การศึกษาคุณลักษณะทางชีวเคมีและทางชีวฟิสิกส์ของไคโตพอริน
จากแบคทีเรียที่ใช้และไม่ใช้ไคติน
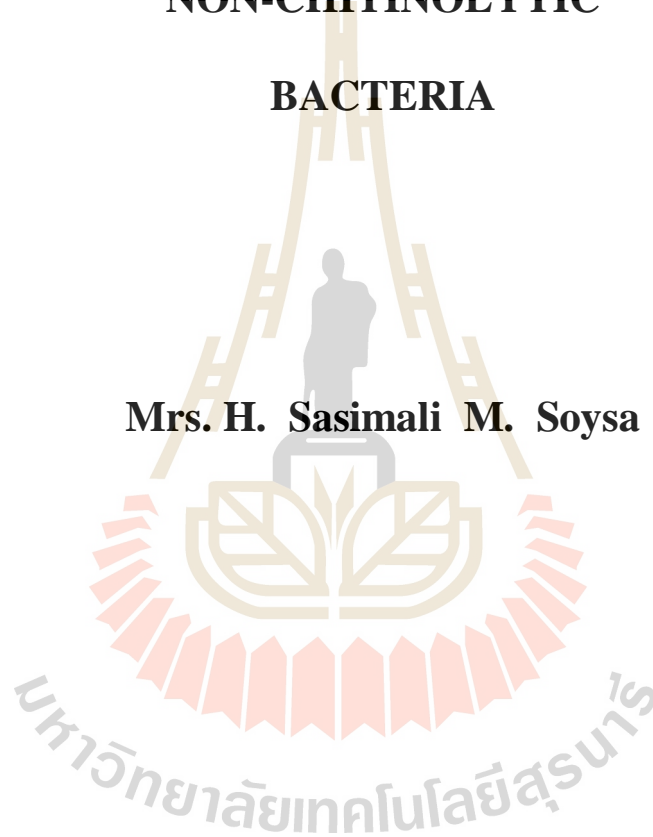
นางเอช ศศิมาลี เอ็ม ซอยซา

BIOCHEMICAL AND BIOPHYSICAL

CHARACTERIZATION OF CHITOPORINS

FROM CHITINOLYTIC AND

NON-CHITINOLYTIC

BACTERIA

Mrs. H. Sasimali M. Soysa

A Thesis Submitted in Partial Fulfillment of the Requirements for the

Degree of Doctor of Philosophy in Biochemistry

Suranaree University of Technology

Academic Year 2016

BIOCHEMICAL AND BIOPHYSICAL CHARACTERIZATION OF CHITOPORINS FROM CHITINOLYTIC AND NON-CHITINOLYTIC BACTERIA

Suranaree University of Technology has approved this thesis submitted in partial fulfillment of the requirements for the Degree of Doctor of Philosophy.

Thesis Examining Committee

_____

(Prof. Dr. Jatuporn Wittayakun)

Chairperson

_____

(Assoc. Prof. Dr. Wipa Suginta)

Member (Thesis Advisor)

_____

(Dr. David Apps)

Member

_____

(Prof. Dr. Albert Schulte)

Member

_____

(Asst. Prof. Dr. M. F. Smith)

Member

_____

(Prof. Dr. Sukit Limpijumnong)

Vice Rector for Academic Affairs

and Innovation

_____

(Prof. Dr. Santi Maensiri)

Dean of Institute of Science

นางเอช ศศิมาลี เอ็ม ซอยซา : การศึกษาคุณลักษณะทางชีวเคมีและทางชีวฟิสิกส์ของ
ไคโตพอรินจากแบคทีเรียที่ใช้และไม่ใช้ไคติน (BIOCHEMICAL AND BIOPHYSICAL
CHARACTERIZATION OF CHITOPORINS FROM CHITINOLYTIC AND NON-
CHITINOLYTIC BACTERIA) อาจารย์ที่ปรึกษาวิทยานิพนธ์ :
รองศาสตราจารย์ ดร.วิภา สุจินต์, 253 หน้า.

ช่องจำเพาะต่อน้ำตาล, ไคโตพอริน, ไอโซเทอร์มอล ไตเตรชัน ไมโครคาลอริเมทรี, การวิเคราะห์
ช่องโปรตีนเดี่ยว

        ไคตินเป็นไบโอโพลีเมอร์ที่ประกอบด้วยน้ำตาล GlcNAc มาเชื่อมต่อกันด้วยพันธะ บีตา-
1,4-ไกลโคซิดิกและเป็นแหล่งคาร์บอนและไนโตรเจนที่เหลือเฟือสำหรับจุลินทรีย์ในทะเล
วิทยานิพนธ์นี้ ประกอบด้วยสามส่วน ซึ่งส่วนแรกจะอธิบายเกี่ยวกับคุณลักษณะของไคโตพอรินที่
ค้นพบใหม่ (เรียกว่า EcChiP) ที่ช่วยในการนำเข้าของน้ำตาลไคตินโอลิโกแซคคาร์ไรด์โดย
แบคทีเรียไม่ใช้ไคติน $E.\ coli$ โดยได้ทำการจำแนกยีน $chip$ ทำการโคลนและการศึกษาการ
แสดงออกของยีนในเซลล์เจ้าบ้าน $E.\ coli$ BL21 (Omp8) Rosetta การศึกษาช่องเดี่ยวโดยเทคนิค
black lipid membrane (BLM) reconstitution พบว่า EcChiP สร้างช่องโมโนเมอร์เสถียรที่มีค่าสภาพ
การนำไฟฟ้าเฉลี่ยเท่ากับ 0.55±0.01 nS และมีความชอบต่อประจุบวก เมื่อหาค่าคงที่การจับ (K) ของ
ช่องเดี่ยวด้วยวิธีทางคณิตศาสตร์สามวิธีพบว่ามีค่าอยู่ในช่วง 0.4-1.0×10^5 M^{-1} การหาค่าเทอร์โม
ไดนามิกส์โดยวิธีไอโซเทอร์มอล ไตเตรชัน ไมโครคาลอริเมทรี (ITC) พบว่าอันตรกิริยาระหว่าง
น้ำตาลไคโตเฮกซะโอสกับช่อง EcChiP เป็นกระบวนการแบบเอนโดเทอร์มิก นอกจากนี้ การ
ทดลองผลของอุณหภูมิพบว่าการขนส่งน้ำตาลผ่านช่อง EcChiP เป็นการแพร่แบบฟาซิลิเทต และ
การศึกษาผลของ pH แสดงให้เห็นว่าหมู่อะซิทะมิโดที่ตำแหน่ง C2 ของไคโตเฮกซะโอสมี
ความสำคัญต่อสัมพรรคภาพของการจับของช่องต่อไคโตโอลิโกแซคคาร์ไรด์ การศึกษาโดยใช้ช่อง
EcChiP เป็นต้นแบบให้องค์ความรู้ใหม่ว่ายีน $chip$ ของแบคทีเรียกลุ่มที่ไม่ใช้ไคตินสามารถถูก
กระตุ้นให้แสดงออกและสร้างไคโตพอรินที่ทำงานได้ ในงานส่วนที่สองทำการศึกษาไคโตพอริน
เหมือน OccD จากเชื้อแบคทีเรียใช้ไคตินคือ $Serratia\ marcescens$ (เรียกว่า SmChiP) การวิเคราะห์
มวลโมเลกุลของ SmChiP โดยวิธี Electrospray MS ให้ค่าเป็น 49,085 Da ซึ่งสอดคล้องกับค่า
น้ำหนักโมเลกุลทางทฤษฎี การหาค่าทางเทอร์โมไดนามิกส์พบว่าน้ำตาลไคโตเฮกซะโอสจับกับ
ช่องด้วยกระบวนการที่ขับเคลื่อนด้วยเอนโทรปี การทดลองด้าน BLM พบว่า SmChiP สร้างช่องเดี่ยว
โมโนเมอร์ที่เสถียรที่มีสภาพการนำไฟฟ้าเฉลี่ยเท่ากับ 0.54±0.01 nS ใน 1M KCl โดย SmChiP ก็มี

ความจำเพาะต่อน้ำตาลไคโตโอลิโกแซคคาร์ไรด์ ผลการทดลองแสดงหน้าที่ของช่องไคโตพอรินที่เหมือน OccD ในการนำเข้าไคโตโอลิโกแซคคาร์ไรด์เป็นครั้งแรกในแบคทีเรียกลุ่มใช้ไคติน ในงานส่วนที่สามเกี่ยวข้องกับคุณลักษณะของไคโตพอรินจากเชื้อ *Vibrio cholerae* (เรียกว่า *Vc*ChiP) จากผลการทดลองที่สอดคล้องกันระหว่างการศึกษาโดย BLM และการดูการเคลื่อนของโปรตีนบนแผ่นเจล SDS-PAGE พบว่า *Vc*ChiP สร้างช่องไตรเมอร์ โดย *Vc*ChiP แสดงคุณสมบัติที่ถูกเหนี่ยวนำโดยความต่างศักย์ไฟฟ้า โดยที่ช่องจะปิดที่ความต่างศักย์ไฟฟ้าต่ำ ๆ เช่น -25 mV และจะเปิดมากขึ้นที่ความต่างศักย์สูง ๆ เช่น -150 mV โดยมีสภาพความสามารถในการนำไฟฟ้าอยู่ที่ 1.6±0.2 nS จากการศึกษาการการผ่านของน้ำตาลเข้าช่องโปรตีนที่ฝังอยู่บนไลโปโซมพบว่าช่อง *Vc*ChiP มีลักษณะเป็นช่องจำเพาะต่อไคโตโอลิโกแซคคาร์ไรด์ การศึกษาด้านเซลล์พบว่าเซลล์ Omp-deficient *E. coli* ที่มียีน *chip* สามารถเจริญเติบโตได้ในอาหารเลี้ยงเชื้อ minimum medium ที่มีน้ำตาลไคโตโอลิโกแซคคาร์ไรด์อยู่ ส่วนเซลล์ที่ไม่มียีน *chip* ไม่สามารถเติบโตได้ โดยรวมผลการทดลองในส่วนนี้แสดงถึงบทบาทของไคโตพอรินในวิถีการใช้ไคตินของแบคทีเรียก่อโรค *V. cholerae.*

สาขาวิชาเคมี   ลายมือชื่อนักศึกษา_____

ปีการศึกษา 2559   ลายมือชื่ออาจารย์ที่ปรึกษา_____

H. SASIMALI M. SOYSA : BIOCHEMICAL AND BIOPHYSICAL CHARACTERIZATION OF CHITOPORINS FROM CHITINOLYTIC AND NON-CHITINOLYTIC BACTERIA. THESIS ADVISOR : ASSOC. PROF. WIPA SUGINTA, Ph.D. 253 PP.

SUGAR-SPECIFIC CHANNEL, CHITOPORIN, ISOTHERMAL TITRATION MICROCALORIMETRY, PROTEIN SINGLE CHANNEL ANALYSIS

Chitin, a biopolymer of β-1,4-glycosidic linked GlcNAc residues, is an abundant source of carbon and nitrogen for marine microorganisms. This thesis is divided into three parts. The first part describes the characterization of a novel chitoporin (so-called *Ec*ChiP) which helps to uptake chitin oligosaccharides in non-chitinolytic *E. coli*. The *chip* gene was identified, cloned and functionally expressed in the Omp-deficient *E. coli* BL21 (Omp8) Rosetta host. Single channel study by black lipid membrane (BLM) reconstitution demonstrated that *Ec*ChiP could readily form a stable monomeric channel, with an average conductance of 0.55 ± 0.01 nS, and showing a slight preference for cations. The binding constant (K) of a single channel binding chitohexaose (the sugar with greatest affinity) was estimated by three mathematical methods and values of $0.4\text{-}1.0\times10^5 \text{ M}^{-1}$ were consistently obtained. Thermodynamic assessment by isothermal titration microcalorimetry (ITC) suggested that chitohexaose-*Ec*ChiP channel interactions are driven by an endothermic process. Moreover, temperature dependence experiments reveal that chitosugar translocation through *Ec*ChiP was achieved by facilitated diffusion. The importance of the acetamido group at C2 of the chitooligosacharide chain for the binding affinity of *Ec*ChiP and its
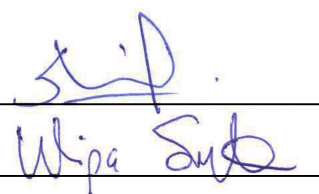
substrate was demonstrated in pH-dependence experiments. Taking *E. coli* as a model, this study offers the first evidence that non-chitinolytic bacteria can activate a quiescent *chip* gene to express a functional chitoporin. The second part is involved with an OccD-like chitoporin from chitinolytic *S. marcescens* (so called *Sm*ChiP). The molecular mass obtained by electrospray ionization spectrometry for the purified *Sm*ChiP was 49,085 Da, which is in good agreement with theoretical molecular weight. The measured ITC parameters indicating that chitosugar binding to *Sm*ChiP is primarily entropy-driven. BLM experiments showed stable monomeric channel with average conductance of 0.54±0.01 nS in 1 M KCl. The channel showed specificity toward chitosugars. For the first time, these data provide insights into chitooligosaccharide uptake by OccD-like chitoporin in chitinolytic bacteria. The third part is involved with the characterization of chitoporin from *V. cholerae* (so called *Vc*ChiP). *Vc*ChiP was shown to be voltage-inducible, being closed at low voltages (i.e. at -25 mV) and more open at high voltages (i.e. -150 mV), and exhibited an average channel conductance of 1.6 ± 0.2 nS. Observed bulk permeation of various chitooligosaccharides through the *Vc*ChiP-reconstituted liposomes together with cell studies confirmed that *Vc*ChiP is a chitooligosaccharide-uptake channel. Cell studies showed that the growth of Omp-deficient *E. coli* cells expressing *chip* gene could be stimulated in the minimum medium supplemented with small chitooligosacharides, while the cells in the absence of *chip* gene could not survive. Overall, the results obtained from this study help to elucidate the role of chitoporin in the chitin utilization pathway of the pathogenic *V.cholerae*.

School of Chemistry   Student's signature_____

Academic Year 2016   Advisor's signature_____
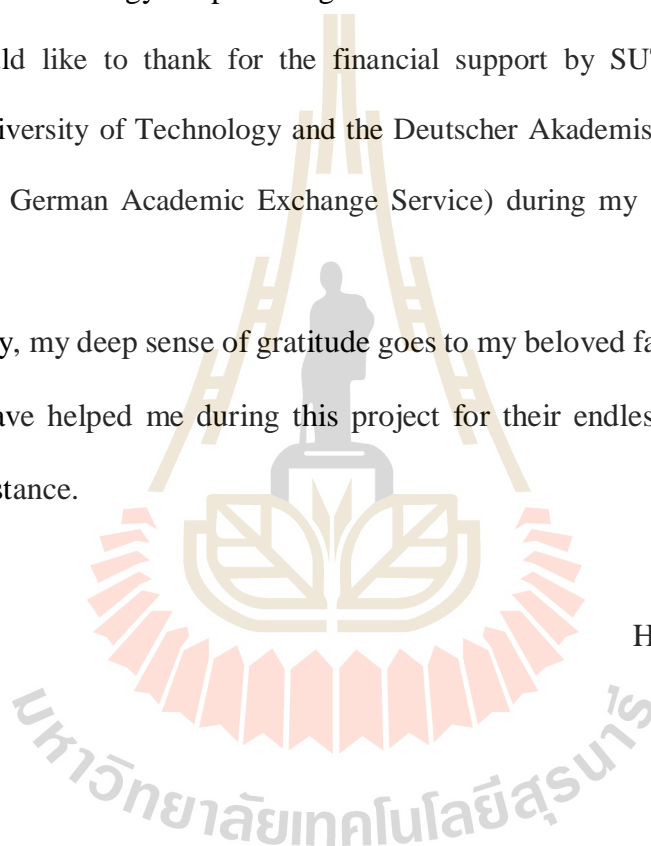
ACKNOWLEDGEMENTS

I am deeply indebted to the Biochemistry-Electrochemistry Research Unit members, School of Chemistry, Suranaree University of Technology, Thailand and Winterhalter's laboratory members, Jacobs University, Bremen, Germany.

I would like to acknowledge the Biochemistry-Electrochemistry Research Unit Laboratory and Center for Scientific and Technological Equipment, Suranaree University of Technology for providing all research facilities.

I would like to thank for the financial support by SUT OROG scholarship, Suranaree University of Technology and the Deutscher Akademischer Austausch Dienst e.V. (DAAD, German Academic Exchange Service) during my 10 months research in Germany.

Finally, my deep sense of gratitude goes to my beloved family members and all those who have helped me during this project for their endless encouragement and heartiest assistance.

<div align="right">H. Sasimali M. Soysa</div>

CONTENTS

CONTENTS (Continued)

CONTENTS (Continued)

CONTENTS (Continued)

CONTENTS (Continued)

CONTENTS (Continued)

CONTENTS (Continued)

LIST OF TABLES

LIST OF TABLES (Continued)

LIST OF FIGURES

LIST OF FIGURES (Continued)

LIST OF FIGURES (Continued)

LIST OF FIGURES (Continued)

LIST OF FIGURES (Continued)

LIST OF FIGURES (Continued)

LIST OF FIGURES (Continued)

LIST OF ABBREVIATIONS

BSA	Bovine serum albumin
BLM	Black lipid membrane
ChiP	Chitoporin
$^{\circ}C$	Degree celsius
Da	Dalton
DPhPC	Diphytanoyl-phosphatidylcholine
*Ec*ChiP	*Escherichia coli* chitoporin
GlcNAc	*N*-acetyl-glucosamine
$GlcNAc_2$	Chitobiose
$GlcNAc_3$	Chitotriose
$GlcNAc_4$	Chitotetraose
$GlcNAc_5$	Chitopentaose
$GlcNAc_6$	Chitohexaose
IPTG	Isopropyl-β-D-thiogaltopyranoside
LDAO	Lauryldimethylamine-oxide
LamB	Maltose-specifc porin
Mr	Molecular weight
μL	Microliter
$\mu g/mL$	Microgram per milliliter
$ng/\mu L$	Nanogram per microliter

LIST OF ABBREVIATIONS (Continued)

Octyl-POE	n-Octylpolyoxyethylene
Omp	Outer membrane proteins
OmpF	Outer membrane protein F
OmpN	Outer membrane protein N
PCR	Polymerase chain reaction
PBS	Phosphate-buffered saline
rpm	Revolutions per minute
ScrY	Sucrose-specific porin
SDS-PAGE	Polyacrylamide gel electrophoresis
SDS	Sodium dodecyl sulphate
*Sm*ChiP	*Serratia marcecens* chitoporin
*Vh*ChiP	*Vibrio harveyi* chitoporin
*Vc*ChiP	*Vibrio cholerae* chitoporin
WT	Wild-type

CHAPTER I

INTRODUCTION

1.1 Structure and composition of Gram-negative bacterial cell walls

Gram-negative cell walls are more complex than Gram-positive cell walls, both structurally and chemically. As Figure 1.1 shows, structurally, a Gram-negative cell wall contains two layers external to the cytoplasmic membrane. Immediately external to the cytoplasmic membrane is a thin peptidoglycan layer. External to the peptidoglycan layer is the outer membrane, which is unique to Gram-negative bacteria. The area between the external surface of the cytoplasmic membrane and the internal surface of the outer membrane is referred to as the periplasmic space. This space is actually a compartment containing a variety of hydrolytic enzymes, which are important to the cell for the breakdown of large macromolecules for metabolism. This space also contains components of the sugar transport systems and other binding proteins to facilitate the uptake of different metabolites and other compounds.
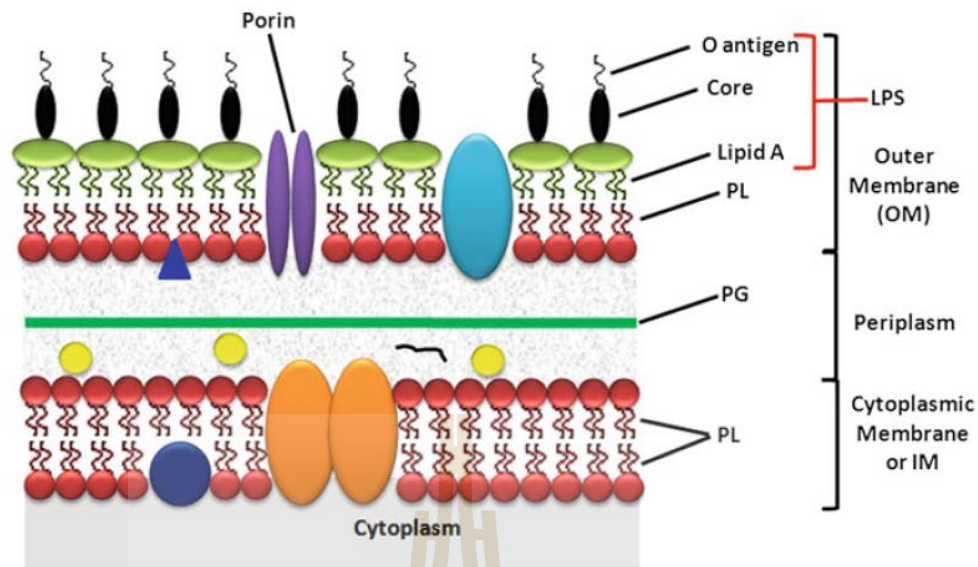
Figure 1.1 Schematic diagram of the bacterial cell wall. It consists of outer membrane (OM), cytoplasmic or inner membrane (IM), and the intermediate periplasmic layer containing the peptidoglycan (PG). The IM consists of the two phospholipid (PL) leaflets and different lipoproteins. The outer membrane consists of two leaflets, the inner leaflet being composed of one phospholipid layer and the outer leaflet of lipid-A, core polysaccharide, and the O-antigen polysaccharide chains projecting outward (Chatterjee and Chaudhuri, 2012).

1.2 Outer membrane proteins (OMPs)

Outer membrane proteins (OMPs), located in the outer membrane, are important for uptaking a variety of hydrophilic compounds into the interior of the bacterial cells. The overall permeability of outer membrane typically depends on the number and properties of the pore-forming proteins, called porins. In Gram-negative bacteria, such as *E. coli*, the uptake of the majority of hydrophilic substrates is mediated by nonspecific porins, such as OmpF and OmpC. Most of these porins form trimeric,

water-filled holes within the outer membrane; they do not bind their substrate with appreciable affinity and mediate the passive diffusion of small molecules (<600 Da) according to their concentration gradients. Although most small molecules utilize this nonspecific pathway, there are some specific channels, such as maltoporin (LamB) (Benz, Schmid, and Vos-Scheperkeuter, 1987; Szmelcman and Hofnung, 1975), and sucrose porin (ScrY) (Schulein, Schmid, and Benzl, 1991), which are responsible for the uptake of maltodextrin and sucrose, respectively. Recently, a newly characterized chitoporin from *V. harveyi* (so-called *Vh*ChiP) was identified (Suginta, Chumjan et al., 2013) with high specificity towards chitooligosaccharides. *Vh*ChiP allows the passage of chitosugars that have an insufficient rate of permeation through non- specific porins and of compounds that are found in the external medium at low concentration. This class of proteins, which includes both monomeric and trimeric channels, contains binding sites for their substrates, allowing for efficient transport at low substrate concentrations.

1.2.1 Substrate-specific porins

The substrate-specific channels bind their substrate with appreciable affinity. For substrates that are present at low concentrations in the external environment, passive diffusion is no longer efficient. So this class of porins contains a binding site for their substrates, and mediates the facilitated diffusion of molecules at low substrate-concentrations. Maltoporin (LamB) was first recognized as a specific porin and as the receptor for λ-phage in *E. coli* (Randall-Hazelbauer and Schwartz, 1973). In addition, LamB was induced in *E. coli* when the cells were grown on maltose or maltodextrins (Szmelcman and Hofnung, 1975). Lipid bilayer experiments were performed with the sugar-specific LamB channel in the presence of a maltodextrin. The

binding site within the channel has been observed from ion flow inhibition studies (Benz et al., 1987) and this information not only showed specific binding of sugars to the interior of the channel, but also allowed the determination of their binding affinity. In maltoporin, there are 18 antiparallel β-strands and three internal loops, namely L1, L3 and L6, which further restrict the channel diameter to 5 Å (Dutzler, Wang, Rizkallah, Rosenbusch, and Schirmer, 1996; Schirmer, Keller, Wang, and Rosenbusch, 1995). The most prominent feature revealed by the X-ray crystallographic structure is a stretch of aromatic residues inside the channel, known as a "greasy slide". Several polar residues are also located at the constriction site and play an important role in maltose and maltodextrin translocation (Figure 1.2) (Ranquin and Van Gelder, 2004).
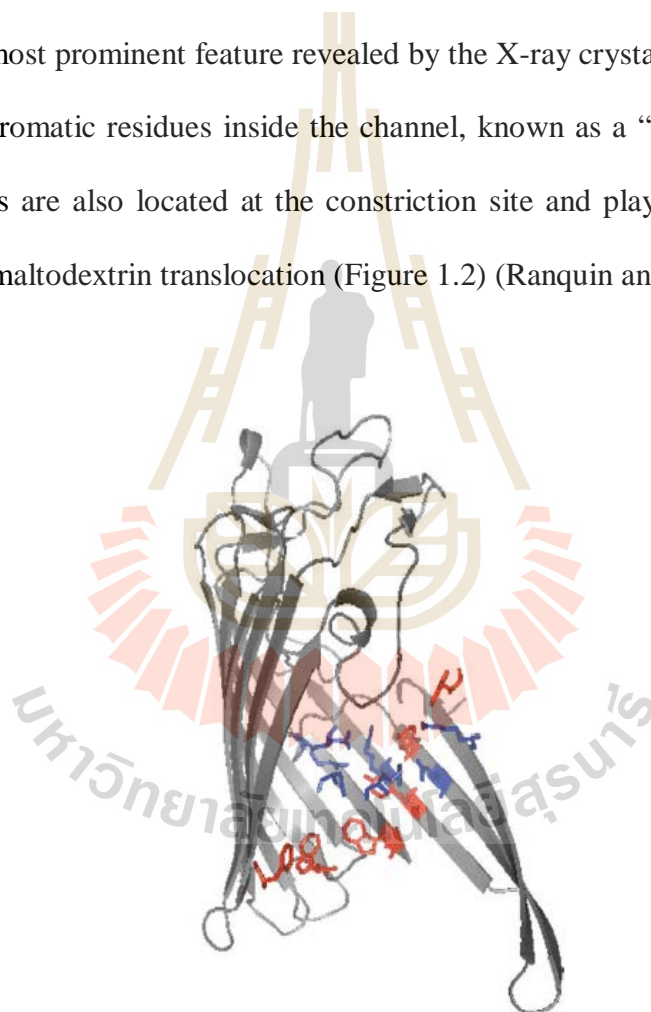
Figure 1.2 Cross-section of the maltoporin monomer. The greasy slide residues are shown in red, in the following sequence: Trp74 (at the top; contributed from the adjacent subunit), Tyr41, Tyr6, Trp420, Trp358 and Phe 227. The polar tracks are shown in blue, comprising the residues: Arg8, Arg33, Glu43, Arg82, Arg109, Asp111

and Asp116 (Ranquin and Van Gelder, 2004).

Furthermore, a sucrose-specific porin (SrcY) (Schulein, Schmid et al., 1991) exhibits high sequence homology to maltoporin with a few residues exchanged (Wang, Dutzler, Rizkallah, Rosenbusch, and Schirmer, 1997). The following Table 1.1 summarizes the previously studied substrate-specific porins.

Table 1.1 Substrate-specific porins.

Porin name	Substrate	References
LamB	Maltose and Maltodextrin	(Luckey and Nikaido, 1980)
SrcY	Sucrose	(Schulein et al., 1991)
Tsx	Nucleosides (purines& pyrimidines)	(Maier, Bremer, Schmid, and Benz, 1988)
OprP	Phosphate	(Benz and Hancock, 1987)
FadL	Long-chain fatty acids	(Hearn, Patel, Lepore, Indic, and van den Berg, 2009)
OprD	Basic amino acids and small peptides containing these amino acids	(Trias and Nikaido, 1990)
Chitoporins	Chitooligosaccharides	(Keyhani, Li, and Roseman, 2000; Suginta, Chumjan, Mahendran, Janning et al., 2013)

1.3 Pore characterization using the black lipid membrane (BLM) technique

Besides site-directed mutagenesis and protein crystallization, several researchers perform current fluctuation analysis using a black lipid membrane technique for channel characterization and for checking the specificity of channels towards substrate. Time-resolved BLM technique is also a high resolution-method for analyzing kinetic parameters for sugar translocation (See section 1.4). Suginta and co-workers recently proved that chitoporin from *V. harveyi* was a chitooligosaccharide-specific porin using black lipid bilayer measurements (Suginta, Chumjan et al., 2013).

The experimental method of choice for characterizing channel-forming proteins is to measure conductance through purified porins that are reconstituted into artificial membranes. Figure 1.3 represents a typical BLM setup, comprising two symmetrical compartments (cuvettes) of a Teflon chamber, separated by a thin Teflon film that contains a round aperture. Each compartment is filled with electrolyte, such as KCl. Across this aperture a lipid membrane is formed. There are two methods for formation of artificial lipid bilayer membrane. One method is a painting approach (Benz, Frohlich, Lauger, and Montal, 1975) in which this type of membrane is formed in the presence of solvent. Another type is the solvent-free membrane that can be formed by lowering and raising the liquid in the cuvettes, following the method described by (Montal and Mueller, 1972). Briefly, solvent-free membrane can form after few microliter of lipid solution in hexane/chloroform is dropped on the top of the surface of electrolyte solution. After allowing solvent to evaporate, a lipid monolayer can be obtained on the top of the electrolyte surface. Then, lowering and raising of the electrolyte level below and above the hole forms a stable bilayer across the aperture. Channel porin insertion

is achieved by adding a porin stock solution on the *cis* side of the BLM chamber (the side of the ground electrode). Choosing the appropriate concentration allows single protein insertion, and multiple insertions can be avoided by flushing the cuvette with fresh buffer. Application of a transmembrane electric field allows the characterization of the electrical properties of the membrane and later of the reconstituted channel. Insertion of a channel gives rise to a measurable jump in ion current. An external voltage applied to the system will cause an ion flux through the inserted porin channel. The strength of the ion flux under different conditions (salt, concentration, pH and external voltage) will reflect the channel's structure and functional properties, such as ion selectivity (Pages, James, and Winterhalter, 2008).
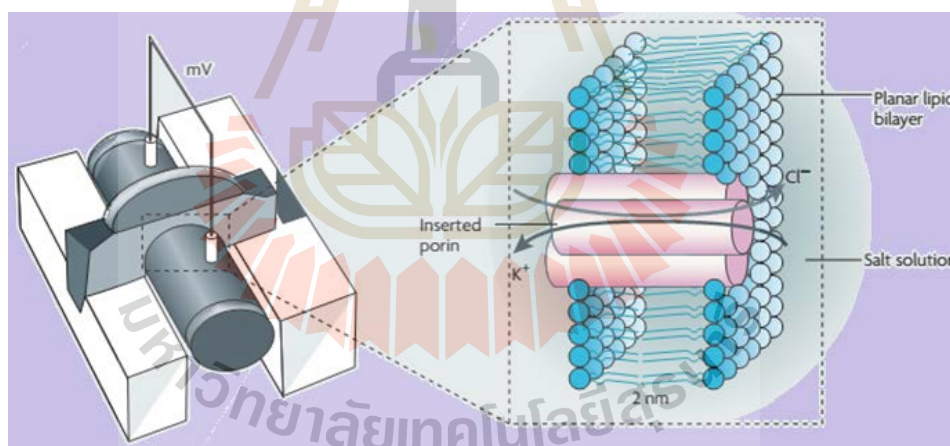
Figure 1.3 Schematic representation of artificial membrane apparatus with expanded view of a single pore within the artificial membrane (Pages et al., 2008).

Figure 1.4 shows a schematic set-up for BLM experiments and normally the BLM set-up is placed in a Faraday cage on a vibration-damping table. A two-electrode bilayer headstage connects to the patch clamp amplifier that connects AD/DA board. A computer interface allows for control of the transmembrane voltage.
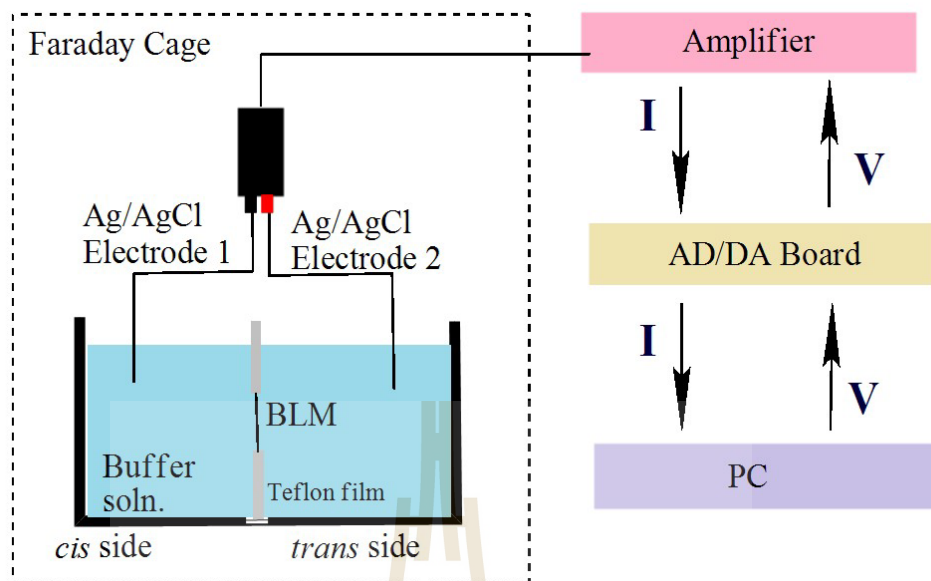
Figure 1.4 Schematic of BLM set-up.

1.4 Kinetic evaluation of substrate-specific channel

Binding of carbohydrates to the maltoporin channels was assumed for a long time to be symmetric, but recent measurements performed on individual maltoporin trimers demonstrated that the association rate was 3–5-fold different depending on the sugar entrance side (Kullman, Winterhalter, and Bezrukov, 2002). The reaction for maltodextrin (M) binding has been proposed to be of first order. The internal binding site, P, is accessible from either side of the membrane (*cis* as well as *trans*). A bound substrate molecule, PM, closes the channel to ion current (Danelon, Brando, and Winterhalter, 2003). The related reaction scheme is written as follows,

$$\text{P} + \text{M}_{cis} \underset{k_{\text{off}}^{cis}}{\overset{k_{\text{on}}^{cis}}{\rightleftharpoons}} \text{PM} \underset{k_{\text{on}}^{trans}}{\overset{k_{\text{off}}^{trans}}{\rightleftharpoons}} \text{P} + \text{M}_{trans}$$
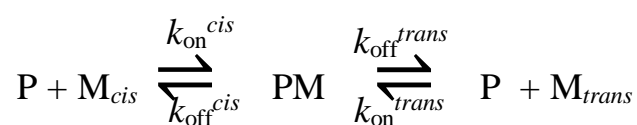
Here k_{on} *cis* and k_{on} *trans* refer to the association rate constants for a sugar molecule entering the channel from the *cis*- and the *trans*-sides, respectively; and k_{off} *cis* and k_{off} *trans* stand for the dissociation rate constants of a sugar molecule exiting from the binding site, respectively, to the *cis* and the *trans*-sides. The two respective pairs of on-off rate constants associated with the *cis*- and *trans*-sides are related to the single thermodynamic equilibrium binding (stability) constant, *K*, according to the detailed balance principle.

$$K = k_{on}^{cis}/k_{off}^{cis} = k_{on}^{trans}/k_{off}^{trans} \qquad \text{Equation 1.1}$$

The on-rate constants k_{on}^{cis} and k_{on}^{trans} can be individually estimated from the respective simple case, where sugar is only added to the *cis*-side or the *trans*-side of the channel. But the off-rate constants k_{off}^{cis} and k_{off}^{trans} can not be obtained from the current fluctuation measurements because they are not distinguishable. Nevertheless, they can easily be derived from the apparent $k_{off} = k_{off}^{cis} + k_{off}^{trans}$ and Equation 1.1.

The relaxation time constant of the binding process, τ, that modulates the ion current depends on the rate constants and sugar concentration, [M],

$$\tau^{-1} = 2\pi f_c = k_{on}^{cis} \cdot [M]^{cis} + k_{on}^{trans} \cdot [M]^{trans} + k_{off}^{cis} + k_{off}^{trans} \qquad \text{Equation 1.2}$$

The parameter f_c can be determined by fitting the power spectral density of the sugar-induced ion fluctuations with the Lorentzian form (Nekolla, Andersen, and Benz, 1994).

Kinetic parameters for sugar transport through LamB were determined by a combination of current fluctuation analysis and site-directed mutagenesis (Danelon et al., 2003; Van Gelder et al., 2002). Referring to Figure 1.5, they showed that analysis of a single greasy slide mutation of LamB at the periplasmic side of the channel resulted in an expected decrease in k_{off} values with single-sided sugar addition on the loop side.
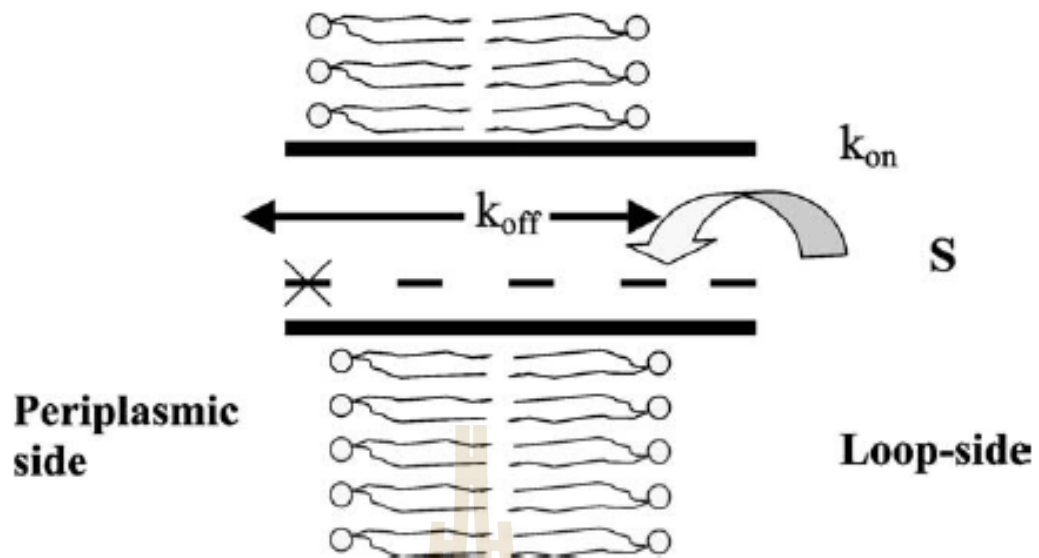
Figure 1.5 Schematic drawing of a single-sided sugar addition experiment. Sugar (S) is added at the loop-side of the channel (*In vivo* this corresponds to the outside medium). Current fluctuation analysis detects k_{on} from the loop side. Once the sugar is bound to the central binding site, it can leave the channel in two directions (length of the arrow is no indication of k_{off} values). Thus, k_{off} values of both exits are measured. The dashed line represents the greasy slide residues; the cross is the mutated greasy slide residue (Ranquin and Van Gelder, 2004).

Conductance data from BLM techniques can be alternatively used to determine the binding constant as shown in Equation 1.3 below (Benz, Schmid, Nakae, and Vos-Scheperkeuter, 1986; Benz et al., 1987).

Suginta and co-workers recently focused on the kinetic evaluation of single chitooligosaccharide translocation through a single *V. harveyi* chitoporin, namely *Vh*ChiP (Suginta, Chumjan, Mahendran, Schulte, and Winterhalter, 2013) and the equilibrium binding constant (*K*) was estimated from the reduction of ion conductance in the presence of increasing concentrations of sugar. As shown in Equation 1.3, G_{max} is

the average conductance of the fully open *Vh*ChiP channel, $G_{[c]}$ is the average

conductance at a given concentration of a chitosugar ($[c]$), I_0 is the initial current

through the fully open channel in the absence of sugar, and $I_{[c]}$ is the current at a

particular sugar concentration. Inversion of Equation 1.3 yields Lineweaver-Burk plot

$(((G_{max} - G_{[c]})/G_{max})^{-1}$ *versus* $([c]^{-1}))$.

$$(G_{max} - G_{[c]})/G_{max} = (I_0 - I_{[c]})/I_0 = K \cdot c / (1 + K \cdot c) \qquad \text{Equation 1.3}$$

Single channel analysis was performed to calculate the rates of association (k_{on})

and dissociation (k_{off}). The off-rate (k_{off}, s^{-1}) was obtained from Equation 1.4, where

τ_c is the average residence (dwell) time (s^{-1}) of the sugar molecule in the channel. The

on-rate (k_{on}, $M^{-1} \cdot s^{-1}$) is given by $k_{on} = K \cdot k_{off}$. The equilibrium binding constant (K)

can be obtained from Equation 1.3.

$$k_{off} = 1/\tau_c \qquad \text{Equation 1.4}$$

Suginta and co-workers further investigated the effects of applied voltages on

sugar translocation. Figure 1.6 presents ion current fluctuations with different

concentrations and different voltages. The number of blocking events was visibly

higher at -100 mV, as well as when high concentration of sugar was used, with the

number of subunit blockages increasing from one subunit to three subunits.
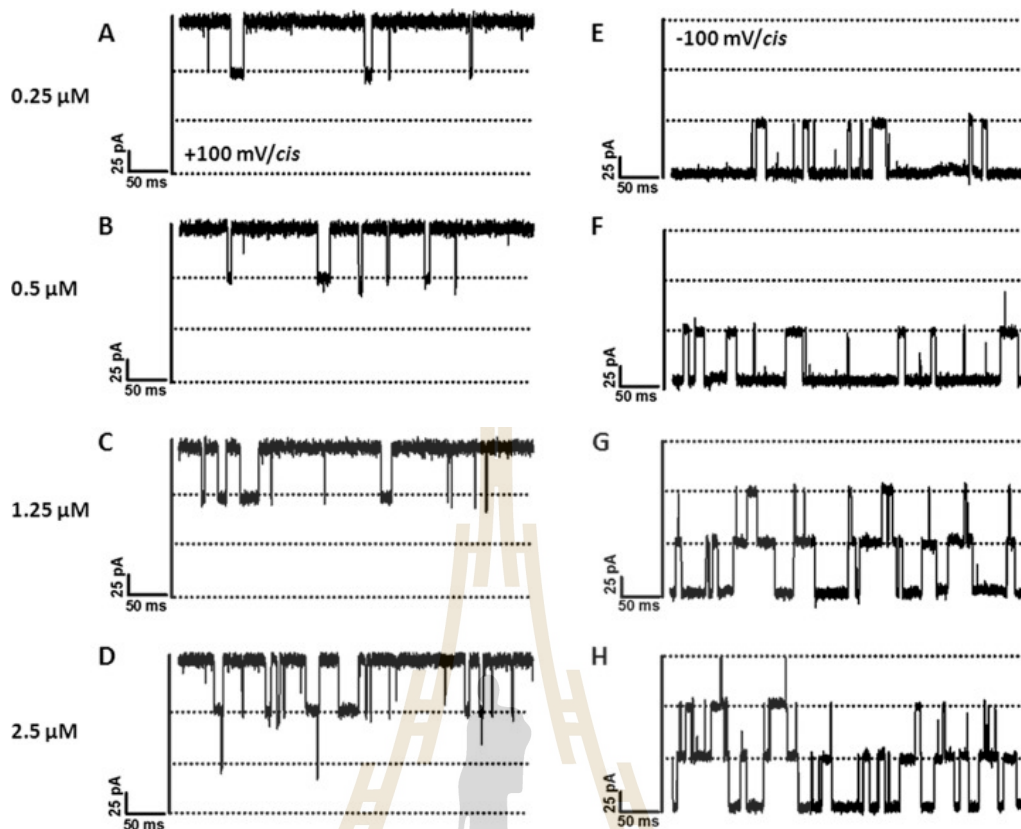
Figure 1.6 Effects of transmembrane potentials and sugar concentrations on ion currents. The fully open *Vh*ChiP trimeric channel was exposed to different concentrations of chitohexaose. Ion current blockages at +100 mV (*A–D*) and −100 mV (*E–H*) (Suginta, Chumjan, Mahendran, Schulte et al., 2013).

Figure 1.7 shows the binding curves of various chitosugars at +100 mV/*cis*. Fitting the curves using a nonlinear regression function derived from Equation 1.3 yielded typical Michaelis-Menten plots. Even though chitohexaose reached saturation at 5 μM, the binding curves of chitotriose, chitotetraose, and chitopentaose did not approach saturation even at 40 μM.
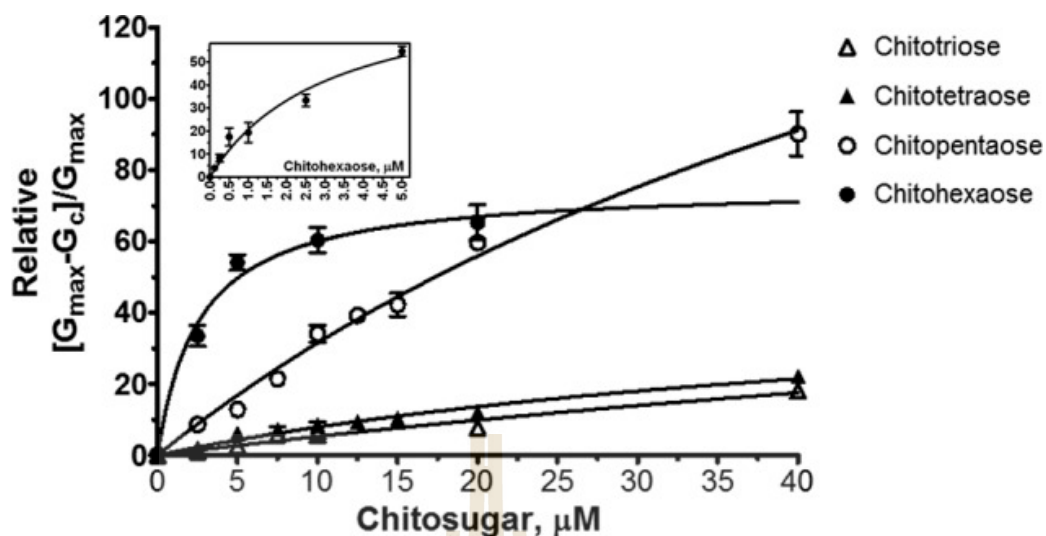
Figure 1.7 Binding of chitohexaose to *Vh*ChiP compared with that of chitopentaose, chitotetraose, and chitotriose. The Michaelis-Menten plots were evaluated from the data acquired on the *cis* side at +100 mV. The values are averaged from the BLM data obtained in triplicate. The plots of $(G_{max} - G_{[c]})/G_{max}$ *versus* sugar concentrations (micromolar) were derived from Equation 1.3. The *inset* shows the plot for chitohexaose at initial concentrations of 0–5 μM (Suginta, Chumjan, Mahendran, Schulte et al., 2013).

Transformation of these binding curves yielded linear double reciprocal plots (Lineweaver-Burk plots) as shown in Figure 1.8. Figure 1.8A shows the Lineweaver-Burk plots for chitotriose, chitotetraose and chitopentaose at +100 mV/*cis*, whereas Figure 1.8B shows the Lineweaver-Burk plots for chitohexaose at +100 mV/*cis* compared with −100 mV/*cis*. These Lineweaver-Burk plots allowed the binding constants (K) to be determined.
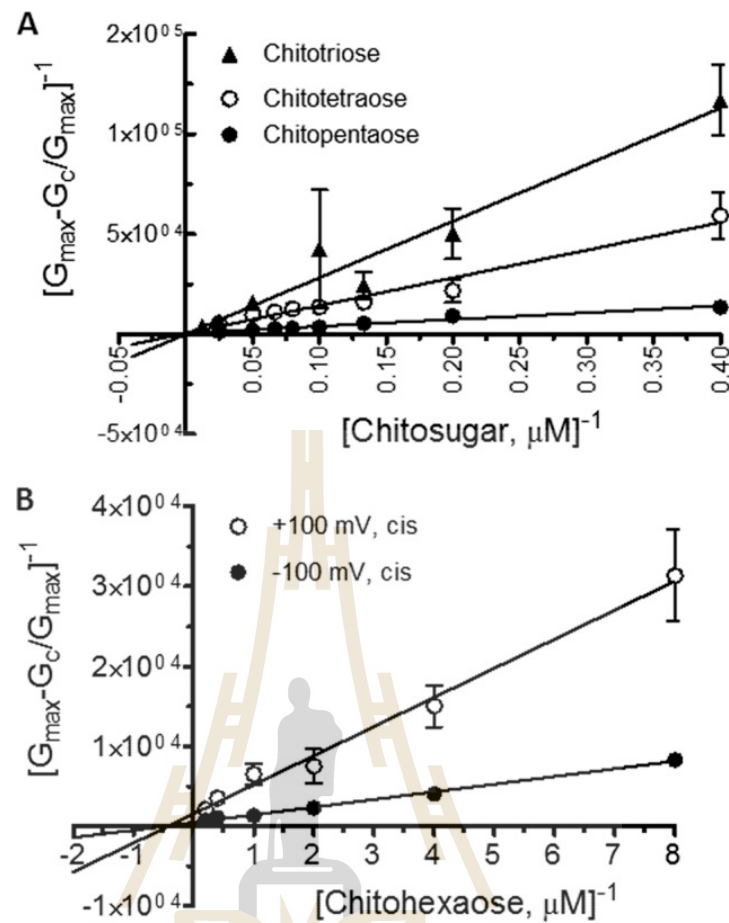
Figure 1.8 Lineweaver-Burk plots for different chitosugars. *A*, Lineweaver-Burk plots of chitotriose, chitotetraose and chitopentaose at a concentration range of 2.5–40 μM. The conditions for data analysis were +100 mV/*cis*. *B*, Lineweaver-Burk plots of chitohexaose at +100 and −100 mV/*cis*. (Suginta, Chumjan, Mahendran, Schulte et al., 2013).

1.5 Characterization of sugar permeation by liposome swelling assay

Liposome swelling assay is a method for studying the permeability of the molecule of interest through multilamellar liposomes reconstituted with a given porin. Normally, the proteoliposomes are filled with 17% (w/v) dextran solution. When they are mixed with aqueous isotonic solution of solutes, the diffusion of such molecules

through the given porin can be investigated. Figure 1.9 shows schematic representation of a liposome swelling assay. In the presence of hypotonic solution, the proteoliposomes will swell and in a hypertonic solution proteoliposomes will shrink. Under isotonic concentration, the scattering signal remains constant through the measuring time.
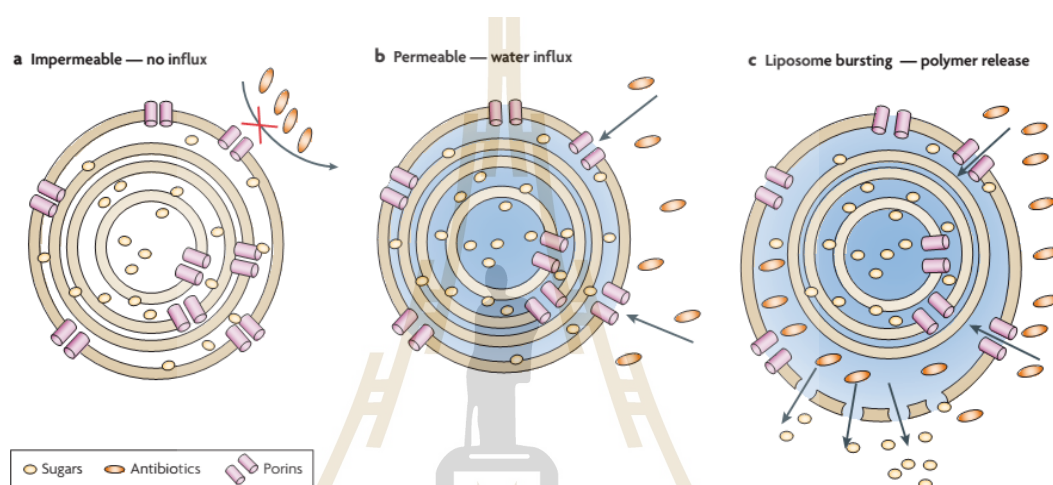
Figure 1.9 Schematic representation of liposome swelling assay. (Pages et al., 2008).

Under isotonic concentration, if solute can enter the proteoliposome, swelling is observed which leads to a decrease in apparent absorbance at 500 nm (A_{500}). The absorbance difference during in the first 60 s gives the swelling rate as follows.

$$\varphi = (1/A_i)dA/dt \qquad \text{Equation 1.5}$$

Where φ is the swelling rate, A_i is the initial absorbance and dA/dt is the rate of absorbance change during the first 60 s. The swelling rate is then normalized by setting the rate for arabinose to 100%, which allows comparison of the permeation rates of different neutral sugar species.

1.6 Statistical analysis of single channels currents

Molecular interactions that take place between the translocating molecule and the protein channel should be considered for understanding permeation on a molecular level. Fluctuations in the ion current that passes through a porin that has been reconstituted into artificial lipid membranes occur when sugars or antibiotics go through the channel and report residence of molecule in a binding pocket inside the porin. Diffusion of maltose through maltoporin (LamB) led to the development of an asymmetric single-binding-site model (Danelon et al., 2003; Kullman et al., 2002). Even though asymmetric translocation was observed in maltoporin, for simplicity they describe only a symmetrical model. However Suginta and co-workers explain a multiple trap design for sugar tranlocation through *V. harveyi* chitoporin (Suginta and Smith, 2013). In that paper, they presented data of ion current fluctuations (I_t) through a bilayer lipid membrane immersed in chitohexaose solution and perforated with one trimeric *Vh*ChiP. (I_t) fluctuates among discrete bands such that $(I_t) = I_n = I_0 (3-n)/3$ when n monomers are blocked by sugar. By analyzing the stochastic integer n, they find that (i) each ChiP monomer functions independently, (ii) a monomer has multiple binding sites (or traps) that can be occupied simultaneously, and (iii) there is evidence that molecules bound in the same monomer attract each other. Ionic current fluctuations can be analyzed in different ways to study channel properties. They characterized the single monomer by U(t) and B(t) functions. U(t) describes trapping by an open monomer and B(t) describes detrapping from an occupied monomer. As shown in Figure 1.10, at the lower times monomers showed multiple trapping states.
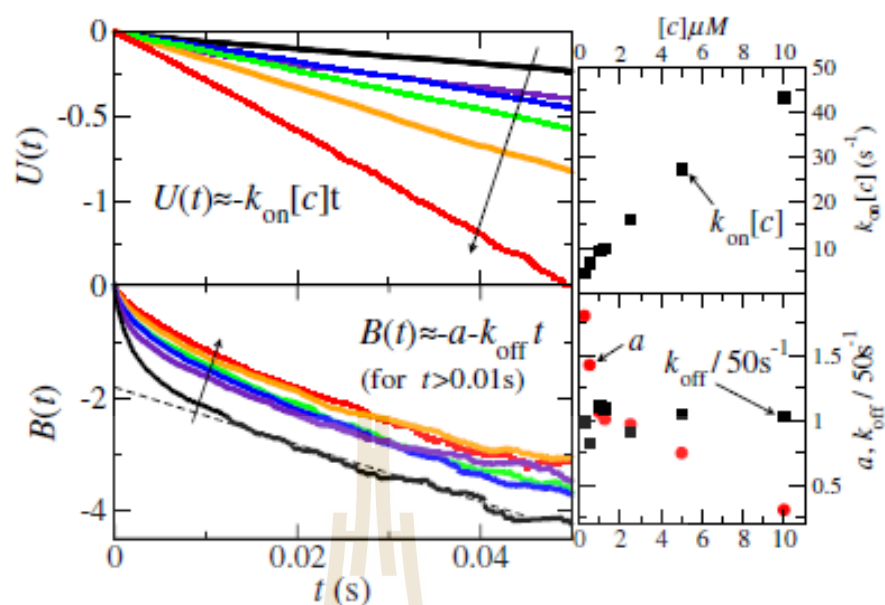
Figure 1.10 Evidence for multiple-molecule trapping by a monomer. Left panels: Horizontal axis is time (t) and vertical axis is logarithm of the probability that a monomer remains unblocked (upper panel) or blocked (lower panel) for longer than t, denoted by U(t) or B(t). Curves are for different sugar concentrations [c], along arrows: [c]= 0.25, 0.5, 1.0, 2.5, 5, and 10 µM. For t > 0.01, linear fits to B(t) (the dashed line) can be made, but at low-t the nonlinear behavior indicates multiple trapping states. Upper right: slope k_{on}[C] of linear fit to U(t), versus [c]. Lower right: slope k_{off} and extrapolated t = 0 intercept a, from linear fit to B(t) for t > 0.01 s, versus [c] (Suginta and Smith, 2013).

1.7 Thermodynamic characteristics of ligand-protein interactions

Isothermal titration calorimetry (ITC) can be effectively used to gain valuable insight into the thermodynamic basis of binding interactions of membrane proteins (Draczkowski, Matosiuk, and Jozwiak, 2014; Evans, Cooper, and Lakey, 1996; Nisius,

Rogowski, Vangelista, and Grzesiek, 2008; Rajarathnam and Rosgen, 2014; Sikora and Turner, 2005a, 2005b; Wohri et al., 2013). To our knowledge, there is not any ITC study of specific bacterial outer membrane protein channel with its substrate to prove binding. Recently outer membrane porin OmpF was used to prove how bacteriocin colE9 recruits OmpF to deliver colE9IUTD (Housden et al., 2010). ITC experiments could be used to determine the binding affinity (K_a), enthalpy changes (ΔH), and binding stoichiometry (n) of the interaction between two or more molecules in solution. From these initial measurements, Gibbs energy changes (ΔG) and entropy changes (ΔS) can be determined using the relationship: (where R is the gas constant and T is the absolute temperature).

$$\Delta G = -RTlnK_a = \Delta H - T\Delta S \qquad \text{Equation 1.6}$$

1.8 Roles of chitoporin in the chitin degradation pathway of Gram-negative bacteria

Chitin, an insoluble polymer of GlcNAc, is an abundant source of carbon, nitrogen and energy for marine microorganisms. Chitin is present in the cell wall of fungi as well as in cuticles and exoskeletons of worms, mollusks and arthropods, and it constitutes a natural source of GlcNAc for many bacteria in respective ecosystems, such as large aquatic reservoirs. An extremely efficient utilization of chitin in the ocean is evidenced by its being nearly undetectable in marine sediments. Marine chitinolytic bacteria, such as marine *Vibrios*, are pre assumed to play a major role in this process (Keyhani and Roseman, 1999). The transformation of GlcNAc to fructose-6-phosphate is catalyzed through consecutive phosphorylation, deacetylation and isomerization-deamination reactions (Yang et al., 2006). This three-step biochemical pathway (NAG

pathway) appears to be conserved in both chitinolytic bacteria (such as *V. cholerae*) (Meibom et al., 2004) and non-chitinolytic bacteria, (such as *E. coli*) (Peri, Goldie, and Waygood, 1990). Chitin degradation by proteobacteria (especially chitinolytic bacteria) is achieved using a complex pathway including various enzymes and transporters. Diffusion of solutes across the outer membrane usually occurs through a porin channel, called chitoporin (ChiP).

Roseman and co-workers first reported identification and molecular cloning of chitoporin (ChiP) from *Vibrio furnissii*. This outer membrane porin was expressed in *V. furnissii* induced by $(GlcNAc)_n$, n= 2-6, but not by GlcNAc or other sugars. In contrast to the parental strain, a mutant of ChiP did not grow on $(GlcNAc)_3$ and this result implied that ChiP was a chitooligosaccharide-specific porin (Keyhani, Li et al., 2000).

Later, Meibom and co-workers identified the gene (VC0972) corresponding to chitoporin in *V. cholerae* using microarray expression results (Meibom et al., 2004). To determine whether VC0972 encodes chitoporin, it was distrupted and the mutant found to grow poorly in a medium containing colloidal chitin. Normal growth was restored by complementation with a plasmid-encoded copy of VC0972 (Figure 1.11).
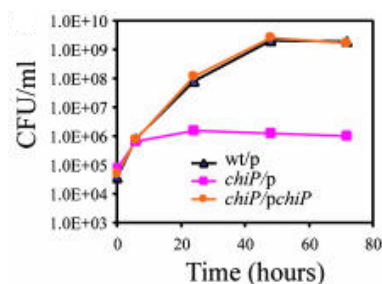
Figure 1.11 Growth in media supplemented with colloidal chitin, mutants with or without a plasmid encoded *ChiP* gene. (Meibom et al., 2004).

Even though chitoporin was identified more than a decade ago, its physiological function as a chitooligosacharide-specific channel remains unproved for bacteria of the family *Vibrionaceae* except for *Vibrio harveyi*. Suginta and co-workers isolated the gene corresponding to an outer membrane chitoporin from *V. harveyi* and proved its function as a chitooligosaccharide-specific porin using black lipid bilayer measurements and liposome swelling assays (Suginta, Chumjan, Mahendran, Janning et al., 2013).

Recently, Watanabe and co-workers studied deletion mutants of genes involved in the chitin utilization pathway in *Serratia marcescens* 2170 (Takanao et al., 2014). The ChiP mutant in their study grew slowly on the lower concentration of $(GlcNAc)_2$ and there was essentially no growth on chitin oligosaccharides larger than $(GlcNAc)_3$.

1.8.1 *E. coli* chitoporin

An outer membrane porin (named in Figure 1.12 as ChiP II) belongs to the OprD family and was mapped in the NagC regulons (transcriptional regulator) of ten γ-proteobacteria. The conserved co-localization of the *ChiP II* and *β-N-acetylglucosaminidase* genes in the chromosomes of the *Yersinia* and *Serratia* species suggests the involvment of ChiP II in the outer membrane uptake of chitooligosachcharides that are substrates for periplasmic β-N-acetylglucosaminidase (*hex*). In non-chitinolytic *Escherichia* and *Salmonella* species that have no Hex hydrolase, ChiP-II (YbfM porin) could be involved in the uptake of chitobiose through the outer membrane, supplying the PTS transporter with this disaccharide (Yang et al., 2006).
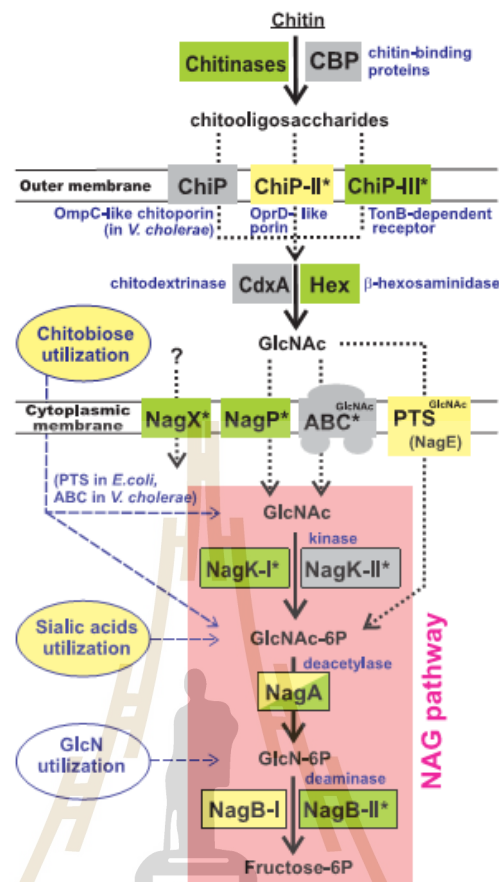
Figure 1.12 Reconstruction of the GlcNAc and chitin utilization pathways in proteobacteria. Functional roles and metabolic blocks (pathways) present in *S. oneidensis* and *E. coli* are shown on green and yellow backgrounds, respectively. Those present in other proteobacteria (but not in *S. oneidensis* and *E. coli*) are shown on a gray background. Solid arrows denote enzymatic reactions, and dotted arrows denote transport. Broken arrows denote links to other catabolic subsystems (utilization of chitobiose, sialic acids, and glucosamine) that are not analyzed in this study (Yang et al., 2006).

In the past few years, an increasing number of small non-coding RNAs (sRNAs) in enterobacteria have been found to negatively regulate the expression of outer membrane proteins (OMPs) at the post-transcriptional level. These RNAs act

under various growth and stress conditions, suggesting an important physiological role of such regulatory RNA molecules in Gram-negative bacteria in modulating the cell surface and/or preventing accumulation of OMPs in the envelope (Figueroa-Bossi, Valentini, Malleret, Fiorini, and Bossi, 2009; Rasmussen et al., 2009). Figueroa and co-workers identified and characterized *ChiP* gene (formerly *YbfM*), in their study. This conserved enterobacterial chitoporin was required for the uptake of chitin-derived oligosaccharides. As shown in Figure 1.13, they identified (*YbfM*) chitoporin as an inducible chitoporin.
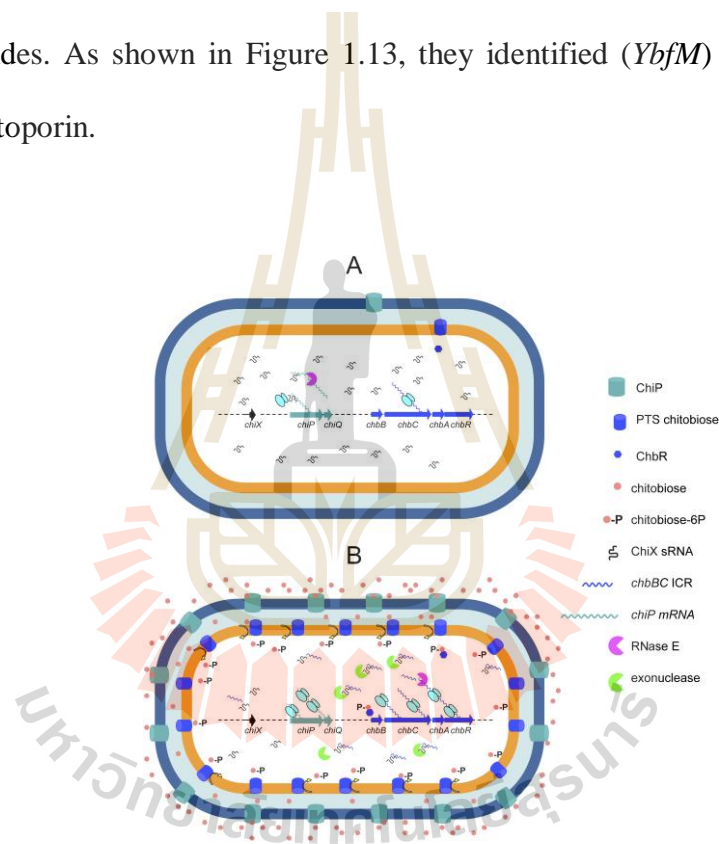
Figure 1.13 Model for ChiP regulation. (A) In the absence of inducers, the chiX gene (black arrow) and the chiPQ operon (green arrows) are transcribed constitutively. Pairing of ChiX sRNA with the 59 UTR of chiPQ mRNA inhibits ChiP synthesis, promoting cleavage of the ChiP mRNA by RNase E. The chb operon (blue arrows; only three genes shown) is expressed just to the level needed to prime the system. (B) In the presence of chitooligosaccharides, inducer binding to ChbR causes this protein to activate transcription of the chb operon and to further stimulate chiPQ transcription.

Processing of the chb transcript (initiated by RNase E) releases chbBC ICR RNA. This RNA base-pairs with ChiX sRNA making it susceptible to the action of a ribonuclease. The drop in ChiX levels, combined with the increase in chiPQ mRNA, relieves ChiP repression leading to a burst of ChiP synthesis. ChiP assembles in the outer membrane, resulting in more inducer uptake (Figueroa-Bossi, Valentini et al., 2009).

In particular research in *E. coli* and *Salmonella* has revealed that sRNAs are key regulators of outer membrane protein (OMP) expression during growth and adaptation to environmental changes and stress conditions (Guillier and Gottesman, 2006; Valentin-Hansen, Johansen, and Rasmussen, 2007; Vogel, 2009; Vogel and Papenfort, 2006). So, it is of great interest to characterize *YbfM* chitoporin from *E. coli* as a chitooligosaccharide-specific porin.

1.8.2 *Serratia marcescens* chitoporin

Serratia marcescens is a Gram-negative bacterium that utilizes chitin, a linear insoluble polymer of β-1,4-linked N-acetylglucosamine (GlcNAc) (Vaaje-Kolstad, Horn, Sorlie, and Eijsink, 2013). This bacterium is now recognized as a main human pathogen, being frequently encountered in nosocomial infections (Hejazi and Falkiner, 1997; Mahlen, 2011) in humans and causing important infections in animals and insects (Mahlen, 2011). The initial step of chitin breakdown by *Serratia* includes four chitin-active enzymes such as ChiA, ChiB, ChiC and a chitin-binding protein (CBP21), a surface-active lytic polysaccharide monooxygenase that introduces chain breaks by oxidative cleavage (Suzuki et al., 2002; Takanao et al., 2014; Vaaje-Kolstad et al., 2013; Watanabe et al., 1997). ChiA and ChiB are processive chitinases that hydrolyze chitin chains in opposite directions while ChiC makes random cuts as an endo-acting non-processive chitinase. Then hydrolyzed products,

chitooligosaccharides, are transported through the bacterial cell wall by chitoporin or ChiP (Takanao et al., 2014). In the periplasm, Chitobiase hydrolyzes the β-1,4-glycosidic bond of $GlcNAc_2$ and the resultant GlcNAc monomers are transported through the inner membrane by the GlcNAc-specific PTS permease while a portion of $GlcNAc_2$ enters the periplasm and is transported into the cytoplasm via $GlcNAc_2$ -specific PTS permease (Takanao et al., 2014). Finally, these products are further metabolized in the cytoplasm, acting as sources of carbon and nitrogen for the bacterium.

1.8.3 *V. cholerae* chitoporin

V. cholerae has evolved mechanisms for attaching to, degrading and using chitin as a carbon and nitrogen source at different stages of its life cycle and at advanced hierarchical scales. Chitin - *V. cholerae* interaction has been proposed to be critical for the pathogenicity of this bacterium during infection of human hosts (Figure 1.14) (Pruzzo, Vezzulli, and Colwell, 2008).
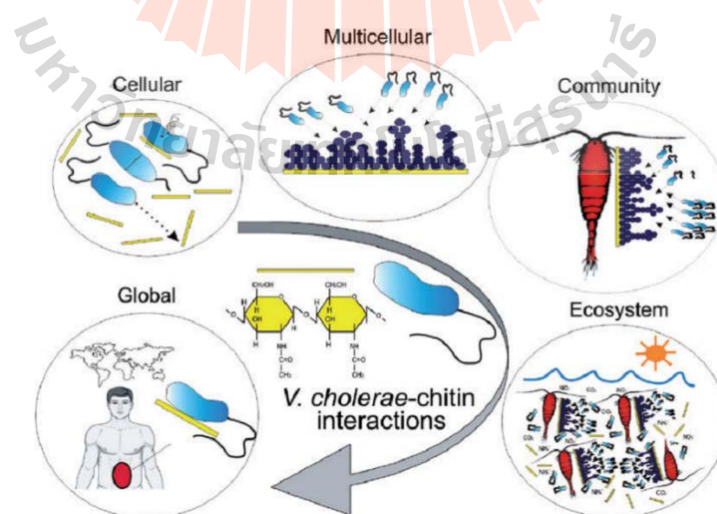
Figure 1.14 Global impact of *V. cholerae*–chitin binding at different hierarchical scales in the environment, comprising: cell response (e.g. cell multiplication, chemotaxis,

competence), biofilm formation, association with chitinous organisms, C and N cycling, and pathogenicity for humans (Pruzzo et al., 2008).

The proposed chitin catabolic cascade in *V. cholerae* begins with the breakdown of chitin polymer into oligomers by extracellular chitinases (Figure 1.15) (Hunt, Gevers, Vahora, and Polz, 2008) and resultant oligosaccharides are transported into the periplasm through a specific porin known as chitoporin (Keyhani, Li, et al., 2000; Meibom et al., 2004).
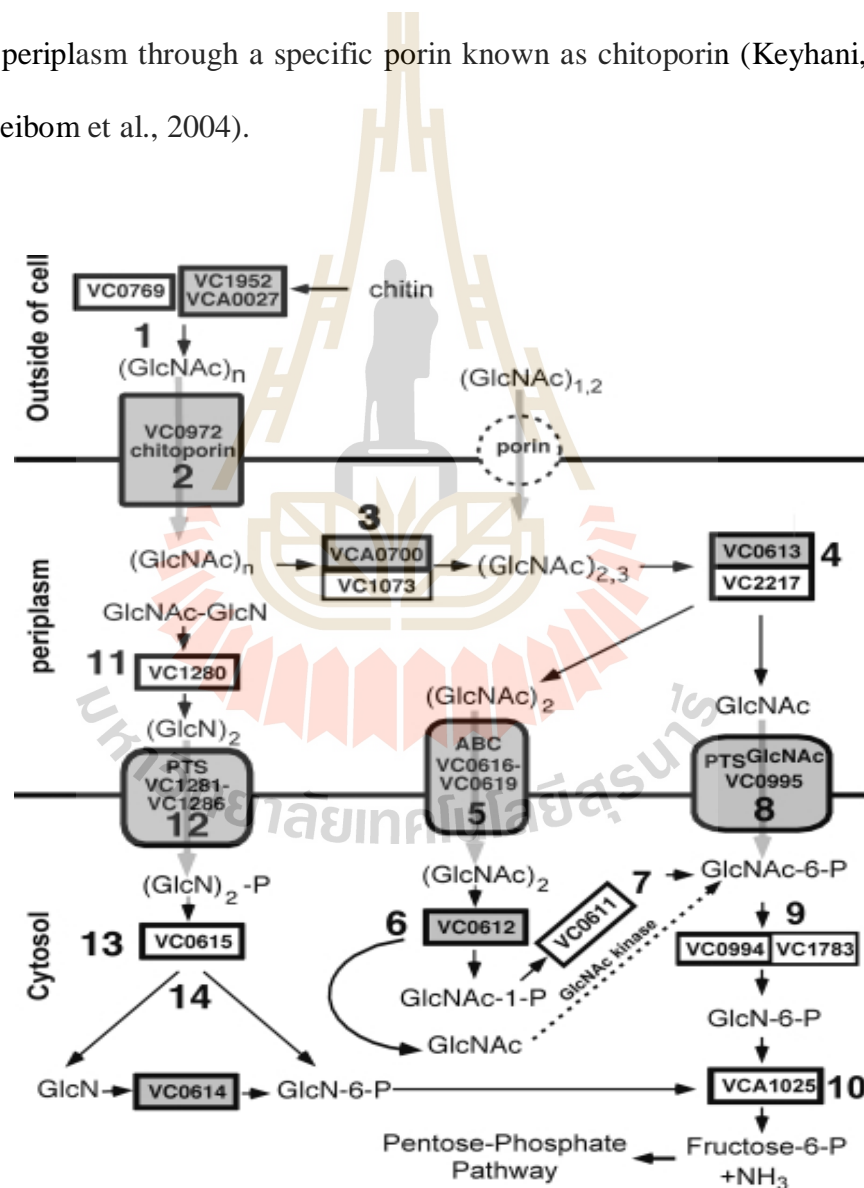
Figure 1.15 Schematic of the chitin catabolic cascade in *V. cholerae*. (Hunt et al., 2008).

In this study, the gene, VC0972 that is responsible for *V. cholerae* chitoporin was selected for cloning to express chitoporin for characterization.

1.9   Research objectives

Escherichia coli is a Gram-negative, heterotrophic bacterium that lives in open environments, such as soil, manure and water, but the persistence of *E. coli* populations depends upon the availability of carbon substrates in each natural environment. *E. coli* usually grows on glucose-enriched nutrients such as starch, cellulose and hemicellulose (Kim and Gadd, 2008), but not on chitin polysaccharides, since it intrinsically lacks competent chitin-utilization machinery (Francetic, Badaut, Rimsky, and Pugsley, 2000; Francetic, Belin, Badaut, and Pugsley, 2000). The chitin-degradation pathway is known to be highly active in marine *Vibrios*, the growth of which depends on the utilization of the chitin biomass as their sole source of cellular energy. The chitin degradation pathway of *Vibrios* incorporates a large number of chitin-degrading enzymes and transporters for chitooligosaccharides and N-acetyl glucosamine (Keyhani, Li et al., 2000; Li and Roseman, 2004; Suginta, Chuenark, Mizuhara, and Fukamizo, 2010). Roseman and co-workers first reported the identification and molecular cloning of the gene encoding chitoporin (*Vf*ChiP) from *Vibrio furnissii* (Keyhani, Li et al., 2000). *Vf*ChiP was expressed on induction with (GlcNAc)n, n= 2-6, but was not induced by GlcNAc nor by other sugars. In contrast to the parental strain, a mutant strain lacking *Vf*ChiP did not grow on GlcNAc$_3$, implying that *Vf*ChiP was selective for chitooligosaccharides (Keyhani, Li et al., 2000). The chitin uptake channel (so-called *Vh*ChiP) from the bioluminescent marine bacterium *V. harveyi* (Suginta, Chumjan,

Mahendran, Janning et al., 2013; Suginta, Chumjan, Mahendran, Schulte et al., 2013) was recently identified and characterized.

*Vh*ChiP is a trimeric OmpC-like porin located in the outer membrane and responsible for the molecular uptake of chitin breakdown products that are generated by the action of secreted chitinases (Meekrathok and Suginta, 2016; Sritho and Suginta, 2012; Suginta et al., 2010; Suginta and Sritho, 2012). Unlike *Vibrio* species, the chitin catabolic cascade of non-chitinolytic bacteria, such as *Candida albicans* (Biswas, Van Dijck, and Datta, 2007), *Xanthomonas campestris* (Boulanger et al., 2010), *Shewanella oneidensis* (Yang et al., 2006) and *E. coli* (Peri et al., 1990; Rasmussen et al., 2009; Verma and Mahadevan, 2012) was innately inactive, although presumed to be preserved. Yang and co-workers proposed the three-step biochemical conversion of GlcNAc (the monomer of chitin) to fructose 6-phosphate in *E. coli* through sequential phosphorylation, deacetylation and isomerization-deamination reactions (Yang et al., 2006). The gene ChiP (formerly ybfM) encoding chitoporin was previously identified in *E. coli* and *Salmonella* sp. as a silent gene controlled by a non-coding small RNA (sRNA) (Rasmussen et al., 2009). However, this ChiP gene was sporadically expressed as an adaptive strategy for the bacterium to thrive in glucose-deficient environments (Figueroa-Bossi et al., 2009; Plumbridge, Bossi, Oberto, Wade, and Figueroa-Bossi, 2014; Rasmussen et al., 2009; Valentin-Hansen et al., 2007; Vogel and Papenfort, 2006). To date, *E. coli* chitoporin (so-called *Ec*ChiP) has not been functionally characterized and our study used electrophysiological and biochemical approaches to uncover the physiological roles of *Ec*ChiP.

Surprisingly, one efficient chitin degrader, *Serratia marcescens,* has an OprD-like chitin uptake channel in its chitinolytic machinery with 75% sequence identity with

*Ec*ChiP (Takanao et al., 2014). In order to expose the role of *Sm*ChiP in chitin utilization by *Serratia marcescens* 2170, the growth rate of wild type and ChiP deletion mutant was monitored on various chitooligosaccharides carbon sources (Takanao et al., 2014). The ΔChiP mutant showed no growth on GlcNAc$_3$, GlcNAc$_4$, GlcNAc$_5$ confirming the role of ChiP for uptaking chitooligosaccharides larger than GlcNAc$_3$. We have now employed biochemical and electrophysiological approaches to characterize the OprD-like chitin uptake channel from chitinolytic *Serratia marcescens*. The aim of this work was to gain insight into how a chitinolytic bacterium uses OprD-like chitoporin for uptaking chitooligosaccharides as sole source of energy.

Vibrio cholerae is a Gram-negative bacterial pathogen and a leading cause of cholera epidemics worldwide (Colwell, 1996; Huq et al., 2005; Pruzzo et al., 2008). The bacteria live in brackish or salt-water, which is a chitin-rich habitat and chitin-*V. cholerae* interactions have been anticipated to be involved at multiple levels in a hierarchical scale and play vital roles in the survival and the pathogenicity of the bacteria (Lutz, Erken, Noorian, Sun, and McDougald, 2013; Nelson, Harris, Morris, Calderwood, and Camilli, 2009; Pruzzo et al., 2008). *V.cholerae* pathogen has both human and environment stages in its life cycle and gene expression pattern is different at different stages of the life cycle (Nelson et al., 2009). *V.cholerae* has evolved mechanisms for attaching to and degrading chitin as a carbon and nitrogen source and this chitin-*V.cholerae* association increases the microbe's resistance to gastric acids during stomach transit (Bartlett and Azam, 2005; Nalin, Daya, Reid, Levine, and Cisneros, 1979). Moreover *V.cholerae* biofilms that develop on single, chitin-containing plankton may increase to the level of an infectious dose (Colwell, 1996).

The gene coding for ChiP is found in most marine members of the *Vibrionaceae*, emphasizing the general importance of a specific chitoporin in the outer membrane for chitin utilization by transporting extracellular chitooligosaccharides, (GlcNAc)$_n$, that are produced by chitinases. Here we report cloning of *ChiP* gene (VC0972, which encodes *Vc*ChiP), recombinant expression and biochemical and biophysical characterization of chitoporin from pathogenic *V. cholerae*.

The objectives of this research include:

1. Isolation of the genes encoding *E. coli* and *V. cholerae* chitoporins using a PCR based strategy, expression and purification of both porins in *E. coli* BL21 (DE3) Omp8 Rossetta.

2. Expression and purification of *S. marcescens* chitoporin in *E. coli* BL21 (DE3) Omp8 Rossetta using commercially purchased expression vector.

3. Functional characterization of all chitoporins, studying pore forming properties, ion conductance, sugar porin interactions and sugar translocation using planar lipid bilayer experiments.

4. Functional characterization of *E. coli* mutants, with pore-lining residues being mutated.

5. Characterization of chitoporins using *in vitro* transport assay (proteoliposome swelling).

6. Kinetic and thermodynamic characterization of sugar-channel interactions of chitoporin from *E. coli* and *S. marcescens* using single channel analysis in planar lipid bilayer experiments and isothermal titration microcalorimetry (ITC).

7. Theoretical characterization of *E. coli* chitoporin, studying dynamic trapping and escape probabilities of chitosugar molecules from the ChiP channel.

CHAPTER II

MATERIALS AND METHODS

2.1 Chemicals and reagents

2.1.1 Bacterial strains and expression plasmids

Escherichia coli type strain DH5α was used for cloning, subcloning and plasmid preparation. Supercompetent *E. coli* XL1Blue (Stratagene, La Jolla, CA, USA) was the host strain for the production of mutagenized plasmid. *E. coli* BL21 (DE3) Omp8 Rossetta (Δ*lamB   ompF*::Tn*5* Δ*ompA* Δ*ompC*) mutant strain was used as expression host. pET23d (+) vector was used as the expression vector.

2.1.2 Cloning, site-directed mutagenesis, and plasmid purification

Chemicals and reagents used for site-directed mutagenesis were of molecular biology grade. The mutagenic primers used for site-directed mutagenesis were ordered from BioDesign (Bangkok, Thailand). *Pfu* DNA polymerase, *Pfu* polymerase 10x buffer, dNTP mix, *Dpn*I, *Bam*H1, *NCoI* and *Xho*I restriction enzymes, were purchased from Promega (Madison, WI, USA). QuickClean II Plasmid Miniprep Kit (GenScript USA Inc. 860 Centennial Ave, Piscataway, NJ 08854, USA) was used for plasmid extraction. QuickClean II Gel Extraction Kit (GenScript USA Inc. 860 Centennial Ave, Piscataway, NJ 08854, USA) was used for agarose gel extraction. SYBR green I nucleic acid gel stain was bought from Invitrogen (Oregon, USA) and Vc 1 kb DNA ladder was bought from Vivantis (USA).

2.1.3 Protein expression, purification and characterization of chitoporins

Chemicals and reagents used for protein expression, purification and characterization of chitoporins were of analytical grade unless stated otherwise. Octyl-POE (n-octyl-polyoxyethylene) was purchased from ALEXIS Biochemicals, Lausanne, Switzerland. LDAO (lauryldimethylamine oxide) was purchased from Sigma-Aldrich Pte. Ltd., Singapore. Novagen BCA protein assay kit (A Brand of EMD Chemicals Inc., San Diego, CA, USA) was used for BCA assay. Chito-oligosaccharides were products of Seikagaku Corporation (Tokyo, Japan) and Dextra Laboratories Ltd, (United Kingdom). Glacial acetic acid, hydrochloric acid, methanol, n-butanol, potassium hydroxide, sodium chloride, sodium hydroxide, sodium dihydrogen phosphate and disodium hydrogen phosphate were obtained from Carlo ERBA (Rodano, Milano, Italy). Acrylamide, tris (hydroxymethyl) aminomethane, glycerol, ammonium persulfate, 2-mercaptoethanol, bromophenol blue, coomassie blue R250, coomassie blue G250, N, N', N'', N'''-tetramethylethylenediamine (TEMED), bis-N, N''-methylenebisacrylamide, calcium chloride, magnesium chloride, sodium dodecyl sulfate (SDS) were products of Sigma-Aldrich (St. Louis, MO, USA). Glycine was from Vivantis (Oceanside, CA, USA). Ampicillin and kanamycin was product of USB Corporation (Cleaveland, OH, USA). DNase I and RNase A were from Bio basic (Markham, Ontario, Canada). Isopropyl thio-β-D-galactoside (IPTG) was from Merck Millipore (Billerica, MA, USA). MF-Millipore Membrane Filters (0.22 μm and 0.45 μm pore size) were purchased from Millipore Corporation (Beverly, MA, USA). Vivaspin-20 ultrafiltration membrane concentrators (10, 30 and 50 kDa molecular-weight cutoff) were product of Vivascience (Hanover, Germany). Hitrap Q HP pre-packed (1×5 mL) anion exchange column, Hitrap Desalting (1×5 mL) column, HiPrep

16/60 Sephacryl S-200 HR and HiPrep 26/60 Sephacryl S-300 HR columns were products of GE Healthcare (Munich, Germany).

2.2 Analytical programs

An amino acid sequence alignment of chitoporins was constructed using the CLUSTALW algorithm in a GCG package and displayed in the DNASTAR package (DNASTAR, Inc., Madison, WI, USA) and the CLC Main Workbench (CLC Bio, Aarhus, Denmark). The structure-based alignment was further generated using the program ESPript, v3.0. PYMOL (www.pymol.org) was used for 3D visualization of protein. Black lipid membrane data acquisition was performed using Clampex software (Axon Instruments, USA) and PULSE program (HEKA Elektronik, Lambrecht, Germany). MicroCal-PEAQ ITC analysis software was used for ITC data analysis (Malvern Instruments Limited, Grovewood Road, Malvern Worcestershire, WR141XZ, UK).

2.3 Instrumentation

The instruments required for site-directed mutagenesis, protein expression, purification and functional characterization were located at the Biochemistry-Electrochemistry Research Unit Laboratory and the Center for Scientific and Technological Equipment, Suranaree University of Technology, Nakhon Ratchasima, Thailand. These instruments included a Sonopuls Ultrasonic homogenizer with a 6-mm diameter probe, a Mastercycler® personal PCR thermocycler (Eppendorf AG., Hamburg, Germany), a DNA gel apparatus (Pharmacia Biotech, SF, USA), a Jenway UV-VIS spectrophotometer (Bibby Scientific Ltd., Staffordshire, UK), a Gel-Doc 2000 Gel document system (Bio-Rad Laboratories, CA, USA), a Mini-PROTEAN® 3 Cell

(Bio-Rad, Hercules, CA, USA), a shaking incubator (MRC, Holon, Israel), a microcentrifuge Denville 26OD (Denville Scientific, Metuchen, NJ, USA), a high-speed microentrifuge CF16RX II (Hitachi, Tokyo, Japan), an ÄKTA purifier system (Amersham Bioscience, Piscataway, NJ, USA), a Thermomixer comfort (Eppendorf AG, Hamburg, Germany), a BenchmarkPlus microplate spectrophotometer (Bio-rad), T80$^+$ UV/Vis Spectrophotometer (PG instrument Ltd, UK), a lyophilizer (Labconco, freezone plus 12 liter cascade console freeze dry system, Kansas city, MO 64132-2696, USA), two-electrode bilayer headstage (PC-ONE plus PC-ONE-50; Dagan Corp., Minneapolis, MN, USA), an A/D converter (LIH 1600, HEKA Elektronik, Lambrecht, Germany), an Axopatch 200B amplifier (Molecular Devices, Sunnywale, CA, U.S.A.) in the voltage clamp mode, an Axon Digidata 1550 digitizer (Molecular Devices, Sunnywale, CA, U.S.A.), and a Microcal PEAQ-ITC (Malvern Instruments Limited, Grovewood Road, Malvern Worcestershire, WR141XZ, UK).

The instruments used for Black lipid membrane techniques located at Jacobs University, Bremen, Germany were an Axopatch 200B amplifier (Molecular Devices, Sunnywale, CA, U.S.A.) in the voltage clamp mode, an Axon Digidata 1440 digitizer (Molecular Devices, Sunnywale, CA, U.S.A.).

2.4 Methodology

2.4.1 PCR amplification and cloning of ChiPs into pET23d(+)

2.4.1.1 *E. coli* chitoporin (*Ec*ChiP)

The nucleotide sequence encoding chitoporin was identified in the *E. coli* strain K-12 sub-strain MG1655 chromosome in the NCBI database (gi

49175990), and the *ChiP* gene was commercially synthesized using the GenScript gene synthesis service. The ChiP DNA fragment ligated in the pUC57 cloning vector was excised and then transferred into the pET23d(+) expression vector using the *Nco*I and *Xho*I cloning sites so that the *ChiP* gene could be expressed under the control of the T7 promoter. The following digestion conditions were used and after incubated at 37 ºC for 10 min. The enzymes were inactivated by heating at 65 ºC for 10 min.

Table 2.1 Digestion of pUC57/*E.coliChiP* using fast digestion enzyme.

Component	pUC57/*E.coliChiP* (150 ng/µL)	pET23d(+)(50 ng/µL)
10× green buffer	2 µL	2 µL
*Nco*I enzyme	1 µL	1 µL
*Xho*I enzyme	1 µL	1 µL
DNA	10 µL	15 µL
Distilled water	6 µL	1 µL
Total	20 µL	20 µL

        Digested products were checked by 1% agarose gel electrophoresis and digested pET23d and inserted gene were excised from the gel for purification. Then according to the following table ligation components were mixed together and incubated at 16 ºC for around 16 hours.

Table 2.2 Ligation reaction.

Component	1.3(insert:vector)	1.5(insert:vector)	1.8(insert:vector)
10× T4 ligase buffer	1 µL	1 µL	1 µL
(pET23d/42 ng/mL)	1.2 µL	1.2 µL	1.2 µL
Insert (34ng/mL)	1.7 µL	2.8 µL	4.5 µL
T4 ligase enzyme	1 µL	1 µL	1 µL
H$_2$O	5.1 µL	4 µL	2.3 µL
Total	10 µL	10 µL	10 µL

After ligation 10 µL sample was added into 100 µL competent cells (DH5α) on ice for transformation and finally pellets were resuspended and spread on LB agar with ampicillin and incubated at 37 °C overnight. Colony PCR was performed to check transformed colonies after ligation. Briefly, half of the colony was kept in a 20 µL of autoclaved water and boiled for 5 min. Then the mixture was centrifuged at 13000 rpm for 10 min. Supernatant was added as PCR template. The oligonucleotides used for colony detection of the ChiP PCR product were 5-ATACCATGGCCATGCGTACGTTTAGT-3 for the forward primer and 5-AACCTCGAGTCAGAAGATGGTGAA-3 for the reverse primer (sequences underlined indicate the restriction sites).

Table 2.3 Colony PCR reactions for *Ec*ChiP.

Component	Control	Test
Distilled water (dH$_2$O)	9.75 μL	-
5× green flexi buffer	5 μL	5 μL
dNTPs (final concn. 0.2 mM each dNTP)	0.5 μL	0.5 μL
MgCl$_2$ (final concn. 2 mM)	2.0 μL	2.0 μL
DNA template	2.5 μL	12.25 μL
Primer forward (final concn. 1μM)	2.5 μL	2.5 μL
Primer reverse (final concn. 1μM)	2.5 μL	2.5 μL
Go Taq DNA polymerase	0.25 μL	0.25 μL
Total reaction volume	25 μL	25 μL

The following cycling parameters were used and PCR products were kept at 4 °C until used.

Initial Denaturation	95 °C	2 min
Denature	95 °C	30 sec
Annealing	55 °C	30 sec 30 cycles
Extension	72 °C	2 min
Polish extension	72 °C	5 min

Then the PCR products were checked by 1% (w/v) agarose gel electrophoresis. Positive colonies were selected for plasmid extraction and following conditions were used for double digestion of recombinant plasmids.

Table 2.4 Double digestion of recombinant pET23d/*Ec*ChiP plasmids.

Component	Amount
10× green buffer	2 µL
*Nco*I enzyme	1 µL
*Xho*I enzyme	1 µL
Recombinant plasmids	15 µL
Distilled water	1 µL
Total	20 µL

Digestion mixture was incubated at 37 $^{\circ}$C for 10 min. and the enzymes were inactivated by heating at 65 $^{\circ}$C for 10 min. Digested recombinant plasmids were checked by 1% agarose gel electrophoresis. Nucleotide sequences of sense and antisense strands of the PCR fragment were determined by automated sequencing (First BASE Laboratories SdnBhd, Selangor DarulEhsan, Malaysia).

2.4.1.2 *S. marcescens* chitoporin (*Sm*ChiP)

The pET23a(+) expression vector carrying the *Serratia marcescens ChiP* gene was obtained from GenScript USA Inc. 860 Centennial Ave, Piscataway, NJ 08854, USA.

2.4.1.3 *V. cholerae* chitoporin (*Vc*ChiP)

After selecting pET23d(+) as expression vector, zero cutters were checked using NEBcutter V2.0 tool for finding restriction enzyme sites. Then for primer designing, a *BamH*I restriction site was selected for forward primer design and

a *Xho*I restriction site was selected for reverse primer design for *V. cholerae* chitoporin gene. Then using Lasergene primer select, the primer catalog was read to get information regarding length, GC percentage and Tm value. Then a primer hairpin also was checked to have a better primer. Finally, in frame was checked for nucleotide bases in plasmid with original translated DNA using Meg Align. Briefly both original *V. cholerae* ChiP translated DNA and inframe checking translated DNA were saved and enter sequences in MegAlign was used to add both file and finally alignment report was viewed. Primers for *V. cholerae*

5'AT<u>GGATCC</u>ATGGTTGACAAAATGTTT3'   Vc_*BamH*I (Forward)

5'AAC<u>CTCGAG</u>TCACAAGAAACCGTA3'   Vc_*Xho*I (Reverse)

Sequences underlined indicate the restriction sites. For the amplification of *V. cholerae* ChiP gene fragment, PCR was carried using following conditions using *Vc*ChiP DNA fragment ligated in the pUC57 cloning vector (commercially synthesized using the GenScript Gene Synthesis Service) as template.

Table 2.5 The PCR reaction for amplification of *V. cholerae* ChiP gene fragment.

Component	Amount per reaction (μL)
Distilled water (dH$_2$O)	17.75
10× pfu buffer	2.5
dNTPs (final concn. 0.2 mM each dNTP)	0.5
MgCl$_2$ (final concn. 2 mM)	1.0
DNA template (pUC57/*V.cholerae*)	0.5
Primer forward (final concn. 0.5 μM)	1.25
Primer reverse (final concn. 0.5 μM)	1.25
pfu polymerase	0.25
Total reaction volume	25

The following cycling parameters were used and PCR products were kept at 4 ^{o}C until used.

Initial Denaturation	95 ^{o}C	2 min
Denature	95 ^{o}C	30 sec
Annealing	50 ^{o}C	30 sec 30 cycles
Extension	72 ^{o}C	2.5 min
Polish extension	72 ^{o}C	5 min

Then the PCR products were purified by QuickClean II PCR extraction kit (GenScript, USA) and verified by 1% (w/v) agarose gel electrophoresis. The DNA insert of expected size was excised and ligated with pGEM-T cloning vector, according to the Promega manufacturer's instruction. For that, first the PCR gene fragment was subjected to A-trailing and the following conditions were used. Reaction mixture comprised 6 µL of purified PCR DNA fragment, 2 µL of 5× Go taq buffer, 0.8 µL of 25 mM MgCl$_2$, 0.2 µL of 10 mM dATP and 1 µL of Go Taq polymerase. The reaction mixture was incubated at 70 ^{o}C for 30 min.

The amounts of DNA insert used for ligation were calculated as follow:

$$\frac{(\text{ng of vector x kb size of insert})}{\text{kb size of vector}} \times (\text{insert : vector molar ratio}) = \text{ng of insert}$$

Ligation reactions comprised 1 µL of 10 x ligase buffer, 50 ng of pGEM-T easy vector (1 µL), 0.5 µL of PCR products with A-trailing and 1 µL of T4 DNA ligase. 6.5 µL of autoclaved deionized water were added to make up a final

volume of 10 μL. The reaction mixture was incubated at 16 °C for 16 hours. The above ligated mixture was transformed into DH5α and spread on LB plate containing ampicillin, X-gal, IPTG and picked white colonies for plasmid extractions using QuickClean II plasmid miniprep kit (GenScript, USA).

The purified plasmids (pGEM-T-easy/*Vc*ChiP) and pET23d (+) were double digested with the restriction enzymes *Bam*HI and *Xho*I to obtain cohesive-end ligation. Double digestion reactions contained 15 μL of DNA inserts (4 μg), 0.2 μL of BSA (10×), 2 μL of 10x NEB buffer3, 0.5 μL of *Bam*HI and *Xho*I and 1.8 μL of autoclaved deionized water were added to make up a final volume of 20 μL. The digestion mixture was incubated at 37 °C for 3 hours and the enzymes were inactivated by heating at 65 °C for 20 min. Digested products were checked by 1 % agarose gel and digested pET23d (+) and inserted gene band (1056 bp) were excised from gel and purified by the QuickClean II gel extraction kit (GenScript, USA). The purified *Vc*ChiP cDNA was used for ligation with pET23d(+). The reaction mixture consisted of 1 μL of 10 x ligase buffer, 50 ng of pET23d(+) vector (1.4 μL), 2 μL of insert (23 ng/mL) and 0.5 μL of T4 DNA ligase and 5.1 μL of autoclaved deionized water were added to make up a final volume of 10 μL. The reaction mixture was incubated at 16 °C for 16 hours. The above ligated mixture was transformed into DH5α. Colony PCR was performed to check transformed colonies after ligation. Briefly half of the colony was kept in a 20 μL of autoclaved water and boiled for 5 min. Then the mixture was centrifuged at 13000 rpm for 10 min. Supernatant was added as PCR template.

Table 2.6 The PCR reaction for colony PCR of pET23d/*Vc*ChiP.

Component	Control (µL)	Test (µL)
Distilled water (dH$_2$O)	14.25	-
5× green flexi buffer	5	5
dNTPs (final concn. 0.2 mM each)	0.5	0.5
MgCl$_2$ (final concn. 2 mM)	2	2
DNA template	0.5	14.75
Primer forward (final concn. 0.5 µM)	1.25	1.25
Primer reverse (final concn. 0.5 µM)	1.25	1.25
Go Taq DNA polymerase	0.25	0.25
Total reaction volume	25	25

Following cycling parameters were used and PCR products were kept at 4 ºC until used.

Initial Denaturation	95 ºC	2 min
Denature	95 ºC	30 sec
Annealing	55 ºC	30 sec 30 cycles
Extension	72 ºC	2 min
Polish extension	72 ºC	5 min

Then the PCR products were checked by 1% (w/v) agarose gel electrophoresis. Then two colonies were selected and recombinant plasmids were isolated by using the QuickClean II plasmid miniprep kit (GenScript, USA). Nucleotide sequences of sense and antisense strands of the PCR fragment were determined by automated sequencing (First BASE Laboratories SdnBhd, Selangor DarulEhsan, Malaysia).

2.4.2 Expression and purification of recombinant ChiPs in *E. coli* BL21 (DE3) Omp8 Rosetta and peptide mass analysis by MALDI-TOF MS

Expression and purification of the recombinant *Ec*ChiP, *Sm*ChiP and *Vc*ChiP were carried out as below. The expression vector pET23d(+), harboring the full-length *ChiP* gene, was transformed into *E. coli* BL21(DE3) Omp8 Rosetta strain, which lacks major endogenous Omps, including OmpF, OmpC, OmpA, and LamB. The transformed cells were grown at 37 °C in Luria Bertani (LB) broth supplemented with 100 μg.mL^{-1} ampicillin and 25 μg.mL^{-1} kanamycin. During the exponential growth phase (A600=0.6–0.8), ChiP expression was induced with 0.5 mM final concentration of isopropyl thio-D-galactoside (IPTG). After 6 h of additional incubation at 37 °C, the cell pellet was harvested by centrifugation at 2,948×g for 20 min at 4 °C.

For protein purification, the cell pellet was resuspended in lysis buffer (20 mM Tris-HCl, pH 8.0, 2.5 mM MgCl$_2$, 0.1 mM CaCl$_2$) containing 10 μg.mL^{-1} RNase A and 10 μg.mL^{-1} DNase I. Cells were disrupted with a high speed ultrasonic processor (EmulsiFlex-C3, Avestin Europe, Mannheim, Germany) for 10 min. After this, 20% (w/v) SDS solution was added to obtain a final concentration of 2%, and the suspension was further incubated at 50 °C for 60 min with 300 rpm shaking to ensure complete lysis. Cell wall components were removed by centrifugation at 100,000 × g at 4 °C for 1 h. The pellet, containing recombinant ChiP, was extracted twice with 2.5% (v/v) *n*-octylpolyoxyethylene (Alexis Biochemicals, Lausanne, Switzerland) in 20mM phosphate buffer, pH 7.4, and centrifuged again. The supernatant was then dialyzed thoroughly against 20 mM phosphate buffer, pH 7.4, containing 0.2% LDAO (v/v) lauryldimethylamine oxide (Sigma). To obtain protein of high purity, the solubilized ChiP was subjected to ion-exchange chromatography using a Hitrap Q HP prepacked

column (5×1 mL) connected to an ÄKTA Prime plus FPLC system (GE Healthcare).
Bound proteins were eluted with a linear gradient of 0–1 M KCl in 20mM phosphate
buffer, pH 7.4, containing 0.2% LDAO (v/v) lauryldimethylamine oxide. The purity of
the eluted fractions was confirmed by SDS-PAGE. Fractions containing *Ec*ChiP were
pooled and subjected to size exclusion chromatography using a HiPrep 16/60 Sephacryl
S-200 high resolution column. The purity of the *Ec*ChiP fractions obtained after the
size exclusion step was verified by SDS-PAGE before they were pooled, and the protein
concentration of the freshly prepared *Ec*ChiP was estimated using the Novagen BCA
protein assay kit (EMD Chemicals Inc., San Diego, CA).

The purified ChiP was electrophoresed on a 12% polyacrylamide gel, and
the ChiP bands were excised and sent to BGI Tech Solutions (HongKong) Co. Ltd. or
First BASE Laboratories SdnBhd, Selangor DarulEhsan, Malaysia for MALDI-TOF
MS analysis. Briefly, protein in the gel was digested with trypsin and eluted to obtain
a peptide mixture, then MALDI-TOF mass spectrographic analysis was performed, and
the obtained peptide masses were identified using Mascot software v2.3.02.

2.4.3 Molecular weight determination of *Ec*ChiP

Standard proteins and dyes of known molecular weight were resolved on a
HiPrep 26/60 Sephacryl S-300 HR column. Dextran-2000 was used to obtain the void
volume (V_0), whereas DNP-lysine was used to calculate the volume of the stationary
phase (V_i) and the elution volume of each protein sample, denoted as V_e. The elution of
a protein sample was characterized by the distribution coefficient (K_d) derived as in
Equation 2.1,

$K_d = (V_e - V_0)/ V_i$ 　　　　　　　　　　　　　　　　　　　　Equation 2.1

A calibration curve was created by plotting K_d *versus* logarithmic values of the corresponding molecular weights of the standard proteins and was used to estimate the molecular weight of *Ec*ChiP. The standard proteins used in this experiment were ferritin (440 kDa), catalase (250 kDa), aldolase (158 kDa), bovine serum albumin (66 kDa), ovalbumin (43 kDa), carbonic anhydrase (29 kDa) and ribonuclease A (13.7 kDa).

2.4.4 Molecular weight determination of *Sm*ChiP by electrospray mass spectrometry

The *Sm*ChiP protein sample was prepared in low salt buffer without detergent for intact mass analysis by electrospray mass spectrometry. Briefly, *Sm*ChiP in 20 mM phosphate buffer pH 7.4, containing 0.05% (v/v) LDAO was subjected to HiTrap desalting column (5×1 mL) filled with 10 mM phosphate buffer pH 7.4. Then 125 µg of *Sm*ChiP was frozen using liquid nitrogen and dried using a lyophilizer (LABCONCO, Freezone Plus 12 Liter Cascade Console Freeze Dry System, Kansas City, MO 64132-2696,USA) to prepare freeze-dried *Sm*ChiP. Then *Sm*ChiP molecular weight was confirmed by electrospray mass spectrometry analysis as described below (First BASE Laboratories Sdn Bhd, Selangor Darul Ehsan, Malaysia). 50 µg of protein sample was loaded onto a Zorbax 300 SB-C8 RRHD 2.1x50 mm 1.8-micron column (Agilent) and eluted with a 2% to 80% acetonitrile gradient. The column output was subject to positive ion electrospray MS analysis on an Agilent 6540 Q-TOF mass spectrometer (Agilent). Spectra were collected from 600 to 3200 *m/z*. A ten-peptide mixture (Agilent) was used for calibration prior to analysis. The MS spectrum (MS TOF) was deconvoluted with the Bayesian protein reconstruct tool using Analyst QS2.0 software.

2.4.5 Production of anti-*Vc*ChiP polyclonal antibodies and immunoblotting analysis

2.4.5.1 Animal model

An adult (10-week-old) New Zealand female rabbit was purchased from the Animal Caring Center, Mahidol University, Bangkok, Thailand. The rabbit was housed in a standard animal facility under conditions of controlled temperature (25 °C) and photoperiod (a 12:12-hour light/dark schedule), with food and water provided ad libitum.

2.4.5.2 Antibody production

Production of anti-*V.cholerae* ChiP polyclonal antibodies was carried out using the in-gel method. Purified chitoporin that was confirmed by mass spectroscopy (100 µg) was resolved on a 12% SDS-PAGE gel. Following electrophoresis, the protein was stained and after destaining thoroughly, the protein band was excised from the gel. The excised band was homogenized with 200 µL of water, and emulsified with 200 µL of Freund's complete/incomplete adjuvant. The emulsified mixture was injected subcutaneously into a female New Zealand white rabbit to produce anti-chitoporin sera. Multiple injections were performed and bleeds was collected as described below.

Week 0: Collection of pre-immune serum (2 mL) and immunization with 100 µg of *Vc*ChiP mixed with the complete Freund's adjuvant.

Week 2: Immunization with 80 ug of *Vc*ChiP antigen mixed with the incomplete Freund's adjuvant.

Week 3: Immunization with 80 µg of *Vc*ChiP antigen mixed with the incomplete Freund's adjuvant.

Week 4: Collection of blood serum (5 mL).

Week 5: Immunization with 80 µg of *Vc*ChiP antigen mixed with the incomplete Freund's adjuvant and collection of blood serum (5 mL).

Week 6: Collection of blood serum (20 mL).

Blood samples were collected from the central ear artery with a 21-gauge needle and the immunized serum was centrifuged at 2500 rpm at 4 °C for 25 min. Collected supernatant was stored at -40 °C until used. The titer of anti-*V.cholerae* ChiP antibodies in serum was determined by Western blotting.

2.4.5.3 Immunological analysis

For Western blotting experiments, first SDS-PAGE was run, and the isolated protein in SDS-PAGE was transferred into nitrocellulose membrane using a semi- dry blotting system. After transfer, the blotted membrane was blocked with 5% (w/v) skimmed milk in 1× PBS buffer at room temperature for 1 hour. The blocked membrane was stained with the respective primary antibodies. After washing, the membrane was further stained with the secondary antibody, goat anti-rabbit HRP-conjugated IgG. Finally, the membrane was washed 3 times with 0.1% Tween 20 in 1×PBS, followed an additional 2 times with 1×PBS buffer. Then, chemiluminescent substrate was added onto the membrane strip to cover the surface of the membrane. The membrane was incubated at room temperature for 3 min and protein bands were detected by developing with X-ray films at various times.

2.4.6 Sequence analysis and homology modeling of ChiPs

Amino acid sequences of bacterial ChiPs from *E. coli* (P75733), *Salmonella* (Q7CQY4), *Serratia marcescens* (L7ZIP1), *Vibrio cholerae* (Q9KTD0) and *V. harveyi*

(L0RVU0) were aligned and displayed using the program CLC Main Workbench v6.0 or CLUSTALW algorithm in the DNASTAR package and displayed in Genedoc. The secondary structure of the *E. coli* ChiP was constructed by ESPript 3.0 (Robert and Gouet, 2014), according to the 3D structure of *Pseudomonas aeruginosa* OprD (pdb 2odj) and the secondary structure of the *Vc*ChiP was constructed according to the 3D structure of *V. harveyi* (unpublished data). The amino acid sequence of the *Vc*ChiP was submitted to Swiss-Model (http://swissmodel.expasy.org/) for tertiary structure prediction using the crystal structure of folded *Vh*ChiP (unpublished data) as a structural template. The annotated structures were edited and displayed in PyMOL (www.pymol.org).

2.4.7 Mutational design and site-directed mutagenesis of *Ec*ChiP

The mutagenic primers were synthesized commercially by BioDesign Co., Ltd Bangkok, Thailand and the oligonucleotide sequences of primers are listed in Table 2.7. The underlined sequences represent the mutated codon.

Table 2.7 Primers used for site-directed mutagenesis.

Mutation	Primer Sequence
W138A (F)	5'CAAACGCTGTTAGCGCCGCAC<u>GCA</u>AGCTTTATGCCAGGTAC3'
W138A (R)	5'GTACCTGGCATAAAGCT<u>TGC</u>GTGCGGCGCTAACAGCGTTTG3'
Y421A (F)	5'CCAAGCTGGGGCGGTGGT<u>GCA</u>GGCAACATCTTCCAG3'
Y421A (R)	5'CTGGAAGATGTTGCC<u>TGC</u>ACCACCGCCCCAGCTTGG3'

The pET23d(+) expression vector harboring the full length *Ec*ChiP was used as DNA template for point mutations.

Table 2.8 The PCR reaction used for site-directed mutagenesis.

Component	Final concentration	(µL)
Distilled water (dH$_2$O)	-	40
Pfu 10× buffer with MgSO$_4$	1×	5
dNTPs (10 mM)	0.2	1
MgCl$_2$ (final concn. 2 mM)	2	2
DNA template	50 ng	1
Primer forward (10 µM)	125 ng	1
Primer reverse (10 µM)	125 ng	1
Pfu DNA polymerase (Promega 3u/ µL)	3u	1
Total reaction volume	-	50

Following cycling parameters were used and PCR products were kept at 4 ºC until used.

Initial Denaturation	95 ºC	2 min
Denature	95 ºC	30 sec
Annealing	55 ºC	1 min 16 cycles
Extension	72 ºC	11 min
Polish extension	72 ºC	13 min

Then the PCR products were checked by 1% (w/v) agarose gel electrophoresis and non-mutated parental DNA template was digested with D*pn*I. Briefly, 44 µL of PCR product was mixed with 5 µL of 10× Tango buffer with BSA and 1 µL of D*pn*I (stock 10 u/µL) and incubated 1 hr at 37 °C. Then 10 µL of D*pn*I digested solution was transformed into XL1-Blue super competent cells. Then two colonies were selected and recombinant plasmids were isolated by using the QuickClean II plasmid miniprep kit (GenScript, USA). Nucleotide sequences of sense and antisense strands of the PCR fragment were determined by automated sequencing (First BASE Laboratories SdnBhd, Selangor Darul Ehsan, Malaysia) to identify correct mutated plasmids.

2.4.8 Liposome swelling assay

The *Ec*ChiP, *Sm*ChiP and *Vc*ChiP-reconstituted proteoliposomes were prepared as follows. 100 µL of Azolectin (20 mg/mL in chloroform) was added into each tube and lipid was dried using gentle stream of N_2. Then 0.2 mL of diethyl ether was added to dissolve lipid again. Then, a smooth lipid film was formed while tubes were rotated in a 50 °C water bath using a gentle stream of N_2. Finally, lipid film-containing tubes were dried in desiccators with silica gel at overnight. For preparation of proteoliposomes, 200 ng of chitoporins was reconstituted into the liposomes by sonication. Then vesicles were dried using a rotary evaporator in a 50 °C water bath. Finally, the lipid vesicles were dried in a dessicator overnight. Preparations of liposomes were carried out as described above, with the exception that no protein was added into the lipid suspension. Then 600 µL of 17% (w/v) dextran, freshly prepared in 5 mM phosphate buffer, pH 7.4 was added to each tube and resuspended. The tube was incubated for 45 minutes at 30 °C with 100 rpm agitation. Then, the tube was

shaken vigorously 3 times and again incubated 30 minutes at 30 ℃. Multilamellar liposomes were stored in a refrigerator until used.

D- raffinose solutions were prepared in phosphate buffer to obtain different concentrations, such as 40 mM, 50 mM, 60 mM and 70 mM for determination of isotonic solute concentration. This value was then used for the adjustment of the isotonic concentration for other solutes. Then, 25 µL of the proteoliposome suspension was added into 600 µL of sugar solution and changes in absorbance at 500 nm were monitored immediately for 60 s. The apparent absorbance change over the first 60 sec was used to estimate the swelling rate (s^{-1}) using the equation: $\varphi = (1/A_i)dA/dt$, in which φ is the swelling rate, A_i the initial absorbance, and dA/dt the rate of absorbance change during the first 60 s. The swelling rate for each sugar was normalized by setting the rate with the smallest sugar, L-arabinose (Mr 150), to 100%. The values presented are averages from three to five independent determinations. Protein-free liposomes and proteoliposomes without sugars were used as negative controls. The sugars tested were D-glucose (180 Da), D-mannose (180 Da), D-galactose (180 Da), *N*-acetylglucosamine (GlcNAc) (221 Da), D-sucrose (342 Da), D-melezitose (522 Da), GlcNAc$_2$ (424Da), GlcNAc$_3$ (628 Da), GlcNAc$_4$ (830 Da), GlcNAc$_5$ (1034 Da), GlcNAc$_6$ (1237 Da) and maltodextrins.

2.4.9 Black lipid bilayer measurements of pore conductance and chitin oligosaccharide translocation

Black lipid membrane (BLM) reconstitution was carried out in electrolyte containing 1 M KCl in 20 mM HEPES, pH 7.4, at room temperature (25 ℃). Solvent-free bilayer (Montal-Mueller type) formation was performed using 5 mg/mL 1,2-diphytanoyl-sn-glycero-3-phosphatidylcholine (DPhPC; Avanti Polar Lipids,

Alabaster, AL) in n-pentane. First, a 25 µm-thick Teflon film with an aperture of 40–70 µm was sandwiched between the two chambers of a Teflon cuvette and the aperture was pre-painted with a few microliters of 1% (v/v) hexadecane in hexane, then a planar bilayer was formed across the aperture by lowering and raising the liquid level (Montal and Mueller, 1972). Ionic currents were detected using Ag/AgCl electrodes (World Precision Instruments, Sarasota, FL), one connected to the *cis* side of the membrane (ground) and the other to the head-stage of the Axopatch 200B amplifier (Axon Instruments, Foster City, CA). Single channel measurements were performed with an Axopatch 200B amplifier (Axon Instruments, Foster City, CA) in the voltage clamp mode and digitized using the Axon Digidata 1440 digitizer, while data acquisition was performed using Clampex software (Axon Instruments). The traces obtained were filtered at 10 kHz, using a low-pass Bessel filter with a sampling frequency of 50 kHz. Single channel analyses were performed using Clampfit software (all from Molecular Devices, Sunnywale, CA). Single protein channels were reconstituted in lipid bilayers, *Ec*ChiP and *Sm*ChiP always being added to the *cis* side of the cuvette while *Vc*ChiP was added to the either *cis* or *trans* side.

Multiple channel insertions experiments were operated with the the patchclamp amplifier connected to a two-electrode bilayer head-stage (PC-ONE plus PC-ONE-50; Dagan Corp., Minneapolis, MN, USA) together with an A/D converter (LIH 1600, HEKA Elektronik, Lambrecht, Germany) and operated using the software PULSE program (HEKA Elektronik, Lambrecht, Germany).

Conductance values were extracted from the current steps observed at different voltages after the addition of the protein. The ion selectivity of *Ec*ChiP was determined using different salt solutions, such as 1 M lithium chloride (LiCl), 1 M

cesium chloride (CsCl), and 1 M potassium acetate (KAc). To investigate sugar translocation, single ChiP channels were reconstituted in the artificial lipid membrane. To prevent multiple insertions during data acquisition, the protein solution in the chamber was gently diluted after the first insertion by sequential additions of the working electrolyte. Then the fully open ChiP channel was titrated with distinct concentrations of different chitooligosaccharides: chitobiose (GlcNAc$_2$), chitotriose (GlcNAc$_3$), chitotetraose (GlcNAc$_4$), chitopentaose (GlcNAc$_5$) and chitohexaose (GlcNAc$_6$). Each sugar was added to either *cis* or *trans* side of the chamber. Fluctuations of ion flow were observed as a result of sugar diffusion through the reconstituted channel and were usually recorded for 2 min at different transmembrane potentials. To test the substrate specificity of the channel toward chitooligosaccharides, maltodextrin sugars were used as controls. To test the effect of N-acetyl side chains chitosan hexamer and chitohexaose were tested at pH 6 and 8.2.

2.4.9.1 Estimation of binding constant

The equilibrium binding constant K (M^{-1}) was calculated using three different methods. As the first method, single channel analysis was performed in order to determine the rates of association (k_{on}) and dissociation (k_{off}) using clampfit v 10. The on-rate (k_{on}, $\text{M}^{-1} \cdot \text{s}^{-1}$) is given by Equation 2.2.

$$k_{on} = \text{N}/[\text{c}] \hspace{4cm} \text{Equation 2.2}$$

where N is number of blocking events per second and [c] is the molar concentration of chitosugar added during titration.

The off-rate (k_{off}, s^{-1}) was obtained from Equation 2.3, where τ_c is the average residence (dwell) time (s) of the sugar molecule in the channel, which can be calculated from the exponential fit of the dwell-time histogram.

$$k_{off\,=}\,1/\tau_c \qquad\qquad \text{Equation 2.3}$$

The equilibrium binding constant (K) is given by K= k_{on}/k_{off}.

As the second method we plotted binding curves from the reduction of the ion conductance in the presence of increasing concentrations of sugar using Equation 2.4 (Andersen, Cseh, Schulein, and Benz, 1998; Benz and Hancock, 1987; Saravolac, Taylor, Benz, and Hancock, 1991; Suginta, Chumjan, Mahendran, Schulte, et al., 2013).

$$(G_{max} - G_{[c]})/G_{max} = (I_0 - I_{[c]})/I_0 = K \cdot c\,/\,(1 + K \cdot c) \qquad \text{Equation 2.4}$$

Here G_{max} is the average conductance of the fully open EcChiP channel, $G_{[c]}$ is the average conductance at a given concentration of a chitosugar ($[c]$), I_0 is the initial current through the fully open channel in the absence of sugar and $I_{[c]}$ is the current at a particular sugar concentration. Inversion of Equation 2.4 yields Lineweaver-Burk plot, of $[(G_{max} - G_{[c]})/G_{max})]^{-1}$ *versus* $[c]^{-1}$.

As the third method, single channel noise analysis was performed using power density spectra, which were fitted to a Lorentzian function according to Equation 2.5.

$$S_{(f)} = S_{(0)}\,/\,[1 + (2\pi f\tau)^2] \qquad\qquad \text{Equation 2.5}$$

Here f is frequency, $S_{(0)}$ is the low frequency spectral limit and τ is the relaxation time of sugar binding and is a parameter of the fit of the power density

spectrum with Lorentzian power 2 and related to corner frequency according to Equation 2.6.

$$1/\tau = 2\pi f_c = k_{on} \cdot c + k_{off} \qquad \text{Equation 2.6}$$

Here f_c is the corner frequency of the power density spectrum, c is the sugar concentration and k_{on} and k_{off} can be calculated from the slope and intercept, respectively, of a plot of $1/\tau$ vs c.

2.4.10 Ion selectivity measurements

Zero-current membrane potential measurements were performed as described below. The membranes were formed in 0.1 M salt solution. A salt concentration gradient was gradually established across the membrane after porin insertions reached a stationary phase by the addition of 0.1 M salt solution to one side and 3 M salt solution to the other. Ions with a higher permeability through the channel cause charge separation across the membrane. As a result, a zero-current membrane potential is established when the electrochemical equilibrium is reached. Potentials were measured at the diluted side with a high impedance electrometer (Keithley 617) and P_{K+}/P_{Cl-} values were calculated and analyzed using the Goldman-Hodgkin-Katz equation (Benz, Janko, and Lauger, 1979).

$$Vm = RT/F \ln [P_{K+} [K^+]^{cis} + P_{Cl-} [Cl^-]^{trans} / P_{K+} [K^+]^{trans} + P_{Cl-} [Cl^-]^{cis}] \qquad \text{Equation 2.7}$$

Where, Vm is the membrane potential (in Volts); R is the ideal gas constant (8.314 J/K/mol); T is the temperature in Kelvins; F is Faraday's constant; Pion is the permeability for that ion.

2.4.11 Temperature-dependence measurements

High-resolution ion current recordings were carried out with planar lipid bilayers at different temperatures (Chimerel, Movileanu, Pezeshki, Winterhalter, and Kleinekathofer, 2008; Jung, Bayley, and Movileanu, 2006; Kang, Gu, Cheley, and Bayley, 2005; Mahendran, Chimerel, Mach, and Winterhalter, 2009). All temperature-dependent experiments were carried out with a teflon septum of 40-50 µm aperture that yielded stable bilayers with low noise and pre-painted with 2% squalene. The electrolyte used was 1 M KCl, 20 mM HEPES in H_2O or D_2O, pH 7.5. The porins were added to the cis chamber. In order to vary the temperature over a broad range we included a Peltier element for temperature regulation (Dagan) (Chimerel et al., 2008). Insertion was carried out at room temperature and after the first insertion the cuvette was carefully rinsed with buffer to remove remaining porins. Subsequently the temperature was lowered to 5 $^{\circ}$C and the measurement started at 5 $^{\circ}$C. The temperature was increased manually and adjusted to the new temperature such as 10, 15, 22, 30 and 35 $^{\circ}$C. Single-channel measurements were recorded by using the same set up as mentioned in section 2.4.9. Ion current blockage events were measured following the addition of chitosugars to the *cis* or *trans* side of the lipid membrane. The energy barrier of k_{on} and k_{off} rates were analyzed using Arrhenius equation; $k = Ae^{-Ea/(RT)}$ where k is the rate constant, T is the absolute temperature (in Kelvins), A is the pre-exponential factor, E_a is the activation energy for the reaction (in Joules mol^{-1}) and R is the universal gas constant.

2.4.12 Theoretical characterization of chitoporins

Theoretical analysis was performed using single channel ion current traces. Briefly, dynamic trapping and escape probabilities of chitosugar molecules from the ChiP channels, voltage-dependent trapping and de-trapping of charged chitosan, voltage-dependent trapping dynamics for neutral chitohexaose, and comparison of the translocation probability of different chitosugars were analyzed.

2.4.13 Isothermal titration calorimetry (ITC)

ITC measurements were performed using Microcal PEAQ-ITC (Malvern Instruments Limited, Grovewood Road, Malvern Worcestershire, WR141XZ, UK) thermostated at 10 $^{\circ}$C with *Ec*ChiP or *Sm*ChiP prepared in 20 mM phosphate buffer pH 7.4 in the presence of 0.05% LDAO. *Ec*ChiP (300 µL) was in the sample cell at a concentration 100 µM, with 40 µL of 1 mM ligand (prepared in dialysis buffer) in the syringe. *Sm*ChiP was in the sample cell at a concentration 60 µM with 40 µL of 1 mM to 2.5 mM ligand (prepared in dialysis buffer) in the syringe, depending on the affinity towards *Sm*ChiP. In order to ensure proper mixing after each injection, a constant stirring speed of 600 rpm was maintained during the experiments. Control experiments were performed by injecting ligand solution into the buffer, buffer solution into the cell material (protein) and buffer into the buffer in an identical manner and the resulting heat changes were subtracted from the measured heat of binding using a composite control type using manufacturer's Microcal PEAQ-ITC analysis software with a 'one set of sites' fitting model.

2.4.14 Growth of the *E. coli* BL21(DE3) Omp8 Rossetta with *Vc*ChiP on various carbon sources

To test the effects of chitoporin expression on the utilization of various carbon sources, *E. coli* (DE3) Omp8 Rossetta with *Vc*ChiP expression were grown in a microtiter plate containing 200 μL of M9 minimal medium supplemented with various carbon sources, and growth was monitored by microplate reader. The protocol used for this experiment was as follows: *E. coli* cultures were first grown aerobically at 37 $^{\circ}$C in LB medium supplemented with 1% Glucose and ChiP expression was induced by adding IPTG. Then the cells were harvested by centrifugation, and resuspended to the desired starting optical density (OD) in appropriate fresh M9 minimal medium. Inoculated cultures were grown aerobically in an Eppendorf mixer (350 rpm) in microtiter plates containing 200 μL of M9 minimal medium supplemented with various carbon sources. The carbon sources used in this experiment were glucose ($C_6H_{12}O_6$) (0.20% w/v), glycerol ($C_3H_8O_3$) (0.20%), GlcNAc (0.20%), GlcNAc$_2$ (0.20%), GlcNAc$_3$ (0.20%), GlcNAc$_4$ (0.20%) and GlcNAc$_6$ (0.20%). *E.coli* (DE3) Omp8 Rossetta and *E.coli* (DE3) Omp8 Rossetta carrying *Vc*ChiP plasmid (without ChiP expression; no IPTG addition) were used as controls.

CHAPTER III

RESULTS

PART I

BIOCHEMICAL AND BIOPHYSICAL CHARACTERIZATION OF CHITOPORIN FROM *ESCHERICHIA COLI*

3.1 Cloning, sequence analysis and structure prediction

The availability of the nucleotide sequence in the genome of *E. coli* strain K-12 sub-strain MG1655, (complete genome NCBI reference sequence: NC_000913) allowed the putative amino acid sequence of *E. coli* ChiP (so-called *Ec*ChiP) to be identified. The full-length *ChiP* gene corresponding to *Ec*ChiP was synthesized commercially, for which the target gene was ligated into the *Nco*I and *Xho*I cloning sites of the pUC57 cloning vector (GenScript, Piscataway Township, NJ, USA). The nucleotide sequence of the *ChiP* gene, comprising 1,407 bps, was translated to a putative polypeptide of 468 amino acids, including the 26-amino acid signal sequence. The theoretical mass of the full-length *Ec*ChiP was 52,780 Da, with a predicted isoelectric point 4.70. The pUC57 cloning vector carrying the *EcChiP* gene was digested with *Nco*I and *Xho*I and checked by 1% agarose gel electrophoresis (Figure 3.1A). *EcChiP* gene showed a band around 1400 bp. Double-digested pET23d and

*EcChi*P gene were excised from the gel for purification. Purified product was ligated to get recombinant plasmids. As expected, transformation of ligated product into DH5α resulted in many colonies on the plate and selected colonies showed positive results as shown in below in Figure 3.1B. Figure 3.1C shows the double digestion of recombinant pET23d/*Ec*ChiP.
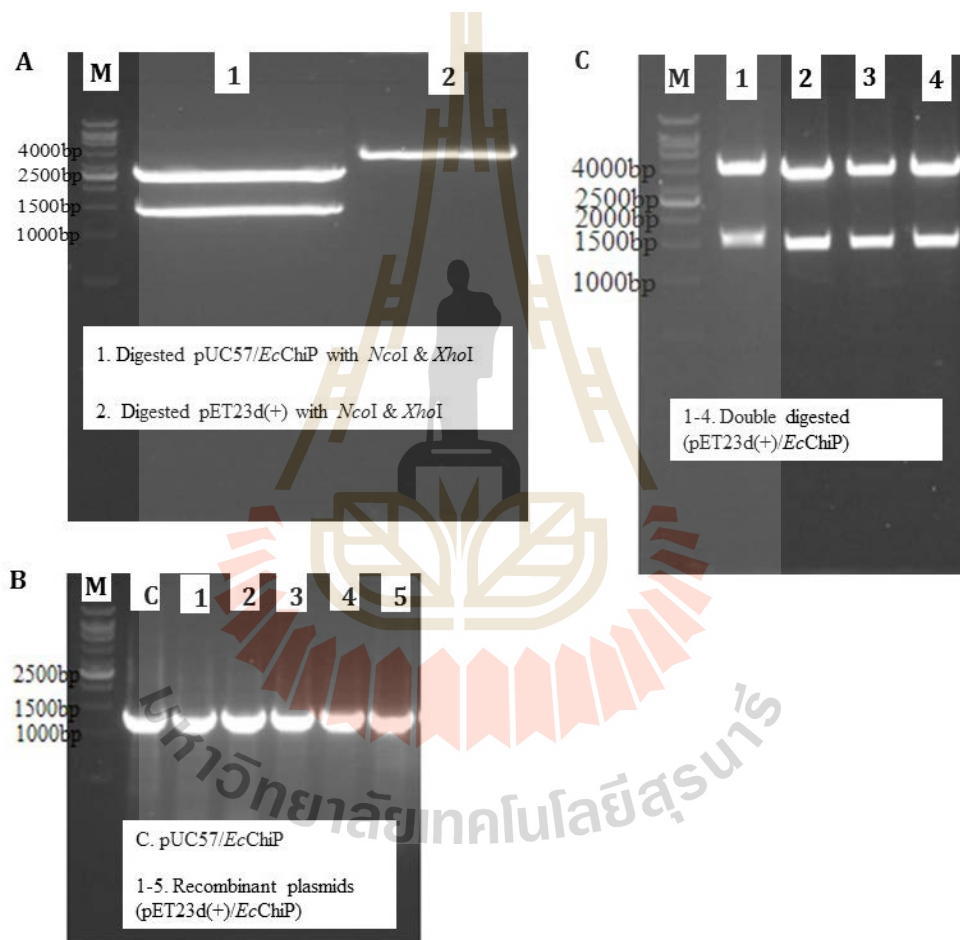
Figure 3.1 Agarose gel electrophoresis for *Ec*ChiP cloning. (A) Double digestion of pUC57/*Ec*ChiP and pET23d (+) expression vector by *Nco*I and *Xho*I restriction enzymes. (B) Colony PCR products using recombinant pET23d (+)/*Ec*ChiP as template. pUC57/*Ec*ChiP used as positive control. (C) Double digestion of pET23d (+) /*Ec*ChiP by *Nco*I and *Xho*I restriction enzymes.

Amino acid sequence comparison of *Ec*ChiP with other bacterial ChiPs in the SwissProt/UniProtKB database is presented in Figure 3.2. The putative sequence of *Ec*ChiP showed highest sequence identity to *S. typhimurium* ChiP (Q7CQY4) (90%) (Figueroa-Bossi et al., 2009), followed by *Serratia marcescens* ChiP (L7ZIP1) (70%) (Takanao et al., 2014). Our sequence analysis indicated that *Ec*ChiP had exceptionally low identity with the ChiP sequences from marine *Vibrios*, such as *V. cholerae* ChiP (Q9KTD0) (Meibom et al., 2004), *V. furnissii* ChiP (Q9KK91) (Keyhani, Li et al., 2000) and *V. harveyi* ChiP (L0RVU0) (Suginta, Chumjan, Mahendran, Schulte et al., 2013), with 13%, 14% and 12% identity, respectively.

Unlike marine *Vibrios*, *E. coli* and *S. typhimurium* are non-chitinolytic bacteria that possess ChiP homologs belonging to the OprD family of porins. The *Ec*ChiP amino acid sequence was submitted to the Swiss-model database for homology structure prediction, and the crystal structure of *Pseudomonas aeruginosa* OprD (pdb 2odj) (Biswas, Mohammad, Patel, Movileanu, and van den Berg, 2007) was computationally selected as a structure template.
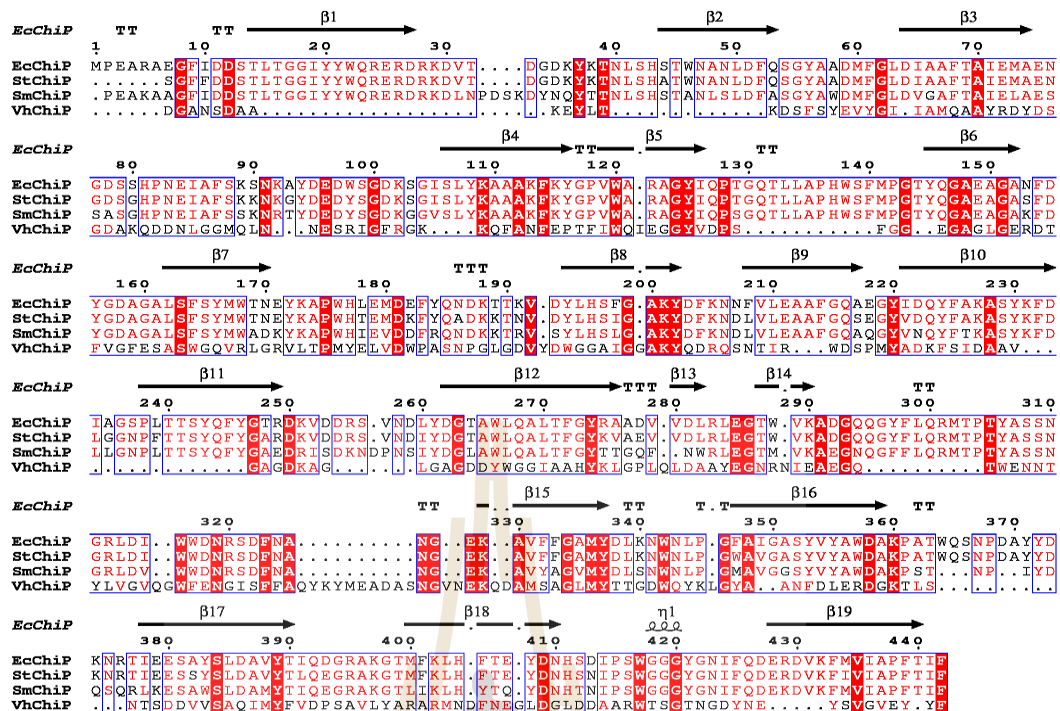
Figure 3.2 Sequence alignment of *Ec*ChiP, showing the secondary structural elements of *Ec*ChiP. The amino acid sequences of *S. typhimurium* ChiP (*St*ChiP), *S. marcescens* ChiP (*Sm*ChiP), and *V. harveyi* ChiP (*Vh*ChiP), without signal peptides, were aligned using CLC Main Workbench 6. The secondary structure of *E. coli* was constructed by ESPript 3.0 according to the structure of *P. aeruginosa* OprD (pdb 2odj). β-strands are marked with black arrows, and α-helices with black spirals. Absolutely conserved residues are highlighted in red (Soysa and Suginta, 2016).

Figure 3.3A shows a side view of the predicted β-barrel structure of *Ec*ChiP, atypically consisting of 19-strands connected by 9 external loops and 9 periplasmic turns. Previous reports of the crystal structures of the maltoporin (LamB) (Wang, Dutzler, Rizkallah, Rosenbusch, and Schirmer, 1997) and sucrose-specific porin ScrY (Forst, Welte, Wacker, and Diederichs, 1998) suggested that aromatic residues are

important for sugar transport. Amino acid residues located within the pore interior, such as W138, D314, R320 and Y421, are predicted to be crucial for sugar transport (residues marked as sticks in Figure 3.3B top view). The predicted *trans*-membrane topology for *Ec*ChiP is shown in Figure 3.3C. The longest loop (L3, Gly124 to Tyr145) found inside the channel lumen presumably acts as the pore-confining loop that controls ion flow.
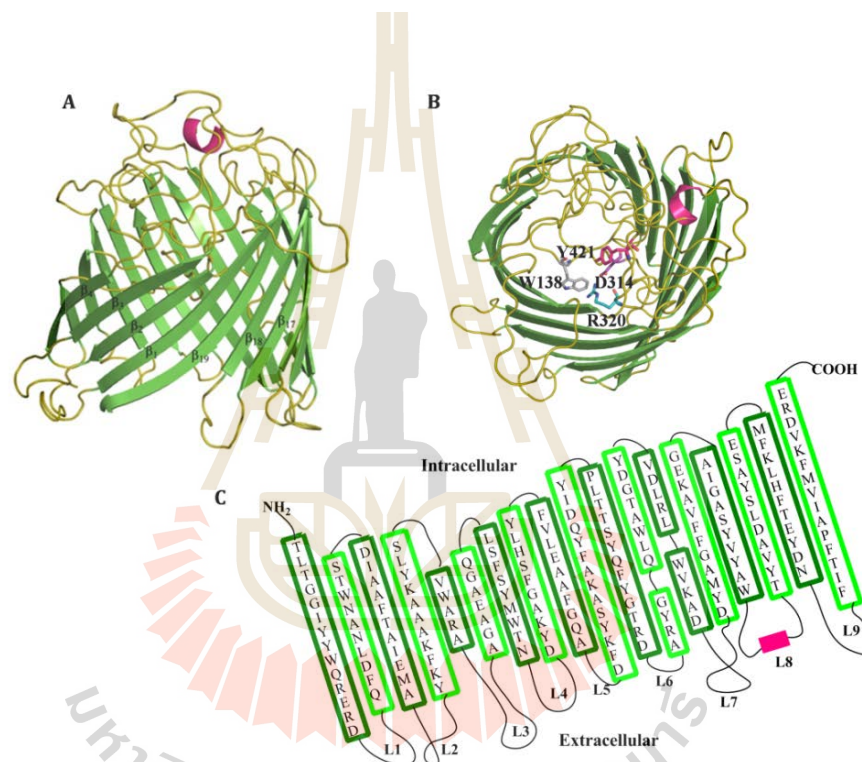
Figure 3.3 The Swiss-model structure of *E. coli* chitoporin. (A) Cartoon of *Ec*ChiP viewed from the side. (B) Top view of the *Ec*ChiP modeled structure. Important residues in the pore that may be involved in sugar transport, W138, D314, R320 and Y421, are presented in gray, purple, teal and pink respectively as stick structures. The X-ray structure of OprD from *Pseudomonas aeruginosa* (pdb 2odj) was selected as the structure template for *E. coli* chitoporins. Green: β-strands; olive: loops and turns; hot pink: α-helices. (C) The predicted transmembrane topology of *Ec*ChiP (Soysa and Suginta, 2016).

3.2 Recombinant expression, purification and mass identification

The plasmid pET23d (+) harboring the *ChiP* gene fragment was designed to express recombinant *Ec*ChiP, with the 26-amino acid N-terminal signal sequence aiding channel insertion into the cell wall of the *E. coli* BL21(DE3) Omp8 Rosetta host. When the transformed cells were grown to exponential phase, expression of the recombinant *Ec*ChiP was induced with 0.5 mM IPTG for a period of 6h at 37 °C. Figure 3.4A shows SDS-PAGE analysis of whole cell lysates of the Omp-deficient *E. coli* expressing *Ec*ChiP. When compared with cells transformed with the empty vector (lane 1: no induction, and lane 2: IPTG induction), uninduced cells transformed with the pET23d (+)/*ChiP* vector did not produce the heterologous protein (lane3), while a prominent band of the expected size (50 kDa) appeared on induction with IPTG (lane 4). These results confirm successful production of *Ec*ChiP in the selected host cells.

For purification of *Ec*ChiP, the induced cells were subjected to a two-step detergent extraction. In the first step using 2% (w/v) SDS, most of *Ec*ChiP remained in the insoluble fraction and in the second step *Ec*ChiP was solubilized with 2.5% (v/v) octyl-POE. The protein purity observed after these steps was above 90%. *Ec*ChiP was further subjected to ion-exchange chromatography using a Hitrap Q HP pre-packed column. Figure 3.4B shows the chromatographic profile, indicating that *Ec*ChiP fractions were eluted in two peaks (P1 and P2) by an applied gradient of 0-1M KCl. SDS-PAGE analysis shows that the *Ec*ChiP fractions in the first peak (P1) were highly purified (Figure 3.4B, inset), while the fractions in P2, contained some contamination from other proteins (not shown); P2 may therefore contain *Ec*ChiP bound to other proteins. Peaks P1 and P2 were therefore applied separately onto a HiPrep 16/60 Sephacryl S-200 high-resolution exclusion chromatography column for final

purification. The highly purified *Ec*ChiP obtained after gel filtration chromatography was subjected to in-gel digestion for MALDI-TOF MS analysis. A MASCOT database search identified 16 peptides (designated P1-P16) that belonged to the internal sequences of the putative chitoporin from *E. coli* (gi|251784171|ref|YP_002998475.1|) (Figure 3.4C, sequences in cyan). The sequence coverage for the identified peptides was 50%. These results confirmed that the 50-kDa protein expressed in *E. coli* BL21(DE3) Omp8 Rosetta host was *Ec*ChiP.
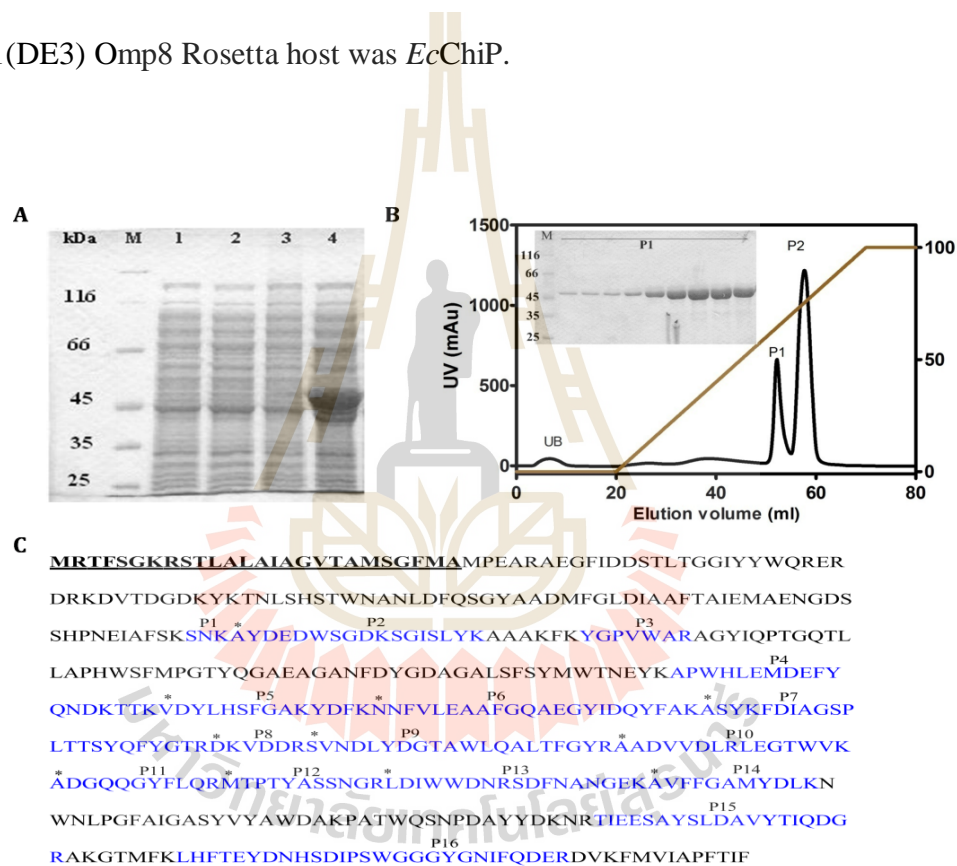
Figure 3.4 Recombinant expression, purification and mass identification. (A) SDS-PAGE analysis of whole-cell lysate with and without IPTG induction for *E. coli* carrying pET23d (+) and pET23d (+)/*Ec*ChiP. Lane M, marker proteins; lane 1, *E. coli* Omp8 Rosetta carrying pET23d (+) without IPTG induction; lane 2, *E. coli* Omp8 Rosetta carrying pET23d(+) with IPTG induction; lane 3, *E. coli* Omp8 Rosetta carrying pET23d(+)/*Ec*ChiP without IPTG induction; lane 4, *E. coli* Omp8 Rosetta

carrying pET23d(+)/*Ec*ChiP with IPTG induction. (B) Chromatographic profile of *Ec*ChiP purification with a Hitrap Q HP prepacked column (5×1 mL) connected to an ÄKTA Prime plus FPLC system. Bound proteins were eluted with a linear gradient of 0–1 M KCl in 20 mM phosphate buffer, pH 7.4, containing 0.2% (v/v) LDAO. SDS-PAGE analysis of bound fraction P1 is shown in an inset. (C) Identification of tryptic digests of the expressed proteins by MALDI-TOF MS. The sixteen identified peptides (P1-P16) that gave a complete match with putative peptides of *Ec*ChiP are shown in cyan. The N-terminal ends of peptides P2, P5, P6, P7, P8, P9, P10, P11, P12, P13 and P14 are indicated by asterisks. The 26 amino-acid signal peptide is in bold and underlined (Soysa and Suginta, 2016).

3.3 Determination of the native state of the *Ec*ChiP channel

All chitoporins identified in marine *Vibrios* are trimeric channels (Suginta, Chumjan, Mahendran, Schulte et al., 2013). In the next series of experiments, we investigated the native state of *Ec*ChiP. Unlike *V. harveyi* ChiP (*Vh*ChiP) (Suginta, Chumjan, Mahendran, Schulte et al., 2013), *Ec*ChiP did not migrate on SDS-PAGE to the position corresponding to a trimer under non-denaturing conditions. Figure 3.5A is an SDS-PAGE analysis showing the migrations of *Vh*ChiP (lane 1; unheated, and lane 2; heated) and *Ec*ChiP (lane 3, unheated, and lane 4; heated). Intact *Vh*ChiP migrated with an apparent molecular mass close to 100 kDa, indicating a trimer (lane 1), but the dissociated subunits migrated close to 40 kDa (lane 2). Different results were observed with the *E. coli* sample: native *Ec*ChiP migrated with an apparent molecular mass of about 35 kDa (lane 3), indicating a monomeric, folded structure according to literature review (Conlan, Zhang, Cheley, and Bayley, 2000; van den Berg, 2012). After boiling,

the apparent molecular mass increased to nearly 50 kDa, presumably due to unfolding of the protein (lane 4). Gel filtration chromatography was used to confirm the monomeric structure of native *Ec*ChiP. Figure 3.4B shows a chromatographic profile of the protein standards eluted from a HiPrep 26/60 Sephacryl S-300 pre-packed column. *Ec*ChiP was eluted at a position between ovalbumin (43 kDa) and bovine serum albumin (66 kDa) (Figure 3.5B, black dotted line), and its apparent molecular mass estimated from its distribution coefficient (K_d) was ca. 60 kDa (Figure 3.5C), consistent with a monomeric molecule. The slightly greater molecular weight than the expected size of *Ec*ChiP (50 kDa) may be added by the MW the detergent LDAO (17 kDa) (Strop and Brunger, 2005) that was included to maintain the protein solubility in form of the detergent-protein complex.
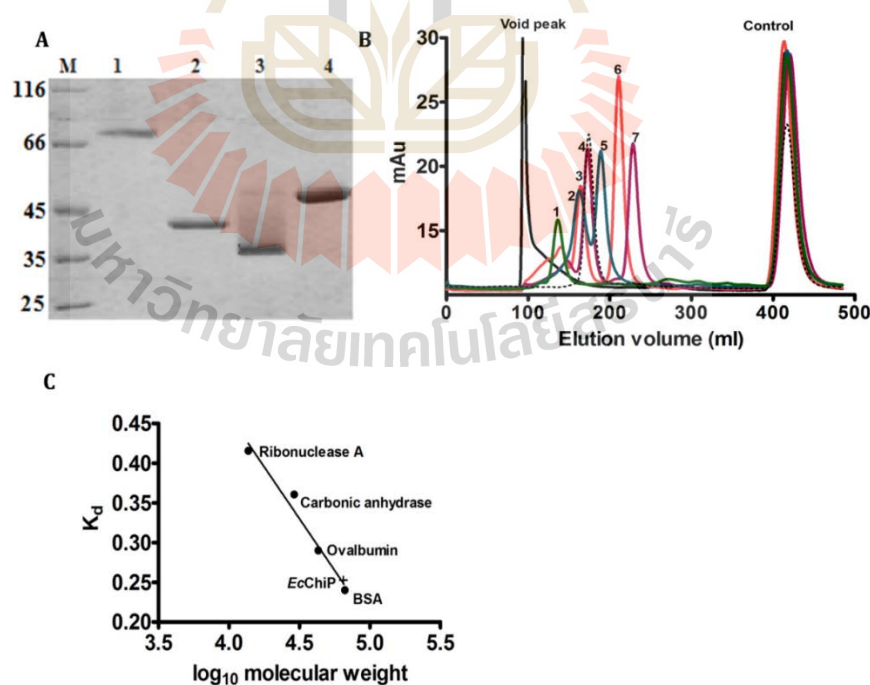
Figure 3.5 SDS-PAGE analysis of *Ec*ChiP and molecular weight determination. (A) SDS-PAGE analysis of purified *Ec*ChiP, with *Vh*ChiP for comparison. Lane 1, *Vh*ChiP

(unheated); 2, *Vh*ChiP (heated); 3, *Ec*ChiP (unheated); 4, *Ec*ChiP (heated). (B) Size exclusion chromatogram of standard proteins with *Ec*ChiP. Standards were run separately, together with DNP-lysine (control). Protein standards: 1, ferritin (440 kDa); 2, catalase (250 kDa); 3, aldolase (158 kDa); 4, bovine serum albumin (66 kDa); 5, ovalbumin (43 kDa); 6, carbonic anhydrase (29 kDa); 7, ribonuclease A (13.7 kDa). Void peak: elution peak of blue dextran 2000. Control: elution peak for DNP-lysine. *Ec*ChiP was eluted (black dotted line) as a monomer within the 43-66 kDa range. (C) Calibration curve to determine the K_d value of *Ec*ChiP (Soysa and Suginta, 2016).

3.4 Channel-forming properties of *Ec*ChiP

To examine the pore-forming properties of the isolated channel, *Ec*ChiP was reconstituted into artificial planar phospholipid membranes. An abrupt increase in ion current in response to an externally applied potential was observed soon after addition of the protein and the induced current remained steady throughout the subsequent period of data acquisition (usually 2 min). The BLM results clearly demonstrated that *Ec*ChiP was a channel-forming protein. Figure 3.6A is a representative ion current recording of around 50 pA at +100 mV, signifying a characteristic single *Ec*ChiP insertion under a given condition (<2 ng.mL^{-1} *Ec*ChiP added on the *cis* side of the chamber filled with 1M KCl, pH 7.5). This channel insertion behavior was observed consistently throughout our study. In Figure 3.6B, we show typical ion current traces obtained from multiple insertions in the presence of a high added concentration of *Ec*ChiP (>10ng.mL^{-1}) in the same electrolyte solution. Figure 3.6B inset shows the Gaussian distribution of the pore conductance, derived from 365 channel insertions. The value was fitted with a mean conductance of 0.54±0.04nS, which corresponded

well with the value obtained from the slope of the I-V curve shown in Figure 3.6C (inset). For individual *Ec*ChiP, currents were recorded at potentials from -100 to +100 mV using 25 mV steps, as shown in Figure 3.6C. The plot of current as a function of transmembrane voltage was constructed from 17 independent single channel insertions. The conductance of the pore (slope of the curve) was constant over the entire voltage range scanned, yielding the conductance value of 0.55±0.01nS. *Ec*ChiP was shown to be a relatively stable channel at both negative and positive potentials with a threshold for channel gating observed at approx. -200 mV and +200 mV. An example of channel gating at +200 mV is shown in Figure 3.6D.
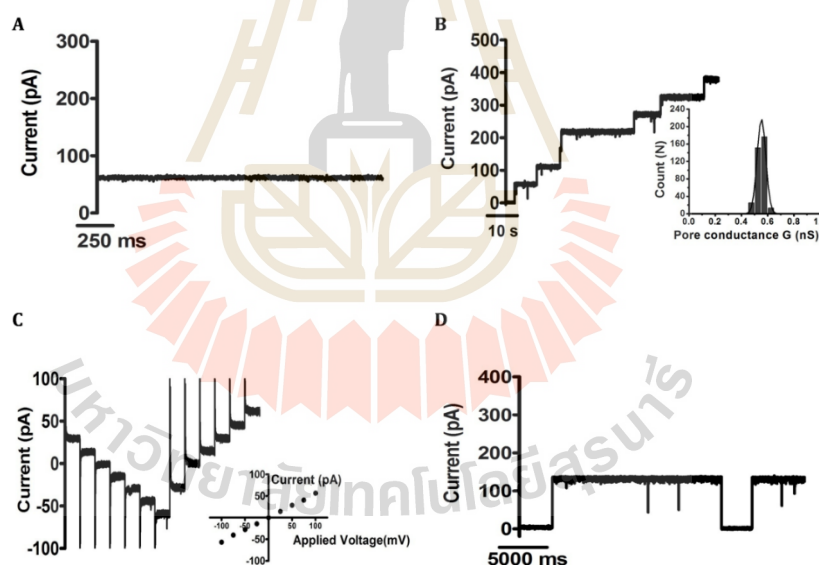
Figure 3.6 Single-channel recordings of *Ec*ChiP in artificial lipid membranes. Lipid bilayers were formed across a 70 µM aperture by the lowering and raising technique, using 5 mg.mL^{-1} 1,2-diphytanoyl-sn-glycero-3-phosphatidylcholine (DPhPC) in n-pentane and 1M KCl in 20 mM HEPES, pH 7.5 on bothsides of the chamber. The protein was added to the *cis* side. (A) Fully open *Ec*ChiP current trace at +100 mV. (B) Multiple channel insertions; Inset: histogram of the conductance steps observed with

1,2-diphytanoyl-sn-glycero-3-phosphatidylcholine (DPhPC) artificial bilayer for 365 independent channel insertions. The black line represents a single Gaussian fit. (C) Stepwise ramping of the potential for single insertion, Inset: I-V plot for a single *Ec*ChiP single channel. The average current values were obtained by varying potential from -100 mV to +100 mV using 25 mV steps for 17 independent channel insertions. (D) Gating behavior of *Ec*ChiP at high potential (+200 mV) (Soysa and Suginta, 2016).

Then single channel measurements were performed using a high resolution Axon setup following reconstitution of single *Ec*ChiP in black lipid membranes (BLM), and all data sets were recorded and analyzed at both *cis* and *tran*s sides and at different applied potentials from ±25 to ±100 mV. Figure 3.7 shows that monomeric *Ec*ChiP could insert stably into the artificial phospholipid bilayers (DPhPC; 1,2-diphytanoyl-sn-glycero-3-phosphatidylcholine), producing ion flow in 1M KCl with an average current of 49±1.0 pA at +100 mV (Figure 3.7A) and 44±2.0 pA at -100 mV (Figure 3.7B). The asymmetry in conductance values was consistently observed over a wide range of applied potentials, from -200 mV to +200 mV. Figure 3.7C, a plot of the average conductance (G) *vs.* applied potential, shows that the channel conductance increased linearly with increasing voltage. The G values are clearly greater at positive potentials than at negative potentials, and such biased responses to opposite polarity were also observed for LamB (Bezrukov, Kullman, and Winterhalter, 2000; Kullman et al., 2002) and CymA (Bhamidimarri, Prajapati, van den Berg, Winterhalter, and Kleinekathofer, 2016). The asymmetric ion conductivity of the *Ec*ChiP channel allowed us to probe the orientation of an individual channel residing in the lipid bilayer

membrane. This intrinsic channel property becomes crucial when the in-depth kinetic parameters, including off/on rate constants, are extracted from sugar titrations and the values must be consistently derived from inserted channels with the same orientation. In our BLM experiments, we worked on a large population of *Ec*ChiP channels that exhibited the larger conductance at positive potentials, discarding a few rare insertions with lower conductance.
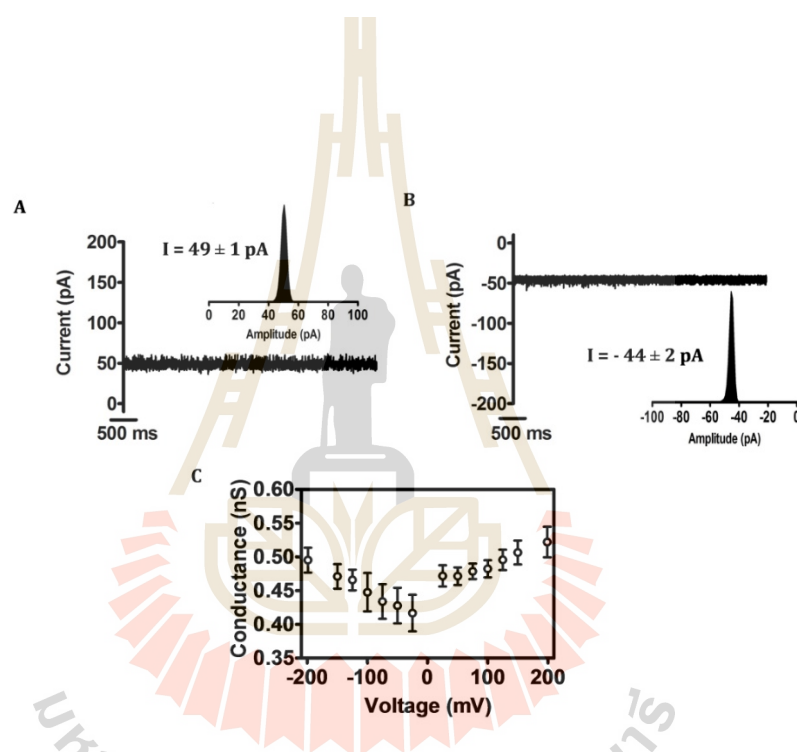
Figure 3.7 Asymmetric behavior of *Ec*ChiP. Lipid bilayers were formed across a 70 µm aperture by the lowering and raising technique, using 5 mg.mL^{-1} 1,2-diphytanoyl-sn-glycero-3-phosphatidylcholine (DPhPC) in n-pentane and 1M KCl in 20 mM HEPES, pH 7.5 on both sides of the chamber. The protein was added to the *cis* side. (A) Fully open *Ec*ChiP current trace at +100 mV. Inset: histogram of the fully open channel at +100 mV (B) Fully open *Ec*ChiP current trace at -100 mV. Inset: histogram of the fully open channel at -100 mV (C) Conductance as a function of the applied potential.

Single-channel experiments were also performed with salts other than KCl, to obtain information on the ion-selectivity of *Ec*ChiP; the results are summarized in Table 3.1. Replacement of Cl$^-$ by CH$_3$COO$^-$, a less mobile anion, slightly reduced the single channel conductance from 0.5 to 0.4 nS. However, replacement of K$^+$ by the less mobile cation Li$^+$ resulted in a much larger decrease, from 0.5 nS to 0.25 nS, indicating a preference of *Ec*ChiP for cations (Table 3.1). Although Li$^+$ and CH$_3$COO$^-$ and K$^+$ and Cl$^-$ have similar aqueous mobilities (Benz et al., 1987; Saravolac et al., 1991), the conductance of *Ec*ChiP channel was lower in LiCl than in KAc. This result supports the conclusion that the *Ec*ChiP channel was cation-selective.

Table 3.1 Average single-channel conductance, G, of *Ec*ChiP in different salt solutions. The pH of the aqueous salt solutions was around 7.5. G was calculated from the single channel recording by averaging single events as indicated within brackets. The applied membrane potential was +100 mV.

Aqueous salt solution	Single channel conductance (G, nS)
1M KCl	0.54 ± 0.04 (n=365)*
1M KAc	0.40 ± 0.03 (n=71)
1M CsCl	0.60 ± 0.04 (n=87)
1M LiCl	0.25 ± 0.02 (n=65)

*n represents the number of BLM measurements in which the data were acquired in this experiment.

3.5 Investigation of chitooligosaccharide interactions with *Ec*ChiP

In these experiments, we carried out time-resolved measurements with BLM in the presence of various chitooligosaccharides (GlcNAc$_n$; n=1-6), to examine the sugar specificity of *Ec*ChiP. Figure 3.8 is an I(t) trace, showing current perturbation induced by the addition of a fixed concentration (20 μM) of different chitooligosaccharides. The frequency of blocking events varied, depending on the chain-length and type of sugar. Figure 3.8A is a control I(t) trace, showing the fully-open state of the monomeric *Ec*ChiP channel in the absence of sugar. When the monosaccharide GlcNAc was added to the working electrolyte, on either the *cis* or the *trans* side of the bilayer, no disturbance of the I(t) trace was observed, because GlcNAc (mol. wt.=221 Da) is smaller than the size exclusion limit of the channel lumen (predicted to be approx. 300 Da). Hence, this sugar can permeate the channel without obstructing the ion flow. When chitobiose (GlcNAc$_2$) was added, occasional current fluctuations were seen, indicating transient blockage of the channel by the sugar, but such events were very brief (Figure 3.8C). Rare, short-lived blocking events suggested that most of sugar molecules could diffuse freely through the channel, but that these molecules occasionally formed weak interactions during passage. Progressive blocking events became clearly visible with the higher molecular weight sugars, which were retarded while traversing the channel lumen. These were seen with chitotriose (GlcNAc$_3$) (Figure 3.8D), chitotetraose (GlcNAc$_4$) (Figure 3.8E), chitopentaose (GlcNAc$_5$) (Figure 3.8F) and chitohexaose (GlcNAc$_6$) (Figure 3.8G). In particular, extensive blockage of ion flow was observed on addition of chitohexaose, indicating that this long-chain sugar entered the channel and stayed for a significant time before exiting. Such events occur when the sugar molecule forms a large network of interactions with the channel interior. Table 3.2

shows that both on- and off-rate constants are greatly dependent on the sugar length. Such results were consistently obtained under all the conditions investigated, and suggest sugar translocation by facilitated diffusion. Under the most favourable conditions, with sugar addition on *cis* side and data recording at +100 mV (hereafter referred as *cis*/+100 mV), the average time for sugar molecules residing inside the *Ec*ChiP channel (defined as the residence time, τ_c) increased from 0.4±0.2 ms for chitotetraose to 3.5±0.9 ms for chitopentaose and 12.0±0.7 ms for chitohexaose, yielding a 10-fold decrease in the off-rate constant (k_{off}, $1/\tau_c$) from chitotetraose (2,550 s^{-1}) to chitopentaose (250 s^{-1}) and a 32-fold decrease to chitohexaose (80 s^{-1}), respectively. The on-rate constant (k_{on}) for the same series of sugars increased instead from $(1.0\pm0.3)\times10^6$ to $(2\pm1.5)\times10^6$ and $(4\pm2)\times10^6$ $M^{-1}s^{-1}$. Hence, the correlated binding constant (K, M^{-1}) was estimated to increase in sequence with increasing length of sugar chain from chitotetraose (400 M^{-1}) to chitopentaose (8,000 M^{-1}) and chitohexaose (50,000 M^{-1}), reflecting an increased affinity in sugar-channel interactions. However, in a control with the glucose analog maltohexaose at a concentration of 200 μM, 20-fold higher than that of chitohexaose (10 μM), there was no significant disturbance of the I(t) trace derived from the *Ec*ChiP channel (Figure 3.8H). We also investigated the interaction of *Ec*ChiP with maltopentaose and observed no current blockage (data not shown). Comparable results were observed, with reduced effects on conductance, when BLM data were acquired with a *trans*/-100 mV setting (see Supplementary Figure 1).
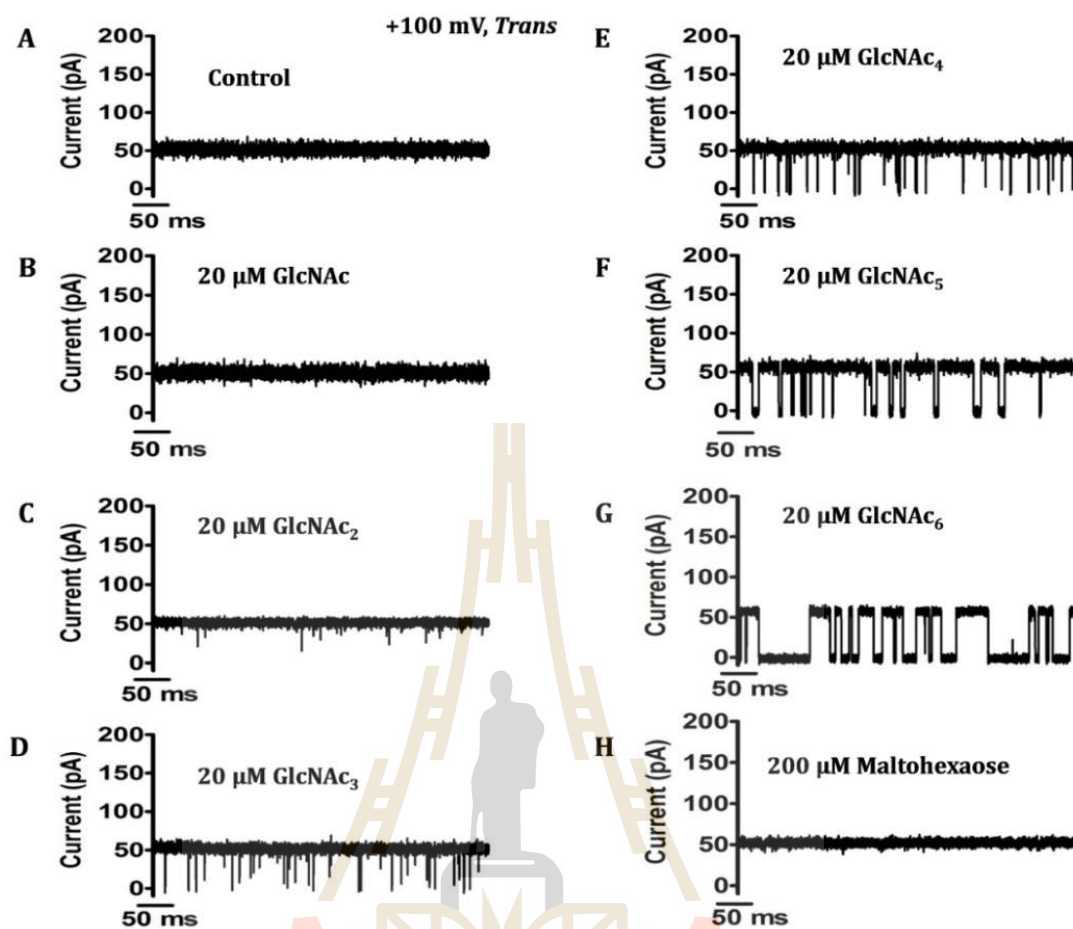
Figure 3.8 Ion current recordings of single *Ec*ChiP channels in solutions of different chitooligosaccharides of various chain lengths. Ion current fluctuations were monitored for 120 s at applied potentials of +/-100 mV with sugars on either the *cis* or the *trans* side. Here, only current traces for 500 ms at +100 mV, *trans* are presented. (A) Fully open state of *Ec*ChiP before sugar addition. Then (B) *N*-acetylglucosamine (GlcNAc), (C) chitobiose (GlcNAc$_2$), (D) chitotriose (GlcNAc$_3$), (E) chitotetraose (GlcNAc$_4$), (F) chitopentaose (GlcNAc$_5$) or (G) chitohexaose (GlcNAc$_6$) were added on the *trans* side of the chamber, to a final concentration of 20 μM. (H) Control recording with maltohexaose at a final concentration of 200 μM.

3.6 Kinetic assessment of sugar-channel interactions in planar lipid membranes

To obtain further information on the kinetics of sugar-channel interactions, we titrated the membrane-inserted EcChiP channel with two-fold increments in the concentration of chitohexaose (GlcNAc$_6$). Figure 3.9A-E (left panel) are I(t) recordings, and show frequent current fluctuations upon the cumulative addition of chitohexaose under $trans$/+100 mV conditions. Histogram analyses indicate progressive decreases in the ratio of the open-to-closed state of the channel, correlating with the increase of sugar concentration from 2.5 to 40 μM (Figure 3.9A-E, right panel).

Subsequent sugar titration experiments allowed us to obtain the kinetic details of sugar-channel interactions. The on-rate constant (k_{on}) (Figure 3.9G), represented by the number of sugar blocking events per unit time (Figure 3.9F), was estimated and expressed by equation 2.2 (section 2.4.9.1), whereas the off-rate constant (k_{off}), represented by inverse value of the residence time ($1/\tau_c$), was expressed by equation 2.3 (section 2.4.9.1). We spected to see linear increment of on-rate in response to increasing concentrations of chitohexaose. However, our experimental data showed deviation of linerarity in the presense of high concentration of sugar. We may speculate that this might be caused by long term blockage of the channel at high concentration. Therefore Figure 3.9G shows the exponential decay characteristic of the k_{on} values in response to increasing concentrations of chitohexaose. On the other hand, the k_{off} values were relatively constant and independent of chitohexaose concentration (Figure 3.9H).
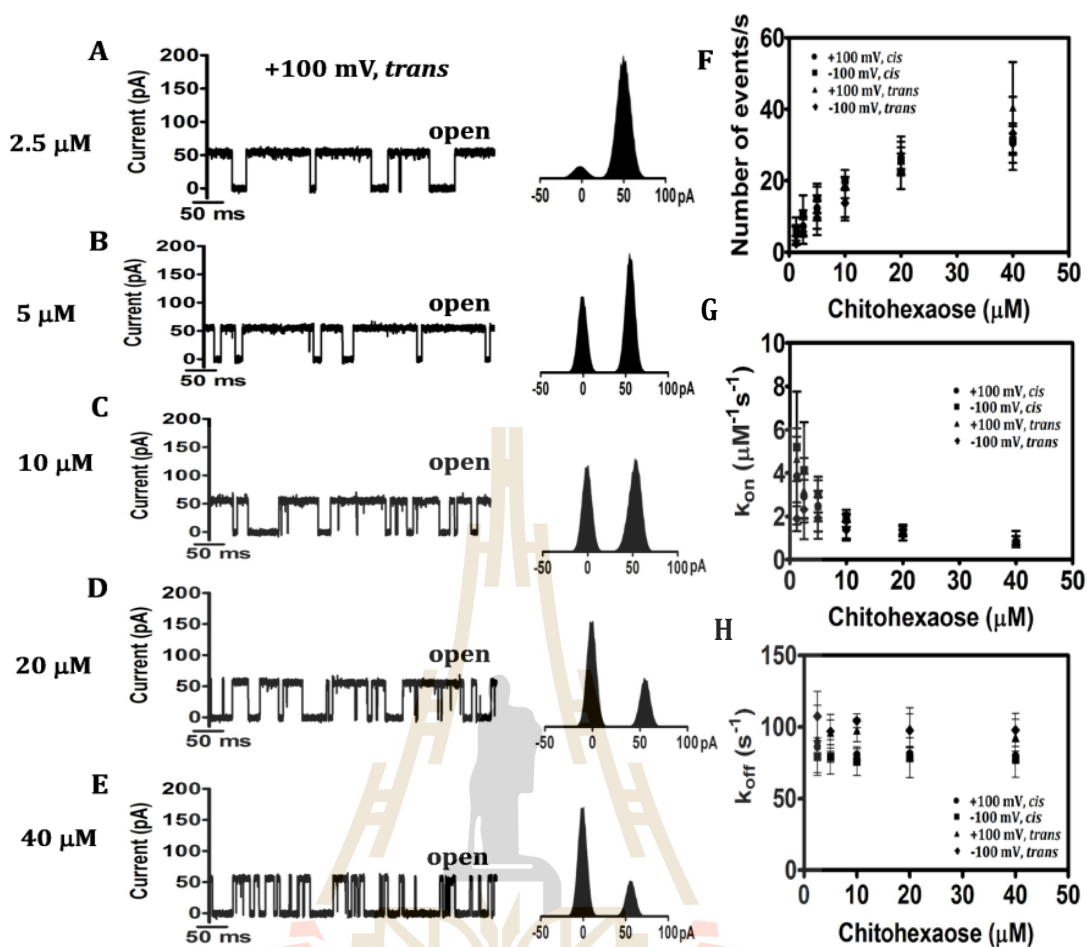
Figure 3.9 Reduction of single *Ec*ChiP channel conductance by increasing concentrations of chitohaxaose. Ion current fluctuations were monitored for 120 s at applied potentials of ±100 mV with sugar addition on either the *cis* or the *trans* side. Here only current traces for 500 ms are presented, with five different chitohaxaose concentrations at *trans*/+100 mV (A-E, left panels) with the corresponding histograms (A-E, right panels. (F) Number of events per unit time (G) Dependence of association rates (k_{on}) and (H) Dependence of dissociation rates (k_{off}) on chitohexaose concentration.

Similarly, dose-dependent current blockages by chitopentaose and chitotetraose are shown in Supplementary Figures 2 and 3, respectively. The k_{on}, k_{off} and the respective K values for the three oligosaccharides tested are summarized in Table 3.2. The data show slight increases in k_{on} with increasing chain length, but much greater decreases in k_{off}. As a result, the resultant K values were increased by more than 20- and 120-fold when the number of GlcNAc units in the chitooligosaccharide chain increased from four to five and six, respectively. These results clearly indicate the preference of EcChiP for a certain length of substrate, which is, indeed, characteristic of a substrate-specific channel.

Table 3.2 Substrate specificity of *Ec*ChiP.

	cis side addition						*trans* side addition					
	+100 mV			-100 mV			+100 mV			-100 mV		
Substrate	(k_{on}) 10^6 $M^{-1}{\cdot}s^{-1}$	(k_{off}) s^{-1}	(K) M^{-1}	(k_{on}) 10^6 $M^{-1}{\cdot}s^{-1}$	(k_{off}) s^{-1}	(K) M^{-1}	(k_{on}) 10^6 $M^{-1}{\cdot}s^{-1}$	(k_{off}) s^{-1}	(K) M^{-1}	(k_{on}) 10^6 $M^{-1}{\cdot}s^{-1}$	(k_{off}) s^{-1}	(K) M^{-1}
GlcNAc$_2$		ND			ND			ND			ND	
GlcNAc$_3$		ND			ND			ND			ND	
GlcNAc$_4$	1	2550± 320	400±10	1.7	2350±255	730±70	3	1608±25	1830±350	1	2642±136	360±50
GlcNAc$_5$	2	250±19	8000±3550	4	280±12	13200±8300	3	255±3	10500±1880	2	385±6	4250±570
GlcNAc$_6$	4	80±1	46600±28700	5	78±1	57900±39200	5	93±2	55000±5100	2	98±1	19600±200

The on-rate (k_{on}, $M^{-1}{\cdot}s^{-1}$) is given by (number of blocking events per second)/[sugar concentration]

In each case sugar concentration= 1.25 μM.

The off-rate (k_{off}, s^{-1}) was obtained from the relationship $k_{off} = 1/\tau_c$ where τ_c is the average residence (dwell) time (s) of the sugar molecule in the channel.

The equilibrium binding constant (M^{-1}) is given by the relationship K= k_{on}/k_{off}

ND indicates that there were no well-resolved blocking events, so that the residence time could not be evaluated with confidence.

To ensure the reliability of the kinetic analysis of single channel recordings, the binding constants (K) for all sugars tested were estimated by three mathematical methods; i) direct quantification from the number of blocking events per unit time and dwell-time analysis (Bhamidimarri et al., 2016; Schwarz, Danelon, and Winterhalter, 2003), ii) from the average reduction of channel conductance induced by elevated sugar concentrations (Andersen et al., 1998; Suginta, Chumjan, Mahendran, Schulte et al., 2013; Andersen, Bachmeyer et al., 1999; Chumjan, Winterhalter, Schulte, Benz, and Suginta, 2015; Pajatsch et al., 1999) and iii) by power spectral (noise) analysis (Andersen et al., 1998; Andersen, Jordy, and Benz, 1995; Andersen, Rak, and Benz, 1999; Bezrukov et al., 2000; Hilty and Winterhalter, 2001; Nekolla et al., 1994). For the first method, we took advantage of the monomeric structure of the channel, which allows the value of K to be estimated directly from k_{on} and k_{off}, which were derived from the number of blocking events and the residence time. The values of K obtained for all four conditions (Table 3.3, left column) depended on the side of sugar addition and the polarity of the applied potential, reflecting the asymmetric nature of the channel, as described previously. In general, larger K values were obtained under the most favorable conditions, *trans*/+100 mV and *cis*/-100 mV. For the second method, we studied the reduction of ionic current produced by increasing sugar concentrations. Figure 3.10 shows non-linear plots of the relative change in ion conductance with increasing sugar concentration for the two representative conditions, *trans*/+100 mV and *trans*/-100 mV (Figure 3.10A), together with their linear transformations as Lineweaver-Burk plots, (Figure 3.10B), which allow the K values to be estimated using the mathematical model shown in equation 2.4 (section 2.4.9.1). The values of K estimated by this method were also affected by the polarity of the applied potential and

the side of sugar entry, the channel responding best to the condition *trans*/+100 mV.

Finally, it has been demonstrated previously that sugar blockages induced current

noises in a concentration-dependent manner (Nekolla et al., 1994). We therefore

performed analysis of sugar-induced noise. The power spectra were satisfactorily fitted

using the Lorentzian function in equation 2.5 (section 2.4.9.1). Figure 3.10C shows

good fits under two different conditions (*cis*/-100 mV and *trans*/+100 mV), with low

frequency spectral density (S_0) increasing, while the average time (τ) between

successive blockages decreased, with increasing sugar concentration. Analysis of the

density spectra at different sugar concentrations yielded the respective corner frequency

(F_c) values, which were used to construct the linear plots shown in Figure 3.10D. Plots

of F_c against sugar concentration allowed both on- and off-rate constants to be

extracted, according to equation 2.6 (section 2.4.9.1).
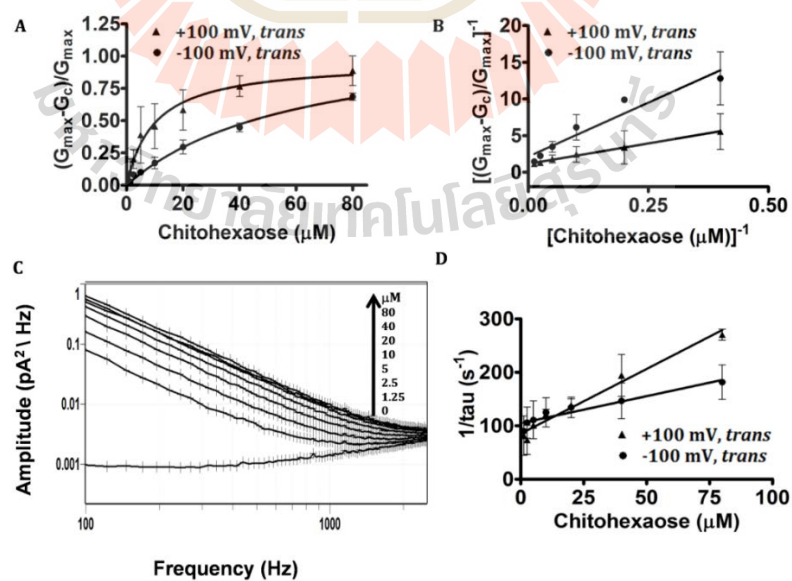
Figure 3.10 Saturation curves and power density spectra of chitohexaose-induced

current noise of *Ec*ChiP. (A) Binding of chitohexaose to *Ec*ChiP. The relative

conductance inhibition $(G_{max}-G_c)/G_{max}$ as a function of chitohexaose concentration plot for membrane potentials +100 mV and -100 mV, with sugar addition on the *trans* side. (B) Lineweaver-Burk double-reciprocal plot of the data in (A). (C) Power density spectra showing the effect of increasing concentration of chitohexaose (from 1.25 to 80 μM chitohexaose, at +100 mV, *trans*) on the current noise amplitude (D) Dependence of $2\pi f_c = 1/\tau$ on the chitohexaose concentration.

For binding of chitohexaose to the *Ec*ChiP channel, the rate constants obtained from noise analysis were; $k_{on} = 3 \times 10^6$ $M^{-1}s^{-1}$ and $k_{off} = 64$ s^{-1} for the condition *cis*/+100 mV and $k_{on} = 3 \times 10^6$ $M^{-1}s^{-1}$ and $k_{off} = 85$ s^{-1} for the condition *trans*/+100 mV, and the corresponding values of K were 46,900 M^{-1} and 35,300 M^{-1}, respectively. Table 3.3 compares the values of K obtained by spectral analysis with those estimated from the number of events and dwell times.
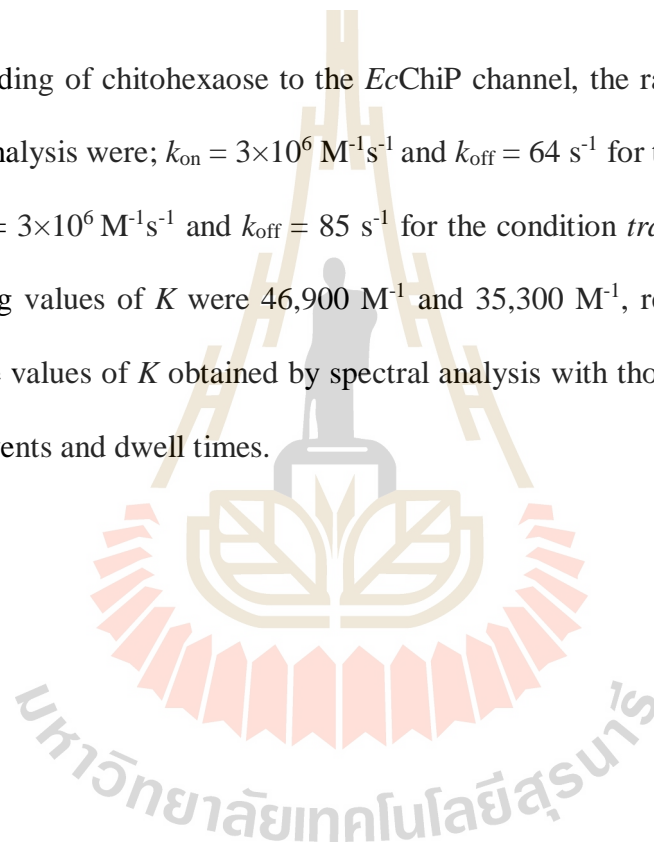
Table 3.3 Comparison of binding parameters of chitohexaose to EcChiP, determined by three different analysis methods.

Side of GlcNAc$_6$ Addition	K (from number of blockage events and tau closed)			(from ionic current reduction)	K (from power density spectra)		
	[a](k_{on}) 10^6 M$^{-1}\cdot$s^{-1}	[b](k_{off}) s^{-1}	[c]K M^{-1}	[d] K M^{-1}	[e](k_{on}) 10^6 M$^{-1}\cdot$s^{-1}	[f](k_{off}) s^{-1}	[g]K M^{-1}
+100 mV, *cis*	4	80 ± 1	46,600±28700	55,600	2	71	28,200
-100 mV, *cis*	5	78 ± 1	57,900±39200	73,100	3	64	46,900
+100 mV, *trans*	5	93 ± 2	55,000±5100	102,800	3	85	35,300
-100 mV, *trans*	2	98 ± 1	19,600±200	44,000	1	104	9,700

[a]The on-rate (k_{on}, M$^{-1}\cdot$s^{-1}) is given by (number of blocking events per second)/[sugar concentration]. Here GlcNAc$_6$ concentration = 1.25 μM.

[b]The off-rate (k_{off}, s^{-1}) was obtained from the relationship $k_{off} = 1/\tau_c$ where τ_c is the average residence (dwell) time (s) of the sugar molecule in the channel.

[c] The equilibrium binding constant K (M^{-1}) is given by K= [a]k_{on} /[b]k_{off}

[d]The equilibrium binding constant K was estimated from the reduction of ion conductance in the presence of increasing concentrations of GlcNAc$_6$.

[e]The on-rate constant (k_{on}, M$^{-1}\cdot$s^{-1}) is given by slope of graph in Figure 3.10.

[f]The off-rate constant (k_{off}, s^{-1}) is given by intercept of graph in Figure 3.10.

[g]The equilibrium binding constant K (M^{-1}) is given by K= [e]k_{on} /[f]k_{off}

3.7 Determination of channel specificity using a liposome swelling assay

Proteoliposome swelling assays were performed to evaluate the bulk permeation of neutral solutes through the *Ec*ChiP channel. *Ec*ChiP-containing proteoliposomes were prepared according to the protocol described elsewhere (Aunkham, Schulte, Winterhalter, and Suginta, 2014; Yoshimura and Nikaido, 1985). Swelling of the proteoliposomes caused by diffusion of solute molecules through the protein channel resulted in a decrease in apparent absorbance at 500nm, while under isotonic conditions constant absorbance was maintained. In this assay, we used *D*-raffinose (504 Da), a branched sugar that is unable to diffuse through the porin, to establish the isotonic concentration and enable the comparison of diffusion rates. *L*-arabinose (150 Da), the smallest sugar tested in this experiment, had the highest diffusion rate through *Ec*ChiP, and the swelling rates in the other sugars tested were normalized relative to that in *L*-arabinose, which was set to 100%.

To address the differences between the *Ec*ChiP channel and the chitooligosaccharide- specific porins from the OmpC family, we compared our data with those obtained with *Vh*ChiP-incorporated proteoliposomes. The two chitoporins showed similar diffusion rates for small sugars such as *D*-glucose, *D*-mannose and *D*-galactose (180 Da) and *N*-acetylglucosamine (GlcNAc, 221 Da) (Figure 3.11A). However, *D*-sucrose (342 Da), maltose (360 Da) and *D*-melezitose (522 Da) showed no diffusion through *Ec*ChiP. In contrast, *D*-sucrose and maltose permeated *Vh*ChiP, albeit with very low diffusion rates, while *D*-melezitose was impermeant. When *Ec*ChiP was tested with long-chain chitooligosacharides it was found that all neutral chitooligosaccharides were permeant (Figure 3.11B), while maltosugars (maltose and

maltahexaose) did not show permeation. The results obtained from the proteoliposome swelling assays additionally confirmed the high selectivity of *Ec*ChiP for chitooligosaccharides.
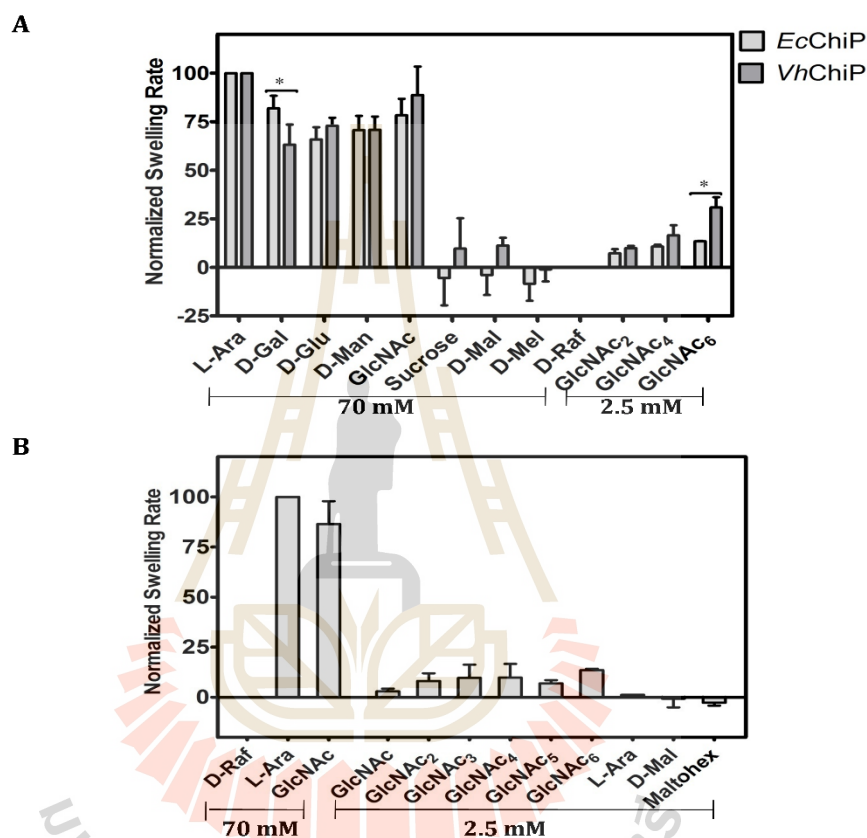
Figure 3.11 Proteoliposome swelling assays. In each preparation, multilamellar liposomes were reconstituted with 200 ng of *Ec*ChiP or *Vh*ChiP. *D*-raffinose was used to determine the isotonic concentrations that produced no change in absorbance at 500 nm of the proteoliposome suspension over 60 s. The swelling rate in *L*-arabinose was set to 100% to obtain normalized swelling rates. The permeability of channels was assumed to be directly proportional to the swelling rate. (A) Permeation of different types of sugar through *Ec*ChiP- and *Vh*ChiP-containing proteoliposomes. Differences between the two data sets were evaluated using a t-test. Statistically significant

differences (P < 0.05) are marked with an asterisk (*). Values are means±SD, obtained from 3-5 independent sets of experiments. (B) Permeation of chitooligosaccharides through EcChiP. Maltodextrins were used as controls. L-Ara, L-Arabinose; D-Gal, D-Galactose; D-Glu, D-Glucose; D-Man, D-Mannose; GlcNAc, N-acetylglucosamine; D-Mal, D-Maltose; D-Mel, D-Melezitose; D-Raf, D-Raffinose, $GlcNAc_2$, Chitobiose; $GlcNAc_3$, Chitotriose; $GlcNAc_4$, Chitotetraose; $GlcNAc_5$, Chitopentaose; $GlcNAc_6$, Chitochexaose; Maltohex, Maltohexaose.

3.8 Thermodynamic evaluation of sugar-channel interactions in solution

Isothermal titration calorimetry (ITC) was employed to assess the binding affinity of EcChiP for its preferred substrate, chitohexaose. After background subtraction (for control traces, see Supplementary Figure 4), the thermographic binding isotherm (Figure 3.12A, top panel) was used to generate a theoretical fit of the integrated heat change, based on a one-site binding model (Figure 3.12A, bottom panel). The normalized thermogram was characteristic of endothermic binding, and yielded an average binding constant (K) of 250,000 M^{-1}, a free energy of binding (ΔG) of -7.0±0.07 kcal·mol^{-1}, an enthalpy change (ΔH) of 4.0±0.11 kcal·mol^{-1} and an entropy change (-TΔS) of -11.0±0.15 kcal·mol^{-1}. The thermograms, the fitted data and the thermodynamic parameter values calculated from three independent experiments were consistent. The entropy gain in the binding process strongly suggests that hydrophobic interactions play a predominant role in chitohexaose-EcChiP interactions (Abraham, Lewis, Hodges, and McElhaney, 2005b; Anbazhagan, Sankhala, Singh, and Swamy, 2011) (see the

Signature plot, Figure 3.12A bottom panel inset). In marked contrast, the structurally

related maltohexaose showed no interaction at all, as shown in the corresponding

thermogram (Figure 3.12A, top panel), displaying an offset of -0.1 µcal·sec^{-1} and zero

integrated heat change (Figure 3.12A bottom panel, open circles). Our ITC data are

completely consistent with the electrophysiological data, since the addition of

chitohexaose (20 µM) to BLM-reconstituted EcChiP displayed clear, frequent channel-

blocking events (Figure 3.12B top panel), while a ten-fold higher concentration of

maltohexaose (200 µM) did not affect the EcChiP channel (Figure 3.12B, bottom

panel).
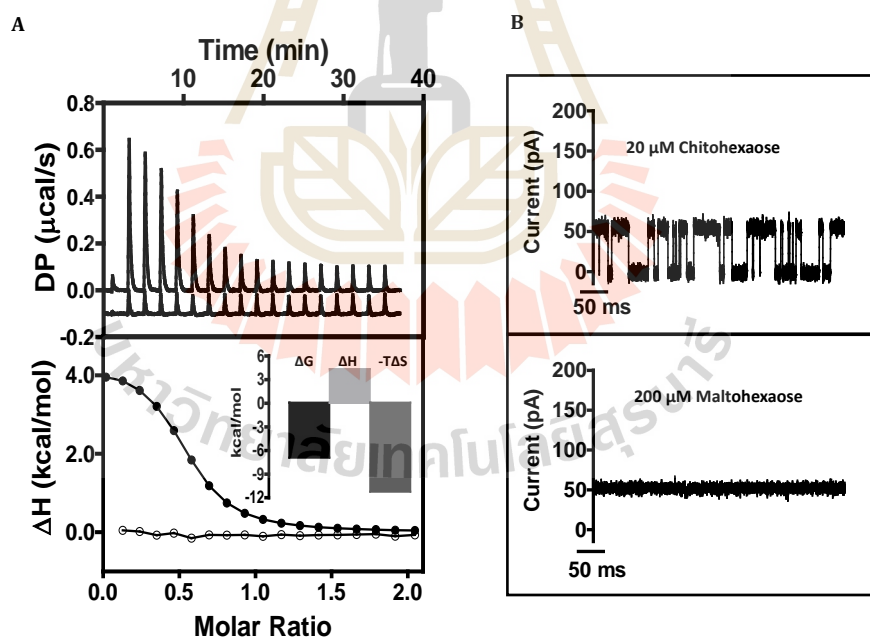
Figure 3.12 Calorimetric titration of EcChiP with chitohexaose and maltohexaose. (A)

Top panel: ITC profile of the binding of chitohexaose to EcChiP, with ITC profile of

the binding of maltohexaose to EcChiP offset by -0.1 µcal/s. Bottom panel: integrated

heat of binding of chitohexaose obtained from raw data, after subtracting the heat of

dilution (closed circles). The solid line represents the best fit to the experimental data using a one-site model from Microcal PEAQ-ITC. Titration of *Ec*ChiP with maltohexaose is shown as open circles. Inset is the signature plot for chitohexaose binding to *Ec*ChiP. (B) Single-channel BLM data showing interaction of chitohexaose with *Ec*ChiP (top panel) and of maltohexaose with *Ec*ChiP (bottom panel).

3.9 Effects of N-acetyl side chains on chitooligosaccharide translocation

The aim of this part was to elucidate the effect of N-acetyl side chains for specificity of chitoporins. To this end two different pH conditions were selected and single *Ec*ChiP channel behavior, reconstituted in planar bilayer, was observed in the absence of sugar. As shown in Figure 3.13 the channel was stable at both pH conditions, showing no ion current fluctuations.
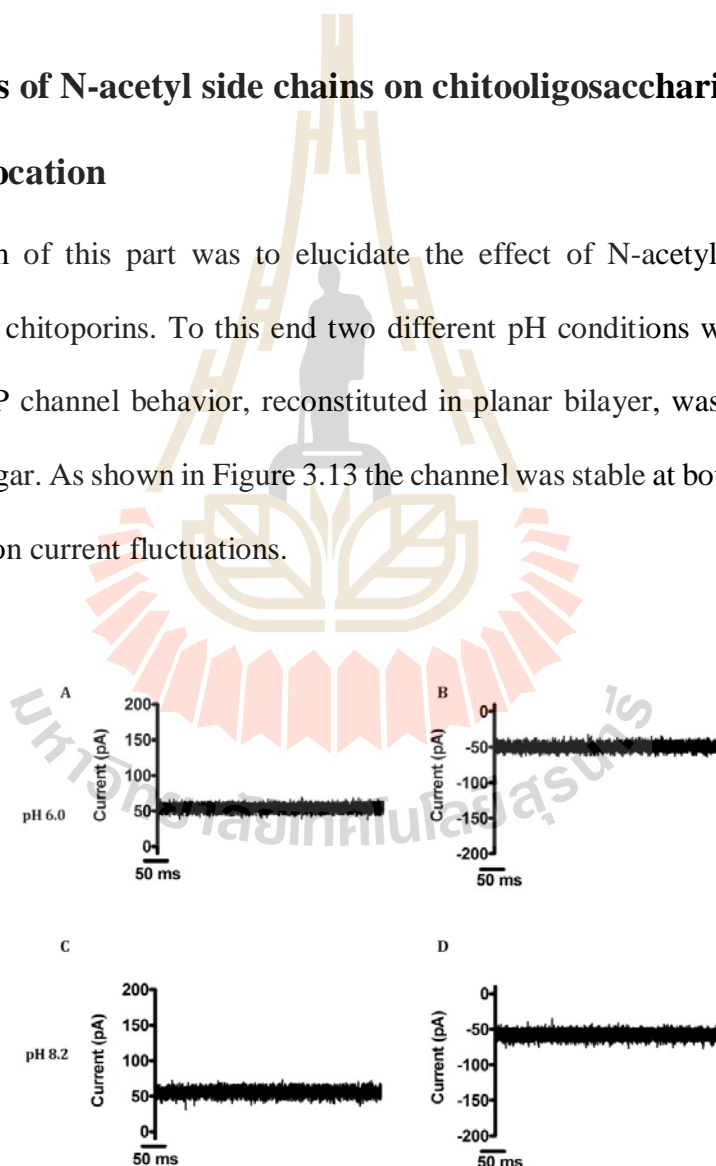
Figure 3.13 Effect of pH on *Ec*ChiP conductance. Typical ion current recordings through a single *Ec*ChiP, at various pH values and in the absence of sugar. The

transmembrane potential of +100 mV (left panel) (A) at pH 6 and (C) at pH 8.2 and right panel potential – 100 mV (B) at pH 6 and (D) at pH 8.2. The bathing solution contained 1 M KCl in 20 mM HEPES pH 8.2 or in 20 mM MES pH 6.0.

Addition of 80 µM chitosan hexaose on the *cis* or *trans* side at pH 8.2 did not cause ion current fluctuations either at positive or negative transmembrane voltage (right panel Figure 3.14). In contrast, at pH 6.0 if chitosan hexaose was added on the *cis* side, blocking events were detectable in negative transmembrane potential. On the other hand, at pH 6.0 if chitosan hexaose was added on the *trans* side, blocking events were detectable in positive transmembrane potential (left panel Figure 3.14) depending on whether the sugar diffusion current flows in the same direction as the electric current flow.
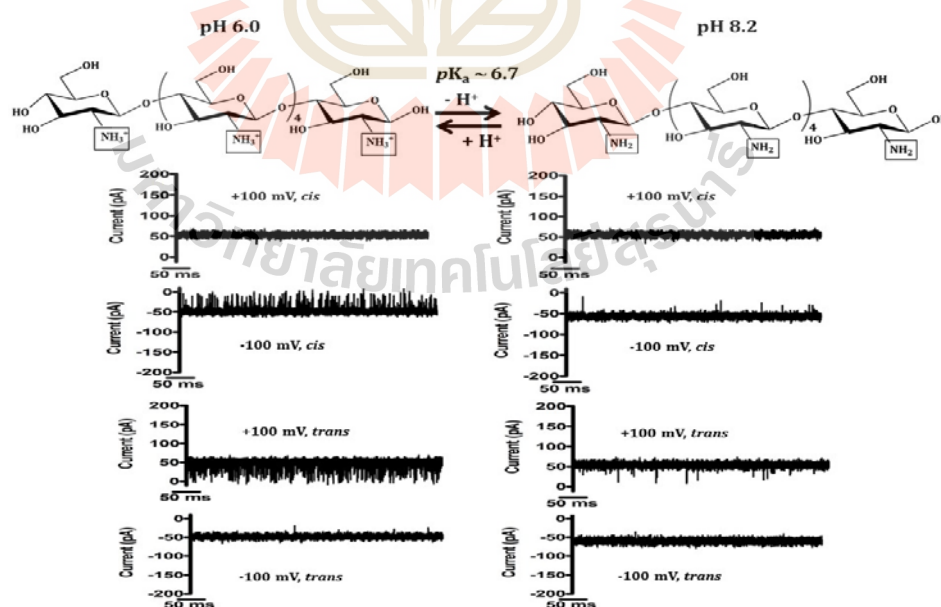
Figure 3.14 Chitosan hexaose interaction with *Ec*ChiP at different pH. Top panel shows the chitosan hexaose structure variation according to the pH. The buffer

contained 1M KCl in 20 mM MES in pH 6 of 80 µM chitosan hexaose either on *cis* or *trans* side (left panel) and buffer contained 1M KCl in 20 mM HEPES in pH 8.2 of 80 µM chitosan hexaose either on *cis* or *trans* side (right panel) with different membrane potential.

Single channel analysis of planar lipid bilayer measurements was displayed high affinity for chitohexaose, but low affinity for chitosan hexaose, lacking the N-acetyl group at C2 of the glucosyl ring at neutral pH (see the chitosan hexaose structure in the top panel, Figure 3.14). But the chitosan hexaose has the primary amine attached to its C2 position making it ionizable at pH below the pKa (6.7) producing protonated catonic sugar.

Addition of chitohexaose on the *trans* side at pH 6.0 caused sugar blocking events with long residence time either with positive (Figure 3.15 right panel) or negative transmembrane voltages (Figure 3.16, right panel). Increasing chitohexaose concentrations from 10 to 80 µM caused more blocking events with channel closure in the most of time at high concentration (Figure 3.15H). If chitosan hexaose was added on the *trans* side, blocking events were detectable at positive voltages (Figure 3.15 left panel) only. Similar to chitohexaose, increasing concentrations of chitosan hexaose caused more blocking events.
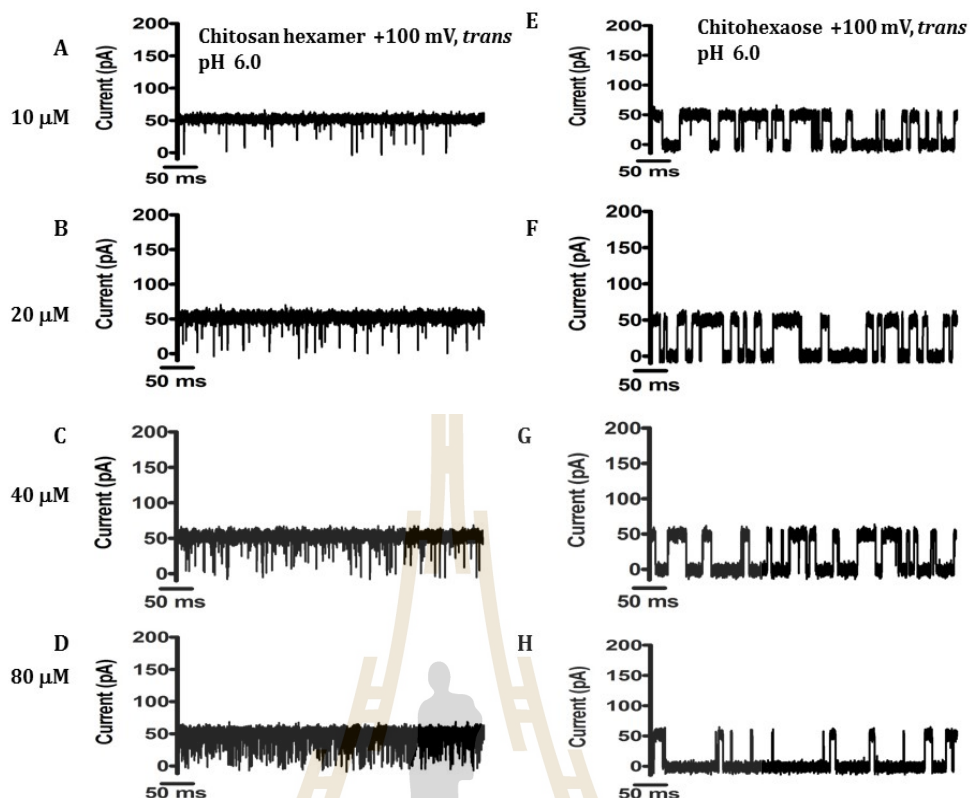
Figure 3.15 Effect of N-acetyl functionality on *Ec*ChiP at pH 6.0 (sugar on the *trans*, positive membrane potentials). Ion current fluctuations were monitored for 120 s at applied potentials of + 100 mV with sugar addition on the *trans* side. Here only current traces for 500 ms are presented, with four different chitosan hexaose concentrations (A-D, left panels) and four different chitohaxaose concentrations (E-H, right panels).

In contrast, chitosan hexaose did not show interactions with the *Ec*ChiP if negative transmembrane voltages were used (Figure 3.16) when sugar was added on the *trans*. Moreover, when sugars were added on the *cis* side, chitohexaose showed similar behavior as *trans,* either at positive or negative voltages, at pH 6. (see Supplementary Figure 5 and 6). But chitosan hexaose showed interactions only at negative voltages (see Supplementary Figure 5 and 6).

91
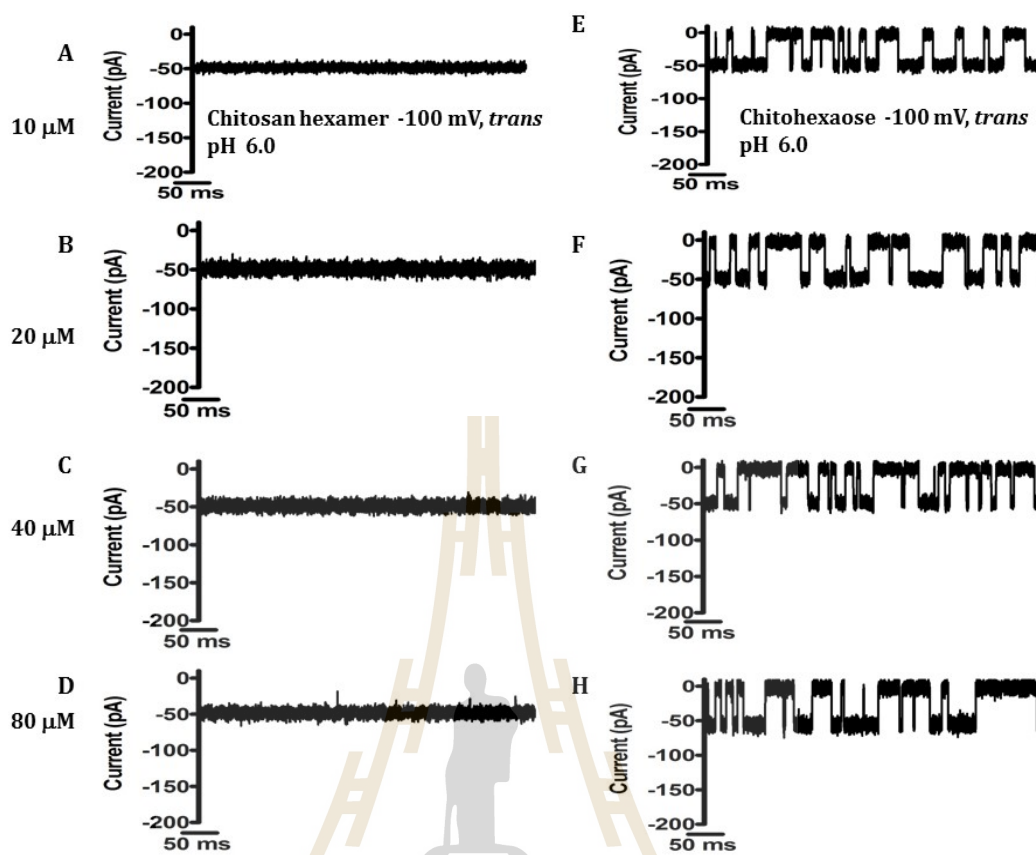
Figure 3.16 Effect of N-acetyl functionality on *Ec*ChiP at pH 6.0 (sugar on the *trans*, negative membrane potentials). Ion current fluctuations were monitored for 120 s at applied potentials of – 100 mV with sugar addition on the *trans* side. Here only current traces for 500 ms are presented, with four different chitosan hexaose concentrations (A-D, left panels) and four different chitohaxaose concentrations (E-H, right panels).

Then we recorded ion current fluctuations at pH 8.2 at which both chitosan hexaose and chitohexaose are uncharged. Figure 3.17 and 3.18 represent the ion current blocking events at pH 8.2 when sugars were added on *trans* side positive and negative transmembrane voltages respectively.
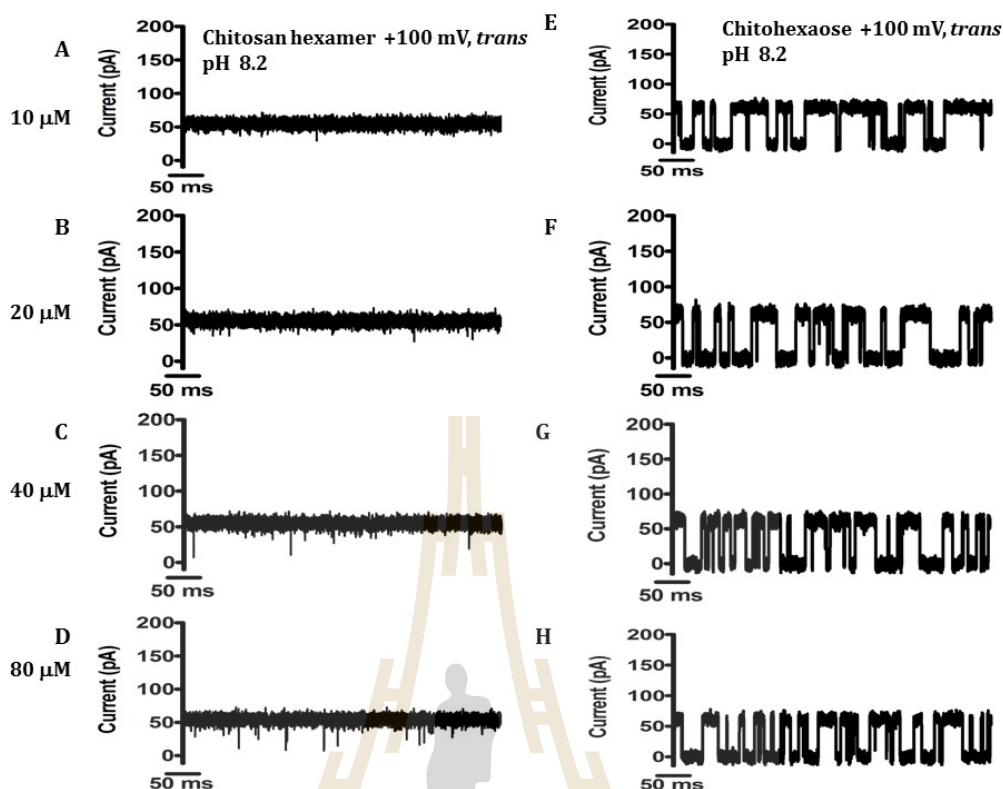
Figure 3.17 Effect of N-acetyl functionality on *Ec*ChiP at pH 8.2 (sugar on the *trans*, positive membrane potentials). Ion current fluctuations were monitored for 120 s at applied potentials of + 100 mV with sugar addition on the *trans* side. Here only current traces for 500 ms are presented, with four different chitosan hexaose concentrations (A-D, left panels) and four different chitohaxaose concentrations (E-H, right panels).

When pH of the working electrolyte was raised above the pK$_a$ of chitosan hexaose to pH 8.2, no disturbance of the I(t) trace was observed. At the very high concentration (80 µM) occasional current fluctuations were seen (Figure 3.17D) only with positive transmembrane potentials and negative transmembrane potentials show the fully-open state of the monomeric *Ec*ChiP channel (Figure 3.18A-D).
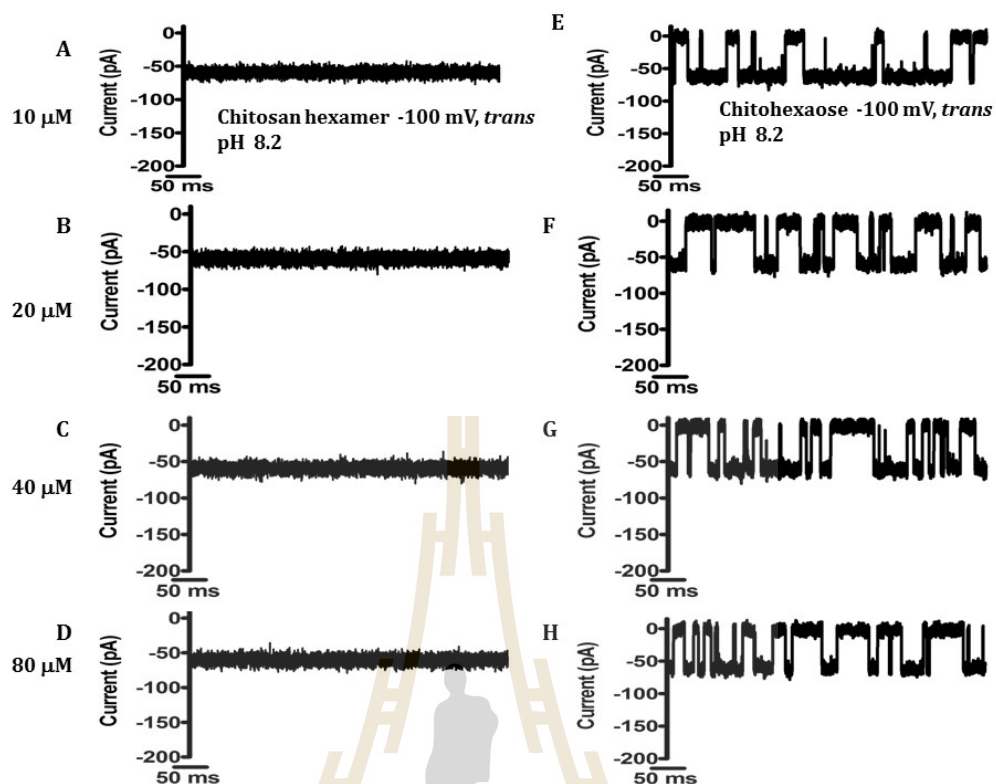
Figure 3.18 Effect of N-acetyl functionality on *Ec*ChiP at pH 8.2 (sugar on the *trans*, negative membrane potentials). Ion current fluctuations were monitored for 120 s at applied potentials of – 100 mV with sugar addition on the *trans* side. Here only current traces for 500 ms are presented, with four different chitosan hexaose concentrations (A-D, left panels) and four different chitohaxaose concentrations (E-H, right panels).

Table 3.4 summarizes the kinetics rates of both charged and uncharged chitooligosaccharides towards *Ec*ChiP when sugars were added on the *trans* side. Supplementary Table 1 summarizes the rates for *cis* side sugar addition.

Table 3.4 Effects of pH on the binding constant of *Ec*ChiP towards charged and uncharged chitooligosaccharides.

pH	Chitohexaose (GlcNAc$_6$), +100 mV, *trans*			Chitosan hexaose (GlcN$_6$), +100 mV, *trans*		
	[a]Binding constant (K, M^{-1})	[b]On-rate constant 10^6 (k_{on}, M^{-1}s^{-1})	[c]Off-rate constant (k_{off}, s^{-1})	[a]Binding constant (K, M^{-1})	[b]On-rate constant 10^6 (k_{on}, M^{-1}s^{-1})	[c]Off-rate constant (k_{off}, s^{-1})
6.0	72450 ± 43000	7.0	98 ± 18	600 ± 250	10	17350 ± 1700
8.2	46140 ± 8600	6.0	126 ± 15	-	ND	ND

[a] The equilibrium binding constant (K)= k_{on} /k_{off}

[b] The on-rate (k_{on}, m^{-1}·s^{-1}) is given by number of blocking events(s^{-1})/[sugar concentration]. Here sugar GlcNAc$_6$ concentration= 1.25 μM, GlcN$_6$ concentration= 1.25 μM.

[c] The off-rate (k_{off}, s^{-1}) was obtained from 1/ τ_c, where τ_c is the average residence (dwell) time of the sugar molecule in the channel.

ND, No well-resolved blocking events.

The on rate and average residence time were plotted as a function of the applied

voltage from -50 to -150 mV for the *cis* side addition of the chitosan hexaose (Figure

3.19) and +50 to +150 mV for the *trans* side addition of the chitosan hexaose (data is

not shown) at pH 6, which chitosan hexaose is positively charged. The plot of average

residence time as a function of the applied voltage proves the translocation of charged

molecules.
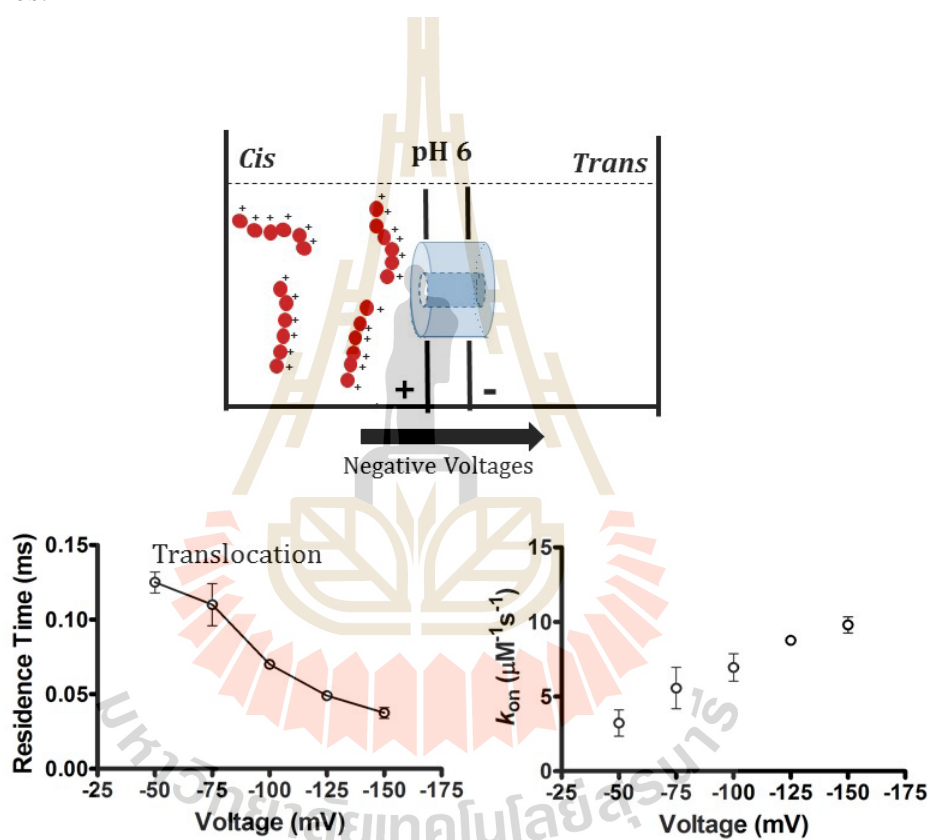
Figure 3.19 Voltage dependence of the residence time and on rates of chitosan hexaose

to *Ec*ChiP.

3.10 Effect of deuterium bonds on sugar transport

Ion current measurements were performed in deuterated water, which is known

to give slightly stronger bonds as compared with hydrogen. A decrease in k_{off} of nearly

50% for chitohexaose was observed in D_2O (Table 3.5 for *cis* side). Figure 3.20 shows

binding curves (top panel) and residence times (bottom panel) for both H_2O and D_2O

on the *cis* side sugar addition at – 100 mV. Similar results were obtained with *trans* side

sugar addition and all binding kinetics rates are shown in Supplimentary Table 2.
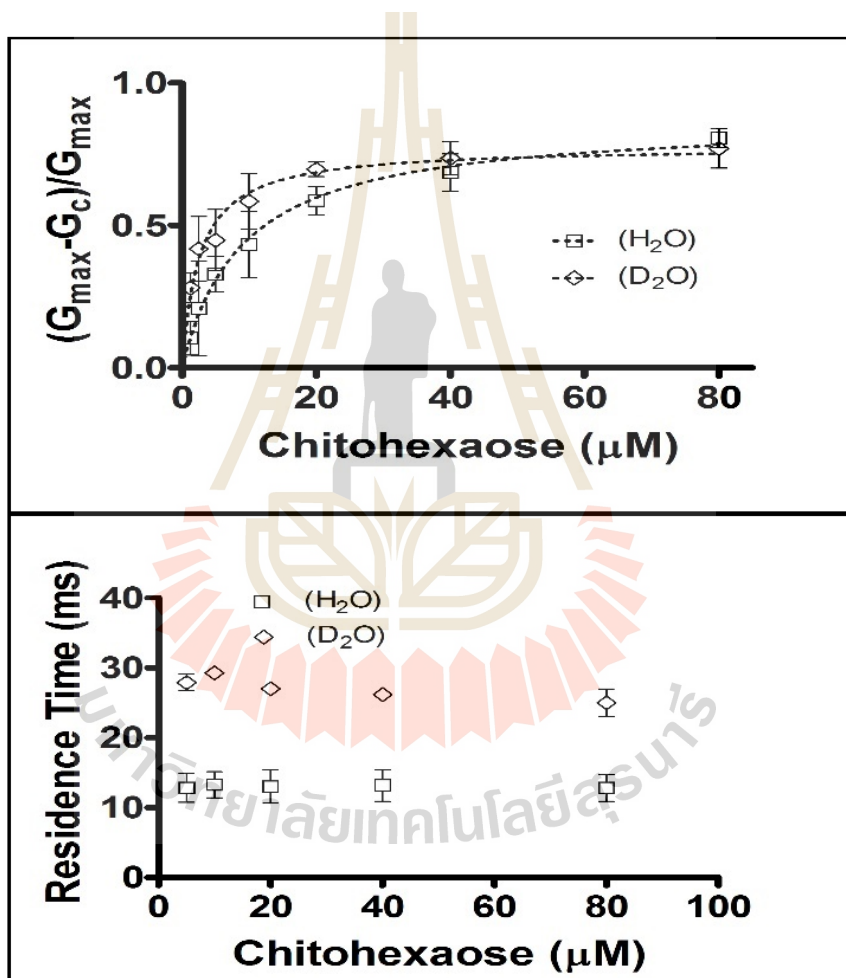
Figure 3.20 Effect of deuterium bonding on sugar transport. (Top panel) binding curves

of chitohexaose using ion current reduction methods. (Bottom panel) residence time of

chitohexaose in *Ec*ChiP in the presence of 1 M KCl 20 mM HEPES in H_2O or D_2O.

Sugar addition on the *cis* side and applied voltage -100 mV.

Table 3.5 Effect of deuterium bonding on sugar transport.

	Cis side addition							
	+100 mV				-100 mV			
Experimental condition	[a](k_{on}) 10^6	[b](k_{off})	[c](K)	[d](K)	[a](k_{on}) 10^6	[b](k_{off})	[c](K)	[d](K)
$GlcNAc_6$ in H_2O	4	80±1	46615±28660	54765	5	78±1	57865±39147	109421
$GlcNAc_6$ in D_2O	3.5	34±1	105948±33648	248570	4	37±2	114063±25610	379795

[a] The on-rate (k_{on}, $M^{-1} \cdot s^{-1}$) is given by number of blocking events(s^{-1})/[sugar concentration].

Here [$GlcNAc_6$] = 1.25μM

[b] The off-rate (k_{off}, s^{-1}) was obtained from Eq. $k_{off} = 1/ \tau_c$ where τ_c is the average residence (dwell) time (s) of the sugar molecule in the channel.

[c] The equilibrium binding constant (K, M^{-1})= k_{on} / k_{off}

[d] The equilibrium binding constant (K, M^{-1}) was estimated from the reduction of ion conductance in the presence of increasing concentrations of sugar.

3.11 Temperature-dependence of ion currents

Single-channel conductance of the EcChiP channel as a function of the temperature is shown in Figure 3.21 (left panel) and ln (EcChiP channel conductance) as a function of 1/T is shown in Figure 3.21 (right panel) in both H_2O and D_2O. As expected EcChiP channel conductance was lower in the presence of D_2O because of lowered bulk conductivity. Prior to adding the 5 µM Chitohexaose, the ion current traces of the single channels were recorded at different temperatures. Temperature range from 5 to 35 °C resulted in a linear slope with an energy barrier of about 6.4 kT and 6.0 kT in 1M KCl in 20 mM HEPES in H_2O and D_2O respectively.
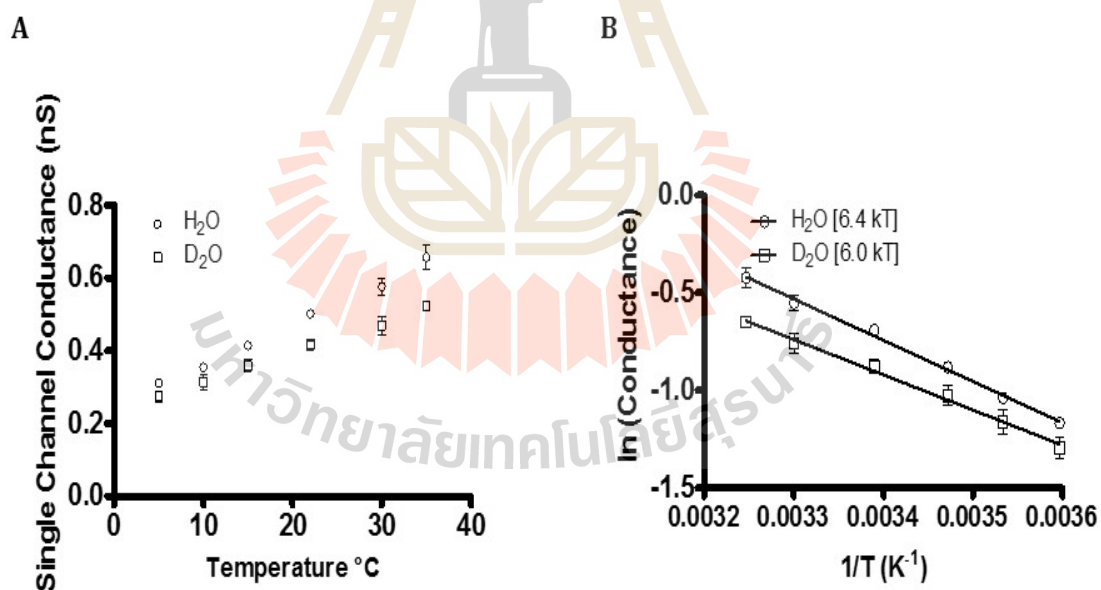
Figure 3.21 Single channel conductance and Arrhenius plot of the conductance as a function of temperature. Experimental conditions are 1M KCl, 20 mM HEPES in H_2O and D_2O, pH 7.4, applied voltage +100 mV.

Subsequently, chitohexaose was added to the *cis* or *trans* side of the lipid membrane. The occurring fluctuations in the ion current were analyzed over a temperature range of 5–35 $^{\circ}$C. The Figure 3.22 shows ion current traces for *cis* side sugar addition at + 100 mV.
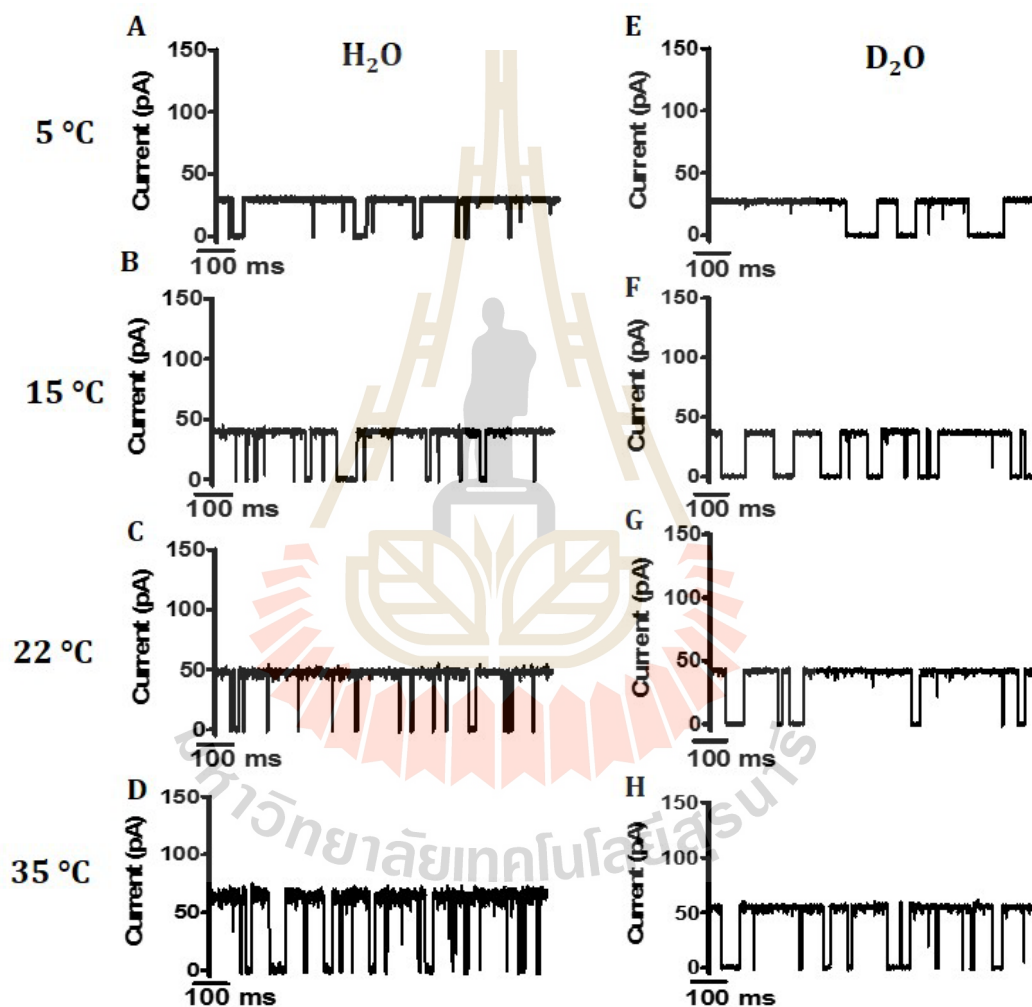
Figure 3.22 Typical ion current recordings through *Ec*ChiP at 5, 15, 22 and 35 $^{\circ}$C in the presence of chitohexaose. (A-D) 1 M KCl, 20 mM HEPES in H_2O (E-H) 1 M KCl, 20 mM HEPES in D_2O. The concentration of chitohexaose was 5 μM added to the *cis* side, applied potential +100 mV.

In both cases, the number of chitohexaose blocking events increased with the increase in the temperature (Figure 3.23A and C). The average residence time of the sugar in the *cis* or *trans* side decreases with the increase in the temperature (Figure 3.23B and D).
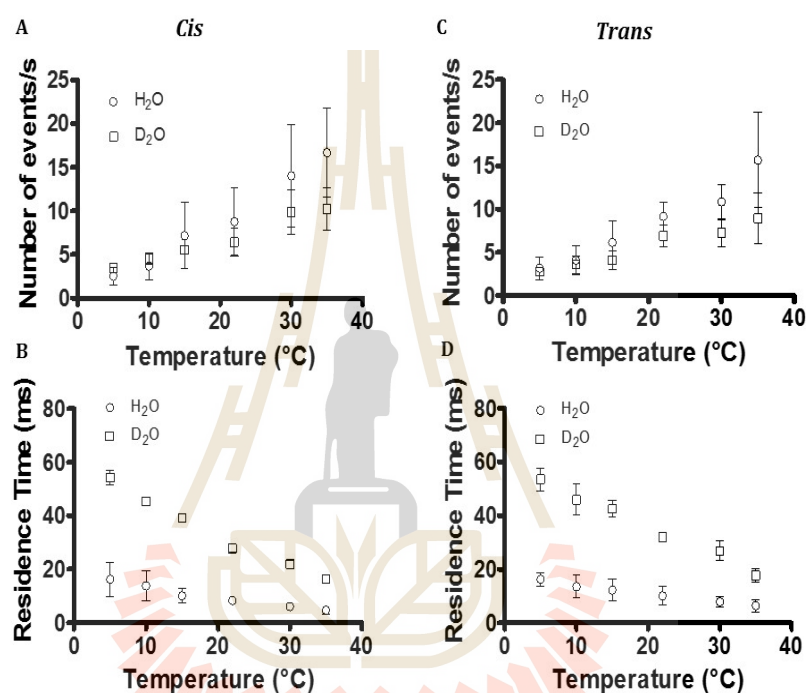
Figure 3.23 Number of events and residence time at different temperatures. (A, C) the number of chitohexaose binding events (B, D) The residence time as a function of temperature from 5 to 35 ºC at + 100 mV. The buffer contained 1M KCl, 20mM HEPES, pH 7.4, in H_2O or D_2O and 5 μM chitohexaose added to the *cis* or *trans* side of the lipid membrane.

The temperature-dependent ion-current blockage events were further analyzed using an Arrhenius plot providing the energy barrier for k_{on} and k_{off} (Figure 3.24). The slope of the Arrhenius plot gives the energy barrier in terms of kT.
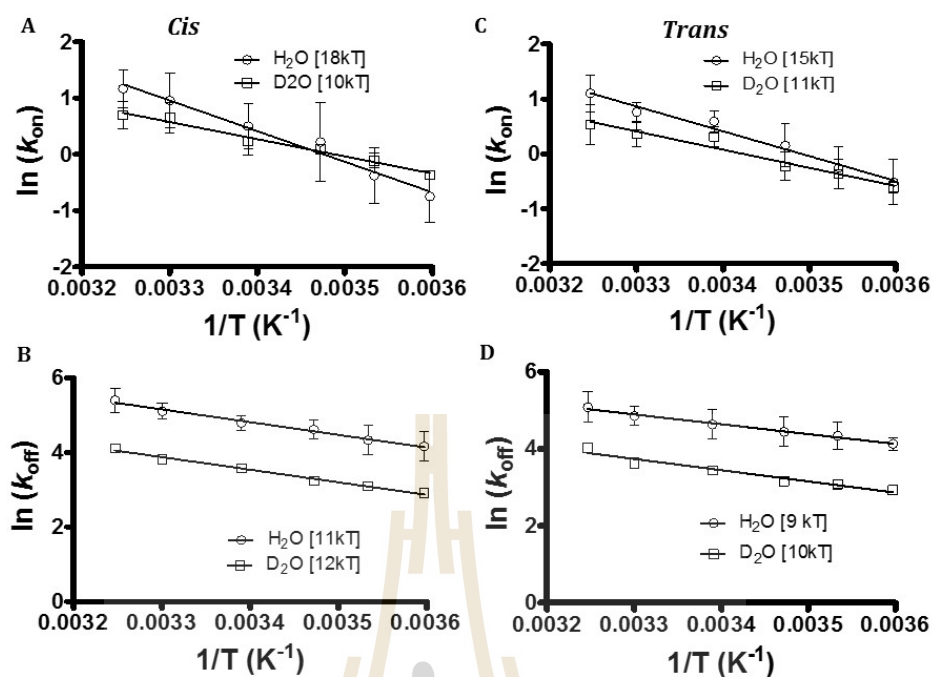
Figure 3.24 The Arrhenius plot of rate constants k_{on} or k_{off} as a function of the inverse of the temperature for chitohexaose. (A, C) k_{on} and (B, D) k_{off} as a function of temperature from 5 to 35 °C resulting in a linear slope with an energy barrier as shown. The buffer contained 1 M KCl, 20 mM HEPES, pH 7.4, in H_2O or D_2O and 5 μM chitohexaose added to the *cis* side of the lipid membrane at applied voltage of + 100 mV (n = 3, mean ± SE).

3.12 Effect of constriction zone mutations of *Ec*ChiP on ion transport and sugar translocation

To determine ion selectivity, hundreds of channels are incorporated in solvent-containing membranes at low voltage (20 mV). After reaching saturation for channel insertion, the voltage is switched off and increasing KCl salt concentration gradients are established followed by determination of the resulting zero- current membrane

potentials (Vm). Since *Ec*ChiP is a cation-selective channel, positive values for Vm are observed for Pcation/Panion. Figure 3.25 shows the measured membrane potentials as a function of the salt concentration ratio in both compartments for *Ec*ChiP wild type and its mutants.
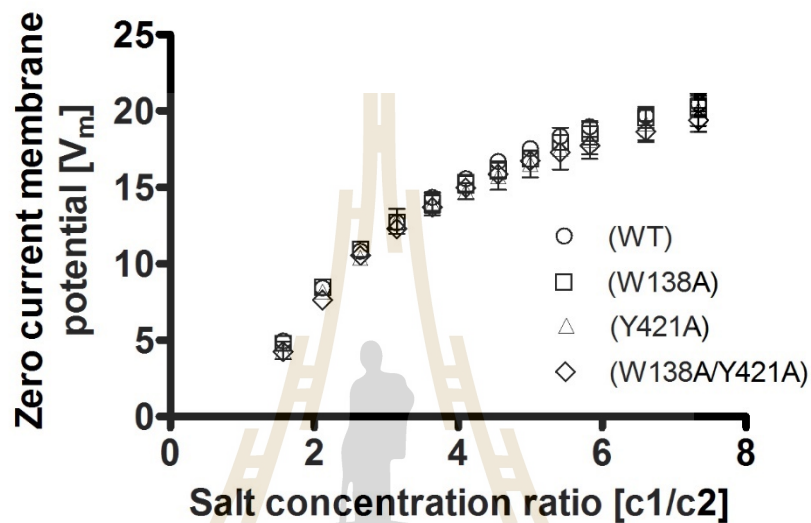
Figure 3.25 Zero-Current Membrane Potentials of *Ec*ChiP and its mutants. Zero-current membrane potential (Vm) is plotted as a ratio of salt concentrations in both compartments for salt solutions ranging from 0.1 to 3 M KCl. Vm values were determined from three independent measurements.

The ratio of cation to anion permeability, (Pc/Pa) was calculated using the Goldman−Hodgkin−Katz equation from at least three individual experiments as shown in Table 3.6 for *Ec*ChiP wild type and its mutant.

Table 3.6 Zero-current measurements to study the ion selectivity of *Ec*ChiP and its mutants.

Protein Name	PK^+/PCl^-
*Ec*ChiP (WT)	2.8
*Ec*ChiP (W138A/Y421A)	2.7
*Ec*ChiP (W138A)	2.8
*Ec*ChiP (Y421A)	2.7

The zero-current membrane potential, Vm, is defined as the difference between the potential at the dilute side and that at the concentrated side of salt solutions.

Chitohexaose interactions with *Ec*ChiP(WT), *Ec*ChiP(W138A), *Ec*ChiP(Y421A/W138A) and *Ec*ChiP(Y421A) were checked with sugar addition either on the *cis* or *trans* side. The most striking effect was observed when sugars were added on *trans* side. Figure 3.26 summarizes the binding curve for *Ec*ChiP wild type and its mutants at + 100 mV when sugars were added on *trans* side.
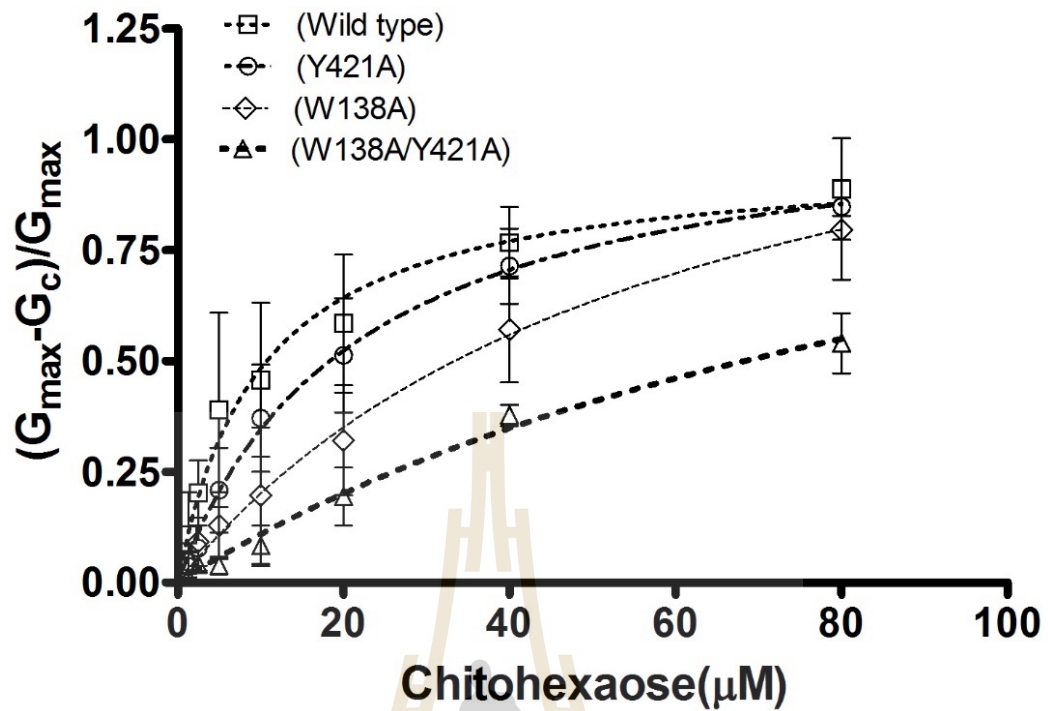
Figure 3.26 Effect of pore constriction mutation on sugar transport.

The binding kinetics for *Ec*ChiP (WT) and its mutants are summarized in Table 3.7 for *trans* side chitohexaose addition (Supplimentary Table 3 summarizes the value for *cis* side sugar addition).

Table 3.7 Binding constant of *Ec*ChiP and its mutants with chitohexaose.

		Trans side addition				
Protein		+100 mV			-100 mV	
	[a]$(k_{on}).10^6$	[b](k_{off})	[c](K)	[a]$(k_{on}).10^6$	[b](k_{off})	[c](K)
	$(M^{-1}s^{-1})$	(s^{-1})	(M^{-1})	$(M^{-1}s^{-1})$	(s^{-1})	(M^{-1})
*Ec*ChiP (WT)	5	93±2	55330±5136	2	98±1	19548±205
(W138A/Y421A)	1	161±14	6537±1254	0.6	168±2	4058±2202
(W138A)	2	124±9	13283±14777	1	182±53	8807±13281
(Y421A)	2	128±8	15012±1716	1	148±7	6837±721

[a] The on-rate (k_{on}, $M^{-1} \cdot s^{-1}$) is given by number of blocking events(s^{-1})/[sugar concentration].

Here [GlcNAc$_6$] = 1.25 μM.

[b] The off-rate (k_{off}, s^{-1}) was obtained from $k_{off} = 1/\tau_c$ where τ_c is the average residence (dwell) time (s) of the sugar molecule in the channel.

The equilibrium binding constant (K, M^{-1}) = k_{on}/k_{off}.

In the next series of experiments, chitohexaose interactions with the *Ec*ChiP(WT), *Ec*ChiP(W138A), *Ec*ChiP(Y421A/W138A) and *Ec*ChiP(Y421A) channels were analyzed at different temperatures. Single-channel conductance of the wild-type and mutant channels as a function of the temperature and ln (conductance) as a function of inverse temperature are shown in Figure 3.27, both at +100 mV. Prior to adding the 5µM chitohexaose, the ion current traces of the single channels were recorded at different temperatures. Temperature range from 5 to 35 ºC resulted in a linear slope with an energy barrier of about 6 - 6.5 kT in 1M KCl in 20 mM HEPES for *Ec*ChiP and its mutants (Figure 3.27 right panel).
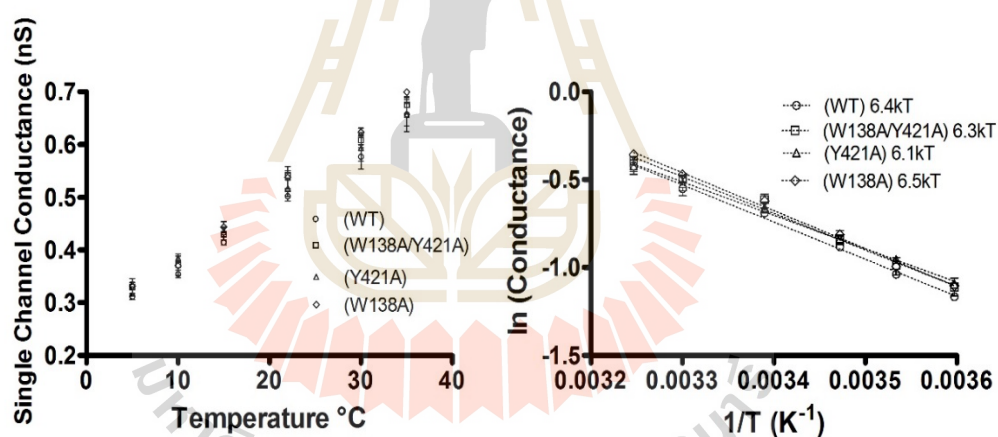
Figure 3.27 Single channel conductance and Arrhenius plot of the conductance as a function of temperature for *Ec*ChiP and its mutants. Experimental conditions are 1M KCl, 20 mM HEPES in H_2O, pH 7.4, applied voltage +100 mV.

Later, 5 µM chitohexaose was added to the *cis* or *trans* side of the lipid membrane in the presence of single *Ec*ChiP or its mutants. The occurring fluctuations in the ion current were analyzed over a temperature range of 5-35 ºC. Figure 3.28 shows ion

current traces comparision for *Ec*ChiP and its mutants on the *trans* side sugar addition

at + 100 mV.
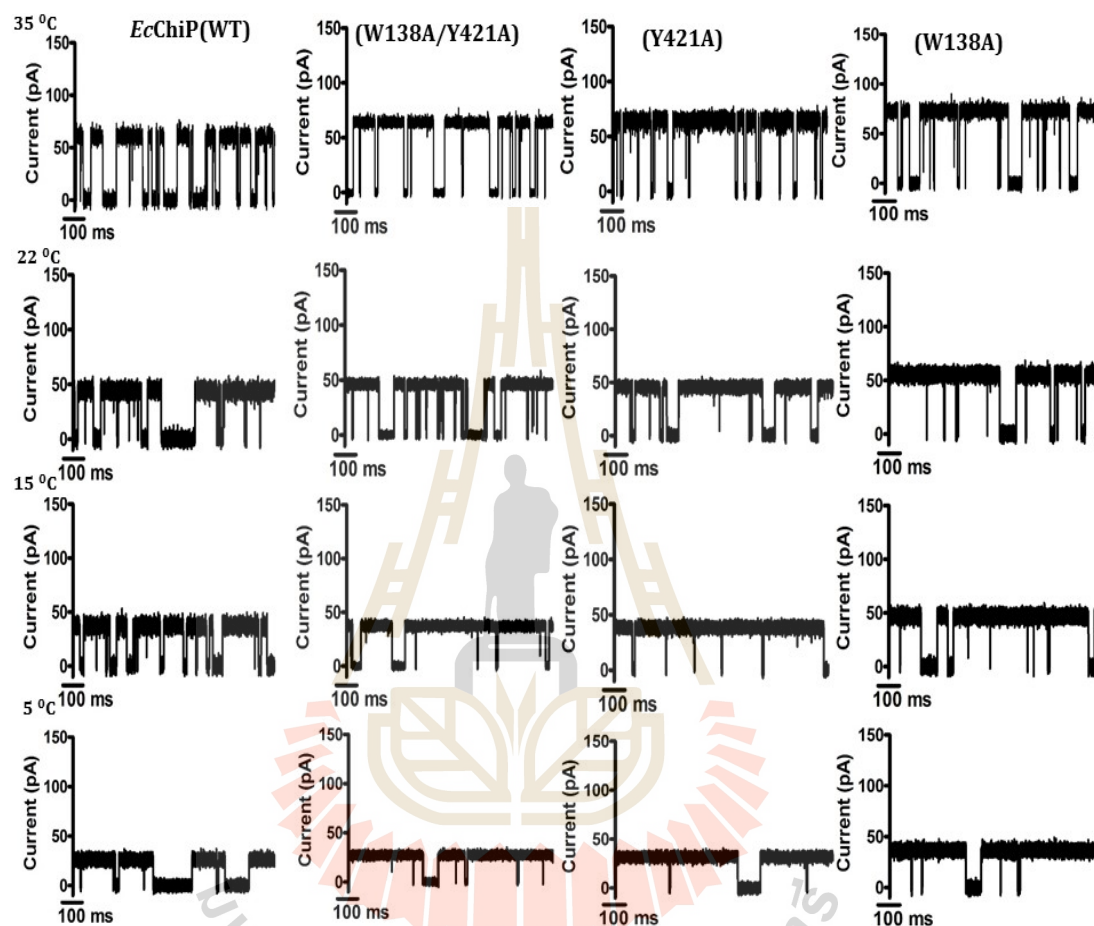
Figure 3.28 Typical ion current recordings through *Ec*ChiP (WT) and its mutants. The

cureent traces are shown at 35, 22, 15 and 5 °C in the presence of 5 µM chitohexaose

at *trans* side, + 100 mV. The experiment was carried out in 1 M KCl in 20 mM HEPES

(pH 7.5).

Ion current fluctuation in the presence of 5 µM chitohexaose caused fully resolved

blockage events and increasing temperature increases the number of events (Figure

3.29A and C) but with substantially shorter residence times (Figure 3.29B and D). It is

interesting to note that the residence time decreases with the increase in temperature, which indicates that at higher temperatures the time spent by the chitohexaose in the channel is shorter for *cis* and *trans* side sugar addition for both wild type and mutants.
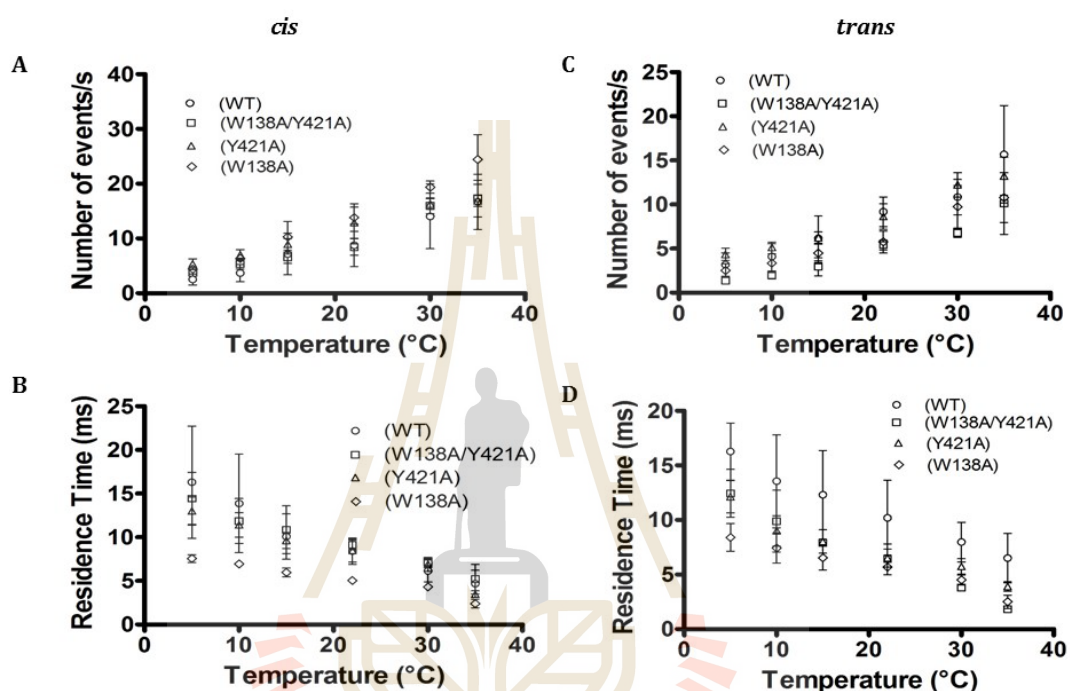
Figure 3.29 Number of events and residence time at different temperatures for *Ec*ChiP and its mutants. (A, C) the number of chitohexaose binding events (B, D) The residence time as a function of temperature from 5 to 35 °C at + 100 mV either sugar on the *cis* or *trans* side. The buffer contained 1MKCl, 20mM HEPES, pH 7.4, and 5 μM chitohexaose added to the *cis* or *trans* side of the lipid membrane (n = 3, mean ± SE).

The temperature-dependent ion-current blockage events were further analyzed using an Arrhenius plot providing the energy barrier for k_{on} and k_{off} (Figure 3.30). The slope of the Arrhenius plot gives the energy barrier in terms of kT.
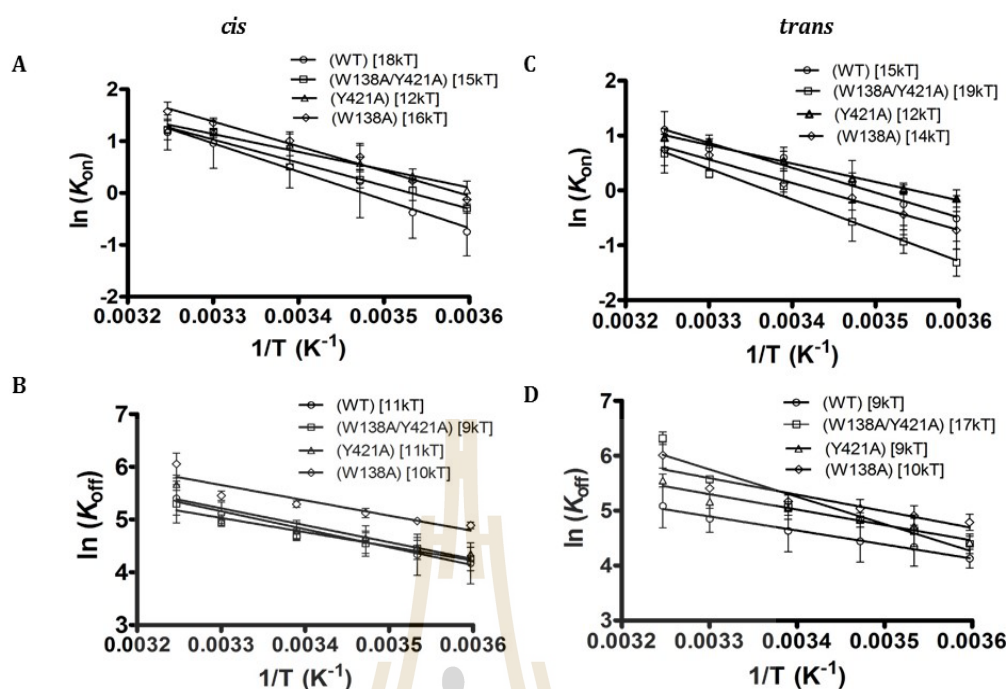
Figure 3.30 The Arrhenius plot of rate constants k_{on} or k_{off} as a function of the inverse of the temperature for chitohexaose. (A, C) k_{on} and (B, D) k_{off} as a function of temperature from 5 to 35 ^{o}C resulting in a linear slope with an energy barrier as shown. The buffer contained 1 M KCl, 20 mM HEPES, pH 7.4, and 5 μM chitohexaose added either to the *cis* or *trans* side of the lipid membrane at applied voltage of + 100 mV (n = 3, mean ± SE).

3.13 Statistical characterization of *Ec*ChiP

From the raw $I(t)$ data (Figure 3.31), it is possible to distinguish two states of the channel as open state ($I(t) \approx I_0$) and close state ($I(t) \approx I_1$) when the monomer is blocked by a sugar molecule. In the absence of sugar, the current $I(t)$ fluctuates about an average value I_0. With $V = 100$ mV, a mean $I_0 \approx 45$ pA was observed (corresponding to a conductance $G = 0.45$ nS) with standard deviation σ_0 about 8 pA. When sugar is added, larger fluctuations in $I(t)$ are observed: the current drops to a value near zero (after the

current decrease, $I(t)$ fluctuates about an average value I_1 of a few pA with a standard deviation similar to σ_0) and can remain low for a period ranging from less than a millisecond to hundreds of milliseconds before returning to values near I_0. As shown in Figure 3.31 top panel in the presence of chitohexaose, on the *cis* or *trans*, open channel I_0 satisfies Ohm's law with $G \approx 0.45$ nS similar to the channel absence of sugar. The current through *Ec*ChiP is always oscillates between two levels I_0 and I_1 (Figure 3.31 bottom panel) confirming *Ec*ChiP as a monomeric channel.
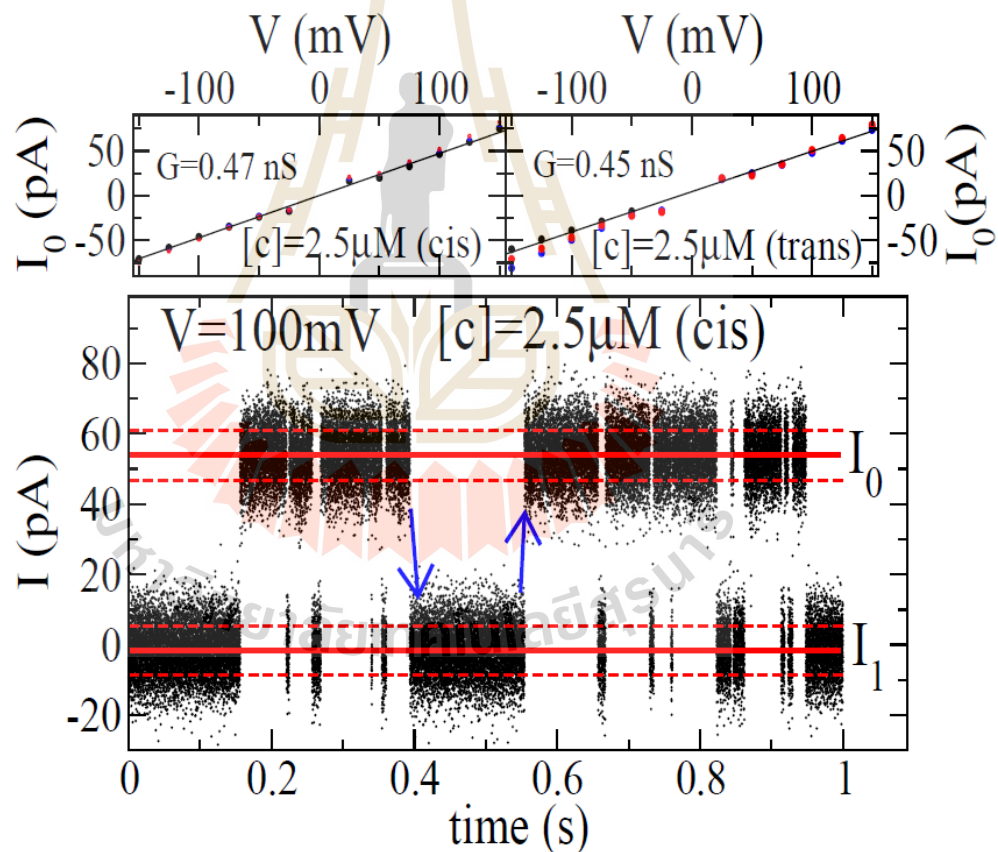
Figure 3.31 The current I through a single monomeric *Ec*ChiP with a concentration $[c]$ of chitohexaose in solution. The electrode on the *cis* side of the channel is at ground while that on the *trans* side has potential V. Lower panel: Current $I(t)$ versus time t with $V = 100$ mV and $[c] = 2.5$ μM on the *cis* side of the membrane (none on the *trans* side).

While the channel is open, $I(t)$ is distributed about a mean I_0 (the solid line indicates I_0 while dashed lanes mark one standard deviation of the distribution). When the channel is blocked by a sugar molecule, the mean I_1 is a within a standard deviation from zero. Trapping (downward arrow) and escape (upward arrow) transitions are seen. Upper panels: The mean current of an open channel versus V with chitohexaose on the *cis* side (left) and *trans* side (right) of the panel. Data for three different *Ec*ChiP samples are shown.

The trapping function $U(t)$ and de-trapping function $B(t)$ can be describes by $U(t) = k_{on}[c]$t and $B(t) = k_{off}$ t. In the case that the probability per unit time for an open monomer to become blocked with sugar is constant and equal to $k_{on}[c]$ then $U(t)$ is linear in time. Similarly, if the probability rate for a blocked monomer to become open is constant and equal to k_{off} then $B(t)$ is linear in time. Figure 3.32 presents experimental results for $U(t)$ and $B(t)$ obtained with varying chitohexaose concentration $[c]$ introduced to the *cis* or *trans* chambers. For these data, the applied voltage was fixed at $V = -100$ mV, so the electric current flows from the *cis* to *trans* chamber. The trapping function $U(t)$ is dependent on concentration and linear in time over its entire range (Figure 3.32 top panel for both *cis* and *trans* side sugar addition), consistent with the behavior of a system with a single constant trapping rate. The de-trapping function $B(t)$ is concentration-independent and non-linear in time (Figure 3.32 bottom panel for both *cis* and *trans* side sugar addition) and represents multiple escape rates. At very small t, (inset of lower left panel in figure 3.32) initial slope is denoted as $B'(0)$ [$B(t) \approx B_0(t) = B'(0) (t - t_{min})$] where $t_{min} = 0.1$ ms. At large t, $B(t)$ is denoted as $B(t) \approx B_\alpha(t)$ where $B_\alpha(t) = \lambda_1 t + B_\alpha(0)$.

The slope of the lines $B_0(t)$ shown are $B'(0) = 0.56$ ms^{-1} and 0.60 ms^{-1} for the *cis* and *trans* sides. The slope for the lines $B_\alpha(t)$ shown, obtained from fits made for $t > 100$ ms, are 0.0070 ms^{-1} and 0.0068 ms^{-1} for the *cis* and *trans* sides. So, $B'(0)$ is nearly two orders of magnitude larger than λ_1. The intercepts $B_\alpha(0)$, obtained by extrapolating the large-t linear behavior back to $t = 0$, are $B_\alpha(0) \approx 2.46$ and 3.02 for the *cis* and *trans* sides.
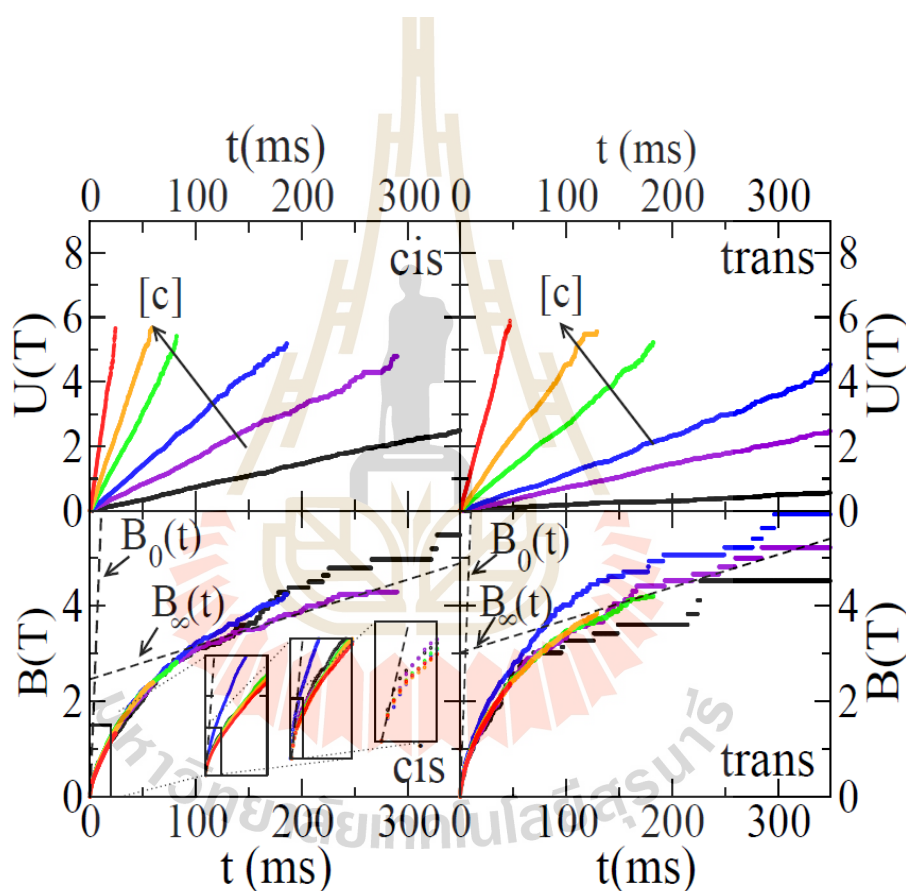
Figure 3.32 Trapping $U(t)$ and de-trapping $B(t)$ functions (the slopes $U'(t)$ and $B'(t)$ are the trapping and de-trapping rates of sugar molecules) of monomeric chitoporin with chitohexaose concentration $[c] =1.25$; 5; 10; 20; 40; 80 µM increasing along arrow (black, violet, blue, green, orange and red curves) on the *cis* (left panels) or *trans* (right) side of the membrane. Data were obtained in 1M KCl solution with a potential $V = -100$ mV on the *trans* side. Upper panels: $U(t) \approx k_{on}[c]t$ is linear in t with a slope

increasing with $[c]$. Lower panels: $B(t)$ is non-linear in t and weakly $[c]$-dependent. In the lower left, successive zooms of the first 20, 5, then 1 ms reveal $t \to 0$ limit of $B(t)$. Dashed lines show a linear fit $B_0(t)$ made in the $t = 0$ limit and another $B\alpha(t)$ made for $t > 100$ ms for $[c] = 5$ µM.

Then assume that all translocation occurs during larger t regions and backwards escape occurs during smaller t regions. Then the fraction P_T (translocation probability) of I_1 events that end with translocation is equal to the fraction of events that end during the large-t regime. That is, $P_T \approx \exp(-B_\alpha[t^*])$ where t^* is the time when the large t regime begins. Since $B_\alpha (0) > \lambda_1 t^*$ in Figure 3.32, we can approximate this by $P_T \approx \exp(-B_\alpha[0])$. So, $\tilde{P}_T \equiv \exp(-B_\alpha[0])$ would provide an experimental measurement of the translocation probability P_T. For the data of Figure 3.32 it gives $\tilde{P}_T = 0.09$ and 0.05 for sugar approaching from the *cis* and *trans* sides.

Similarly, to BLM experiments, voltage-dependent trapping of charged chitosan hexaose sugar was investigated using current traces which obtain at pH 5.5. When chitosan hexaose was added on *cis* side all negative transmembrane potentials result molecular diffusion current flow in the same direction as the electric current while on *trans* side protein addition, all positive transmembrane potentials result molecular diffusion current flow in the same direction as the electric current. Figure 3.33 represents measured $U(t)$ and $B(t)$ for different transmembrane potential in presence of 5 µM chitosan hexaose on the *cis* or *trans* side. Figure 3.33 top panel shows linear behavior of $U(t)$ in time with a slope of $k_{on}[c]$ both *cis* and *trans* side sugar addition and slope increases with increasing potential. When sugars flow against the current (*cis* V>0 and *trans* V<0), $U(t)$ appears noisy as shown in inset on the top panel. As shown in

bottom panel of Figure 3.33, B(t) increases less rapidly in small *t* as membrane potential is increased. For chitosan hexaose on the *cis* side the increase of *B(t)* measured over the first 1ms is $B(t = 1 ms) = 1.8, 1.4, 1.1, 0.95$ for $|V| = 50; 75; 100; 125$ mV, respectively. For chitosan hexaose on the *trans* side, we find $B(t = 1ms) = 2.0; 1.9; 1.7; 1.5$ for $|V| = 50; 75; 100; 125$ mV. The λ_l values are weakly $|V|$-dependent and $B\alpha(0)$ decreases with increasing $|V|$ at larger *t* region Figure 3.33 bottom panel.
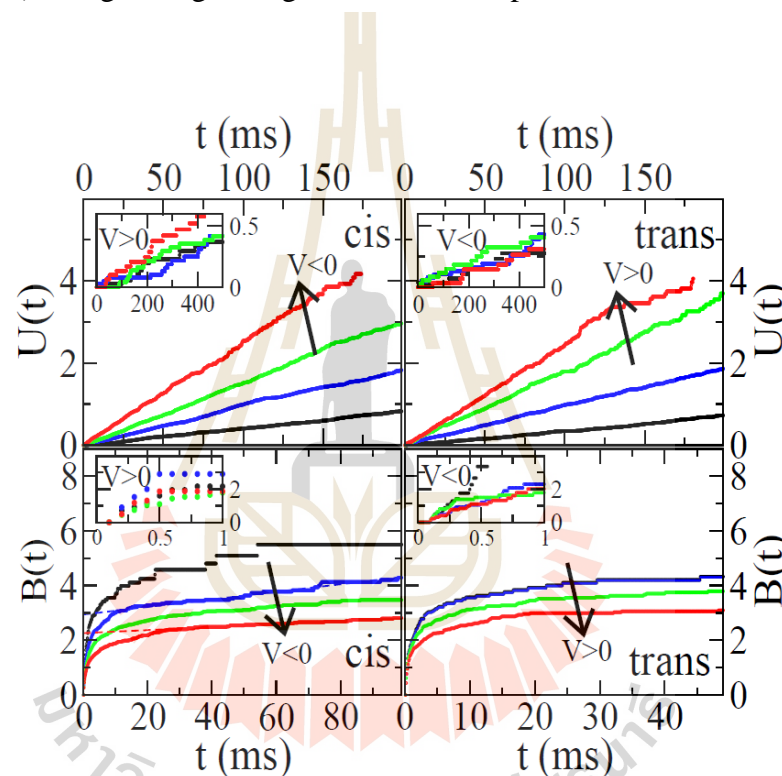
Figure 3.33 Trapping (upper panels) and de-trapping (lower panels) functions measured with concentration $[c] = 5$ µM of chitosan hexaose on *cis* or *trans* sides of the membrane in acidic solution (in which chitosan hexaose acquires positive charge). The potential *V* on the *trans* side is $|V| = 50; 75; 100; 125$ mV in direction of arrow (black, blue, green, red curves) with sign indicated. In main panels (insets), the molecular diffusion current flows in the same (opposite) direction as the electric current. The axes for plots in the insets are the same as for those in main panels. The

fact that $B(t)$ increases more rapidly at small t when $|V|$ is small suggests that $B(t)$ is dominated by backwards escape of chitosan hexaose at small t.

Next, translocation probability of different chitosugars were investigated. Figure 3.34 top panels show trapping rate $k_{on}[c]$ and average residence time τ_c with different concentration $[c]$ of chitohexaose and pentaose. The magnitude of $k_{on}[c]$ appear similar while chitohexaose residence time is nearly five time larger than for chitopentaose. Figure 3.34 bottom panel represents de-trapping function $B(t)$ both chitohexaose and pentaose. The best fit parameters for chitohexaose are $B_\alpha(0) = 1.63$ and $\lambda_1 = 15.8$ s^{-1} while those for chitopentaose are $B_\alpha(0) = 3.86$ and $\lambda_1 = 11.4$ s^{-1}. The associated value of $\tilde{P}_T$ is roughly 0.2 for chitohexaose and 0.02 for chitopentaose.
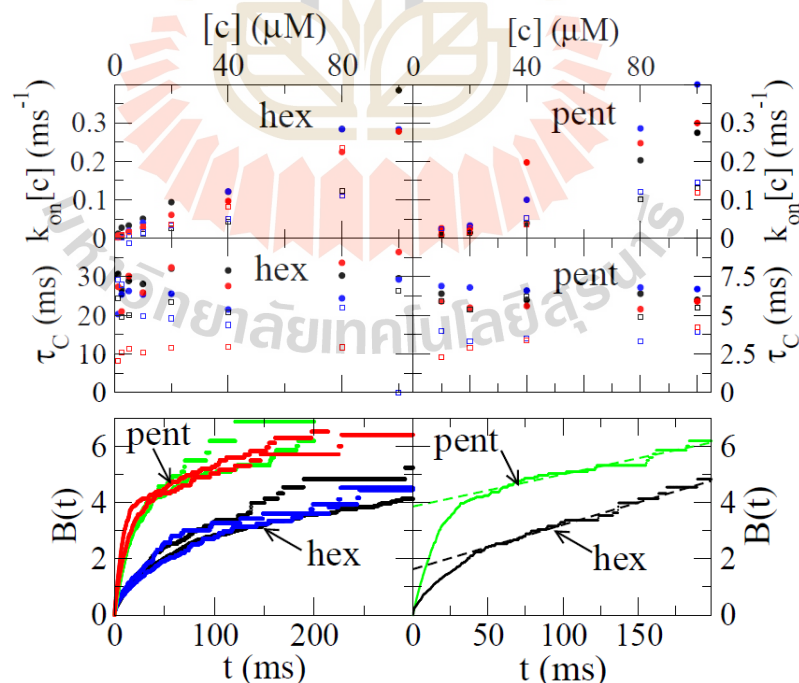
Figure 3.34 Upper four panels: trapping rate $k_{on}[c]$ and average residence time τ_c with concentration $[c]$ of chitohexaose (left) or chitopentaose (right) on the *cis* (closed

circles) or *trans* (open squares) side of membrane. Different colors correspond to different channel samples. Lower left: De-trapping function $B(t)$ for two channel samples, with sugar added to the *cis* (black, green) and *trans* (blue, red) side at concentration $[c]=1.25\,\mu M$ for chitohexaose and $[c] = 10\,\mu M$ for chitopentaose. Lower right: two of the $B(t)$ curves from left shown along with high-t linear fits. The channel appears to preferentially translocate chitohexaose.

PART II

BIOCHEMICAL AND BIOPHYSICAL CHARACTERIZATION OF CHITOPORIN FROM *SERRATIA MARCESCENS*

3.14 Sequence analysis and structure prediction

pET23a(+) expression vector carrying *Serratia marcescens* chitoporin gene containing the 27-amino acid signal sequence was obtained from GenScript USA Inc. Piscataway, USA. The *Sm*ChiP was functionally expressed in Omp-deficient *E. coli* BL21 (DE3) Omp8 Rossetta and the theoretical mass of the full-length (with signal peptide) *Sm*ChiP was 52,066 Da, with a predicted isoelectric point 5.4. The amino acid sequence of *Sm*ChiP (A0A0G8BBQ7) from chitinolytic *Serratia* is 70% identical to the amino acid sequence of *Ec*ChiP (P75733) from non-chitinolytic *E. coli* (Soysa and Suginta, 2016). The amino acid sequence alignment was carried out in ClustalW, and the structure-based alignment was further produced using the program ESPript, v3.0 (Robert and Gouet, 2014). The sequence alignment of both porins is shown in Figure 3.35 and the putative amino acid residues that are important for chitosugar interactions are indicated in red color.
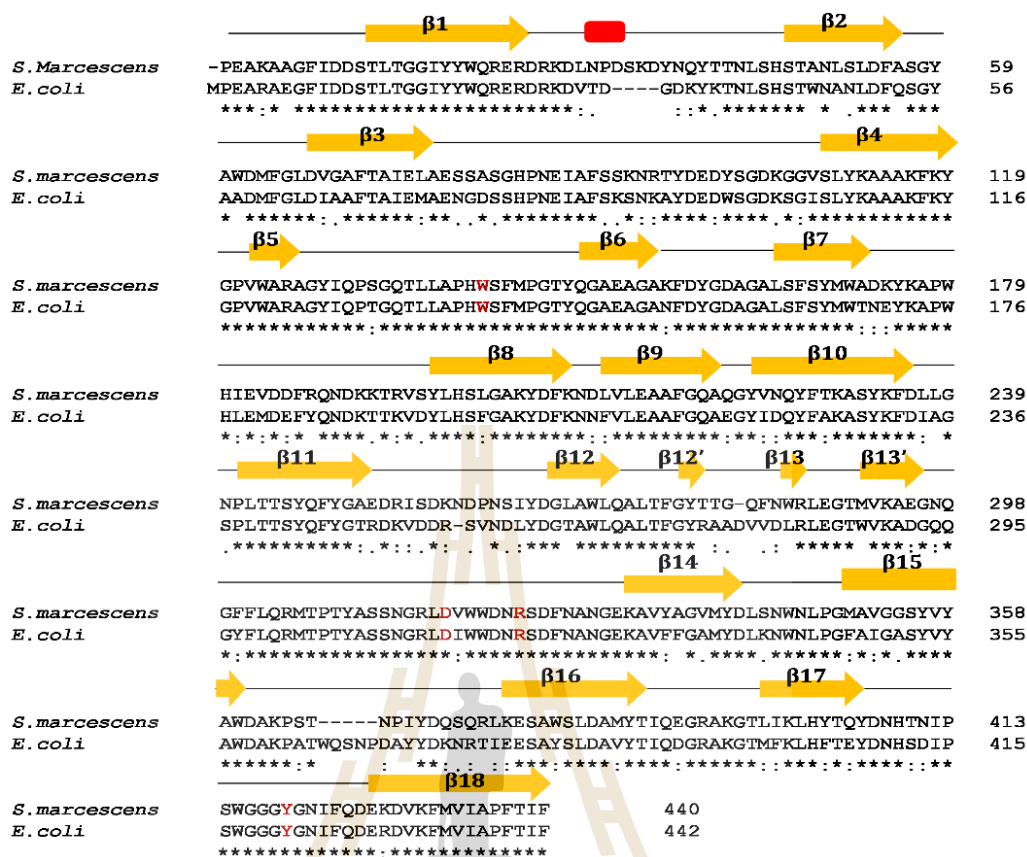
Figure 3.35 Sequence analysis. Multiple sequence alignment of OprD like chitoporins. Amino acid sequences of *Sm*ChiP (A0A0G8BBQ7) and *Ec*ChiP (P75733) were retrieved from Uniprot database. The putative amino acid residues that are important for sugar interaction are indicated in red color. The secondary structure of *Sm*ChiP OprD was constructed by ESPript v3.0 according to the model structure of *Ec*ChiP. β-strands are represented as yellow arrows and α-helix as a red barrel.

To investigate in more detail how the *Sm*ChiP is related structurally to *Ec*ChiP, *Ec*ChiP model structure (Soysa and Suginta, 2016) was used as template for building a model structure of *Sm*ChiP. Figure 3.36 shows a top view of the superimposed predicted β-barrel structure of *Sm*ChiP, consisting of 18 β-strands with *Ec*ChiP modeled structure. *Ec*ChiP structure is shown with β-sheet in green color while *Sm*ChiP structure

is shown with β- sheet in yellow color. Figure 3.35 also shows secondary structural features of *Sm*ChiP with β-strands represented as yellow arrow. Previous reports of the maltoporin (LamB) (Dumas, Koebnik, Winterhalter, and Van Gelder, 2000; Wang et al., 1997) and sucrose-specific porin ScrY (Forst et al., 1998) suggested that aromatic residues and charged amino acids are important for sugar transport. Amino acid residues located within the pore constriction, such as W141, D317, R323 and Y419, (Figure 3.36) are predicted to be crucial for sugar transport and are well aligned with W138, D314, R320 and Y421 respectively, of *Ec*ChiP.
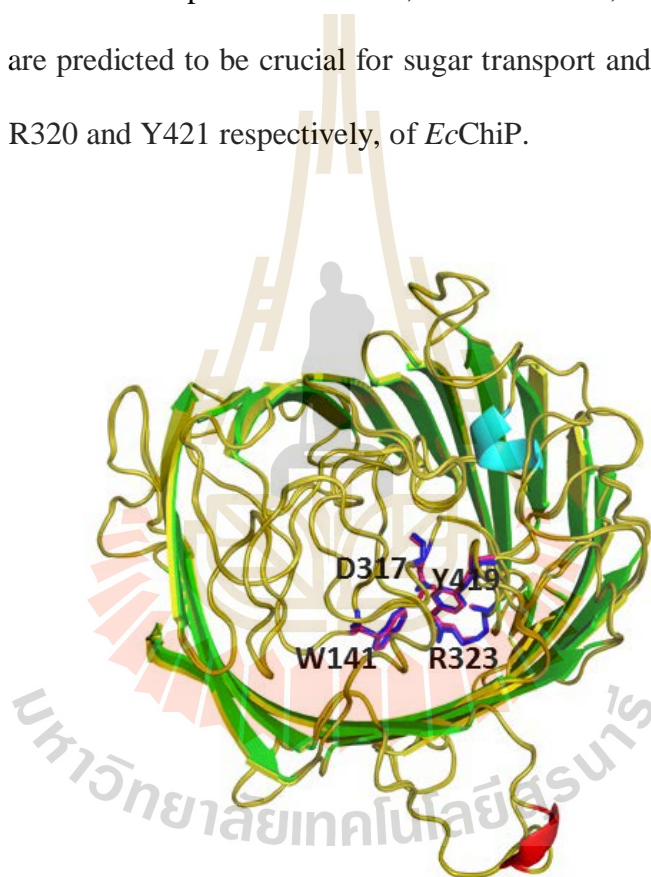
Figure 3.36 Structure prediction of *Sm*ChiP. Top view of superimposition of both conserved amino acids of modeled *Sm*ChiP (in pink stick) with modeled *Ec*ChiP (in blue stick). *Sm*ChiP structure is shown with β-sheet in yellow color, α-helix in red and loops in olive while *Ec*ChiP structure is shown with β-sheet green color, α-helix in cyan and loops in olive.

3.15 Recombinant expression, purification and peptide mass analysis

The recombinant *Sm*ChiP was expressed in the cell wall of the *E. coli* BL21(DE3) Omp8 Rosetta host with the aid of 27-amino acid N-terminal signal sequence. The expressed outer membrane porin of *Sm*ChiP was purified to homogeneity using ion exchange chromatography on a Hitrap Q HP pre-packed column and gel filtration chromatography using a HiPrep 16/60 Sephacryl S-200 high-resolution exclusion chromatography column. Unlike the classical trimeric chitoporins from chitinolytic bacteria (Suginta, Chumjan, Mahendran, Janning et al., 2013), purified *Sm*ChiP shows monomeric behavior on SDS-PAGE (Figure 3.37). *Sm*ChiP did not migrate on SDS-PAGE gel to the position corresponding to a trimer under non-denaturing conditions (Figure 3.37 lane 1; unheated *Sm*ChiP) while it showed similar molecular weight to heated *Sm*ChiP (lane 2; heated *Sm*ChiP).
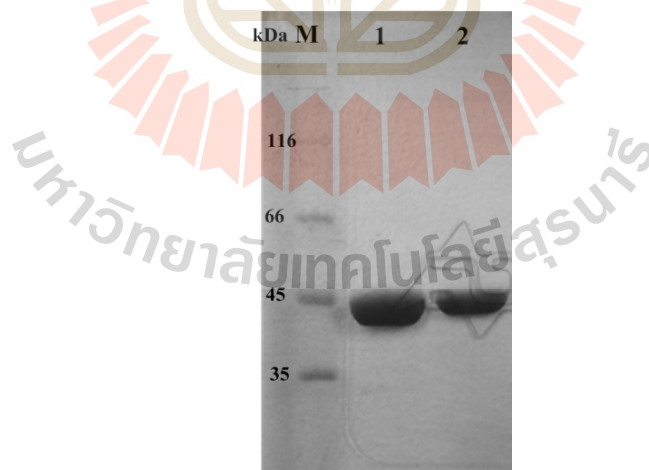
Figure 3.37 Purified *Sm*ChiP, Lane 1, *Sm*ChiP (unheated); 2, *Sm*ChiP (heated).

The purified *Sm*ChiP was subjected to MALDI-TOF mass analysis for confirming the identity of the newly purified protein channel. As summarized in Table 3.8, tryptic

peptides were identified in *Sm*ChiP sequence providing 20% sequence coverage by MALDI-TOF mass spectrometry, confirming that the 50-kDa protein expressed in *E. coli* BL21(DE3) Omp8 Rosetta host was *Sm*ChiP.

Table 3.8 Mass identification of tryptic peptides of *Sm*ChiP by MALDI-TOF mass spectrometry.

Position in the sequence	Expected mass	Observed mass	Peptide AA sequence
144 - 152	1122.5	1123.5	FKYGPVWAR
146 - 152	847.4	848.4	YGPVWAR
202 - 214	1674.7	1675.7	YKAPWHIEVDDFR
204 - 214	1383.8	1384.6	APWHIEVDDFR
258 - 281	2755.1	2756.1	ASYKFDLLGNPLTTSYQFYGAEDR
262 - 281	2305.9	2306.9	FDLLGNPLTTSYQFYGAEDR
321 - 331	1265.5	1266.5	AEGNQGFFLQR
343 - 350	1102.4	1103.4	LDVWWDNR
403 - 420	2112.9	2113.9	LKESAWSLDAMYTIQEGR
405 - 420	1871.7	1872.7	ESAWSLDAMYTIQEGR

3.16 Molecular weight determination of *Sm*ChiP by electrospray

The monomeric behavior of newly purified protein was confirmed by intact mass analysis by electrospray. Intact mass analysis by ESI-LC mass spectrometry allows determining the molecular weight with high precision (Banerjee and Mazumdar, 2012).

ESI-LC MS analysis of the *Sm*ChiP sample is shown as individual spectra (Figure 3.38) and all the peaks appearing in the ESI-mass spectrum represent the intact molecular species with variable charging. The vertical axis represents the relative abundances (intensity) of multiply charged species of the *Sm*ChiP, and the horizontal axis represents the mass to charge ratio (m/z) of the multiply charged analyte. Then the molecular mass of the *Sm*ChiP was determined by charge deconvolution (Covey, Bonner, Shushan, and Henion, 1988) and deconvoluted ion series of *Sm*ChiP is shown Figure 3.38 inset. The observed intact mass of *Sm*ChiP (49085 Da) from electrospray was consistent with the predicted theoretical mass of monomeric protein (49470 Da).
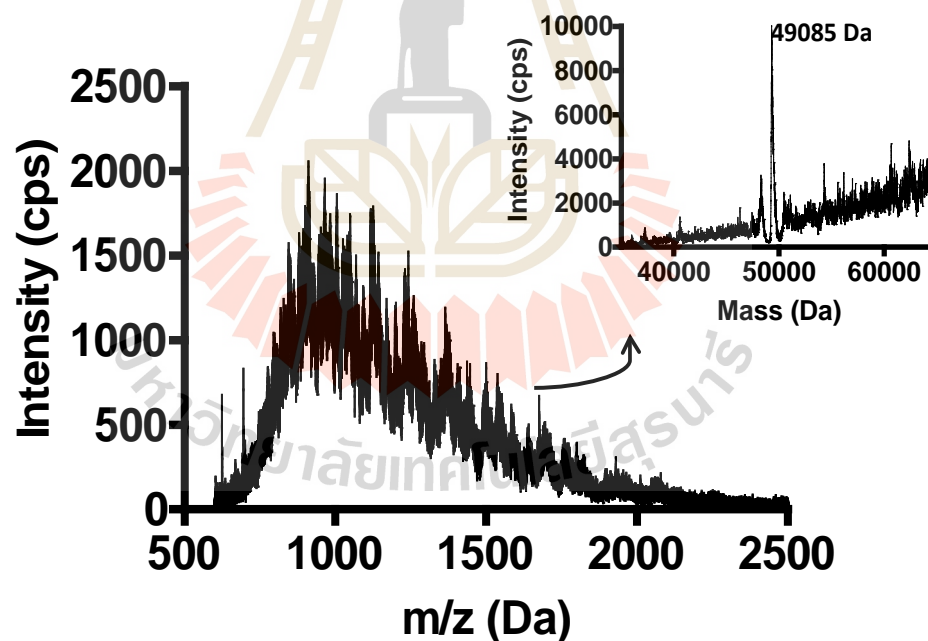
Figure 3.38 Molecular weight determination by electrospray. ESI Spectrum of *Sm*ChiP collected from 600 to 3200 m/z from positive ion electrospray MS analysis. Inset; deconvoluted ion series of *Sm*ChiP.

3.17 Assay of sugar permeation by proteoliposome swelling

Liposome assays give an idea of sugar permeability through protein channels. As shown in Figure 3.39A, we first checked the channel permeability with different sugar molecules varying in molecular weight from 180 Da to 600 Da. The smallest sugar, arabinose, was set to 100% permeability while branched raffinose, a non-permeant sugar, was used to determine isotonicity. Isotonic concentration was found to be 70 mM and the same concentration of sugar was then used in the swelling experiments (Figure 3.39A). All monosaccharides, glucose, galactose and mannose permeated at nearly 100% swelling rate. 70 mM GlcNAc, the monomeric sugar from chitin, also showed a higher permeation rate. But in contrast to normal diffusion porins (Aunkham et al., 2014; Nikaido and Rosenberg, 1983; Saint et al., 1996) we could not see permeation by sucrose, maltose and melezitose, reflecting a pore constriction limit of >200 Da, similar to *Ec*ChiP (Soysa and Suginta, 2016). Then in the next set of experiments we checked the permeation rate of different length chitooligosaccharides, for checking channel specificity towards chitosugars. Only 2.5 mM concentration was used by adjusting isotonic concentration with raffinose (Figure 3.39B). More interestingly, permeation by chitosugars was observed irrespective of the molecular weight. When compared to chitotriose (GlcNac$_3$) and chitohexaose (GlcNAc$_6$), chitotetraose and chitopentaose showed better permeation. Maltohexaose could not permeate through *Sm*ChiP.
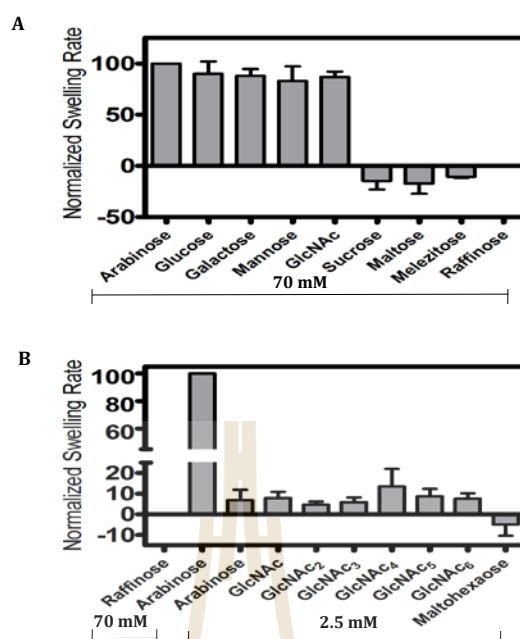
Figure 3.39 Proteoliposome swelling assays. D-raffinose was used to determine isotonic concentration, with no change in absorbance at 500 nm of the proteoliposome suspension over 60s and L-arabinose swelling rate was set to 100% to obtain normalized swelling rate. The permeability of the channel was assumed to be proportional to the swelling rate. (A) Permeation of different types of sugars through *Sm*ChiP reconstituted liposomes. (B) Permeation of chitooligosaccharides through *Sm*ChiP. Maltodextrins were used as control. Values are as means ± SD, obtained from 3 independent sets of experiments.

3.18 Thermodynamics of chitohexaose and chitopentaose binding to *Sm*ChiP

To gain thermodynamic insight into binding of chitooligosaccharides $GlcNAc_6$ and $GlcNAc_5$ to *Sm*ChiP, ITC experiments were carried out. To confirm *Sm*ChiP specificity towards chitoligosaccharides, structurally related maltohexaose was

checked in ITC. Figures 3.40A and 3.40B show the typical ITC profiles for the binding of $GlcNAc_6$ and $GlcNAc_5$ to SmChiP. No measurable binding occurs when using structurally related maltohexaose (Figure 3.40C). Figure 3.40D and 3.40E show the theoretical fit of the integrated heat using a one-site binding model for $GlcNAc_6$ and $GlcNac_5$ respectively. Visible integrated heat was not observed since maltohexaose is not binding to SmChiP (Figure 3.40F).
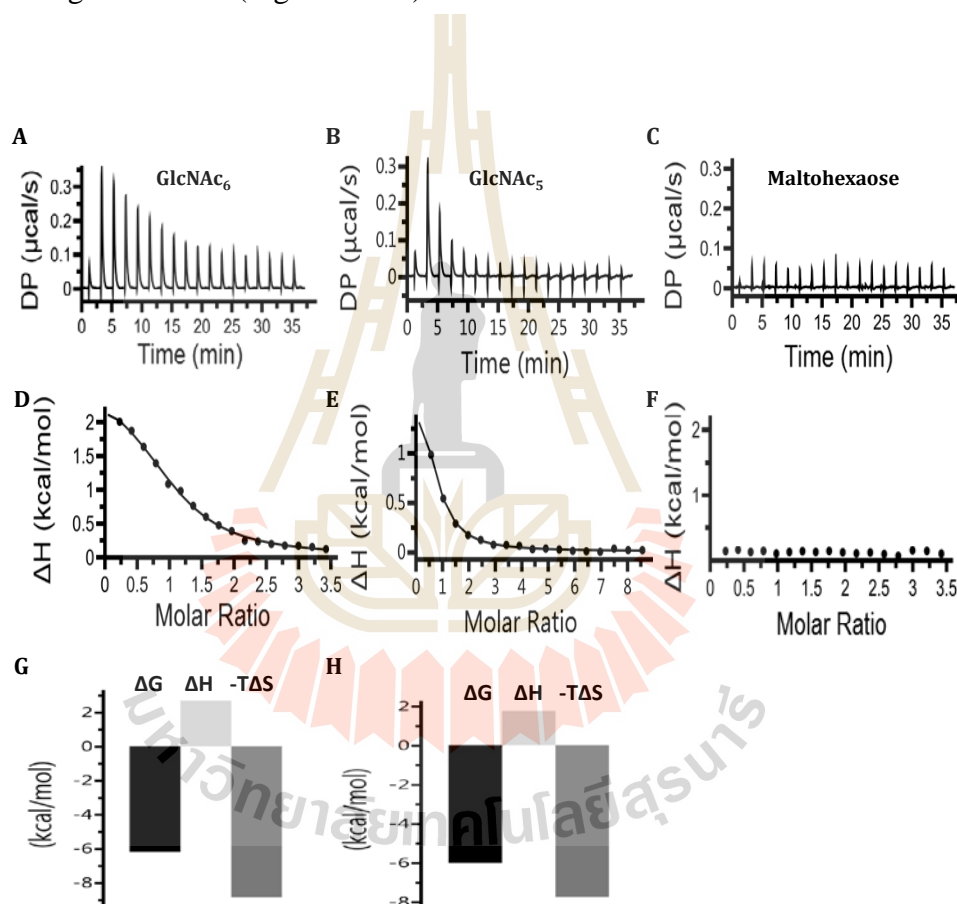
Figure 3.40 Calorimetric titration for the binding of chitohexaose, chitopentaose and maltohexaose to SmChiP. ITC profile corresponding to the (A) binding of chitohexaose (B) binding of chitopentaose (C) binding of maltohexaose to SmChiP. (D) Integrated heat of binding for chitohexaose obtained from raw data, after subtracting the heat of dilution. The solid line represents the best curve fit to the experimental data using one set of sites model from Microcal PEAQ-ITC. (E) Integrated heat of binding for

chitopentaose obtained from raw data, after subtracting the heat of dilution. (F) Integrated heat of binding obtained from raw data for maltohexaose (G) Signature plot representation for comparison of free energy change (ΔG), enthalpy change (ΔH) and the entropy change ($-T\Delta S$) of chitohexaose binding. (H) Signature plot representation for comparison of free energy change (ΔG), enthalpy change (ΔH) and the entropy change ($-T\Delta S$) of chitopentaose binding.

Since ITC is extremely sensitive, it is vital to measure enthalpy changes only from binding interactions, and eliminate or significantly minimize enthalpy changes from other processes. Three control reactions were used for getting the binding interactions of *Sm*ChiP with all sugars as mentioned in above. Especially buffer to protein control was used to compare any mismatch in detergent concentrations. Analysis of ITC data yields the K_d for $GlcNAc_6$ and $GlcNAc_5$, which are 17 µM and 23 µM, and all the fitted parameters for a single site binding model from three independent titrations in ITC experiments are listed in Table 3.9. As shown in the signature plot (Figure 3.30G and 3.40H for $GlcNAc_6$ and $GlcNAc_5$ respectively), the enthalpy change (ΔH), entropy change ($-T\Delta S$) and free energy change (ΔG) gained from ITC experiments prove that chitohexaose and chitopentaose binding to *Sm*ChiP is solely driven by favorable entropy change ($-T\Delta S$) and opposed by positive enthalpy change (ΔH). The results indicate that hydrophobic interactions are the major forces governing chitosugar binding.

Table 3.9 Thermodynamic parameters obtained by isothermal titration calorimetry for chitohexaose and chitopentaose binding to *Sm*ChiP.

	N (sites)	K_D (μM)	ΔH (kcal/mol)	ΔG (kcal/mol)	-TΔS (kcal/mol)
$GlcNAc_6$	1.00 ± 0.03	16.96 ± 0.64	2.81 ± 0.25	-6.18 ± 0.02	-8.99 ± 0.26
$GlcNAc_5$	0.60 ± 0.09	23.00 ± 2.00	1.97 ± 0.22	-6.02 ± 0.05	-7.98 ± 0.20

3.19 Channel properties of *Sm*ChiP and channel specificity

The monomeric behavior on SDS-PAGE is fully consistent with BLM measurements, which indicate a stable monomeric channel. Figures 3.41A and 3.41B show typical ion current traces acquired over 2000 ms at +100 mV and -100 mV respectively. The channel was found to open almost constantly with applied transmembrane potential from ±25 mV to ±150 mV. Multi-channel reconstitution experiments (Figure 3.41C) further confirm the mean channel conductance of 0.53 ± 0.4 nS from 65 independent channel insertions, obtained from Gaussian distribution fitting of the histogram as shown in Figure 3.41C inset. Slop of the I/V curve (Figure 3.41D for 9 independent single channel insertions) obtained from single channel analysis yields a channel conductance of 0.54±0.01 nS, fully consistent with multi-channel insertions channel conductance.
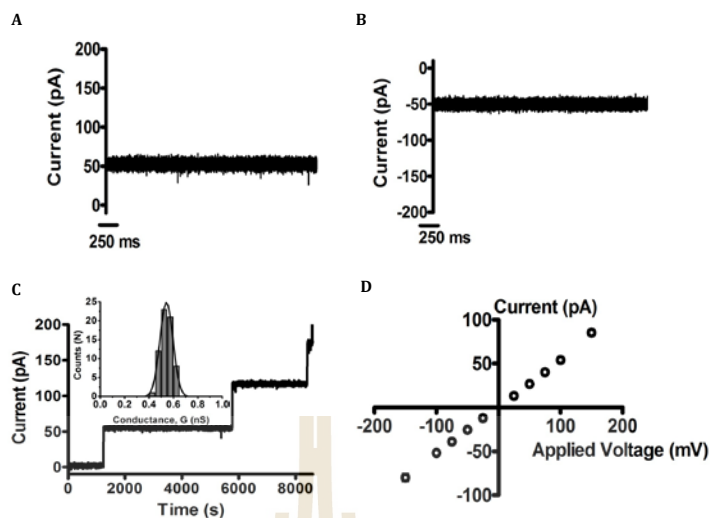
Figure 3.41 Pore-forming properties of *Sm*ChiP in artificial lipid membranes. Lipid bilayers were formed across a 60 μm aperture by the lowering and raising technique, using 5 mg.mL^{-1} DPhPC and bathed on either side in 1M KCl in 20 mM HEPES, pH 7.4. The protein was added to the *cis* side of the chamber. (A) Fully open *Sm*ChiP current trace at +100 mV (B) Fully open *Sm*ChiP current trace at -100 mV (C) Multiple channel insertions. Inset: Histogram of the conductance steps observed for 65 independent channel insertions. The black line represents a single Gaussian fit. (D) I-V plot for *Sm*ChiP single channel. The average current values were obtained for 9 independent channel insertions.

So far, ITC experiments together with liposome swelling assays showed *Sm*ChiP channel specificity toward chitosugars. In the next series of experiments, the channel specificity was confirmed by electrophysiology. Sugar was added into either *cis* or *trans* side and ion current blockages were observed at both negative and positives voltages for 2 min. Before addition of sugars, *Sm*ChiP fully open channel was stable in

the bilayer (Figure 3.42A) and only 500 ms current traces for sugar addition in *cis* side are shown, at -100 mV for all sugars. The chitosugars with different length were tested with single channels which were reconstituted in artificial bilayer. GlcNAc and GlcNAc$_2$ (Figure 3.42B and 3.42C respectively) showed no frequent blockages, indicating rapid passage of sugar molecules through channel, and infrequent current spikes indicate the weak interactions of sugar molecules with the channel constriction. GlcNAc$_3$ addition (Figure 3.42D) showed noticeable ion current fluctuations with short-lived transient blockages. Addition of the chitooligosaccharides chitotetra-, penta-, and hexaose resulted in frequent complete current blockages in *Sm*ChiP, reflecting strong sugar-channel interactions (Fig. 3.42E-G). In contrast, subsequent addition of 200 µM maltohexaose (Figure 3.42H) had no detectable effect of ion current blockage, confirming the results from both ITC and swelling experiment of *Sm*ChiP's specificity for chitosugars.
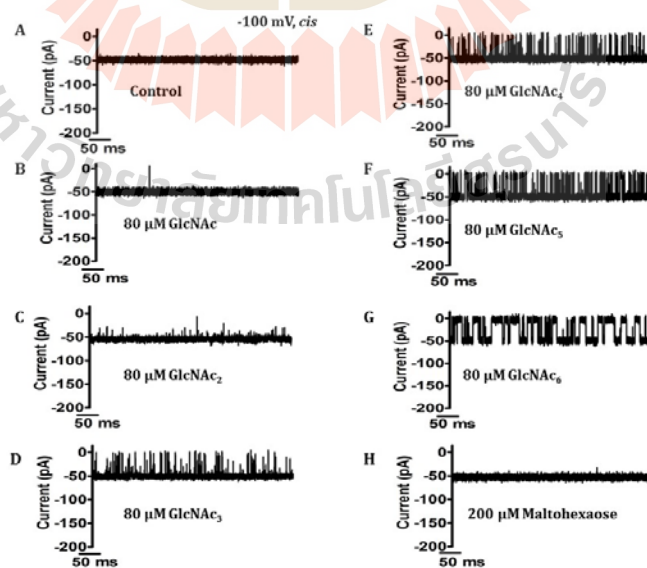
Figure 3.42 *Sm*ChiP channel specificity. Ion current fluctuations were monitored for 120s at applied potentials of +/-100 mV with sugars on either *cis* or *trans* side. Here,

only current traces for 500 ms at -100 mV, *cis* are presented. (A) A fully open state of *Sm*ChiP before sugar addition. Then (B) GlcNAc (*N*-acetylglucosamine), (C) Chitobiose (GlcNAc$_2$), (D) Chitotriose (GlcNAc$_3$), (E) Chitotetraose (GlcNAc$_4$), (F) Chitopentaose (GlcNAc$_5$) and (G) Chitohexaose (GlcNAc$_6$) were added on the *cis* side of the chamber to a final concentration of 80 µM. (H) Control recording with maltohexaose at a concentration of 200 µM.

3.20 Kinetics of chitooligosaccharide translocation through *Sm*ChiP

To complement the results of proteoliposome swelling assays and ITC experiments, BLM experiments were performed to monitor the interaction of chitooligosaccharides with *Sm*ChiP and evaluate binding kinetics. The sugar-induced current blocking is clearly concentration-dependent similar to maltoporin (Bezrukov et al., 2000) and chitoporin from *V.* harveyi (Suginta, Chumjan, Mahendran, Schulte et al., 2013). The effect of applied voltages on sugar passage was investigated from both *cis* and *trans* sides at various concentrations. Figure 3.43A-E shows ion current fluctuations with five different concentrations of chitohexoase (2.5, 5, 10, 20 and 40 µM), addition at *cis*, +100 mV. Then the quantitative analysis of the binding kinetics was carried out to access the channel affinity. The k_{on} rate of chitohexaose is shown in Figure 3.43F for all four regimes and shows no significant difference when sugar is entering channel from *cis* or *trans* side. The k_{on} values are slightly decreased with increasing concentration due to saturation of the channel with high concentration of sugar. Figure 3.43G shows a dwell-time histrogram for 2.5 µM chitohexaose at *cis*, +100 mV where we obtain τ_c, the average residence (dwell) time (s) of the sugar molecule in the channel by the exponential fit of the dwell-time histogram. The calculated k_{off} from residence time is shown in Figure 3.43G inset for all concentration

ranges tested for four different regimes. However, the τ_c values did not alter significantly with sugar concentration, indicating that the time taken by sugar molecule to stay inside channel is concentration-independent.
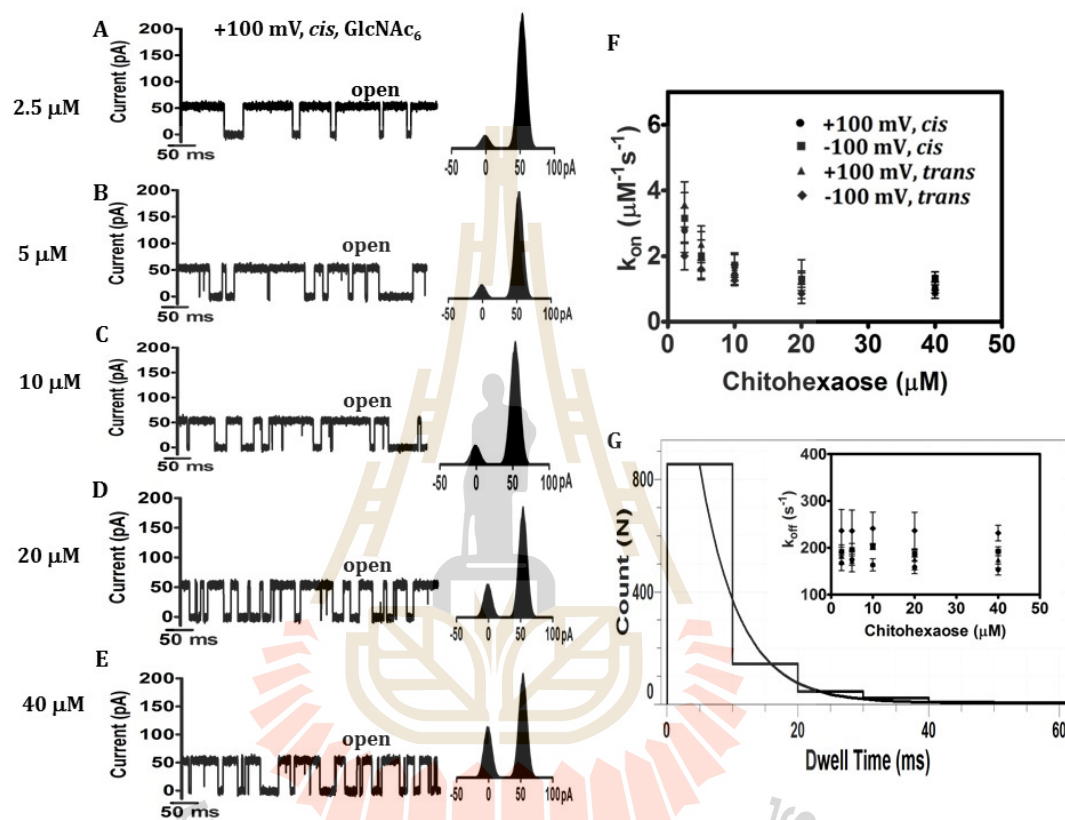
Figure 3.43 Single channel analysis. (A-E) left panel; Typical ion current recording at *cis*, +100 mV, in the presence of chitohexaose for five different concentrations. (A-E) right panel; Histogram for open and closed states of the channel (F) Association rate of chitohexaose as a function of sugar concentration; sugar at either *cis* or *trans* ± 100 mV (G) Dwell-time histogram of chitohexaose, inset: dissociation rate of chitohexaose as a function of sugar concentration; sugar at either *cis* or *trans* ± 100 mV.

Table 3.10 summarizes the kinetic values obtained from four different regimes. The k_{on} values for chitotetraose and chitopentaose differ by a factor of ~2 when compared with chitohexaose. Moreover, a fifteen-fold change k_{off} was observed for chitotetraose when compared with chitohexaose. To elucidate the binding affinity, binding constants for each chitooligosaccharide were calculated (Table 3.10). Based on the calculation, we see that with increasing sugar length, there is an increase in binding affinity, which implies that longer chain sugar molecules stay longer inside the channel during their passage through it. However, there is no significant difference when sugar molecules are added *cis* or *trans*. The relative values of K determined by BLM were consistent with those obtained from ITC.
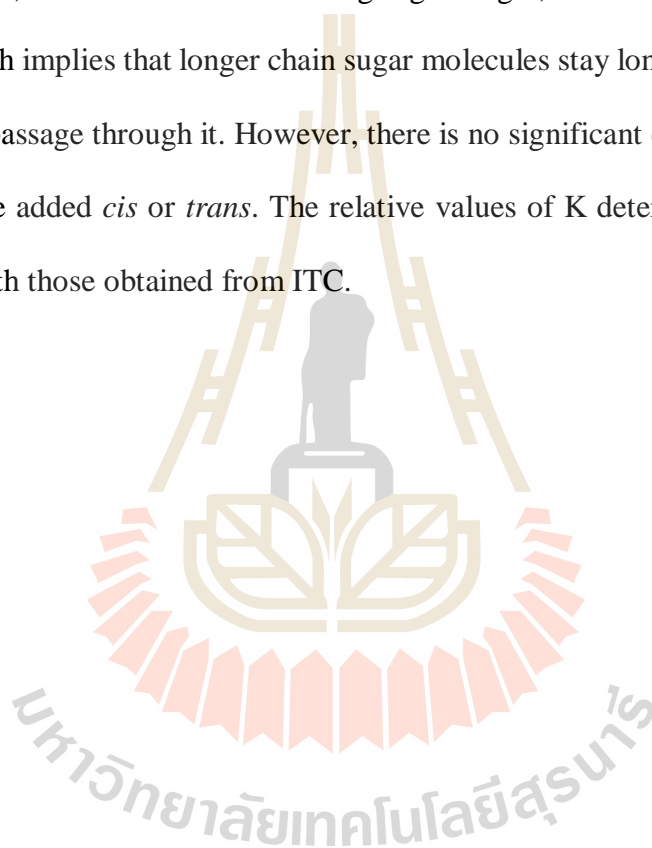
Table 3.10 Substrate specificity of *Sm*ChiP.

Substrate	*cis* side addition						*trans* side addition					
	+100 mV			-100 mV			+100 mV			-100 mV		
	(k_{on}) 10^6 $M^{-1}{\cdot}s^{-1}$	(k_{off}) s^{-1}	(K) M^{-1}	(k_{on}) 10^6 $M^{-1}{\cdot}s^{-1}$	(k_{off}) s^{-1}	(K) M^{-1}	(k_{on}) 10^6 $M^{-1}{\cdot}s^{-1}$	(k_{off}) s^{-1}	(K) M^{-1}	(k_{on}) 10^6 $M^{-1}{\cdot}s^{-1}$	(k_{off}) s^{-1}	(K) M^{-1}
GlcNAc$_2$		ND			ND			ND			ND	
GlcNAc$_3$		ND			ND			ND			ND	
GlcNAc$_4$	6±2.5	3197±447	2000±106	6±2	2810±160	2200±870	8±1.7	3690±414	2222±374	5±1.2	3790±885	1288±486
GlcNAc$_5$	6±2	756±84	8160±2912	6±2	777±96	8190±2676	6±1	760±40	7833±1406	4±0.6	870±39	4447±901
GlcNAc$_6$	3±0.6	168±16	16660±4074	3±0.7	192±14	16530±4240	4±0.6	183±18	19690±4457	2±0.4	236±45	8497±930

The on-rate (k_{on}, $M^{-1}{\cdot}s^{-1}$) is given by number of blocking events (s^{-1})/[sugar concentration]. Here sugar concentration = 2.5 µM.

The off-rate (k_{off}, s^{-1}) was obtained from Eq. $k_{off} = 1/\tau_c$ where τ_c is the average residence (dwell) time (s) of the sugar molecule in the channel.

The equilibrium binding constant (K, M^{-1}) = k_{on}/k_{off}

ND, No well-resolved blocking events (residence time could not be evaluated with confidence).

3.21 Effects of N-acetyl side chains on chitooligosaccharide

translocation through *Sm*ChiP

Similarly to *Ec*ChiP, two different pH conditions were selected and single *Sm*ChiP channel behavior, reconstituted in planar bilayer, was observed in the absence of sugar. As shown in Figure 3.44 the channel was stable at both pH conditions without ion current fluctuations.
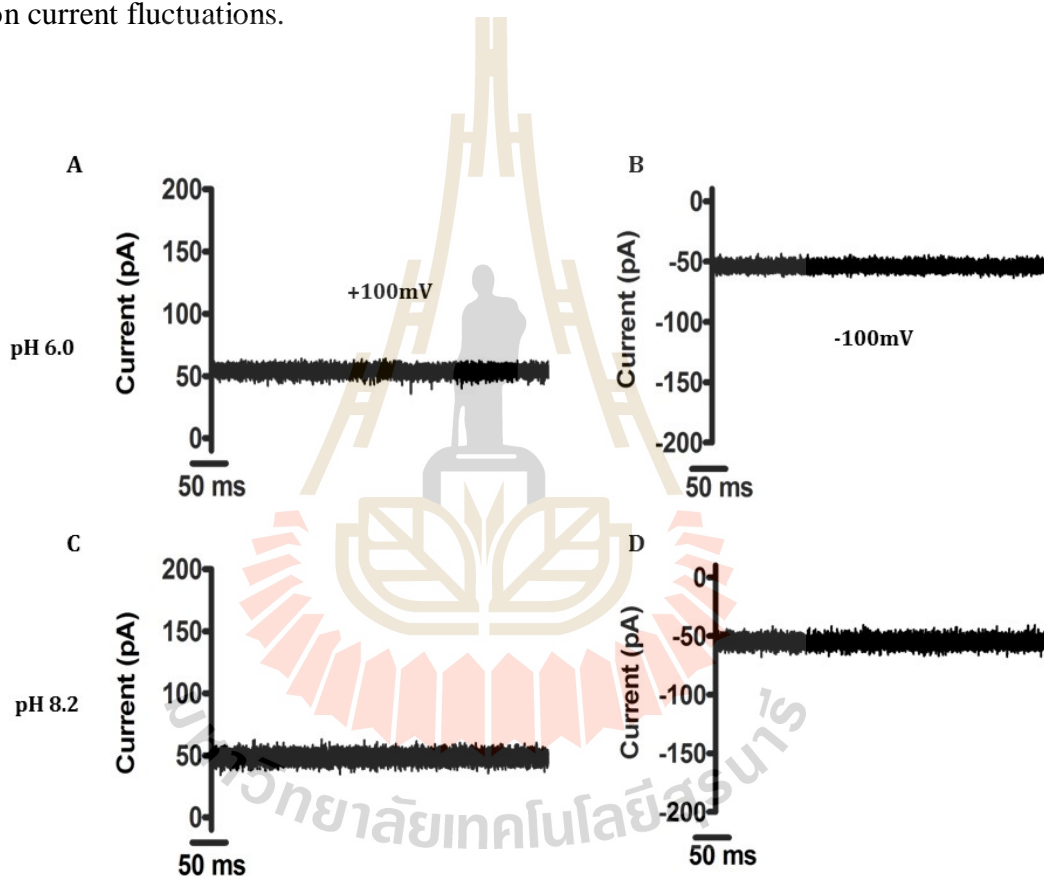
Figure 3.44 Effect of pH on *Sm*ChiP conductance. Typical ion current recording through a single *Sm*ChiP, at various pH values and in the absence of sugar. The transmembrane potential was +100 mV (left panel) (A) at pH 6 and (C) at pH 8.2 and right panel potential – 100 mV (B) at pH 6 and (D) at pH 8.2. The bathing solution contained 1 M KCl in 20 mM HEPES pH 8.2 or in 20 mM MES pH 6.0.

Single channel analysis of planar lipid bilayer measurements showed low affinity for chitosan hexaose, lacking the N-acetyl group at C2 of the glucosyl ring, at neutral pH (see the chitosan hexaose structure in the top panel, Figure 3.14). Addition of chitohexaose on the *trans* side at pH 6.0 caused sugar blocking events with long residence time either with positive (Figure 3.45 right panel) or negative transmembrane voltages (Figure 3.46, right panel). Increasing chitohexaose concentrations from 10 to 80 μM caused more blocking events. If chitosan hexaose was added on the *trans* side, blocking events were detectable at positive voltages (Figure 3.45 left panel) only. Similarly to chitohexaose, increasing concentrations of chitosan hexaose caused more blocking events.
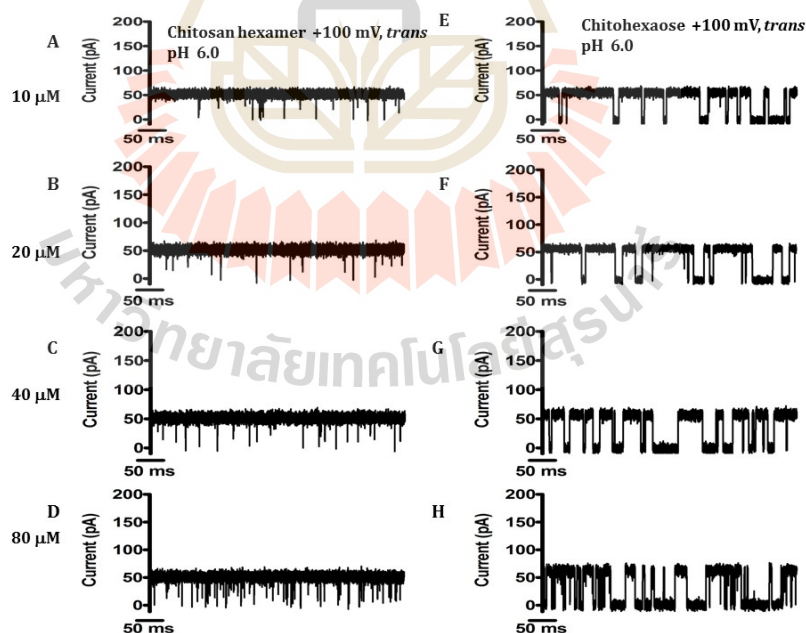
Figure 3.45 Effect of N-acetyl functionality on *Sm*ChiP at pH 6.0 (sugar on the *trans*, positive membrane potentials). Ion current fluctuations were monitored for 120 s at applied potentials of + 100 mV with sugar addition on the *trans* side. Here only current

traces for 500 ms are presented, with four different chitosan hexaose concentrations (A-D, left panels) and four different chitohaxaose concentrations (E-H, right panels).

In contrast, chitosan hexaose did not show interactions with *Sm*ChiP if negative transmembrane voltages were used (Figure 3.46) when sugar was added on the *trans*. Moreover, when sugars were added on the *cis* side, chitohexaose showed similar behavior to *trans* either at positive or negative voltages (see Supplementary Figure 9 and 10), but chitosan hexaose showed interactions only at negative voltages (see Supplementary Figure 9 and 10).
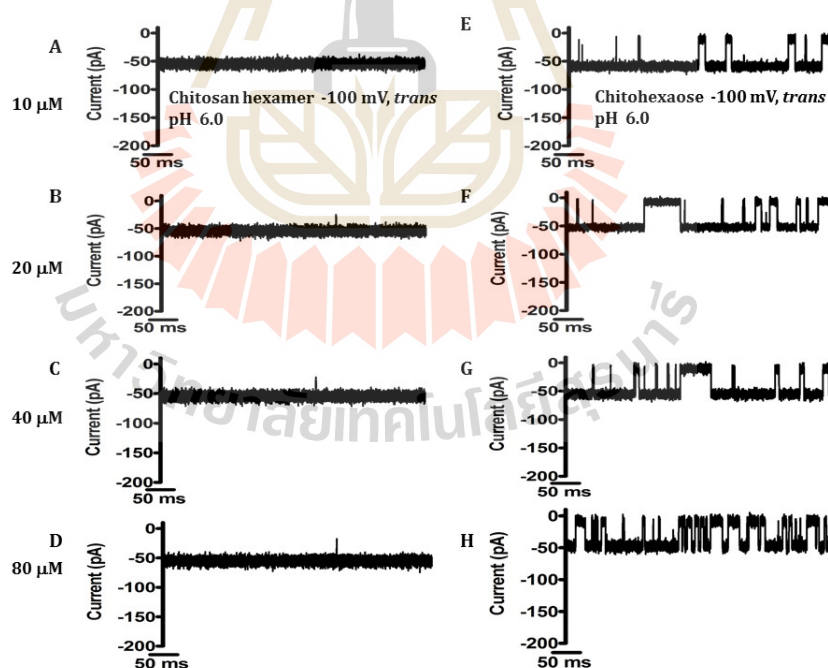
Figure 3.46 Effect of N-acetyl functionality on *Sm*ChiP at pH 6.0 (sugar on the *trans*, negative membrane potentials). Ion current fluctuations were monitored for 120 s at applied potentials of – 100 mV with sugar addition on the *trans* side. Here only current

traces for 500 ms are presented, with four different chitosan hexaose concentrations (A-D, left panels) and four different chitohaxaose concentrations (E-H, right panels).

Then we recorded ion current fluctuations at pH 8.2, at which both chitosan hexaose and chitohexaose are uncharged. Figure 3.47 and 3.48 represent the ion current blocking events at pH 8.2 when sugars were added on *trans* side positive and negative transmembrane voltages respectively.
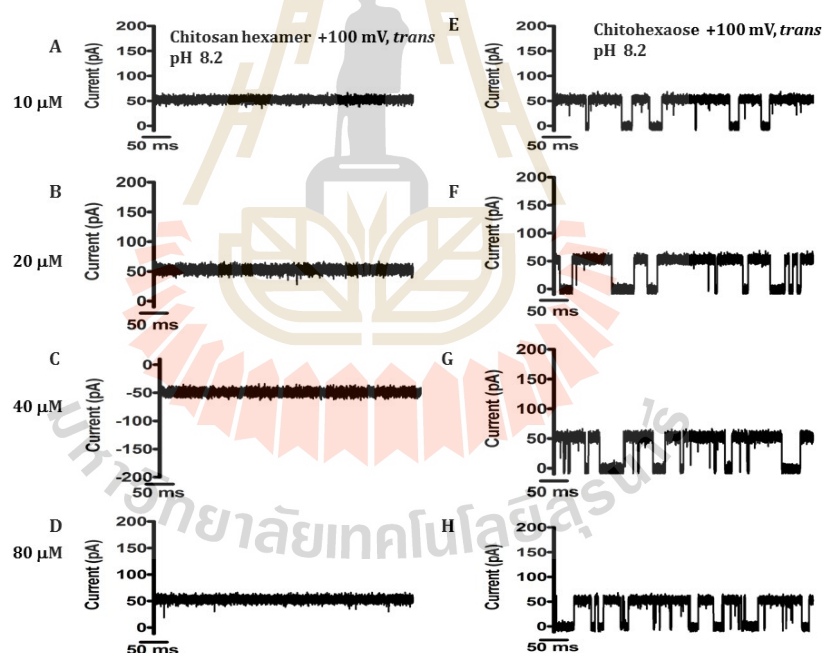
Figure 3.47 Effect of N-acetyl functionality on *Sm*ChiP at pH 8.2 (sugar on the *trans*, positive membrane potentials). Ion current fluctuations were monitored for 120 s at applied potentials of + 100 mV with sugar addition on the *trans* side. Here only current traces for 500 ms are presented, with four different chitosan hexaose concentrations (A-D, left panels) and four different chitohaxaose concentrations (E-H, right panels).

When the pH of the working electrolyte was raised above the $p\text{K}_a$ of chitosan hexaose to pH 8.2, no disturbance of the I(t) trace was observed. Both positive transmembrane potentials and negative transmembrane potentials show the fully-open state of the monomeric *Sm*ChiP channel (Figure 3.47 and 3.48).
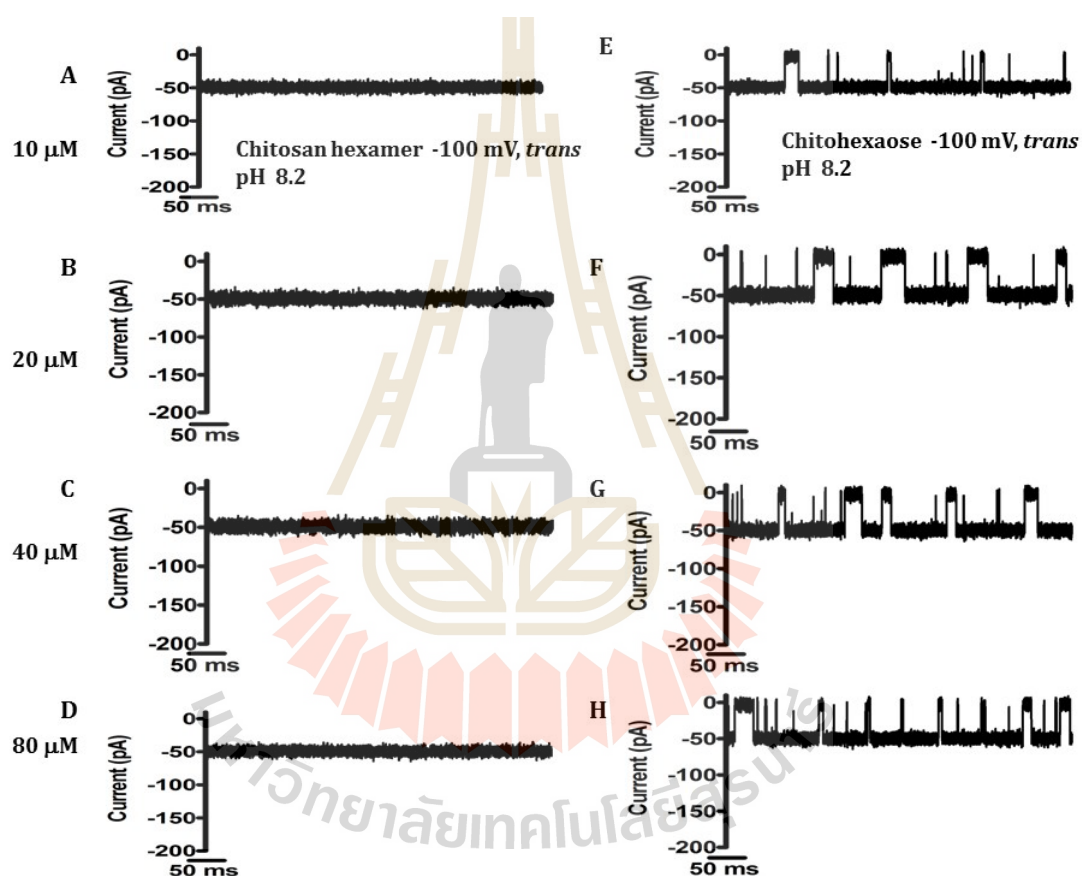
Figure 3.48 Effect of N-acetyl functionality on *Sm*ChiP at pH 8.2 (sugar on the *trans* side, negative membrane potentials). Ion current fluctuations were monitored for 120 s at applied potentials of -100 mV with sugar addition on the *trans* side. Here only current traces for 500 ms are presented, with four different chitosan hexaose concentrations (A-D, left panels) and four different chitohaxaose concentrations (E-H, right panels).

Table 3.11 summarizes the kinetic rates of both charged and uncharged chitooligosaccharides towards *Sm*ChiP when sugars were added on the *trans* side. Supplementary Table 4 summarizes the rates for *cis* side sugar addition.
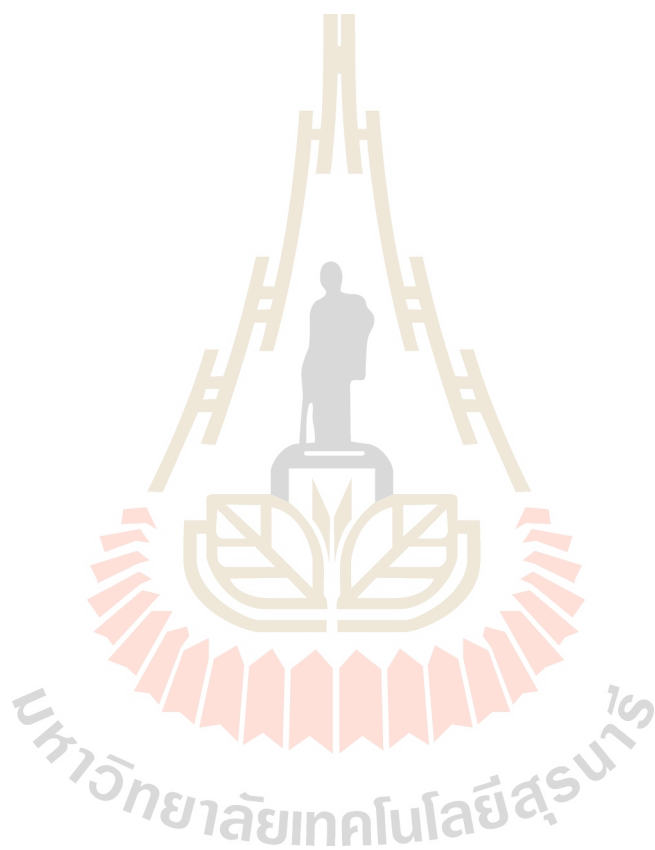
Table 3.11 Effects of pH on the binding constant of *Sm*ChiP towards charged and uncharged chitooligosaccharides.

	Chitohexaose (GlcNAc$_6$), +100 mV, *trans*			Chitosan hexaose (GlcN$_6$), +100 mV, *trans*		
pH	[a]Binding constant (K, M^{-1})	[b]On-rate constant 10^6 (k_{on}, M^{-1}s^{-1})	[c]Off-rate constant (k_{off}, s^{-1})	[a]Binding constant (K, M^{-1})	[b]On-rate constant 10^6 (k_{on}, M^{-1}s^{-1})	[c]Off-rate constant (k_{off}, s^{-1})
6.0	8930 ± 1700	2.2	250 ±36	430 ± 178	7	16000 ± 1500
8.2	11200 ± 1870	3.5	300 ±43	-	ND	ND

[a] The equilibrium binding constant (K) = k_{on}/k_{off}

[b] The on-rate (k_{on}, m$^{-1}\cdot$s^{-1}) is given by number of blocking events(s^{-1})/[sugar concentration]. Here sugar GlcNAc$_6$ concentration = 2.5 μM, GlcN$_6$ concentration = 5 μM.

[c] The off-rate (k_{off}, s^{-1}) was obtained from 1/ τ_c, where τ_c is the average residence (dwell) time of the sugar molecule in the channel.

ND, No well-resolved blocking events.

The on-rate and average residence time were plotted as a function of the applied voltage from -50 to -150 mV for the *cis* side addition of the chitosan hexaose (Figure 3.49) and +50 to +150 mV for the *trans* side addition of the chitosan hexaose (data is not shown) at pH 6 which chitosan hexaose is positively charged. The plot of average residence time as a function of the applied voltage proves the translocation of charged molecules.
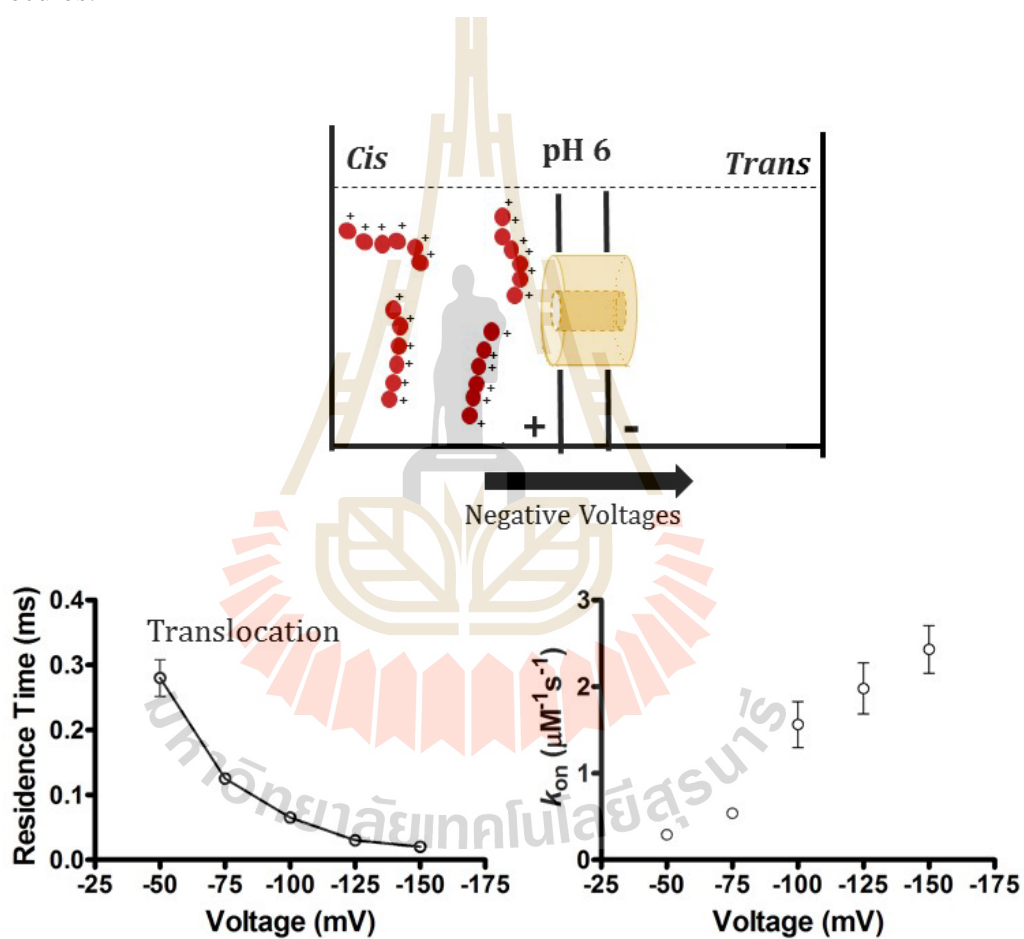
Figure 3.49 Voltage dependence of the residence time and on rates of chitosan hexaose to *Sm*ChiP.

PART III

BIOCHEMICAL AND BIOPHYSICAL CHARACTERIZATION OF CHITOPORIN FROM *VIBRIO CHOLERAE*

3.22 Clonning, Sequence analysis and structure prediction of *Vc*ChiP

The full-length *ChiP* gene corresponding to *Vc*ChiP was synthesized commercially, for which the target gene was ligated into the pUC57 cloning vector (GenScript, Piscataway Township, NJ, USA). The pUC57 cloning vector carrying *VcChiP* gene was used as template for PCR amplification and *VcChiP* gene showed expected band around 1056 bp in 1% agarose gel (Figure 3.50A). Then A-trailing PCR product was successfully ligated into pGEM-Teasy vector and Figure 3.50B represents double digested pGEM-Teasy vector carrying *Vc*ChiP gene and pET23d(+) with *BamH*I and *Xho*I. Purified product was ligated to get recombinant plasmids. As expected, transformed of ligated product into DH5α was resulted many colonies on the plate and selected colonies show positive results as shown in below Figure 3.50C. Figure 3.50D is shown for double digestion of recombinant pET23d/*Vc*ChiP and correct sequence of *Vc*ChiP was confirmed by automated sequencing (First BASE Laboratories SdnBhd, Selangor DarulEhsan, Malaysia). Various physical and chemical parameters for a *Vc*ChiP were obtained from ProtParam tool in ExPASy bioinformatics resource portal. The theoretical mass of the full-length (without signal peptide) *Vc*ChiP was 35,584 Da, with a predicted isoelectric point 4.7.
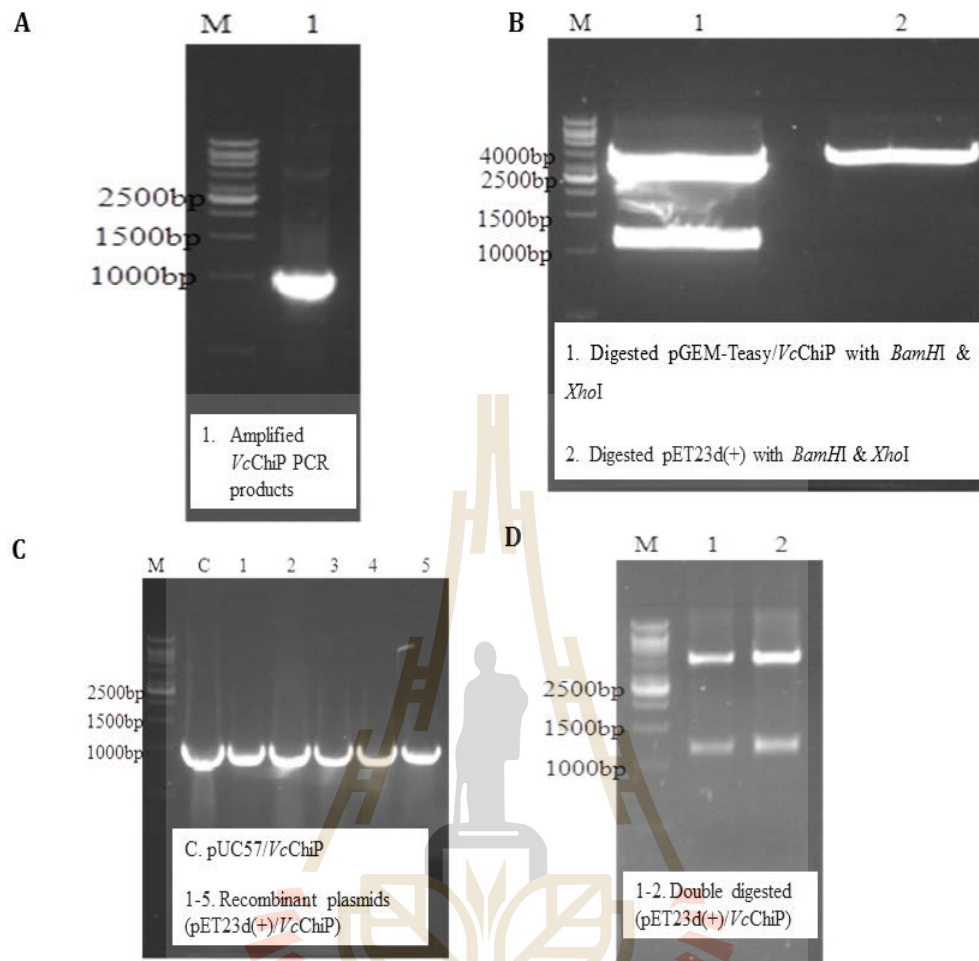
Figure 3.50 Agarose gel electrophoresis for *Vc*ChiP cloning. (A) PCR amplification of *VcChiP* gene (B) Double digestion of pGEM-Teasy/*Vc*ChiP and pET23d (+) expression vector by *BamH*I and *Xho*I restriction enzymes. (C) Colony PCR products using recombinant pET23d (+)/*Vc*ChiP as template. pUC57/*Vc*ChiP used as positive control. (D) Double digestion of pET23d (+) /*Vc*ChiP by *BamH*I and *Xho*I restriction enzymes.

The gene encoding for ChiP is found in most marine members of the *Vibrionaceae*, highlighting the general importance of chitoporin for cellular acquisition of soluble chitin oligosaccharides (Hunt et al., 2008; Keyhani, Li et al., 2000; Meibom

et al., 2004; Suginta, Chumjan, Mahendran, Janning et al., 2013). The sequence similarity between *Vh*ChiP (newly characterized chitoporin) (Suginta, Chumjan, Mahendran, Schulte et al., 2013; Suginta and Smith, 2013) and *Vc*ChiP were analyzed. The amino acid sequence of *Vc*ChiP (UniProtKB entry: Q9KTD0) is 38% identical to the amino acid sequence of *Vh*ChiP (UniProtKB entry: L0RVU0). The amino acid sequence alignment was carried out in ClustalW, and the structure-based alignment was further produced using the program ESPript, v3.0 (Robert and Gouet, 2014). The sequence alignment of both porins is shown in Figure 3.51 together with secondary structural features of *Vc*ChiP. The newly resolved high-resolution X-ray crystal structure of *Vh*ChiP (unpublished data) provided a good template and was used as a template for model structure determination of *Vc*ChiP. In Figure 3.51, N-terminal amino acid residues are shown in orange color including α-helix whereas loop3 (L3) residues, protruding into the pore, are shown in red color including three α- helices.
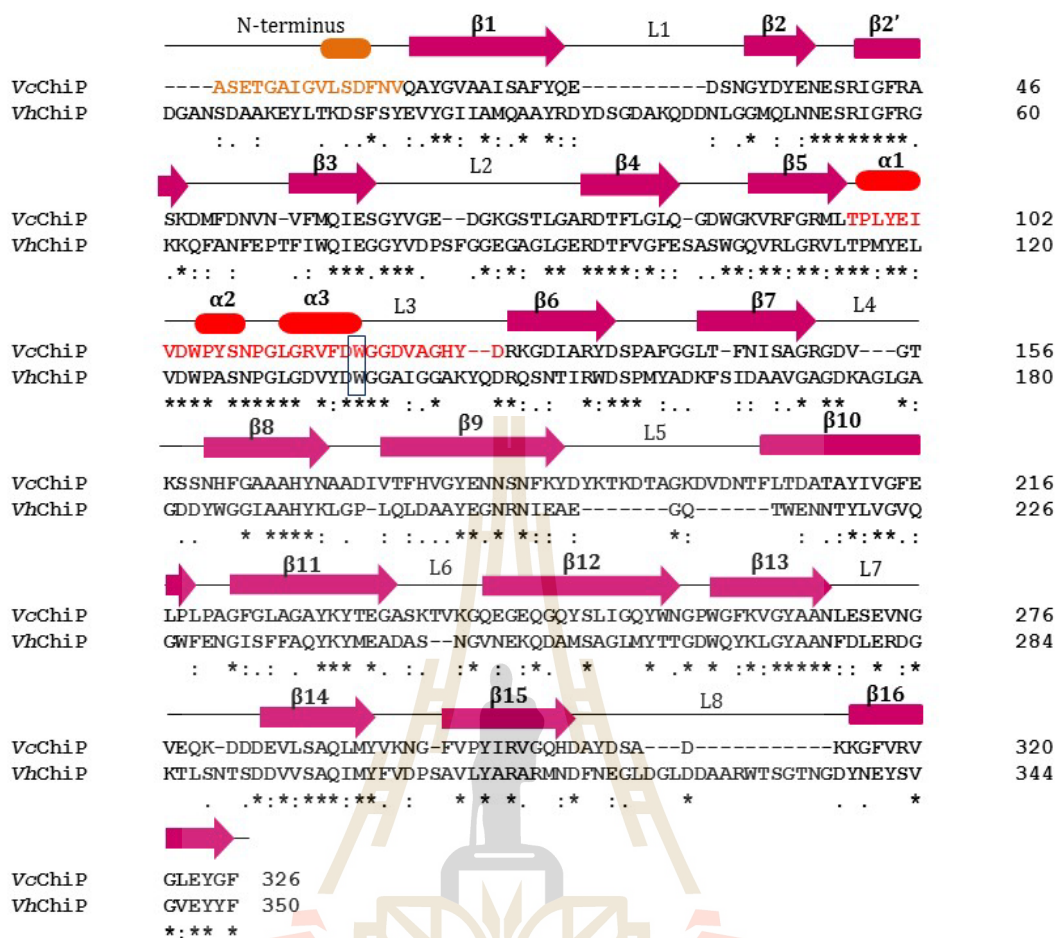
Figure 3.51 Alignment of *Vc*ChiP with ortholog from *Vibrio harveyi*. Amino acid sequences of *Vc*ChiP (Q9KTD0) and *Vh*ChiP (L0RVU0) were retrieved from Uniprot database. The secondary structure of *Vc*ChiP was constructed by ESPript v3.0 according to the X-ray crystal structure of *Vc*ChiP. The N-terminal sequence is indicated in orange color with a short helix consisting of 3 amino acids (L10-D12). The pore-confining loop (L3) is presented in red color with 3 helices whereas β-strands are represented as pink arrows. The Trp (W) amino acid residue that is important for chitooligosaccharides binding is indicated with a blue box.

To explore in more detail how the *Vc*ChiP is related structurally to *Vh*ChiP, the model structure of *Vc*ChiP was obtained using *Vh*ChiP as template. The overall structure of *Vc*ChiP is shown in Figure 3.52 and Figure 3.52A shows a side view of the predicted β-barrel structure of *Vc*ChiP, with each monomer consisting of 16 β -strands. Each monomer is shown in three different colors such as pink, green and yellow respectively. *Vc*ChiP shows an extended periplasmic N-terminus consisting of a helix (shown as cylindrical shape) which located on the periplasmic side. Figure 3.52B (top view of the Figure 3.52A with 90-degree rotation) clearly shows that prominent elongated loop 3 contains α -helices inside the channel lumen. This loop is mainly responsible for the size and constriction of the pore as shown in other porin structures (Moraes, Bains, Hancock, and Strynadka, 2007; Tanabe, Nimigean, and Iverson, 2010). Superimposition of the modelled structure of *Vc*ChiP with the crystal structure of *Vh*ChiP gave an R.M.S.D. of 0.147 Å for 290 Cα atoms (Figure 3.52C). The pore lining residues in loop3 of *Vh*ChiP was conserved with loop3 residues of *Vc*ChiP (highlighted with a star in Figure 3.51) which suggested that these amino acids could play a role in specificity towards chitooligosachacharides. Recently, the importance of the pore-lining residue Trp 136 in loop3 of *Vh*ChiP was studied (Chumjan et al., 2015) and the location is equivalent to that of Trp118 in loop3 of *Vc*ChiP (The location of Trp residues is indicated with a blue box in Figure 3.51).
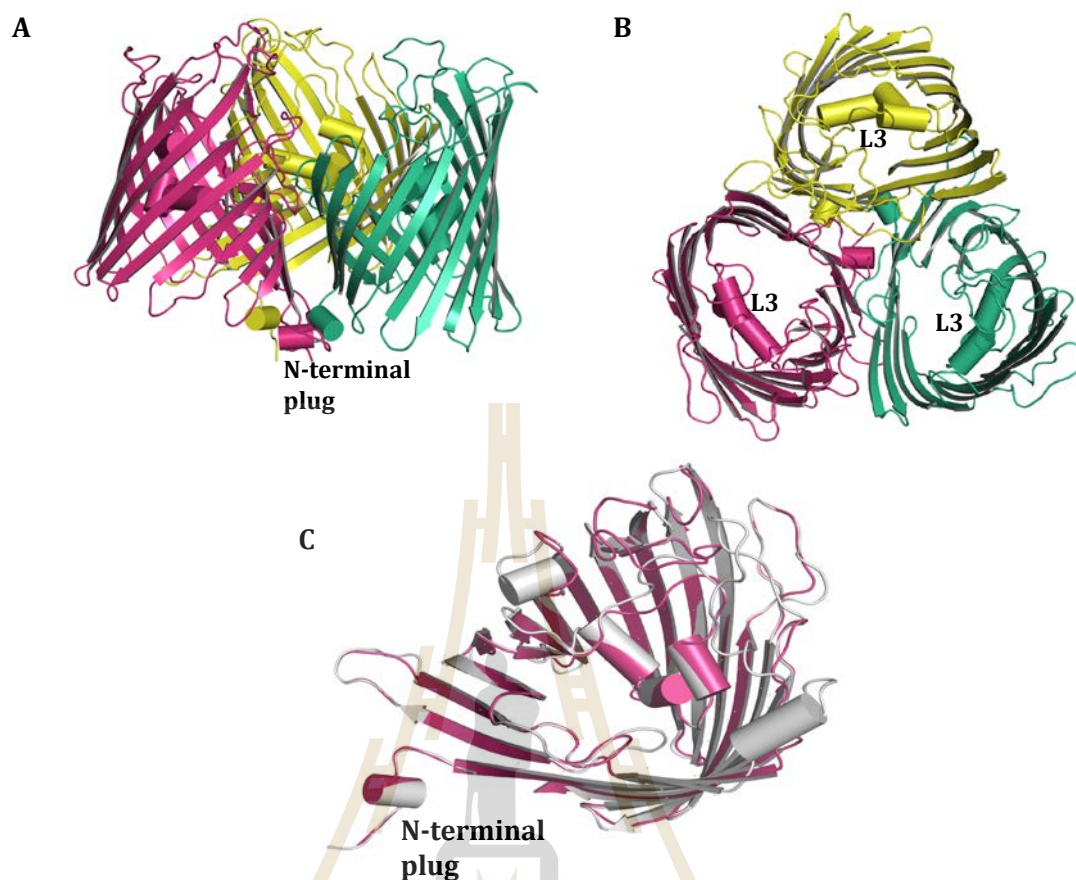
Figure 3.52 *Vc*ChiP forms trimers with N-terminus. (A) Modeled *Vc*ChiP is shown in cartoon representation from a side view, with monomers shown in pink, green and yellow. (B) Top view of the modeled structure, showing L3 as the pore-confining loop with the 3 short helices (C) Superimposition of the modelled structure of *Vc*ChiP (in pink) with the X-ray crystal structure of *Vh*ChiP (in gray).

3.23 Recombinant expression, purification and peptide mass analysis

by MALDI-TOF MS

After the correct nucleotide sequence was confirmed, pET23d (+) expression vector was transformed into *E. coli* BL21(DE3) Omp8 Rosetta and was ready to be expressed in the outer membrane of the *E. coli* host with the aid of 23-amino acid signal

sequence. *Vc*ChiP was successfully extracted with 3.5% (v/v) octyl-POE and was further purified to homogeneity using ion exchange using a Hitrap Q HP pre-packed column (Figure 3.53) and gel filtration chromatography using HiPrep 16/60 Sephacryl S-200 high-resolution exclusion chromatography column.
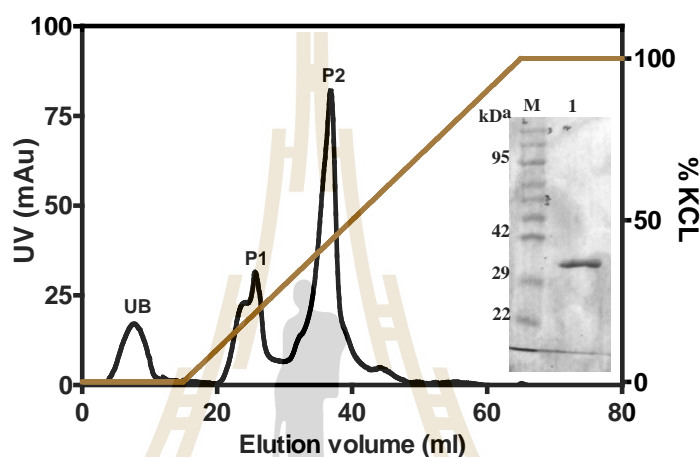
Figure 3.53. Recombinant expression and purification. Chromatographic profile of *Vc*ChiP purification with a Hitrap Q HP prepacked column (5×1 mL) connected to an ÄKTA Prime plus FPLC system. Bound proteins were eluted with a linear gradient of 0–1 M KCl in 20 mM phosphate buffer, pH 7.4, containing 0.5% (v/v) LDAO. SDS-PAGE analysis of bound fraction P2 is shown in an inset. SDS-PAGE gel of OM-expressed *Vc*ChiP loaded as boiled sample.

The purified *V. cholerae* chitoporin was subjected to MALDI-TOF mass analysis for confirming the identity of newly purified protein. As summarized in Table 3.12, tryptic peptides were identified in *Vc*ChiP sequence providing 41 % sequence coverage by MALDI-TOF mass spectrometry confirming that the 35-kDa protein expressed in *E. coli* BL21(DE3) Omp8 Rosetta host was *Vc*ChiP.

Table 3.12 Mass identification of tryptic peptides of *Vc*ChiP by MALDI-TOF mass spectrometry.

Position in the sequence	Expected mass	Calculated mass	Peptide AA sequence
72 - 93	2494.09	2493.08	DMFDNVNVFMQIESGYVGEDGK
101-112	1336.65	1335.65	DTFLGLQGDWGK
118 - 137	2321.15	2320.16	MLTPLYEIVDWPYSNPGLGR
138 - 152	1721.79	1720.8	VFDWGGDVAGHYDRK
158 - 174	1772.85	1771.85	YDSPAFGGLTFNISAGR
264 - 286	2629.24	2628.2	GQEGEQGQYSLIGQYWNGPWGFK
304 - 317	1625.69	1624.77	DDDEVLSAQLMYVK
318 - 325	965.52	964.51	NGFVPYIR
326 - 338	1433.67	1432.66	VGQHDAYDSADKK

To guarantee that the recombinant protein obtained is *Vc*ChiP in future purification, polyclonal antibodies against *Vc*ChiP were raised using MOLDI/TOF confirmed protein. Figure 3.54A top panel shows a Coomassie Blue stained gel of different porins, corresponding to the immunoblot (bottom panel) with anti-*Vc*ChiP antiserum. The antibody recognized only the *Vc*ChiP band and showed no cross-reactivity with *Vh*ChiP. Anti- *Vh*ChiP (Suginta, Chumjan, Mahendran, Janning, et al., 2013) also did not cross react with *Vc*ChiP. The produced antibody was used to confirm *Vc*ChiP expression in *E. coli* BL21(DE3) Omp8 Rossetta in growth rate determination experiments. Figure 3.54B shows the corresponding SDS-PAGE and immunological analysis blot for *Vc*ChiP expression.
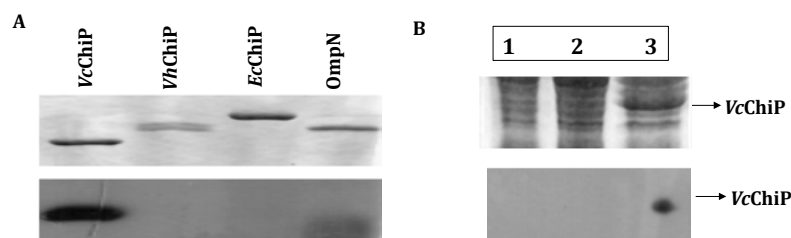
Figure 3.54 Immunoblot analysis of *V. cholera*e chitoporin. (A) Cross-reactivity of *Vc*ChiP antiserum with other outer membrane porins. (top panel) Coomassie blue-stained SDS-polyacrylamide gel, and (bottom panel) The corresponding immunoblots detected with anti *Vc*ChiP antibody (B) *Vc*ChiP expression for growth rate determination. (top panel) Coomassie blue-stained SDS-polyacrylamide gel, (1) *E. coli* BL21 (DE3) Omp8 Rosseta (2) *E. coli* BL21 (DE3) Omp8 Rosseta/*Vc*ChiP carrying plasmid/no *Vc*ChiP expression (3) *E. coli* BL21 (DE3) Omp8 Rosseta/*Vc*ChiP carrying plasmid/*Vc*ChiP expression (bottom panel) The corresponding immunoblots detected with anti *Vc*ChiP antibody.

3.24 Growth of the *E. coli* BL21(DE3) Omp8 Rossetta with *Vc*ChiP

on various carbon sources

The growth of *E. coli* host carrying *Vc*ChiP on the M9 minimal medium supplemented with various carbon sources was monitored. As shown in Figure 3.55, *E. coli* cells, with chitoporin expression or without chitoporin, were able to grow on glucose, glycerol and GlcNAc with a short lag phase (Figure 3.55A-C). We also examined the growth of *E. coli* host without carbon sources in M9 minimal medium and as expected cells were unable to grow without a carbon source. The growth of cells was slightly slower on GlcNac$_2$ and chitoporin-containing cells grew with a modest lag

phase of 18 hr whereas cells without chitoporin were able to grow on $GlcNAc_2$ with

long lag phase of 35 hr (Figure 3.55D). When M9 medium was supplemented with

$GlcNAc_3$, *E. coli* cells with chitoporin grew with a 25 hr lag phase. But without

chitoporin, cells were unable to grow on $GlcNAc_3$ (Figure 3.55E). There was essentially

no growth on chitin oligosaccharides larger than $GlcNAc_3$ (Figure 3.55F).
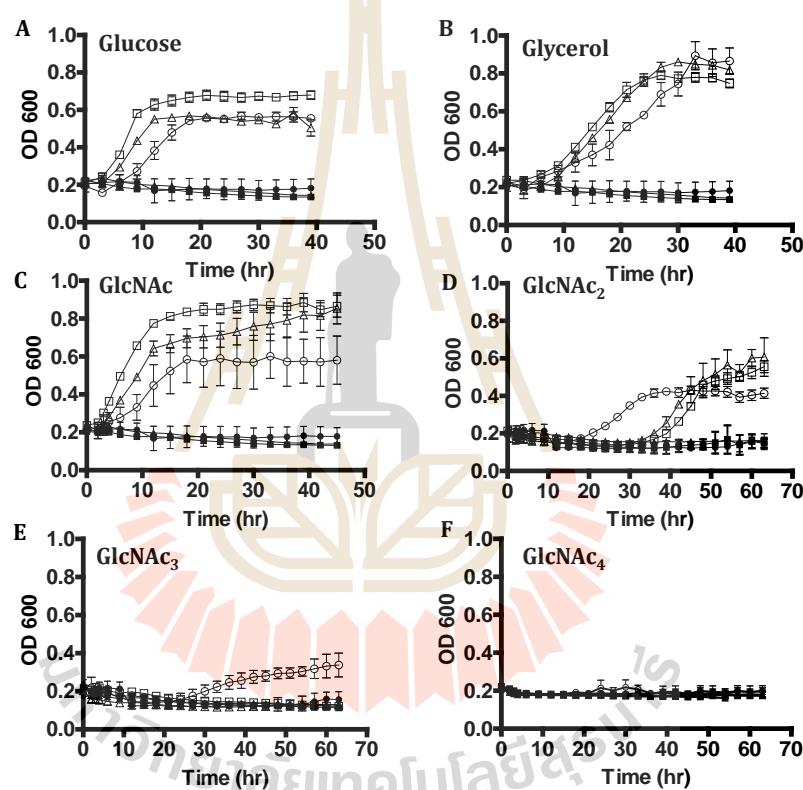
Figure 3.55 Growth of *E. coli* BL21(DE3) Omp8 Rossetta on various carbon sources.

E. coli BL21 (DE3) Omp8 Rosseta (*Ec*Omp8) were grown on M9 minimal medium

supplemented with 0.2% (A) Glucose, (B) Glycerol, (C) GlcNAc, (D) $GlcNAc_2$, (E)

$GlcNAc_3$, (F) $GlcNAc_4$. Symbols: solid squares, *Ec*Omp8 without carbon source; open

squares, *Ec*Omp8 with carbon source; solid triangles, *Ec*Omp8/*Vc*ChiP carrying

plasmid/no *Vc*ChiP expression without carbon source; open triangles,

*Ec*Omp8/*Vc*ChiP carrying plasmid/no *Vc*ChiP expression with carbon source; solid

circles, *Ec*Omp8/*Vc*ChiP carrying plasmid/*Vc*ChiP expression without carbon source; open circles, *Ec*Omp8/*Vc*ChiP carrying plasmid/*Vc*ChiP expression with carbon source.

3.25 Assay of sugar permeation by proteoliposome swelling

To functionally probe the chitooligosaccharide specificity of *V. cholerae* chitoporin, we reconstituted *Vc*ChiP into proteoliposomes and performed *in vitro* transport assays. Additionally, to address the differences between the *Vc*ChiP channel and the chitooligosaccharide- specific porins from *V. harveyi*, we compared our data with those obtained with *Vh*ChiP-incorporated proteoliposomes. As shown in Figure 3.56 top panel, we first checked the channel permeability with different sugar molecules, of varying molecular weight from 180 Da to 600 Da. Various monomeric sugars such as *D*-glucose, *D*-mannose and *D*-galactose (180 Da) and *N*-acetylglucosamine (GlcNAc, 221 Da) translocate efficiently through both ChiPs in an identical manner whereas maltose (360 Da) permeated through both chitoporins with very low diffusion rates. The smallest sugar, arabinose, was set to 100% permeability while branched raffinose a non-permeant sugar, was used to determine isotonic concentration in the swelling experiments. However, sucrose (342 Da), and melezitose (522 Da) showed no diffusion through *Vc*ChiP while sucrose permeated very slowly through *Vh*ChiP. In contrast, different lengths of chitooligosaccharides (chitobiose; $GlcNAc_2$ (424 Da), chitotetraose; $GlcNAc_4$ (830 Da), and chitohexaose; $GlcNAc_6$ (1237 Da)) translocated efficiently through both chitoporins. $GlcNAc_2$ and $GlcNAc_4$ permeate through *Vc*ChiP at higher rates while $GlcNAc_6$ translocated through *Vh*ChiP with the highest permeation rate. Then in the next set of experiments (Figure 3.56

bottom panel) we checked the permeating rate of different lengths of chitooligosaccharide for checking channel specificity towards chitosugars. Only 2.5 mM concentration was used, adjusting the isotonic concentration with raffinose. More interestingly, permeation by chitosugars was observed irrespective of their molecular weight. Maltohexaose could not permeate through *Vc*ChiP.
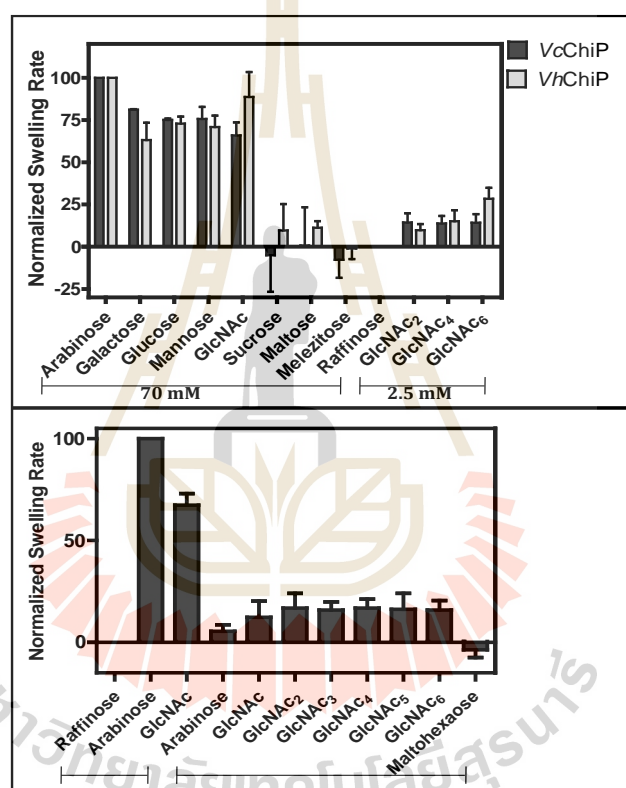
Figure 3.56 Proteoliposome swelling assays.

D-raffinose was used to determine isotonic concentration; (no change in absorbance at 500 nm of the proteoliposome suspension over 60 s) and L-arabinose swelling rate was set to 100% to obtain the normalized swelling rate. The permeability of channel was assumed to be proportional to the swelling rate. (Top panel) Permeation of different types of sugars through *Vc*ChiP and *Vh*ChiP reconstituted liposomes.

(Bottom panel) Permeation of chitooligosaccharides through VcChiP. Maltohexaose was used as control. Values are means ± SD, obtained from 3 independent sets of experiments. GlcNAc, N-acetylglucosamine; $GlcNAc_2$, chitobiose; $GlcNAc_3$, chitotriose; $GlcNAc_4$, chitotetraose; $GlcNAc_5$, chitopentaose; $GlcNAc_6$, chitohexaose.

3.26 Spontaneous gating of the pore with voltage-induced channel opening

Pore-forming activity of VcChiP was checked in the planar lipid bilayer by adding protein into the *cis* side. The addition of VcChiP into the *cis* side of the planar lipid membrane raised the current level, confirming the pore-forming properties of VcChiP. Surprisingly, the channel was nearly closed at low applied potential (~25 mV). Besides channel closing at low applied potential, the single-channel reconstitution shows pronounced asymmetry in ion conductance with positive (Figure 3.57A-D left panel) and negative applied potentials (Figure 3.57E-H left panel). The first observation is that the inserted channel is nearly closed at low applied potentials and opened at high applied potentials with spontaneous gating. The second observation is that when protein is added on the *cis* side, negative applied potentials produce nice trimeric channel opening without sub-states whereas positive applied potentials produces partly opened channels with sub-states. It is clearly seen with the comparison of all point histograms that positive and negative potentials differ in their gating pattern. At negative applied potential, the current fluctuations occurred among O_1 (monomeric open), O_2 (dimeric open) and O_3 (trimeric open), which were three open subunits of the channel, as observed for many trimeric protein channels (Kullman et al., 2002; Suginta, Chumjan,

Mahendran, Schulte et al., 2013; Tran et al., 2010) and Figure 3.57E-H right panel shows corresponding histograms for each current trace. In contrast, at positive applied potentials current fluctuations occurred among main subunits as well as among other sub-states in an asymmetric manner. Sub-states were named as O_1'(sub-state of first subunit), O_2' (sub-state of second subunit) and O_3' (sub-state of third subunit) and Figure 3.57A-D right panel shows corresponding histograms for each current trace together with sub-states. This asymmetry in single channel reconstitution allowed exploration of the directional properties of the channel.
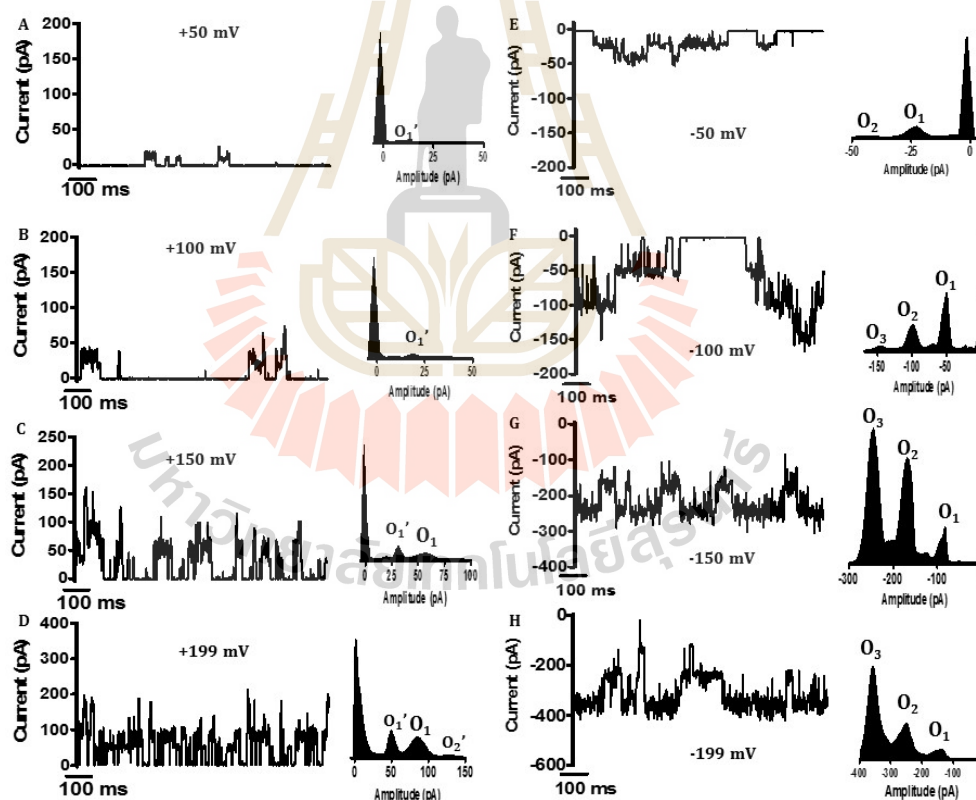
Figure 3.57 Single channel recording of *Vc*ChiP (protein addition: *cis* side). Current traces (500 ms) from a *Vc*ChiP pore at various applied potentials. Lipid bilayers were formed across a 70 µM aperture by the lowering and raising technique, using 5 mg.mL$^-$ ^{1} 1,2-diphytanoyl-sn-glycero-3-phosphatidylcholine (DPhPC) in n-pentane and 1M

KCl in 20 mM HEPES, pH 7.5 on both sides of the chamber. Ion current fluctuations are presented with four different positive voltages (A-D, left panels) with the corresponding histograms (A-D, right panels) and four different negative voltages (E-H, left panels) with the corresponding histograms (E-H, right panels).

The insertion of *Vc*ChiP into the planar lipid bilayers is unidirectional. When we added protein to the *cis* side of the chamber, an applied negative potential showed full opening of the channel without sub-states gating at high voltages (the current values are clearly greater at negative potentials than at positive potentials) and the channel conductance obtained at -100 mV was 1.65 ± 0.20 nS (n=33) as shown in histogram in Figure 3.58. In our planar lipid bilayer experiments, we worked on a large population of *Vc*ChiP (n=34) channels that exhibited the larger conductance at negative potentials, and only single insertions showed different behavior (larger conductance at positive potentials and channel gating with sub-states with lower conductance at negative potentials), confirming the unidirectional properties of the channel.
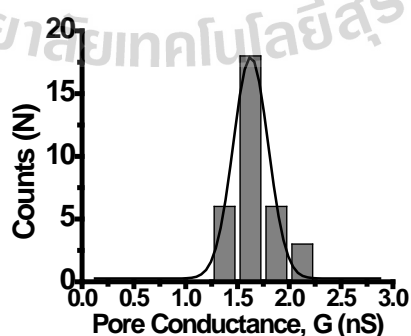
Figure 3.58 Histogram of the conductance steps observed with 1,2-diphytanoyl-sn-glycero-3-phosphatidylcholine (DPhPC) artificial bilayer for 33 independent channel insertions (protein addition *cis* side). The black line represents a single Gaussian fit.

In the next series of experiments, we probed the unidirectional orientation by adding protein into the *trans* chamber. As we expected, since channel insertion is unidirectional we see an ion fluctuation pattern exactly the opposite way around from *cis* side protein addition. As shown in Figure 3.59, increased positive potentials produce fully open channels with only three main subunits gating (Figure 3.59A-D) whereas negative potentials produce partly open channels with more sub-states gating among main subunits. Apart from this asymmetric channel gating with negative and positive applied potential, the most striking effect of *Vc*ChiP single channel insertion is voltage-induce channel opening. We worked with a voltage range from ±25 to ±200 mV and always voltage-induced channel opening was observed (channel more open at higher voltage than low voltage).
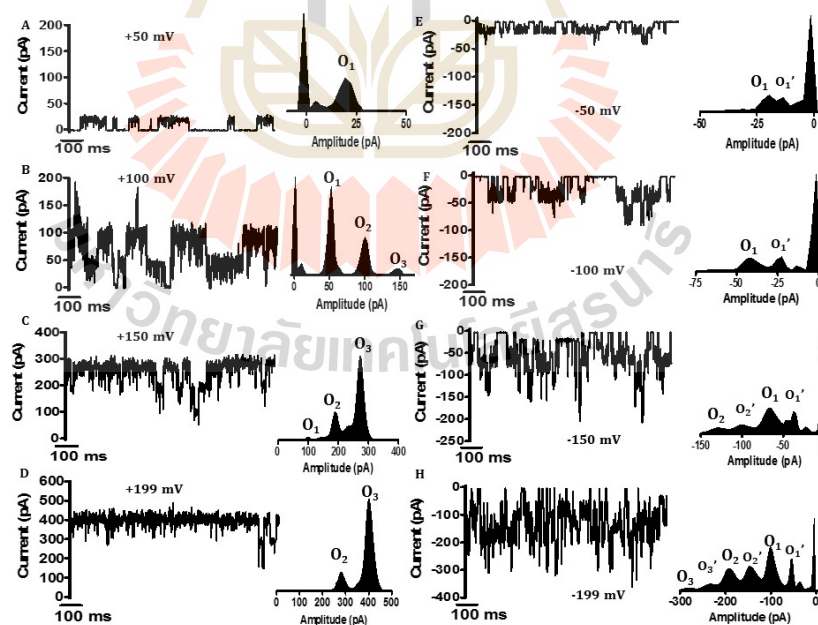
Figure 3.59 Single-channel recording of *Vc*ChiP (protein addition: *trans* side). Current traces (500 ms) from a *Vc*ChiP pore at various applied potentials. Lipid bilayers were formed across a 70 µm aperture by the lowering and raising technique, using 5 mg/mL

1,2-diphytanoyl-sn-glycero-3-phosphatidylcholine (DPhPC) in n-pentane and 1M KCl in 20 mM HEPES, pH 7.5 on both sides of the chamber. Ion current fluctuations are presented with four different positive voltages (A-D, left panels) with the corresponding histograms (A-D, right panels) and four different negative voltages (E-H, left panels) with the corresponding histograms (E-H, right panels).

3.27 Asymmetric gating patterns with unidirectional orientation

Next, we consider asymmetric channel gating patterns and unidirectional orientation in detail. About 70 – 80% of the reconstituted channels are oriented with the extracellular entrance toward the side to which the protein was added and with the periplasmic opening on the opposite side (Andersen, Schiffler, Charbit, and Benz, 2002; Danelon et al., 2003; Kullman et al., 2002). We also assume that our *Vc*ChiP pore is inserted into the lipid bilayer with its short turns first because considerably lower energy is needed to move these turns through the hydrophobic membrane interior when compared with extracellular side with its huge hydrophilic loops. Since our protein insertion is unidirectional we provide a schematic model of channel orientation in lipid bilayer with respect to the side of protein addition. As shown in Figure 3.60 top panel, the extracellular side is the side of protein addition. As we have seen in model structures the N-terminal plug is located on the periplasmic side and we assume that channel gating and voltage-induced opening is due to the N-terminal plug. Supporting this hypothesis, we can see voltage-induced fully open channel with negative applied potential when protein is added to *cis* side independently of the sign of the potential applied during channel incorporation (Figure 3.60 left side). If protein is added to the *cis* side, at the negative voltage the current flow is from extracellular to periplasmic

side and it may help to remove the periplasmic N- terminal plug from the inside pore, resulting in the I-V curve shown in Figure 3.60 left side bottom panel. O1-O3 show the main subunit opening whereas O1'-O3' correspond to sub-states among main subunits which are mainly observed at positive voltages (protein addition: *cis*). The Figure 3.60 bottom right panel shows the corresponding I-V curve when protein is added to *trans* side. It shows the exact reciprocal of the *cis* side addition. We assume that when protein is inserted from *trans* side, positive potential (current flow from extracellular to periplasmic) helps to remove N-terminal plug while negative potential shows asymmetric channel gating with sub-states because of N-terminal plug movement inside the pore. Moreover, it is clearly seen that we have to apply high potential (> 100 mV) to get a fully open channel (at low voltages cannot see a second or third subunit opening). The single-channel electrical signature of *Vc*ChiP shows three open subunits either at positive voltages, >100 mV (protein addition: *trans*) or negative voltages, > -100 mV (protein addition: *cis*).
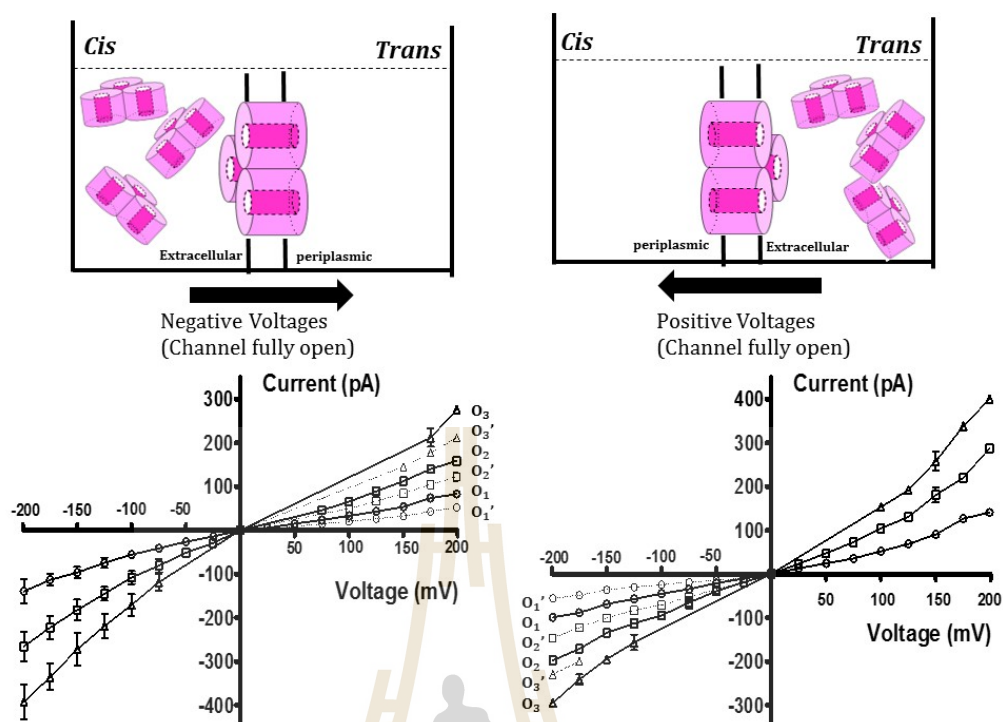
Figure 3.60 Schematic model of protein orientation and I-V curves of *Vc*ChiP (protein addition: *cis* side or *trans* side). The top panel is the schematic representation of channel orientation in the bilayer with protein addition at *cis* or *trans*. The bottom panel is the I-V curve of *Vc*ChiP voltage ranging from ± 25 to ± 199 mV either protein addition at *cis* or *trans*. The data represent the mean values from three independent pores. The bars show the standard deviations. O1-O3 are the current fluctuations occurred among main subunits and O1'-O3' are the current fluctuations occurred among sub-states through main subunits.

Interestingly, we found no statistically significant alterations of the conductance values for *cis* negative potentials and *trans* positive potential (or vice versa) for both subunits and sub-states (see Table 3.13 and 3.14 for the values), which confirms the unidirectional orientation of *Vc*ChiP.

Table 3.13 The single-channel subunit conductance of *Vc*ChiP. The chamber solution contained 1 M KCl in 20 mM HEPES pH 7.5. The data were determined from at least three distinct single channel electrical recordings.

Subunits	Protein: *cis* side at +175 mV (G; nS)	Protein: *cis* side at - 175 mV (G; nS)	Protein: *trans* side at + 175 mV (G; nS)	Protein: *trans* side at - 175 mV (G; nS)
O1	0.42 ± 0.01	0.64 ± 0.07	0.72 ± 0.02	0.50 ± 0.01
O2	0.80 ± 0.04	1.27 ± 0.15	1.25 ± 0.01	0.98 ± 0.01
O3 (fully open)	1.20 ± 0.10	1.92 ± 0.17	1.93 ± 0.01	1.38 ± 0.06

The sub-states of each subunit have approximately half subunit channel conductances, as Table 3.14 shows clearly.

Table 3.14 The single channel sub-states conductance of *Vc*ChiP. The chamber solution contained 1 M KCl in 20 mM HEPES pH 7.5. The data were determined from at least three distinct single channel electrical recordings.

Sub-states	Protein: *cis* side at +175 mV (G; nS)	Protein: *trans* side at - 175 mV (G; nS)
O1'	0.24 ± 0.02	0.28 ± 0.01
O2'	0.59 ± 0.01	0.7 ± 0.02
O3'	1.00 ± 0.02	1.1 ± 0.01

In detail, voltage-dependence of open channel conductance values is shown in Figure 3.61 for either protein addition; *cis* or *trans*. Only the main three subunit conductance values are presented, clearly showing the voltage-induced channel opening with asymmetry in the voltage-dependence of conductance.
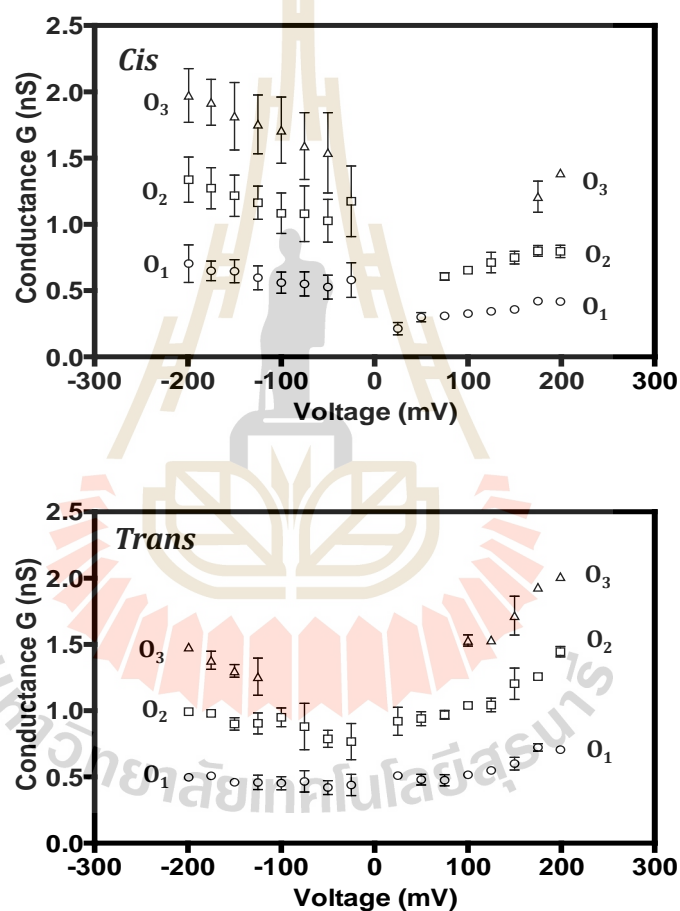
Figure 3.61 Voltage-dependence of open channel conductance (protein addition: *cis* side or *trans* side). The data represent the mean values from three independent pores. The bars show the standard deviations. O1-O3 are the conductances responsible for current fluctuations occurring among main subunits and O1'-O3' are the conductances responsible for current fluctuations occurring among sub-states of main subunits.

3.28 Substrate specificity

In these experiments, we studied the substrate specificity of *Vc*ChiP which is added to *cis* side of the chamber. Due to spontaneous gating of the channel itself it was difficult to clearly separate sugar-induced channel gating. So, we selected a high applied potential (-199 mV) (channel is nearly fully opened and less noisy) (Figure 3.62) and a low applied potential (-50 mV) (channel is nearly closed and less noisy) (Figure 3.63) for comparing the traces and sugars were added into *cis* chamber. As shown in Figure 3.62 we tested 80 μM chitotetraose and chitohexaose. Maltohexaose was tested to confirm the channel specificity towards chitosugars. Addition of chitotetraose resulted in additional channel gating while chitohexaose also showed sugar-induced channel gating at -199 mV (Figure 3.62). On the other hand, no clearly distinguishable modification occurred upon addition of maltohexaose following chitohexaose to the same channel (after diluting the *cis* chamber with 20 mL of electrolyte to remove chitohexaose) at -199 mV.
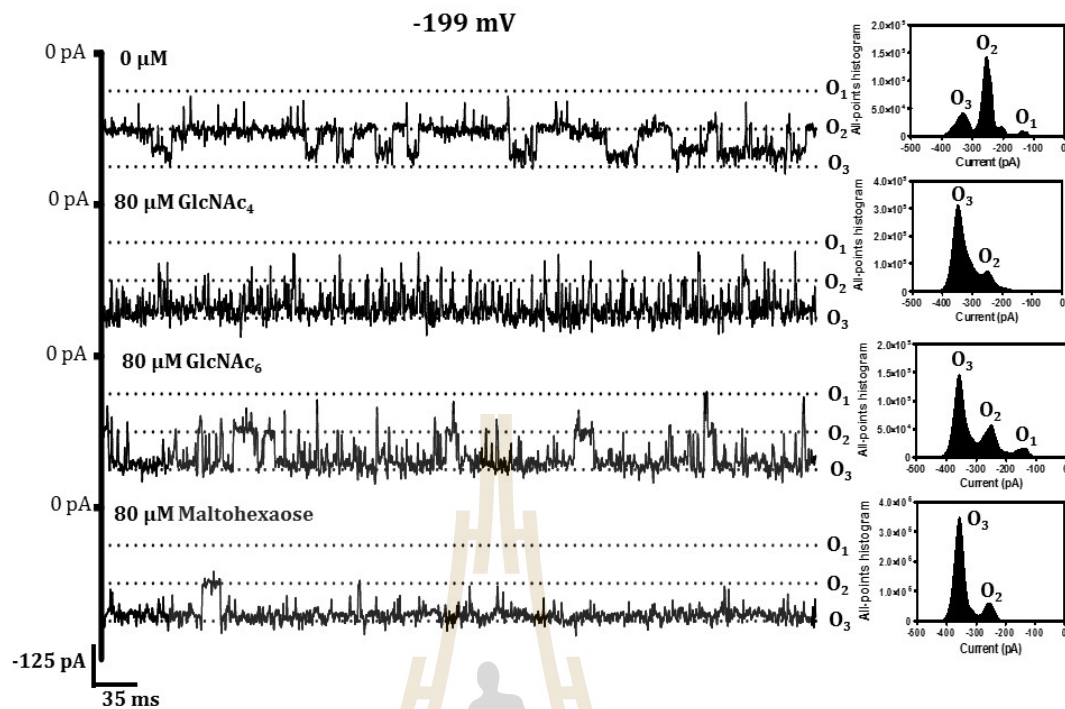
Figure 3.62 Current recordings of single *Vc*ChiP channels at -199 mV (protein addition and sugar addition: *cis* side). Ion current fluctuations were monitored for 120 s. Here, only current traces for 500 ms at – 199 mV are presented. Ion current traces represent the same *Vc*ChiP channel before sugar addition and with 80 µM of chitotetraose (GlcNAc$_4$), chitohexaose (GlcNAc$_6$) and maltohexaose.

Interestingly, addition of chitohexaose at -50 mV displayed sugar-induced channel opening together with extra gating for substrate when compared with control (Figure 3.63), but addition of chitotetraose or maltohexaose did not show significant differences with controls.
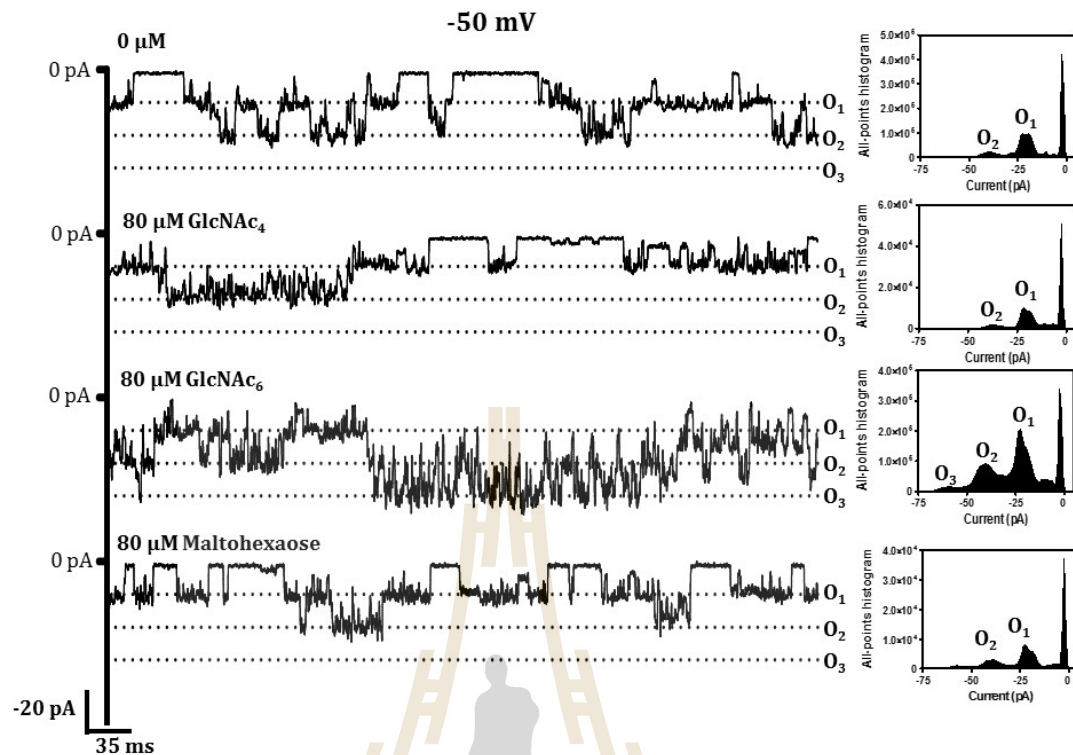
Figure 3.63 Current recordings of single *Vc*ChiP channels at -50 mV (protein addition and sugar addition: *cis* side). Ion current fluctuations were monitored for 120 s. Here, only current traces for 500 ms at – 50 mV are presented. Ion-current traces represent the same *Vc*ChiP channel before sugar addition and with 80 μM of chitotetraose (GlcNAc$_4$), chitohexaose (GlcNAc$_6$) and maltohexaose.

CHAPTER IV

DISCUSSION

PART I

BIOCHEMICAL AND BIOPHYSICAL CHARACTERIZATION OF CHITOPORIN FROM *ESCHERICHIA COLI*

4.1 Cloning, sequence analysis and structure prediction of *E. coli*

E. coli is a non-chitinolytic bacterium living primarily in the gastrointestinal tract of animals and its generation of cellular energy relies on glucose-enriched nutrients. Although the *ChiP* gene, encoding a chitoporin that is responsible for the uptake of chitin-derived chitooligosaccharides, is evolutionarily conserved, it is usually quiescent in non-chitinolytic bacteria. A previous report on *Salmonella* and *E. coli* (Figueroa-Bossi et al., 2009; Rasmussen et al., 2009) showed that in the absence of any inducer, the *ChiP* gene (formerly *ybfM*) was constantly suppressed by forming a DNA-RNA duplex with a conserved sRNA, namely *ChiX*. However, silencing was relieved in the presence of chitooligosaccharides, since these sugars produced accumulation of anti-*ChiX* sRNA that paired with *ChiX*, allowing the *ChiP* gene to be expressed. Another study reported co-localization of *ChiP* and *Hex* (encoding β-N-acetylglucosaminidase) in the chromosomes of *Yersinia* and *Serratia* species (Yang et al., 2006).

This suggested a sequential action of ChiP and *β*-N-acetylglucosaminidase in chitin uptake and chitin degradation respectively, and *E. coli* and *Salmonella* ChiPs have been proposed to be involved in the uptake of chitobiose, an end-product of chitin breakdown that is readily transported through the inner membrane by the phosphoenolpyruvate transferase system (PTS).

In this study, the *ChiP* gene was identified, encoding a hypothetical outer-membrane chitoporin (*Ec*ChiP) from the genome of the *E. coli* strain K-12, sub-strain MG1655. Amino acid sequence analysis showed that *Ec*ChiP had exceptionally low sequence identity (<14%) to all ChiPs from the OmpC family, such as *Vh*ChiP from *V. haveryi* and *Vf*ChiP from *V. Furrnissi* (Keyhani, Li et al., 2000; Suginta, Chumjan, Mahendran, Schulte et al., 2013). This suggested that the *ChiP* genes from *E. coli* and from *Vibrio sp*. did not share common ancestors, and further sequence analysis showed that *Ec*ChiP was similar to *Sm*ChiP from *S. marcescens* (75% identity), both of which are members of the OprD family.

4.2 Channel forming properties of *Ec*ChiP and ion selectivity

The recombinant *Ec*ChiP displayed quite different channel behavior from other sugar-specific porins. Its most distinctive feature was that it formed a monomeric channel, rather than the trimeric channel observed with other known ChiPs, and that the channel was stably open over a wide range of external membrane potentials, with only occasional gating at high voltages (+/-200 mV). At 0.55±0.01 nS, the single-channel conductance of *Ec*ChiP was approximately one-third of that of the well-studied

*Vh*ChiP (1.8±0.3 nS) (Suginta, Chumjan, Mahendran, Schulte et al., 2013), consistent with our observation that *Ec*ChiP formed a monomeric channel, while *Vh*ChiP worked as a trimer. Comparison with the monomeric OprD from *Pseudomonas aeruginosa*, a basic amino acid uptake channel (Biswas, Mohammad, et al., 2007), revealed that *P. aeroginosa* OprD had a narrow central constriction zone and displayed a much smaller conductance (28 pS) than that of *Ec*ChiP under the same electrolyte conditions (1M KCl and pH 7.5). This suggests differences in the amino acids that line the channel interior and regulate the net ion flow in *Ec*ChiP, as compared to those in OprD.

Measuring changes in ion flow upon varying the cationic/anionic species could provide some information regarding ion selectivity. For examples, Benz and coworkers (Benz et al., 1987; Saravolac et al., 1991) used LiCl and KAc to test the channel selectivity of the maltodextrin-specific channel LamB and the glucose-inducible channel OprB. Both channels showed preference for cations over anions. Following their method, our channel also exhibited similar preference. We also measured the K^+/Cl^- selectivity by observing changes in reverse membrane potential at zero current under 0.1-3.0 M gradients of KCl. The value of the P_c/P_a ratio = 2.8 was obtained, which was slightly less than the value obtained for the trimeric *Vh*ChiP (P_c/P_a = 3.2) (Chumjan et al., 2015). Nonetheless, the ion selectivity obtained from both techniques confirmed that *Ec*ChiP was a cationic-selective channel.

4.3 *Ec*ChiP channel specificity

We examined sugar-channel interactions with various chitooligosaccharides. Our BLM data showed that *Ec*ChiP interacted strongly with long-chain chitooligosaccharides, but not with maltooligosaccharides, implying that the channel

was specific for chitooligosaccharide uptake. Strong interaction with the higher-molecular weight substrates is also a characteristic of other sugar-specific channels, such as LamB (Bezrukov et al., 2000; Danelon et al., 2003; Kullman et al., 2002), *Vh*ChiP (Chumjan et al., 2015; Suginta, Chumjan, Mahendran, Schulte et al., 2013) and CymA (Bhamidimarri et al., 2016). Consistent with this is an earlier *in vivo* study that showed no growth of *S. marcescens* expressing the null ChiP mutant in the presence of chitooligosaccharides larger than chitotriose (Takanao et al., 2014). Both results confirmed the physiological roles of the OprD-related ChiP in chitooligosaccharide uptake.

*Ec*ChiP was tested for its ability to transport neutral sugars of various sizes by use of a liposome swelling assay. All the monosaccharides tested could permeate into *Ec*ChiP-reconstituted liposomes. Similar results were obtained with *Vh*ChiP. Neither channel allowed the passage of neutral sugars of >221 Da, such as maltose, sucrose, melezitose and raffinose, reflecting the size exclusion limit for small molecules that traverse the channel by general diffusion. In our BLM measurements, we did not observe the occlusion of *Ec*ChiP by GlcNAc, presumably because the short-lived blocking events (<100 µs) produced a residence time too short to be resolved by the currently-available BLM setup. This is also the case when molecules with a molecular weight below the size exclusion limit pass through the channel without interacting with it. However, the behavior of the *Ec*ChiP channel was not equivalent to that of other known non-specific porins, such as *Bps*Omp38 from *Burkholderia pseudomallei* (Aunkham et al., 2014; Siritapetawee, Prinz, Krittanai, and Suginta, 2004; Siritapetawee, Prinz, Samosornsuk, Ashley, and Suginta, 2004) and OmpF from *E. coli* (Saint et al., 1996), which typically have a size-exclusion limit of around 650 Da. In

liposome swelling experiments, in agreement with the electrophysiological data, *Ec*ChiP showed sugar-selective behavior, allowing the bulk permeation of chitooligosaccharides at rates that depended on the sizes of the sugar chains, longer chain chitooligosaccharides (chitotetra-, penta- and hexaose) tending to show greater permeation rates than short-chain sugars such as chitobiose and -triose. Additionally, the channel operated even at the low sugar concentration of 2.5 mM, a characteristic of solute-specific channels that has been reported for other well characterized porins, including *E. coli* LamB (Dumas et al., 2000; Van Gelder, Dumas, Rosenbusch, and Winterhalter, 2000) and *V. harveyi* ChiP (Suginta, Chumjan, Mahendran, Schulte, et al., 2013). In the liposome swelling assay, the rate of permeation of chitohexaose through *Vh*ChiP was much greater than those for other sugars, while the permeation rates of chitotetra-, penta-and hexaose through *Ec*ChiP were comparable. Both the liposome swelling assays and the BLM data generally showed the lower affinity of *Ec*ChiP than of *Vh*ChiP for the same sugars, and suggested high substrate specificity of the *Vibrio* channel and broad substrate specificity of the *E. coli* channel. This is not surprising, since *Vh*ChiP uses chitin as its sole source of energy, so the channel has evolved to provide very efficient chitooligosaccharide uptake, enabling the bacterium to thrive even in rough seas. On the other hand, *E. coli* uses mainly glucose as a nutrient, its ChiP functioning only under certain environmental conditions, such as a scarcity of glucose in the growth medium. Moreover, the data obtained indicate that *Ec*ChiP is specific for chitooligosaccharides, and does not conduct maltooligosaccharides. Previous reports showed that *E. coli* constitutively expresses a maltodextrin-specific porin, namely LamB or maltoporin, to allow growth in glucose-containing media (Berkane et al., 2005; Schulein and Benz, 1990; Van Gelder et al., 2002). Our data,

which show no interaction of *Ec*ChiP with maltooligosaccharides but strong interactions with chitooligosaccharides, provide strong evidence that the C_2-*N*-acetamido groups on the GlcNAc moieties serve as major determinants for chitooligosaccharide-*Ec*ChiP interactions and define the channel specificity. The nature of the amino acid side-chains lining the channel interior that interact with the C_2-*N*-acetamido groups of the chitooligosaccharide chain is presumed to play an important role in the binding affinity of the *Ec*ChiP channel.

4.4 Kinetic assessment of sugar-channel interactions in planar lipid membranes

Sugar blocking events occurred through the trapping of individual sugar molecules within the elongated channel lumen followed shortly by departure, and therefore reduction of the overall channel conductance. The residence time observed for individual current deflections defined how long the entrapped sugar molecules would remain in the channel, which set the first-order rate constant k_{off}. On the other hand, the frequency of the sugar blocking events accounts for the rate of sugar binding, which is directly related to the second-order rate constant k_{on}. The transport of long-chain oligosaccharides (chitotetra-, penta-, and hexaose) through the membrane occurred by facilitated diffusion that was driven by specific interactions between the sugar molecule and the amino acid residues lining the protein pore. Ion-current fluctuation I(t) of *Vh*ChiP (the trimeric analog of the *Ec*ChiP channel) was recently analyzed and demonstrated that the movement of a chitin oligomer through the channel interior occurred by a multi-step process (Suginta and Smith, 2013). The sequence of

multiple trap/untrap events helped to explain how the energy barrier to translocation of a long-chain sugar (chitohexaose) through the outer membrane could be more easily lowered than in a single-trap translocation.

Here the binding constant value was confirmed by three different methods. Noise spectral analysis and ion-current reduction method kinetic values are in line with the values estimated from the number of events and dwell time analysis, with slight deviations. Note that the K values calculated by direct quantitation of the number of binding events per second and from dwell time analysis may be systematically underestimated, since short-lived binding events (<10 µs) were omitted because of the detection limit of our BLM setup. On the other hand, all binding events contributed to the overall change in ion conductance used in ion reduction analysis.

However, the binding affinity significantly increased if the sugar chain was longer. Sugar blocking events occurring during which individual sugar molecules were trapped and then detrapped inside the narrow passage of the channel lumen, eventually causing transient occlusions of the ion flow. The amplitude of each binding/departing peak, indeed, depends on the strength of interactions, while the frequency of the sugar blocking events accounted for the rates of sugar binding. Note that we did not observe such current fluctuations when short-chain chitooligosaccharides, such as GlcNAc and GlcNAc$_2$, were tested, due to no/weak interactions. This is the case when the size of the travelling species is smaller than the size exclusion limit of the protein pore. The small sugar molecules moved through the channel by a simple diffusion process. Unlike short-chain sugars, the transport of long-chain sugars (chitotetra-, penta-, and hexaose) across the membrane was achieved by facilitated diffusion that was essentially driven by specific interactions between the sugar molecule and the amino acid residues

underlying the inner surface of the protein pore. Stochastic ion-current fluctuation I(t) of *Vh*ChiP was recently analyzed (the trimeric analog of the *Ec*ChiP channel) and demonstrated that the movement of a chitin oligomer along the channel interior was achieved by a multi-step process (Suginta and Smith, 2013). The multiple-trap/untrap design helped to explain that the energy barrier required for translocation of a long-chain sugar (chitohexaose) across the outer membrane could be easily overcome as compared to the single-trap translocation.

4.5 Thermodynamic assessment of sugar-channel interactions in solution

Although ITC has afforded valuable insights into the thermodynamic basis of the action of several membrane proteins (Draczkowski et al., 2014; Evans et al., 1996; Nisius et al., 2008; Rajarathnam and Rosgen, 2014; Sikora and Turner, 2005a, 2005b; Wohri et al., 2013), this approach has been limited in its application to outer membrane channels, due to the highly dynamic nature of these channels. Nevertheless, an ITC study of the outer membrane porin OmpF has been reported (Housden et al., 2010), in which it was demonstrated that bacteriocin colE9 recruited OmpF to deliver colE9 intrinsically unstructured translocation domain (colE9IUTD). The data obtained from this study allow us to assess the thermodynamic characteristics of sugar-channel interactions and *Ec*ChiP was titrated with chitohexaose. The entropy gain in the binding process strongly suggest that hydrophobic interactions play a predominant role in chitohexaose *Ec*ChiP interactions (Abraham et al., 2005b; Anbazhagan et al., 2011).

4.6 pH-dependence of the rates of charged and uncharged chitosugar translocation

pH-dependence experiments show the remarkable difference in the interaction of chitohexaose and chitosan hexaose with EcChiP. Chitohexaose shows interactions with the channel at both pH 6.0 and 8.2. In contrast, chitosan hexaose did not interact with channel when it is in uncharged form, suggesting that the C_2-NHCOCH$_3$ groups are crucial for the interaction with the affinity sites lining the EcChiP pore, and that this – NHCOCH$_3$ group defines the high specificity of EcChiP for chitooligosaccharides. When the pH of the measuring solution was lowered below the pK$_a$ of chitosan hexaose to 6, the amino group of the chitosan hexaose became cationic through protonation. If chitosan hexaose was added on the cis side at pH 6, negative transmembrane potential ($trans$ Ag/AgCl electrode was negative) helped catonic chitosan hexaose to pass through the EcChiP. The applied voltage serves as the main driving force to pull the cationic chitosan hexaose through EcChiP. With the aid of different transmembrane potential as shown in previous work (Singh et al., 2012), translocation of cationic chitosan hexaose was confirmed and we did not observe binding within the range of transmembrane potentials that we used. Noticeably increasing the transmembrane voltage increases the driving force for translocation. Increases of transmembrane potential increase the frequency of cationic chitosan hexaose being pulled into the pore (the k_{on}) and decreases residence time (Figure 3.19). If sugar is translocated the time spent by the molecules in the pore should decrease with applied voltage. Similarly the residence time decreases with an increase in applied voltage, (Figure 3.19) confirming translocation.

4.7 Temperature-dependence of rates and effect of deuterium bonds on the sugars' translocation

As expected, channel conductance was less in the presence of D_2O due to lower bulk conductivity (Figure 3.21). Moreover, when we used D_2O in the electrolyte, sugar-protein interaction resulted in a longer residence time at the binding site due to stronger bond formation as compared with H_2O, and k_{on} was not effected much in titration experiments (Table 3.5). Inspection of the rates at different temperatures reveals that sugar translocation is not simply diffusion-limited. Free diffusion of KCl in water gives about 6 kT (Lamichhane et al., 2013; Mahendran, Lamichhane, Romero-Ruiz, Nussberger, and Winterhalter, 2013), whereas the barrier for KCl inside EcChiP is slightly higher (6.4 kT) (Figure 3.21). The obtained energy barriers using an Arrhenius plot resulted in 15 (k_{on}) and 9 kT (k_{off}) in H_2O, and 11 (k_{on}) and 10 kT (k_{off}) in D_2O with the sugar addition *trans* side (Figure 3.24). This additional energy in both cases reflects the additional interaction of chitohexaose with channel. The energy barrier for k_{off} in D_2O was slightly higher than in H_2O, reflecting the difficulty of escape by sugar molecules in D_2O because of stronger bonding in D_2O than in H_2O.

4.8 Site-directed mutagenesis for chitohexaose translocation through EcChiP pore

EcChiP mutants with pore-lining residues mutated did not show any remarkable difference in ion selectivity (Figure 3.25 and Table 3.6). It is obvious that we did not mutate any charged residues. In the titration experiments, double mutant (W138A/Y421A) showed a significant change in ion-current reduction in comparison to wild type when sugars were added on *trans* side (Figure 3.26). This is an interesting

result, which shows that residues W138 and Y421 both play a crucial role in the substrate binding. As shown in Table 3.7 the double mutant binding constant is 8-fold lower than that of wild type EcChiP. Moreover, a 5-fold lower k_{on} value was observed, causing an unfavorable interaction with chitohexaose. Measurement of temperature-dependence showed a similar profile to titration experiments. A slight increment of channel conductance was observed for mutants due to the lack of bulk residues in the channel contriction zone (Figure 3.27). The temperature dependence of ion-current fluctuations in single channels allows determination of energy barriers for taking sugar molecules inside the pore and a sugar molecule escaping from the pore. The resulting higher energy barrier for k_{on} in the double mutant (19kT) compared with wild type (15kT) on *trans* side sugar addition reflects the difficulty of getting sugar molecule inside the pore of mutant ChiP.

4.9 Statistical characterization of EcChiP

The trapping function $U(t)$ has a linear time dependence with a slope that increases with [c]. The de-trapping function $B(t)$ has a non-linear time dependence showing two different slope at smaller t and larger t. This qualitative t dependence of $B(t)$ allows to predict backwards escape at small t and translocation at large t. Voltage dependent chitosan hexaose experiments help to confirm backwards escape at smaller t. The initial escape rate $B'(0)$ (dominated by backward escape) is decreased when the potential $|V|$ is increased, by confirming translocation of chitosan molecules with the aid of potential $|V|$. The EcChiP channel is designed to transport chitooligosaccharides through the membrane and, therefore, some translocation of chitohexaose during the experiment can be assumed. If one accepts these points, then the translocation

probability P_T is related to the measurable parameter $\tilde{P}_T$, which thus becomes a key parameter for channel characterization.

4.10 Chitooligosaccharide utilization pathway of *E. coli*

Taking all of our data together, the chitooligosaccharide utilization pathway of *E. coli* was reconstructed based on the GlcNAc-utilization pathway suggested previously (Verma and Mahadevan, 2012; Yang et al., 2006). As shown in Figure 4.1, *E. coli* chitoporin facilitates the uptake of extracellular chitooligosaccharides into the periplasm. The breakdown of high-molecular weight chitosugars (chitotriose, -tetraose, -pentaose and -hexaose) within the periplasm may be initiated by an uncharacterized β-N-acetylglucosaminidase (Hex), yielding GlcNAc and $GlcNAc_2$. In the subsequent step, GlcNAc is transported through the inner membrane by a GlcNAc-specific PTS transporter, forming GlcNAc-6-phosphate, while $GlcNAc_2$ is transported and phosphorylated by the $(GlcNAc_2)$-specific Enzyme II permease of a different PTS system.

Utilization of chitobiose is further mediated by the Chb-BCARFG gene products of the Chb operon (Keyhani, Bacia, and Roseman, 2000; Keyhani, Boudker, and Roseman, 2000; Keyhani, Wang, Lee, and Roseman, 2000). The deacetylase ChbG removes one acetyl group from chitobiose-6-P, generating monoacetyl chitobiose-6-P which is then the substrate for a β-glucosidase, ChbF. Its product, GlcNAc-6-P (Verma and Mahadevan, 2012), is deacetylated to GlcN-6-P by NagA and then deaminated by NagB to fructose-6-P. This final product of the pathway is metabolized as a carbon source for the bacterial cells.
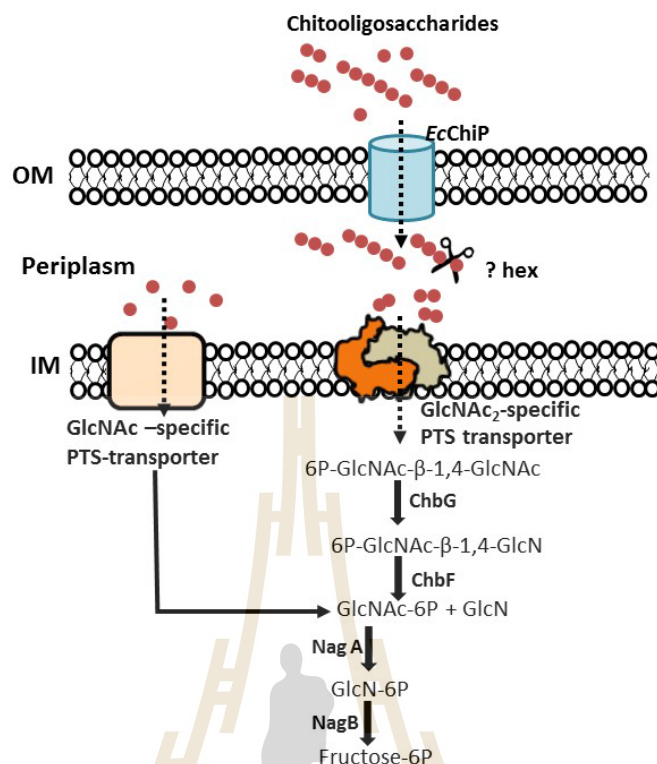
Figure 4.1 The chitooligosaccharide-utilization pathway in *E. coli*. The scheme is based on the GlcNAc-utilization pathway proposed by Yang et al. (Yang et al., 2006) and Verma and Mahadevan (Verma and Mahadevan, 2012). Solid arrows denote enzymic reactions, and dotted arrows denote the direction of sugar transport. *Ec*ChiP, *E. coli* chitoporin; OM, outer membrane; IM, inner membrane; ?Hex, uncharacterized β-N-acetylglucosaminidase (E.C.3.2.1.52); ChbG, chitooligosaccharide mono-deacetylase (E.C.3.5.1.105); ChbF, monoacetyl-chitobiose 6-phosphate hydrolase (E.C.3.2.1.86); NagA, N-acetylglucosamine-6-phosphatedeacetylase (E.C.3.5.1.25); NagB, glucosamine-6-phosphatedeaminase (E.C.3.5.1.10).

PART II

BIOCHEMICAL AND BIOPHYSICAL CHARACTERIZATION OF CHITOPORIN FROM *SERRATIA MARCESCENS*

4.11 Chitin degradation by *Serratia marcescens* and role of chitoporin

Chitin, a highly insoluble β,1-4 linked polymer composed primarily of GlcNAc and one of the most abundant organic substances in nature, is consumed by chitinolytic bacteria such as *Vibrio* species (Chumjan et al., 2015; Keyhani, Li et al., 2000; Li, Wang, Wang, and Roseman, 2007) and *Serratia* species (Vaaje-Kolstad et al., 2013). These chitinolytic bacteria have unique chitinolytic machinery to degrade chitin into chitooligosaccharides and finally use as sole source of carbon and nitrogen (Li and Roseman, 2004; Meibom et al., 2004; Vaaje-Kolstad et al., 2013) and this is achieved using a complex pathway including various enzymes and transporters. It is well known that the outer membrane permeability plays a major role in the Gram-negative bacteria, in terms of uptaking nutrients (Nikaido, 2003). Moreover, diffusion of solutes across the outer membrane usually occurs through porin channels and it is therefore important to first identify the functions of outer membrane protein channels. The chitinolytic machinery of *Serratia marcescens* is one of the best-known systems for chitin degradation. Nevertheless, the physiological function of chitoporin from *Serratia* chitinolytic machinery remains unproved. The role of chitoporins *in vivo* with respect to the permeation of chitosugars across the outer membrane of *Serratia marcescens*

2170 has been studied (Takanao et al., 2014) and proved that chitoporin is essential for uptake higher molecular weight chitosugars, from $GlcNac_3$.

In the present study, chitoporin from *Serratia marcescens* was expressed and purified to elucidate its physiological function as chitooligosaccharide-specific porin. In contrast to other characterized chitoporins from chitinolytic bacteria (Suginta, Chumjan, Mahendran, Janning et al., 2013) *Sm*ChiP showed a monomeric behavior on SDS-PAGE very similar to *Ec*ChiP (Soysa and Suginta, 2016), both of which are members of the OprD family. Monomeric behavior of *Sm*ChiP was further confirmed by calculating molecular weight by intact mass analysis of electrospray.

4.12 *Sm*ChiP specificity

Liposome swelling assays together with ITC experiments and time-resolved single channel analysis in the presence of different sugars showed that the *Sm*ChiP channel responded specifically to chitooligosachcharides and our results clearly indicate no significant interaction from other sugar such as maltodextrins. Swelling assays give an idea of size exclusion cutoffs in *Sm*ChiP by measuring the transport of various size sugars. Generally, nonspecific porins permit entry of di- and sometimes trisaccharides, depending on the shapes of the molecules, up to 600 Da by general diffusion (Siritapetawee, Prinz, Krittanai et al., 2004). There are a few sugar-specific porins, the best characterized being LamB (Baldwin, Bhatia, and Luckey, 2011; Dumas et al., 2000), which permits the entry of high molecular weight maltosugars by a facilitated diffusion process while ScrY porin allows sucrose passage (Van Gelder, Dutzler, Dumas, Koebnik, and Schirmer, 2001).

In the ITC experiments, it is essential to measure enthalpy changes only from binding interactions, and to considerably decrease enthalpy changes from other processes such as buffer mismatch, ligand dilution, and here with the membrane proteins, mismatch in detergent concentrations. Although many literature reviews show only a single control such as ligand to buffer, in this study we have considered three types of control to confirm that calculated enthalpy changes occur only from sugar binding to *Sm*ChiP. Here the binding of $GlcNac_6$ and $GlcNAc_5$ to *Sm*ChiP are an entropy-driven process with a negative $T\Delta S$ of -8.99 kcal/mol and -7.98 kcal/mol. It is interesting to note that no measurable binding occurs when structurally related maltohexaose was used with *Sm*ChiP. In particular, this confirms that binding of chitosugars inside the channel pore and all the thermodynamic parameters are related to binding of sugar inside the channel and not from interaction of sugar molecules with channel exterior walls. Since *Sm*ChiP is specific for chitosugars, it will not allow passage of other sugars. Here the major factor in the net endothermic heat changes may arise from the displacement of ordered water molecules inside the channel (enthalpically unfavorable) (Abraham, Lewis, Hodges, and McElhaney, 2005a) upon binding of sugar. Moreover, binding of chitosugars to *Sm*ChiP is hydrophobic which is enthalpically unfavorable and entrophycally favorable, yielding K_D of 16.96 ± 0.60 μM (K, 58,970 M^{-1}) for chitohexaose and K_D of 23.00 ± 2.00 μM (K, 43,480 M^{-1}) for chitopentaose. The obtained binding constant values from ITC agreed well with the values determined from BLM though the values of binding constant obtained from ITC are a little higher than those from BLM. This may reveal the two different environments by the two methods. BLM experiments give the binding kinetics for single *Sm*ChiP

molecules, reconstituted in an artificial membrane, while ITC experiments give average binding constants for thousands of *Sm*ChiP molecules in solution.

For GlcNAc$_2$, the major product of chitin hydrolysis by *Serratia*, uptake was essential for induction of chitinases and CBP21 production and it seems to be a vital molecule in chitin utilization by *S. marcescens* (Uchiyama et al., 2003). But the presence of chitoporin in the chitin utilization pathway confirms the importance of the porin for larger chitooligosacchrides uptake (Takanao et al., 2014). Our data here further confirm that chitoporin has specificity towards high molecular weight chitooligosaccharides. The presence of chitoporin helps the bacterium to uptake high-molecular weight compounds which help to shield from 'cheaters' that do not invest in the production of extracellular enzymes but do take advantage of the degradation products (Fritsche et al., 2008). One tactic to undermine the effect of chitin cheaters is to degrade chitin only partially into oligomers that supposedly less bacteria can utilize and thus draw less cheaters, and to use an uptake system for further degradation (Allison, 2005).

PART III

BIOCHEMICAL AND BIOPHYSICAL CHARACTERIZATION OF CHITOPORIN FROM *VIBRIO CHOLERAE*

4.13 Chitin degradation by *Vibrio cholerae* and role of chitoporin

Chitin, a polymer of β1,4-linked GlcNAc residues, is an abundant source of carbon and nitrogen for marine microorganisms. Many *Vibrio* species that live in aquatic environments are capable of using chitin as their sole carbon source. Among *Vibrio* species, chitin-*Vibrio cholerae* interactions play important roles including food availability, tolerance to stress and protection from predators (Pruzzo et al., 2008). The chitinolytic cascade in *Vibrios* has been studied in detail and corresponding proteins in chitin utilization program have been characterized such as from *V.cholerae*, *V.harveyi* and *V. furnissii* (Hunt et al., 2008; Keyhani, Li, et al., 2000; Li and Roseman, 2004; Li et al., 2007; Meekrathok and Suginta, 2016; Meibom et al., 2004; Park, Keyhani, and Roseman, 2000; Suginta et al., 2010; Suginta, Sirimontree, Sritho, Ohnuma, and Fukamizo, 2016). But still some data are missing in the chitin utilization pathway. One of example is how chitinase degradation products are taken into the cell. Recently chitoporin from *V. harveyi* was studied and a high resolution X-ray crystal structure became available for the first time, helping understanding of the mechanism of substrate transport at the molecular level (unpublished data).

4.14 Spontaneous gating of the channel

Here the gene responsible for ChiP from *V. cholerae* (VC0972) was cloned into pET23d(+) expression vector and expressed successfully in the outer membrane of *E.coli* BL21(DE3) Omp8 Rossetta. Protein was purified to homogeneity and confirmed by mass spectroscopy. *Vc*ChiP was used to produce polyclonal antibodies, and anti-*Vc*ChiP did not cross-react with *Vh*ChiP, which shares common ancestors. But the *Vh*ChiP X-ray crystal structure provided a good template giving 38% sequence identity, with R.M.S.D. of 0.147 Å for superimposition. The model structure derived from the three-dimensional structure of folded *Vh*ChiP shows that longest loop (L3) protrudes into the channel lumen (Figure 3.47). Many structural analyses of membrane proteins showed that this longest loop constricts the pore (Andersen, Bachmeyer et al., 1999; Eppens, Saint, Van Gelder, van Boxtel, and Tommassen, 1997; Tanabe et al., 2010). Moreover, the modeled structure of *Vc*ChiP shows that the N-terminal extends into the periplasm, similar to *Vh*ChiP. A similar structure has been observed for OprP from the pathogenic bacterium *Pseudomonas aeruginosa* (Moraes et al., 2007) and the voltage-dependent anion channel (VDAC1) which is a eukaryotic membrane protein (Ujwal et al., 2008). There is a general consensus that the N-terminal segment of VDAC is involved in voltage gating and in VDAC1, they proposed a model of the transition from open to closed state by moving the N-terminal (Ujwal et al., 2008). Similarly, in OM-expressed *Vh*ChiP the N-terminal plug was in the pore of a neighboring β-barrel within the trimeric assembly, effectively blocking all β-barrels and the channel for substrate transport (unpublished data). We also assume that the N-terminal of *Vc*ChiP could play a role in channel gating. Supporting this hypothesis, recording of *Vc*ChiP in planar lipid bilayer shows spontaneous gating of the channel.

4.15 Unidirectional channel orientation in planar lipid bilayer

Additionally, the asymmetric gating pattern that is sensitive to the sign of the applied potential allowed us to gain an idea of the channel orientation. The *Vc*ChiP insertion in the bilayer was unidirectional. We further confirmed unidirectional insertion by adding protein into *cis* or *trans* side of the chamber. Basically, many studied outer membrane proteins in planar bilayer studies were added into *cis* side which allowed the extracellular loop to be located on the *cis* side (Andersen, Bachmeyer et al., 1999; Andersen et al., 2002; Danelon et al., 2003). There are some exceptional cases such the simple monomeric OmpG, which shows bi-directional orientation (Chen, Li, and Bayley, 2008). When protein is added into the *trans* side, the gating pattern was exactly reciprocal to *cis* side addition. Our hypothesis of channel gating from the N-terminal was further confirmed by two side (*cis* or *trans*) protein addition experiments. Besides, voltage-induced channel opening of *Vc*ChiP was exhibited, in contrast to voltage-induced gating in many channels at higher applied potential (Arbing, Hanrahan, and Coulton, 2001; Bainbridge, Gokce, and Lakey, 1998; Brunen and Engelhardt, 1993; Heginbotham, LeMasurier, Kolmakova-Partensky, and Miller, 1999; Mauro, Blake, and Labarca, 1988). The single-channel analysis of the *Vc*ChiP channel at high membrane potential (150 -199 mV) shows a high conductance, indicative of a fully open channel. As voltage is decreased, a lower conductance, indicative of a closed channel, is obtained. We assume this is due to the N-terminal plug. Voltage-induced trimeric channel opening is observed with current flow from the direction extracellular to the periplasmic side (negative potential for protein addition: *cis* and positive potential for protein addition: *trans*). Our schematic model (Figure 3.55 top) nicely explains this phenomenon. When current flow is from periplasmic to extracellular (positive potential

for protein addition: *cis* and negative potential for protein addition: *trans*) the N-terminal is inside the pore and produces many sub-states with partial openings of the channel. In the presence of chitosugars, especially with chitohexaose, we assume that since chitohexaose is a bulky molecule with six sugar rings it may stay inside the channel for a long time, so that we can catch all three subunits open upon passage through channel at low potential with sugar-induced channel opening (Figure 3.58). However due to spontaneous channel gating it was difficult to do kinetic evaluation of substrate transport.

4.16 *Vc*ChiP channel specificity

Liposome swelling assays further confirmed that *Vc*ChiP is a chitooligosaccharide- specific channel. Swelling assays give an idea of size exclusion cut-offs of *Vc*ChiP, by measuring the transport of various size sugars. Generally, nonspecific porins are trimeric outer membrane proteins with pore sizes that permit entry of di- or tri-saccharides of < 600 Da, depending on the shape of molecule (Aunkham et al., 2014; Saint et al., 1996; Siritapetawee, Prinz, Krittanai, et al., 2004). This contrasts with sugar-specific porins, the best characterized being LamB (Baldwin et al., 2011; Dumas et al., 2000), which permits the entry of high-molecular weight maltosugars by a facilitated diffusion process, while ScrY porin allows passage of sucrose (Van Gelder et al., 2001). Moreover, previous studies of *Vh*ChiP showed no permeation of oligosaccharides other than chitosugars, including maltose, sucrose, maltopentaose, maltohexaose and raffinose, indicating that *Vh*ChiP is a highly specific channel for chitooligosaccharides (Suginta, Chumjan, Mahendran, Janning, et al.,

2013). Similar results were obtained in the current study with VcChiP and permeation rates of chitosugars were comparable.

In the growth-rate determination experiments, *E. coli* strains with and without VcChiP expression were grown in 0.2 % glycerol, 0.2 % glucose and 0.2 % GlcNAc and the lag-phases were comparable. But when cells were grown with 0.2% $GlcNAc_2$, the lag-phase was short with cells expressing VcChiP, confirming the use of chitoporin for uptaking $GlcNAc_2$ efficiently. Moreover, only chitoporin-expressing cells grew with $GlcNAc_3$, though they showed a prolonged lag-phase during growth, further confirming the importance of chitoporin for uptaking long chain chitooligosaccharides. In the presence of high-molecular weight chitosugars (chito-tetraose and -hexaose) (chitohexaose data is not shown) cells were unable to grow, probably due to lack of periplasmic β-N-acetylglucosaminidase (Hex), to yield low molecular weight chitosugars for further processing.

Taking all of our data together, some questions in our work still remain an unanswered. The main question is why the channel is gated and whether all orthologs from *Vibrio* species share same behavior. This may be due to their marine environments, since gating would be an effective means of restricting the entry of ions in a high-osmolarity environment.

4.17 Chitin uptake efficiency in chitinolytic *versus* non-chitinolytic bacteria

Form a physiological point of view, it may be worth comparing the chitin uptake efficiency of chitinolytic *versus* non-chitinolytic bacteria. *V. harveyi* is a marine

bacterium that requires chitin biomaterials as its sole source of energy. *V. harveyi* contributes significantly to a rapid turnover of chitin in marine ecosystems and the chitin transport protein, known as *Vh*ChiP, of *V. harveyi* has been proved to be highly active (Suginta, Chumjan, Mahendran, Schulte et al., 2013; Suginta and Smith, 2013). When considering their kinetics of chitooligosaccharide transport, it is clearly seen that the binding constant of *Vh*ChiP binding to chitohexaose (500,000 M^{-1}) (cis/-100 mV)(Suginta, Chumjan, Mahendran, Schulte et al., 2013) is ca. 5-fold greater than that of *Ec*ChiP binding to chitohexaose (102,800 M^{-1}) for their most preferable conditions. The results suggested weaker binding of *Ec*ChiP toward chitohexaose than that of *Vh*ChiP to the same sugar.

Table 4.1 contains the on- and off-rate constants together with the binding constant. Binding constants for *Ec*ChiP and *Sm*ChiP were calculated from single channel analysis while *Vh*ChiP binding constant was obtained from ion-current reduction methods (Table 4.1). Considering the on- and off rate constants, *Vh*ChiP showed k_{on} of 85×10^{6} $M^{-1}s^{-1}$ and k_{off} of 170 s^{-1}, while *Ec*ChiP showed a 17-fold lower k_{on} (5×10^{6} $M^{-1}s^{-1}$) and 2-fold lower k_{off} (78 s^{-1}). *Sm*ChiP showed nearly the same k_{off} (190 s^{-1}) as *Vh*ChiP, but k_{on} (3×10^{6} $M^{-1}s^{-1}$) was even less than for *Ec*ChiP. The values suggested that both entrapping and detrapping processes contributed to the binding affinity of the channel but the entrapping step (represented by k_{on}) predominantly determined the distinct interactions of the three channels. The kinetic features confirm the rapid turnover of chitooligosacharide uptake in *V. harveyi*, as compared *E. coli* and *Serratia*.

189

Table 4.1 Comparison of the kinetics of chitohexaose binding to chitoporins from chitinolytic and non-chitinilytic bacteria.

Channel Type	Substrate	k_{on} ($M^{-1}s^{-1}$ $\times 10^6$)	k_{off} (s^{-1})	K(M^{-1})	Ref.
*Ec*ChiP	Chitohexaose	5	78	57,900	This study
*Sm*ChiP	Chitohexaose	3	190	16,500	This study
*Vh*ChiP	Chitohexaose	85	170	500,000	(Suginta, Chumjan et al., 2013)

Moreover, comparision of *in vitro* sugar permeation assays (Figure 4.2) confirm each channel's preference for different chitooligosaccharides.
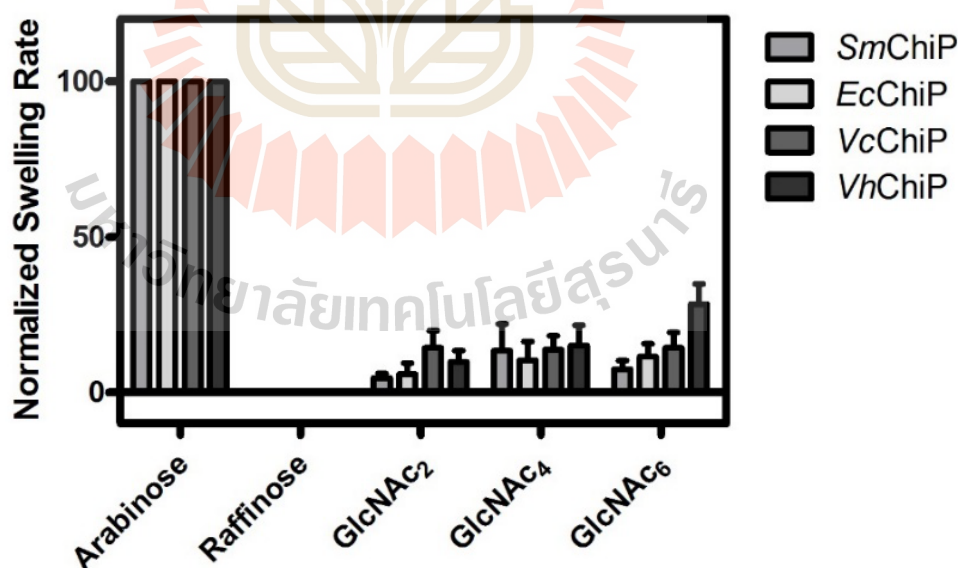
Figure 4.2 Permeation of Chitosugar sugar through *Sm*ChiP, *Ec*ChiP, *Vc*ChiP and *Vh*ChiP-containing proteoliposomes.

*Vh*ChiP shows higher preference for chitohexaose. *Vc*ChiP transports GlcNAc$_2$ and GlcNAc$_4$ much more efficiently than other chitoporins. *Ec*ChiP shows a higher permeation rate for chitooligosaccharides when compared with similar OccD like *Sm*ChiP. The rapid turnover of chitooligosacharides by *E. coli* by taking high amount of sugar molecules may be due to this porin functioning under glucose-deficient conditions while SmChiP uptakes chitosugars in its day-to-day life.
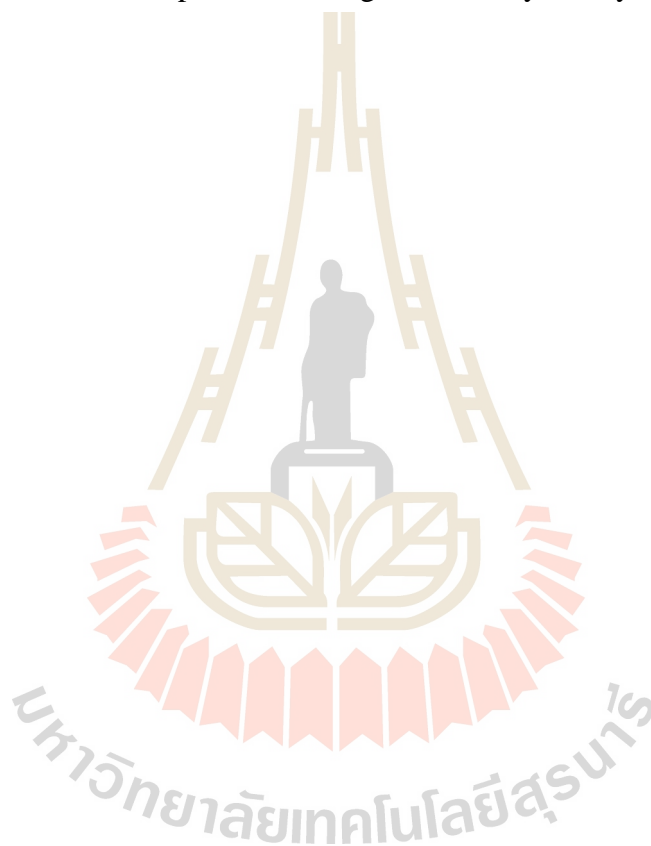
CHAPTER V

CONCLUSION

This study elucidates the physiological function of the chitoporins, and provides an insight into how non-chitinolytic and chitinolytic bacteria can utilize chitin as a source of cellular energy. The study is divided into three parts. The first part is focused on the biochemical and biophysical characterization of *Ec*ChiP. The *Ec*ChiP gene was successfully cloned into pET23d(+) expression vector and expressed in Omp-deficient *E. coli* BL21 (Omp8) Rosetta strain. In this study, we have employed both electrophysiological and biochemical approaches to demonstrate the binding characteristics of the monomeric *Ec*ChiP channel towards chitosugars. The liposome swelling assay suggests that *Ec*ChiP is a chitooligosaccharide-specific channel. Kinetic analysis of sugar transport at the single- molecule level in planar lipid bilayer, using three different analytical approaches, produced fairly consistent K values. ITC data confirmed sugar-channel interactions in solution, with the resultant K value supporting the values obtained by electrophysiological analysis. The ITC data obtained in this study provide some thermodynamic insight into the nature of substrate binding by the *Ec*ChiP channel, which is endothermic, with enthalpy gain and entropy gain. The temperature-dependence experiments helped to gain ideas about the energy barriers involved in sugar-channel interaction while the effect of D_2O on sugar transport showed enhanced sugar-channel interaction through stronger bonding as compared with H_2O. The optimal substrate for *Ec*ChiP was N-acetylated chitooligosaccharides.

The combination of kinetic and thermodynamic data obtained from the studies provides mechanistic details of chitin uptake by non-chitinolytic bacteria.

The second part provides the electrophysiological and thermodynamics insights into the translocation and binding of chitosugars to *Sm*ChiP, which plays an important role in the chitin degradation pathway in *Serratia* by transporting chitooligosaccharides into the periplasm. *Sm*ChiP was expressed in Omp-deficient *E. coli* strain and successfully purified into homogeneity. Here transport of sugars through chitoporin reconstituted into planar lipid membranes has been addressed using single-channel experiments while we show that isothermal titration calorimetry (ITC) offers new possibilities to reveal thermodynamic details of the interaction between the sugar and the channel. The chitosugar binding to *Sm*ChiP is primarily entropy-driven. In conclusion, our study is the first elucidation of the physiological function of the OccD-like ChiP from chitinolytic bacteria, and provides an insight into how *Serratia* uses chitoporin in its chitin degradation pathway.

The third part involved recombinant expression, biochemical and biophysical characterization of chitoporin from *V. cholera*. *Vibrio* species are regarded as important marine chitin degraders and *Vibrio cholerae's* interactions with chitin not only reflect a nutrient-rich habitat but could play a role in cholera epidemics and pandemics worldwide.

The recombinant *Vc*ChiP was successfully cloned into pET23d(+) vector, which was suitable to be expressed in the Omp-deficient *E. coli* BL21 (Omp8) rosetta host strain. The antibody production was done using mass-spectroscope identified purified *Vc*ChiP. *Vc*ChiP was sucssefully reconstituted in planar lipid bilayers and shown to be a voltage-inducible channel, being closed at low voltages (i.e. at -25 mV) and more

open at high voltages (i.e. -150 mV). Observed bulk permeation of various chitooligosaccharides through the *Vc*ChiP-reconstituted liposomes helped to confirm *Vc*ChiP as a chitooligosaccharide-uptake channel. Our cell study indicated that GlcNAc$_3$ clearly induced the growth of the Omp-deficient *E. coli* cells expressing *Vc*ChiP, when grown on the minimal medium, while the control cells without *Vc*ChiP expression could not grow. Overall, the results obtained from this study help to elucidate the role of chitoporin in the chitin utilization pathway of the pathogenic *Vibrio cholerae*.
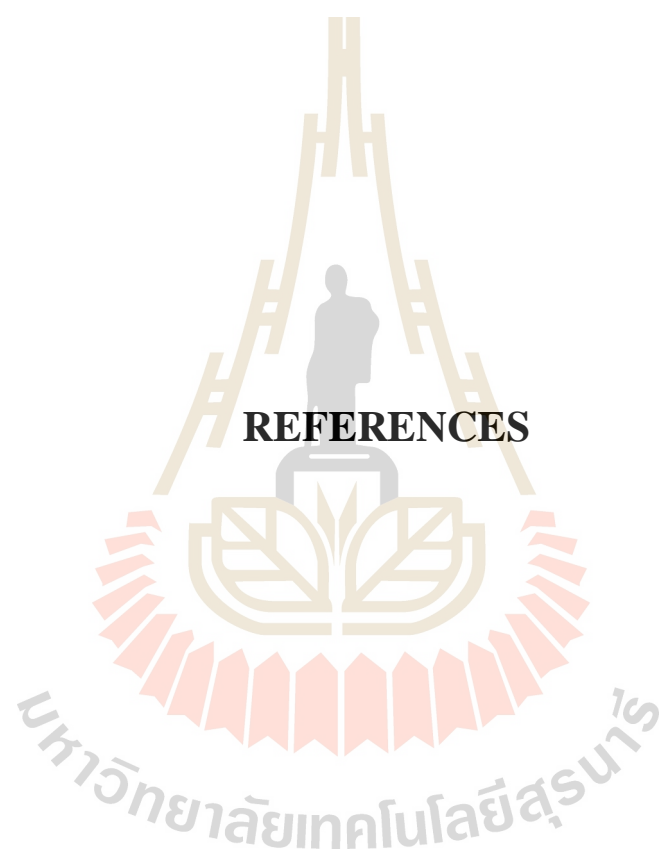
REFERENCES

REFERENCES

Abraham, T., Lewis, R. N., Hodges, R. S., and McElhaney, R. N. (2005a). Isothermal titration calorimetry studies of the binding of a rationally designed analogue of the antimicrobial peptide gramicidin s to phospholipid bilayer membranes. **Biochemistry.** 44(6): 2103-2112.

Abraham, T., Lewis, R. N., Hodges, R. S., and McElhaney, R. N. (2005b). Isothermal titration calorimetry studies of the binding of the antimicrobial peptide gramicidin S to phospholipid bilayer membranes. **Biochemistry.** 44(33): 11279-11285.

Allison, S. D. (2005). Cheaters, diffusion and nutrients constrain decomposition by microbial enzymes in spatially structured environments. **Ecol. Lett.** 8(6): 626-635.

Anbazhagan, V., Sankhala, R. S., Singh, B. P., and Swamy, M. J. (2011). Isothermal titration calorimetric studies on the interaction of the major bovine seminal plasma protein, PDC-109 with phospholipid membranes. **PLoS One.** 6(10): e25993. doi:10.1371/journal.pone.0025993.

Andersen, C., Bachmeyer, C., Tauber, H., Benz, R., Wang, J., Michel, V., and Charbit, A. (1999). In vivo and in vitro studies of major surface loop deletion mutants of the *Escherichia coli* K-12 maltoporin: contribution to maltose and maltooligosaccharide transport and binding. **Mol. Microbiol.** 32(4): 851-867.

Andersen, C., Cseh, R., Schulein, K., and Benz, R. (1998). Study of sugar binding to the sucrose-specific ScrY channel of enteric bacteria using current noise analysis. **J. Membr. Biol.** 164(3): 263-274.

Andersen, C., Jordy, M., and Benz, R. (1995). Evaluation of the rate constants of sugar transport through maltoporin (LamB) of *Escherichia coli* from the sugar-induced current noise. **J. Gen. Physiol.** 105(3): 385-401.

Andersen, C., Rak, B., and Benz, R. (1999). The gene bglH present in the bgl operon of Escherichia coli, responsible for uptake and fermentation of beta-glucosides encodes for a carbohydrate-specific outer membrane porin. **Mol. Microbiol.** 31(2): 499-510.

Andersen, C., Schiffler, B., Charbit, A., and Benz, R. (2002). PH-induced collapse of the extracellular loops closes Escherichia coli maltoporin and allows the study of asymmetric sugar binding. **J. Biol. Chem.** 277(44): 41318-41325.

Arbing, M. A., Hanrahan, J. W., and Coulton, J. W. (2001). Mutagenesis identifies amino acid residues in extracellular loops and within the barrel lumen that determine voltage gating of porin from Haemophilus influenzae type b. **Biochemistry.** 40(48): 14621-14628.

Aunkham, A., Schulte, A., Winterhalter, M., and Suginta, W. (2014). Porin involvement in cephalosporin and carbapenem resistance of Burkholderia pseudomallei. **PloS one**. 9(5): e95918. doi:10.1371/journal.pone.0095918.

Bainbridge, G., Gokce, I., and Lakey, J. H. (1998). Voltage gating is a fundamental feature of porin and toxin beta-barrel membrane channels. **FEBS Lett.** 431(3): 305-308.

Baldwin, V., Bhatia, M., and Luckey, M. (2011). Folding studies of purified LamB protein, the maltoporin from the *Escherichia coli* outer membrane: trimer dissociation can be separated from unfolding. **Biochim. Biophys. Acta.** 1808(9): 2206-2213.

Banerjee, S., and Mazumdar, S. (2012). Electrospray ionization mass spectrometry: a technique to access the information beyond the molecular weight of the analyte. **Int. J. Anal. Chem.** 2012: 282574. doi:10.1155/2012/282574.

Bartlett, D. H., and Azam, F. (2005). Microbiology. Chitin, cholera, and competence. **Science.** 310(5755): 1775-1777.

Benz, R., Frohlich, O., Lauger, P., and Montal, M. (1975). Electrical capacity of black lipid films and of lipid bilayers made from monolayers. **Biochim. Biophys. Acta.** 394(3): 323-334.

Benz, R., and Hancock, R. E. (1987). Mechanism of ion transport through the anion-selective channel of the *Pseudomonas aeruginosa* outer membrane. **J. Gen. Physiol.** 89(2): 275-295.

Benz, R., Janko, K., and Lauger, P. (1979). Ionic selectivity of pores formed by the matrix protein (porin) of *Escherichia coli*. **Biochim. Biophys. Acta.** 551(2): 238-247.

Benz, R., Schmid, A., Nakae, T., and Vos-Scheperkeuter, G. H. (1986). Pore formation by LamB of *Escherichia coli* in lipid bilayer membranes. **J. Bacteriol.** 165(3): 978-986.

Benz, R., Schmid, A., and Vos-Scheperkeuter, G. H. (1987). Mechanism of sugar transport through the sugar-specific LamB channel of *Escherichia coli* outer membrane. **J. Membr. Biol.** 100(1): 21-29.

Berkane, E., Orlik, F., Charbit, A., Danelon, C., Fournier, D., Benz, R., and Winterhalter, M. (2005). Nanopores: maltoporin channel as a sensor for maltodextrin and lambda-phage. **J. nanobiotechnology.** 3(1): 3. doi:10.1186/1477-3155-3-3.

Bezrukov, S. M., Kullman, L., and Winterhalter, M. (2000). Probing sugar translocation through maltoporin at the single channel level. **FEBS Lett.** 476(3): 224-228.

Bhamidimarri, S. P., Prajapati, J. D., van den Berg, B., Winterhalter, M., and Kleinekathofer, U. (2016). Role of Electroosmosis in the Permeation of Neutral Molecules: CymA and Cyclodextrin as an Example. **Biophys. J.** 110(3): 600-611.

Biswas, S., Mohammad, M. M., Patel, D. R., Movileanu, L., and van den Berg, B. (2007). Structural insight into OprD substrate specificity. **Nat. Struct. Mol. Biol**. 14(11): 1108-1109.

Biswas, S., Van Dijck, P., and Datta, A. (2007). Environmental sensing and signal transduction pathways regulating morphopathogenic determinants of *Candida albicans*. **Microbiol. Mol. Biol. Rev.** 71(2): 348-376.

Boulanger, A., Dejean, G., Lautier, M., Glories, M., Zischek, C., Arlat, M., and Lauber, E. (2010). Identification and regulation of the N-acetylglucosamine utilization pathway of the plant pathogenic bacterium *Xanthomonas campestris pv. campestris*. **J. Bacteriol.** 192(6): 1487-1497.

Brunen, M., and Engelhardt, H. (1993). Asymmetry of orientation and voltage gating of the *Acidovorax delafieldii* porin Omp34 in lipid bilayers. **Eur. J. Biochem.** 212(1): 129-135.

Chatterjee, S.N. and chaudhuri, K. (2012). Outer membrane vesicle of bacteria. DOI:10.1007/978-3-642-30526-9.

Chen, M., Li, Q. H., and Bayley, H. (2008). Orientation of the monomeric porin OmpG in planar lipid bilayers. **Chembiochem.** 9(18): 3029-3036.

Chimerel, C., Movileanu, L., Pezeshki, S., Winterhalter, M., and Kleinekathofer, U. (2008). Transport at the nanoscale: temperature dependence of ion conductance. **Eur. Biophys. J.** 38(1): 121-125.

Chumjan, W., Winterhalter, M., Schulte, A., Benz, R., and Suginta, W. (2015). Chitoporin from the Marine Bacterium *Vibrio harveyi*: PROBING THE ESSENTIAL ROLES OF TRP136 AT THE SURFACE OF THE CONSTRICTION ZONE. **J. Biol. Chem.** 290(31): 19184-19196.

Colwell, R. R. (1996). Global climate and infectious disease: the cholera paradigm. **Science.** 274(5295): 2025-2031.

Conlan, S., Zhang, Y., Cheley, S., and Bayley, H. (2000). Biochemical and biophysical characterization of OmpG: A monomeric porin. **Biochemistry.** 39(39): 11845-11854.

Covey, T. R., Bonner, R. F., Shushan, B. I., and Henion, J. (1988). The determination of protein, oligonucleotide and peptide molecular weights by ion-spray mass spectrometry. **Rapid Commun. Mass Spectrom.** 2(11): 249-256.

Danelon, C., Brando, T., and Winterhalter, M. (2003). Probing the orientation of reconstituted maltoporin channels at the single-protein level. **J. Biol. Chem.** 278(37): 35542-35551.

Draczkowski, P., Matosiuk, D., and Jozwiak, K. (2014). Isothermal titration calorimetry in membrane protein research. **J. Pharm. Biomed. Anal.** 87: 313-325.

Dumas, F., Koebnik, R., Winterhalter, M., and Van Gelder, P. (2000). Sugar transport through maltoporin of Escherichia coli. Role of polar tracks. **J. Biol. Chem.** 275(26): 19747-19751.

Dutzler, R., Wang, Y. F., Rizkallah, P., Rosenbusch, J. P. and Schirmer, T. (1996). Crystal structures of various maltooligosaccharides bound to maltoporin reveal a specific sugar translocation pathway. **Structure.** 4: 127-134.

Eppens, E. F., Saint, N., Van Gelder, P., van Boxtel, R., and Tommassen, J. (1997). Role of the constriction loop in the gating of outer membrane porin PhoE of Escherichia coli. **FEBS Lett.** 415(3): 317-320.

Evans, L. J., Cooper, A., and Lakey, J. H. (1996). Direct measurement of the association of a protein with a family of membrane receptors. **J. Mol. Biol.** 255(4): 559-563.

Figueroa-Bossi, N., Valentini, M., Malleret, L., Fiorini, F., and Bossi, L. (2009). Caught at its own game: regulatory small RNA inactivated by an inducible transcript mimicking its target. **Genes Dev.** 23(17): 2004-2015.

Forst, D., Welte, W., Wacker, T., and Diederichs, K. (1998). Structure of the sucrose-specific porin ScrY from *Salmonella typhimurium* and its complex with sucrose. **Nat. Struct. Biol.** 5(1): 37-46.

Francetic, O., Badaut, C., Rimsky, S., and Pugsley, A. P. (2000). The ChiA (YheB) protein of *Escherichia coli* K-12 is an endochitinase whose gene is negatively controlled by the nucleoid-structuring protein H-NS. **Mol. Microbiol.** 35(6):

1506-1517.

Francetic, O., Belin, D., Badaut, C., and Pugsley, A. P. (2000). Expression of the endogenous type II secretion pathway in *Escherichia coli* leads to chitinase secretion. **EMBO J.** 19(24): 6697-6703.

Fritsche, K., de Boer, W., Gerards, S., van den Berg, M., van Veen, J. A., and Leveau, J. H. (2008). Identification and characterization of genes underlying chitinolysis in *Collimonas fungivorans* Ter331. **FEMS Microbiol. Ecol.** 66(1): 123-135.

Guillier, M., and Gottesman, S. (2006). Remodelling of the *Escherichia coli* outer membrane by two small regulatory RNAs. **Mol. Microbiol.** 59(1): 231-247.

Hearn, E. M., Patel, D. R., Lepore, B. W., Indic, M., and van den Berg, B. (2009). Transmembrane passage of hydrophobic compounds through a protein channel wall. **Nature.** 458(7236): 367-370.

Heginbotham, L., LeMasurier, M., Kolmakova-Partensky, L., and Miller, C. (1999). Single streptomyces lividans K(+) channels: functional asymmetries and sidedness of proton activation. **J. Gen. Physiol.** 114(4): 551-560.

Hejazi, A., and Falkiner, F. R. (1997). *Serratia marcescens*. **J. Med. Microbiol.** 46(11): 903-912.

Hilty, C., and Winterhalter, M. (2001). Facilitated substrate transport through membrane proteins. **Phys. Rev. Lett.** 86(24): 5624-5627.

Housden, N. G., Wojdyla, J. A., Korczynska, J., Grishkovskaya, I., Kirkpatrick, N., Brzozowski, A. M., and Kleanthous, C. (2010). Directed epitope delivery across the *Escherichia coli* outer membrane through the porin OmpF. **Proc. Natl. Acad. Sci. U.S.A.** 107(50): 21412-21417.

Hunt, D. E., Gevers, D., Vahora, N. M., and Polz, M. F. (2008). Conservation of the chitin utilization pathway in the *Vibrionaceae*. **Appl. Environ. Microbiol.** 74(1): 44-51.

Huq, A., Sack, R. B., Nizam, A., Longini, I. M., Nair, G. B., Ali, A., Colwell, R. R. (2005). Critical factors influencing the occurrence of *Vibrio cholerae* in the environment of Bangladesh. **Appl. Environ. Microbiol.** 71(8): 4645-4654.

Jung, Y., Bayley, H., and Movileanu, L. (2006). Temperature-responsive protein pores. **J. Am. Chem. Soc.** 128(47):15332-15340.

Kang, X. F., Gu, L. Q., Cheley, S., and Bayley, H. (2005). Single protein pores containing molecular adapters at high temperatures. **Angew. Chem. Int. Ed.Engl.** 44(10): 1495-1499.

Keyhani, N. O., Bacia, K., and Roseman, S. (2000). The transport/phosphorylation of N,N'-diacetylchitobiose in *Escherichia coli.* Characterization of phospho-IIB(Chb) and of a potential transition state analogue in the phosphotransfer reaction between the proteins IIA(Chb) AND IIB(Chb). **J. Biol. Chem.** 275(42): 33102-33109.

Keyhani, N. O., Boudker, O., and Roseman, S. (2000). Isolation and characterization of IIAChb, a soluble protein of the enzyme II complex required for the transport/phosphorylation of N, N'-diacetylchitobiose in *Escherichia coli*. **J. Biol. Chem.** 275(42): 33091-33101.

Keyhani, N. O., Li, X. B., and Roseman, S. (2000). Chitin catabolism in the marine bacterium *Vibrio furnissii*. Identification and molecular cloning of a chitoporin. **J. Biol. Chem.** 275(42): 33068-33076.

Keyhani, N. O., and Roseman, S. (1999). Physiological aspects of chitin catabolism in marine bacteria. **Biochim. Biophys. Acta.** 1473(1): 108-122.

Keyhani, N. O., Wang, L. X., Lee, Y. C., and Roseman, S. (2000). The chitin disaccharide, N,N'-diacetylchitobiose, is catabolized by *Escherichia coli* and is transported/phosphorylated by the phosphoenolpyruvate: glycosephospho transferase system. **J. Biol. Chem.** 275(42): 33084-33090.

Kim, B. H., and Gadd, G. M. (2008). Bacterial physiology and metabolism. Cambridge New York: Cambridge University Press.

Kullman, L., Winterhalter, M., and Bezrukov, S. M. (2002). Transport of maltodextrins through maltoporin: a single-channel study. **Biophys. J.** 82(2): 803-812.

Lamichhane, U., Islam, T., Prasad, S., Weingart, H., Mahendran, K. R., and Winterhalter, M. (2013). Peptide translocation through the mesoscopic channel: binding kinetics at the single molecule level. **Eur. Biophys. J.** 42(5): 363-369.

Li, X., and Roseman, S. (2004). The chitinolytic cascade in *Vibrios* is regulated by chitin oligosaccharides and a two-component chitin catabolic sensor/kinase. **Proc. Natl. Acad. Sci. U.S.A.** 101(2): 627-631.

Li, X., Wang, L. X., Wang, X., and Roseman, S. (2007). The chitin catabolic cascade in the marine bacterium *Vibrio cholerae*: characterization of a unique chitin oligosaccharide deacetylase. **Glycobiology.** 17(12): 1377-1387.

Luckey, M., and Nikaido, H. (1980). Specificity of diffusion channels produced by lambda phage receptor protein of *Escherichia coli*. **Proc. Natl. Acad. Sci. U.S.A.** 77(1): 167-171.

Lutz, C., Erken, M., Noorian, P., Sun, S., and McDougald, D. (2013). Environmental reservoirs and mechanisms of persistence of *Vibrio cholerae*. **Front. Microbiol.**

4: 375. doi:10.3389/fmicb.2013.00375.

Mahendran, K. R., Chimerel, C., Mach, T., and Winterhalter, M. (2009). Antibiotic translocation through membrane channels: temperature-dependent ion current fluctuation for catching the fast events. **Eur. Biophys. J.** 38(8): 1141-1145.

Mahendran, K. R., Lamichhane, U., Romero-Ruiz, M., Nussberger, S., and Winterhalter, M. (2013). Polypeptide Translocation Through the Mitochondrial TOM Channel: Temperature-Dependent Rates at the Single-Molecule Level. **J. Phys. Chem. Lett.** 4(1): 78-82.

Mahlen, S. D. (2011). *Serratia* infections: from military experiments to current practice. **Clin. Microbiol. Rev.** 24(4): 755-791.

Maier, C., Bremer, E., Schmid, A., and Benz, R. (1988). Pore-forming activity of the Tsx protein from the outer membrane of *Escherichia coli*. Demonstration of a nucleoside-specific binding site. **J. Biol. Chem.** 263(5): 2493-2499.

Mauro, A., Blake, M., and Labarca, P. (1988). Voltage gating of conductance in lipid bilayers induced by porin from outer membrane of *Neisseria gonorrhoeae*. **Proc. Natl. Acad. Sci. U.S.A.** 85(4): 1071-1075.

Meekrathok, P., and Suginta, W. (2016). Probing the Catalytic Mechanism of *Vibrio harveyi* GH20 beta-N-Acetylglucosaminidase by Chemical Rescue. **PLoS One.** 11(2): e0149228. doi:10.1371/journal.pone.0149228

Meibom, K. L., Li, X. B., Nielsen, A. T., Wu, C. Y., Roseman, S., and Schoolnik, G. K. (2004). The *Vibrio cholerae* chitin utilization program. **Proc. Natl. Acad. Sci. U.S.A.** 101(8): 2524-2529.

Montal, M., and Mueller, P. (1972). Formation of bimolecular membranes from lipid monolayers and a study of their electrical properties. **Proc. Natl. Acad. Sci. U.**

S.A. 69(12): 3561-3566.

Moraes, T. F., Bains, M., Hancock, R. E., and Strynadka, N. C. (2007). An arginine ladder in OprP mediates phosphate-specific transfer across the outer membrane. **Nat. Struct. Mol. Biol.** 14(1): 85-87.

Nalin, D. R., Daya, V., Reid, A., Levine, M. M., and Cisneros, L. (1979). Adsorption and growth of *Vibrio cholerae* on chitin. **Infect. Immun.** 25(2): 768-770.

Nekolla, S., Andersen, C., and Benz, R. (1994). Noise analysis of ion current through the open and the sugar-induced closed state of the LamB channel of *Escherichia coli* outer membrane: evaluation of the sugar binding kinetics to the channel interior. **Biophys. J.** 66(5): 1388-1397.

Nelson, E. J., Harris, J. B., Morris, J. G., Jr., Calderwood, S. B., and Camilli, A. (2009). Cholera transmission: the host, pathogen and bacteriophage dynamic. **Nat. Rev. Microbiol.** 7(10): 693-702.

Nikaido, H. (2003). Molecular basis of bacterial outer membrane permeability revisited. **Microbiol. Mol. Biol. Rev.** 67(4): 593-656.

Nikaido, H., and Rosenberg, E. Y. (1983). Porin channels in *Escherichia coli*: studies with liposomes reconstituted from purified proteins. **J. Bacteriol.** 153(1): 241-252.

Nisius, L., Rogowski, M., Vangelista, L., and Grzesiek, S. (2008). Large-scale expression and purification of the major HIV-1 coreceptor CCR5 and characterization of its interaction with RANTES. **Protein. Expr. Purif.** 61(2): 155-162.

Pages, J. M., James, C. E., and Winterhalter, M. (2008). The porin and the permeating antibiotic: a selective diffusion barrier in Gram-negative bacteria. **Nat. Rev.**

Microbiol. 6(12): 893-903.

Pajatsch, M., Andersen, C., Mathes, A., Bock, A., Benz, R., and Engelhardt, H. (1999). Properties of a cyclodextrin-specific, unusual porin from *Klebsiella oxytoca*. **J. Biol. Chem.** 274(35): 25159-25166.

Park, J. K., Keyhani, N. O., and Roseman, S. (2000). Chitin catabolism in the marine bacterium *Vibrio furnissii*. Identification, molecular cloning, and characterization of A N, N'-diacetylchitobiose phosphorylase. **J. Biol. Chem.** 275(42): 33077-33083.

Peri, K. G., Goldie, H., and Waygood, E. B. (1990). Cloning and characterization of the N-acetylglucosamine operon of *Escherichia coli*. **Biochem. Cell Biol.** 68(1): 123-137.

Plumbridge, J., Bossi, L., Oberto, J., Wade, J. T., and Figueroa-Bossi, N. (2014). Interplay of transcriptional and small RNA-dependent control mechanisms regulates chitosugar uptake in *Escherichia coli* and *Salmonella*. **Mol. Microbiol.** 92(4): 648-658.

Pruzzo, C., Vezzulli, L., and Colwell, R. R. (2008). Global impact of *Vibrio cholerae* interactions with chitin. **Environ. Microbiol.** 10(6): 1400-1410.

Rajarathnam, K., and Rosgen, J. (2014). Isothermal titration calorimetry of membrane proteins - progress and challenges. **Biochim. Biophys. Acta.** 1838(1 Pt A): 69-77.

Ranquin, A., and Van Gelder, P. (2004). Maltoporin: sugar for physics and biology. **Res. Microbiol.** 155(8): 611-616.

Randall-Hazelbauer, L. and Schwartz, M. (1973). Isolation of the bacteriophage lambda receptor from *Escherichia coli*. **J. Bacteriol**. 116: 1436-1446.

Rasmussen, A. A., Johansen, J., Nielsen, J. S., Overgaard, M., Kallipolitis, B., and Valentin-Hansen, P. (2009). A conserved small RNA promotes silencing of the outer membrane protein YbfM. **Mol. Microbiol.** 72(3): 566-577.

Robert, X., and Gouet, P. (2014). Deciphering key features in protein structures with the new ENDscript server. **Nucleic Acids Res.** 42(Web Server issue): W320-324. doi:10.1093/nar/gku316.

Saint, N., Lou, K. L., Widmer, C., Luckey, M., Schirmer, T., and Rosenbusch, J. P. (1996). Structural and functional characterization of OmpF porin mutants selected for larger pore size. II. Functional characterization. **J. Biol. Chem.** 271(34): 20676-20680.

Saravolac, E. G., Taylor, N. F., Benz, R., and Hancock, R. E. (1991). Purification of glucose-inducible outer membrane protein OprB of *Pseudomonas putida* and reconstitution of glucose-specific pores. **J. Bacteriol.** 173(16): 4970-4976.

Schulein, K., and Benz, R. (1990). LamB (maltoporin) of *Salmonella typhimurium*: isolation, purification and comparison of sugar binding with LamB of *Escherichia coli.* **Mol. Microbiol.** 4(4): 625-632.

Schulein, K., Schmid, K., and Benzl, R. (1991). The sugar-specific outer membrane channel ScrY contains functional characteristics of general diffusion pores and substrate-specific porins. **Mol. Microbiol.** 5(9): 2233-2241.

Schwarz, G., Danelon, C., and Winterhalter, M. (2003). On translocation through a membrane channel via an internal binding site: kinetics and voltage dependence. **Biophys. J.** 84(5): 2990-2998.

Schirmer, T., Keller, T. A., Wang, Y. F. and Rosenbusch, J. P. (1995). Structural basis for sugar translocation through maltoporin channels at 3.1 Å resolution.

Science. 267: 512-514.

Sikora, C. W., and Turner, R. J. (2005a). Investigation of ligand binding to the multi-drug resistance protein EmrE by isothermal titration calorimetry. **Biophys. J.** 88(1): 475-482.

Sikora, C. W., and Turner, R. J. (2005b). SMR proteins SugE and EmrE bind ligand with similar affinity and stoichiometry. **Biochem. Biophys. Res. Commun.** 335(1): 105-111.

Singh, P. R., Barcena-Uribarri, I., Modi, N., Kleinekathofer, U., Benz, R., Winterhalter, M., and Mahendran, K. R. (2012). Pulling peptides across nanochannels: resolving peptide binding and translocation through the hetero-oligomeric channel from *Nocardia farcinica*. **ACS Nano.** 6(12): 10699-10707.

Siritapetawee, J., Prinz, H., Krittanai, C., and Suginta, W. (2004). Expression and refolding of Omp38 from *Burkholderia pseudomallei* and *Burkholderia thailandensis*, and its function as a diffusion porin. **Biochem. J.** 384(3): 609-617.

Siritapetawee, J., Prinz, H., Samosornsuk, W., Ashley, R. H., and Suginta, W. (2004). Functional reconstitution, gene isolation and topology modelling of porins from *Burkholderia pseudomallei* and *Burkholderia thailandensis*. **Biochem. J.** 377(3): 579-587.

Soysa, H. S., and Suginta, W. (2016). Identification and Functional Characterization of a Novel OprD-like Chitin Uptake Channel in Non-chitinolytic Bacteria. **J. Biol. Chem.** 291(26): 13622-13633.

Sritho, N., and Suginta, W. (2012). Role of Tyr-435 of *Vibrio harveyi* chitinase A in chitin utilization. **Appl. Biochem. Biotechnol.** 166(5): 1192-1202.

Strop, P., and Brunger, A. T. (2005). Refractive index-based determination of detergent concentration and its application to the study of membrane proteins. **Protein Sci.** 14(8): 2207-2211.

Suginta, W., Chuenark, D., Mizuhara, M., and Fukamizo, T. (2010). Novel beta-N-acetylglucosaminidases from *Vibrio harveyi* 650: cloning, expression, enzymatic properties, and subsite identification. **BMC Biochem.** 11: 40. doi:10.1186/1471-2091-11-40.

Suginta, W., Chumjan, W., Mahendran, K. R., Janning, P., Schulte, A., and Winterhalter, M. (2013). Molecular uptake of chitooligosaccharides through chitoporin from the marine bacterium *Vibrio harveyi*. **PloS one.** 8(1): e55126. doi:10.1371/journal.pone.0055126

Suginta, W., Chumjan, W., Mahendran, K. R., Schulte, A., and Winterhalter, M. (2013). Chitoporin from *Vibrio harveyi*, a channel with exceptional sugar specificity. **J. Biol. Chem.** 288(16): 11038-11046.

Suginta, W., Sirimontree, P., Sritho, N., Ohnuma, T., and Fukamizo, T. (2016). The chitin-binding domain of a GH-18 chitinase from *Vibrio harveyi* is crucial for chitin-chitinase interactions. **Int. J. Biol. Macromol.** 93(Pt A): 1111-1117.

Suginta, W., and Smith, M. F. (2013). Single-molecule trapping dynamics of sugar-uptake channels in marine bacteria. **Phys. Rev. Lett.** 110(23): 238102. doi:10.1103/PhysRevLett.110.238102.

Suginta, W., and Sritho, N. (2012). Multiple roles of Asp313 in the refined catalytic cycle of chitin degradation by *Vibrio harveyi* chitinase A. **Biosci. Biotechnol. Biochem.** 76(12): 2275-2281.

Suzuki, K., Sugawara, N., Suzuki, M., Uchiyama, T., Katouno, F., Nikaidou, N., and Watanabe, T. (2002). Chitinases A, B, and C1 of *Serratia marcescens* 2170 produced by recombinant *Escherichia coli*: enzymatic properties and synergism on chitin degradation. **Biosci. Biotechnol. Biochem.** 66(5): 1075-1083.

Szmelcman, S., and Hofnung, M. (1975). Maltose transport in *Escherichia coli* K-12: involvement of the bacteriophage lambda receptor. **J. Bacteriol.** 124(1): 112-118.

Takanao, S., Honma, S., Miura, T., Ogawa, C., Sugimoto, H., Suzuki, K., and Watanabe, T. (2014). Construction and basic characterization of deletion mutants of the genes involved in chitin utilization by *Serratia marcescens* 2170. **Biosci. Biotechnol. Biochem.** 78(3): 524-532.

Tanabe, M., Nimigean, C. M., and Iverson, T. M. (2010). Structural basis for solute transport, nucleotide regulation, and immunological recognition of *Neisseria meningitidis* PorB. **Proc. Natl. Acad. Sci. U.S.A.** 107(15): 6811-6816.

Tran, Q. T., Mahendran, K. R., Hajjar, E., Ceccarelli, M., Davin-Regli, A., Winterhalter, M., and Pages, J. M. (2010). Implication of porins in beta-lactam resistance of *Providencia stuartii*. **J. Biol. Chem.** 285(42): 32273-32281.

Trias, J., and Nikaido, H. (1990). Protein D2 channel of the *Pseudomonas aeruginosa* outer membrane has a binding site for basic amino acids and peptides. **J. Biol. Chem.** 265(26): 15680-15684.

Uchiyama, T., Kaneko, R., Yamaguchi, J., Inoue, A., Yanagida, T., Nikaidou, N., and Watanabe, T. (2003). Uptake of N,N'-diacetylchitobiose [(GlcNAc)2] via the phosphotransferase system is essential for chitinase production by *Serratia marcescens* 2170. **J. Bacteriol.** 185(6): 1776-1782.

Ujwal, R., Cascio, D., Colletier, J. P., Faham, S., Zhang, J., Toro, L., and Abramson, J. (2008). The crystal structure of mouse VDAC1 at 2.3 Å resolution reveals mechanistic insights into metabolite gating. **Proc. Natl. Acad. Sci. U.S.A.** 105(46): 17742-17747.

Vaaje-Kolstad, G., Horn, S. J., Sorlie, M., and Eijsink, V. G. (2013). The chitinolytic machinery of *Serratia marcescens*--a model system for enzymatic degradation of recalcitrant polysaccharides. **FEBS J.** 280(13): 3028-3049.

Valentin-Hansen, P., Johansen, J., and Rasmussen, A. A. (2007). Small RNAs controlling outer membrane porins. **Curr. Opin. Microbiol.** 10(2): 152-155.

Van den Berg, B. (2012). Structural basis for outer membrane sugar uptake in *pseudomonads*. **J. Biol. Chem.** 287(49): 41044-41052.

Van Gelder, P., Dumas, F., Bartoldus, I., Saint, N., Prilipov, A., Winterhalter, M., and Schirmer, T. (2002). Sugar transport through maltoporin of *Escherichia coli*: role of the greasy slide. **J. Bacteriol.** 184(11): 2994-2999.

Van Gelder, P., Dumas, F., Rosenbusch, J. P., and Winterhalter, M. (2000). Oriented channels reveal asymmetric energy barriers for sugar translocation through maltoporin of *Escherichia coli*. **Eur. J. Biochem.** 267(1): 79-84.

Van Gelder, P., Dutzler, R., Dumas, F., Koebnik, R., and Schirmer, T. (2001). Sucrose transport through maltoporin mutants of *Escherichia coli*. **Protein Eng.** 14(11): 943-948.

Verma, S. C., and Mahadevan, S. (2012). The chbG gene of the chitobiose (chb) operon of *Escherichia coli* encodes a chitooligosaccharide deacetylase. **J. Bacteriol.** 194(18): 4959-4971.

Vogel, J. (2009). A rough guide to the non-coding RNA world of *Salmonella*. **Mol.**

Microbiol. 71(1): 1-11. doi:10.1111/j.1365-2958.2008.06505.

Vogel, J., and Papenfort, K. (2006). Small non-coding RNAs and the bacterial outer membrane. **Curr. Opin. Microbiol.** 9(6): 605-611.

Wang, Y. F., Dutzler, R., Rizkallah, P. J., Rosenbusch, J. P., and Schirmer, T. (1997). Channel specificity: structural basis for sugar discrimination and differential flux rates in maltoporin. **J. Mol. Biol.** 272(1): 56-63.

Watanabe, T., Kimura, K., Sumiya, T., Nikaidou, N., Suzuki, K., Suzuki, M., and Regue, M. (1997). Genetic analysis of the chitinase system of *Serratia marcescens* 2170. **J. Bacteriol.** 179(22): 7111-7117.

Wohri, A. B., Hillertz, P., Eriksson, P. O., Meuller, J., Dekker, N., and Snijder, A. (2013). Thermodynamic studies of ligand binding to the human homopentameric glycine receptor using isothermal titration calorimetry. **Mol. Membr. Biol.** 30(2): 169-183.

Yang, C., Rodionov, D. A., Li, X., Laikova, O. N., Gelfand, M. S., Zagnitko, O. P., and Osterman, A. L. (2006). Comparative genomics and experimental characterization of N-acetylglucosamine utilization pathway of *Shewanella oneidensis.* **J. Biol. Chem.** 281(40): 29872-29885.

Yoshimura, F., and Nikaido, H. (1985). Diffusion of beta-lactam antibiotics through the porin channels of *Escherichia coli* K-12. **Antimicrob. Agents Chemother.** 27(1): 84-92.

APPENDICES
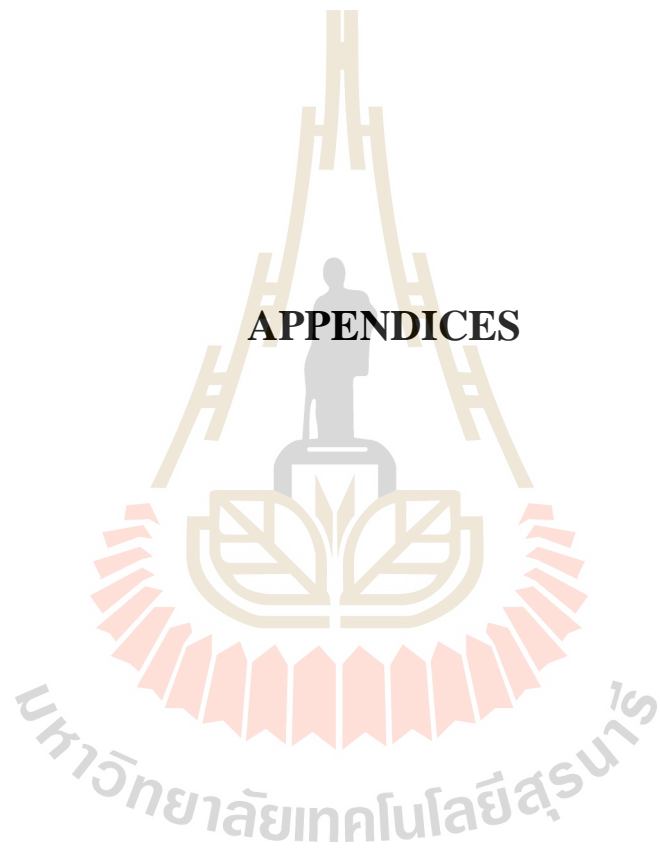
APPENDIX A

PREPARATION OF SOLUTIONS AND REAGENTS

1. Reagents for bacterial culture and competent cell transformation

1.1 Preparation of Luria-Bertani (LB) broth containing antibiotics

10 g Bacto tryptone, 5 g Bacto yeast extract and 10 g NaCl were dissolved in 950 ml distilled water. Mixture was stirred until the solutes have been dissolved. The volume of the solution was adjusted to 1,000 ml with distilled water. The solution is then sterilized by autoclaving at 121 °C for 15 min. The medium is allowed to cool down to 40 °C before antibiotic addition to the final concentration of 100 μg/ml of ampicillin or/and 25 μg/ml of kanamycin. The medium was freshly used or stored at 4 °C until used.

1.2 LB agar medium containing antibiotics

Dissolve 10 g Bacto tryptone, 5 g Bacto yeast extract and 10 g NaCl and 15 g Bacto agar in 950 ml distilled water. Stir until the solutes have been dissolved. Adjust the volume of the solution to 1,000 ml with distilled water. The solution is then sterilized by autoclaving at 121 °C for 15 min. the medium is allowed to cool down to 50 °C before antibiotics addition to the final concentration of 100 μg/ml of ampicillin or/and 25 μg/ml of kanamycin. Pour medium into petri-dishes and allowed the agar to harden and store at 4 °C.

1.3 Antibiotic stock solutions

1.3.1 Ampicillin stock solution (100 mg/ml)

1 g of ampicillin was dissolved in 10 ml of sterile distilled water, filtered solution through 0.2 μm filter, aliquoted and stored at -20 ºC until used.

1.3.2 Kanamycin stock solution (50 mg/ml)

0.5 g of kanamycin 1 g of ampicillin was dissolved in 10 ml of sterile distilled water, filtered solution through 0.2 μm filter, aliquoted and stored at -20 ºC until used.

1.4 Isopropyl thio-β-D-galactoside (IPTG) stock solution (1 M)

2.38 g of IPTG was dissolved in distilled water and adjusted final volume to 10 ml. The stock solution was filtered and aliquoted to small volume and stored at -20 ºC.

2. Reagents for competent *E. coli* cell preparation

2.1 1M CaCl$_2$ stock solution

14.7 g of calcium chloride was dissolved in 100 ml of water and autoclaved at 121 ºC, for 15 min.

2.2 30% glycerol

30% (v/v) glycerol was autoclaved at 121 ºC, for 15 min.

3. Reagent for agarose gel electrophoresis

3.1 10x TAE buffer

48.2 g of Tris-base, 3.7 g of EDTA and 11. 4 ml of glacial acetic acid were mixed together and final volume was adjusted to 1000 ml. Solution was stored at room temperature.

3.2 6x DNA loading solution (10 ml)

0.025 g Bromophenol blue and 0.025 g xylene cyanol were mixed and 3 ml of 100% (v/v) of glycerol was added. Then the final volume was adjusted to 10 ml with ditilled water and stored at -20 °C.

4. Solutions for protein expression and purification

4.1 Lysis buffer pH 8.0 (200 mM Tris-HCl, 25 mM $MgCl_2$, 1 mM $CaCl_2$)

4.84 g of Tris-base, 1 g of $MgCl_2$, and 29.4 mg of $CaCl_2$ were dissolved in 100 ml of distilled water and pH was adjusted to 8.0 with 6 M HCl and filled water upto 200 ml.

4.2 0.2 M Na_2HPO_4 (Mr = 141.96 g/mol)

28.39 g of Na_2HPO_4 was dissolved in 500 ml of distilled water and adjusted volume to 1,000 ml with distilled water.

4.3 0.2 M NaH_2PO_4 (Mr = 137.99 g/mol)

27.6 g of NaH_2PO_4 was dissolved in 500 ml of distilled water and adjusted volume to 1000 ml with distilled water.

4.4 0.1 M phosphate buffer (PB), pH 7.4

Preparation of 100 ml of 0.1 M PB, pH 7.4 working solution, the stock solution was mixed as follows:

- 40.5 ml of 0.2 M Na_2HPO_4

- 9.5 ml of 0.2 M NaH_2PO_4

The volume was adjusted to 100 ml with distilled water and stored the solution at 4 °C.

4.5 20% SDS stock solution

10 g of SDS was dissolved in distilled water to final volume of 50 ml and stored at room temperature.

4.6 DNase I (10 mg/ml)

0.001 g of DNase I was dissolved in 20 mM PB (pH 7.4) to the final volume of 100 μl and kept at -20 °C before used.

4.7 RNase A (10 mg/ml)

0.01 g of RNase A was dissolved in 20 mM PB (pH 7.4) to the final volume of 1,000 μl and kept at -20 °C before used.

4.8 3% Octyl-POE

3 ml of octyl-POE was diluted in 20 mM PB (pH 7.4) to the final volume of 100 ml and stored at 4 °C before used.

4.9 0.125% Octyl-POE

0.125 ml of octyl-POE was diluted in 20 mM PB (pH 7.4) to the final volume of 100 ml and stored at 4 °C before used.

4.10 0.2% LDAO

6.6 ml of LDAO was diluted in 20 mM PB (pH 7.4) to the final volume of 1000 ml and stored at 4 °C before used.

4.11 5x reducing buffer

5 ml of 0.5 M Tris-HCl (pH 6.8), 1 g SDS, 0.5 ml of 5% bromophenol blue and 2.5 ml of 100% glycerol and 0.5 ml of 2-mercaptoethanol was mixed and final volume was adjusted to the 10 ml. The solution was stored at -30 °C.

4.12 1.5 M Tris-HCl (pH 8.8)

18.17 g of Tris-base was dissolved in 80 ml distilled water. pH was adjusted to 8.8 with 6 M HCl and the volume was adjusted up to 100 ml with distilled water and stored at 4 °C.

4.13 0.5 M Tris-HCl (pH 6.8)

6 g of Tris-base was dissolved in 80 ml distilled water. pH was adjusted to 6.8 with 6 M HCl and the volume was adjusted up to 100 ml with distilled water and stored at 4 °C.

4.14 30% (w/v) Acrylamide solution

30 g of acrylamide (MW. 71.08) and 0.8 g of bis-acrylamide (MW.154.2) was mixed in distilled water to a final volume of 100 ml. The solution was filtered with 0.45 µm filter paper and stored in the dark bottle at 4 °C.

4.15 Tris-glycine electrode buffer (10x stock solution)

30.29 g of Tris-base (MW 121.14), 144 g of glycine (MW 75.07) and 10 g of SDS were mixed in distilled water and final volume was adjusted to 1 liter with distilled water.

4.16 Staining solution with Coomassie Brilliant Blue for protein

1 g of Coomassie Brilliant Blue R-250, 400 ml methanol, 530 ml distilled water and 70 ml glacial acetic acid were mixed together and filtered through a whatman filter paper membrane No. 1 and Stored the solution in the dark bottle at room temperature.

4.17 Destaining solution I

400 ml methanol and 70 ml glacial acetic acid were mixed and then added distilled water to the final volume of 1,000 ml.

4.18 Destaining solution II

50 ml methanol and 70 ml glacial acetic acid were mixed and then added distilled water to the final volume of 1,000 ml.

4.19 10% (w/v) Ammonium persulphate

1 g of ammonium persulphate was dissolved in 10 ml of distilled water and stored the solution at -20 °C.

4.20 12% (w/v) Separating SDS-PAGE gel

The solution was mixed as follows:

1.5 M Tris-HCl (pH 8.8) 2.5 ml

Distilled water 3.3 ml

10% (w/v) SDS 0.1 ml

30% (w/v) Acrylamide solution 4.0 ml

10% (w/v) Ammonium persulphate 0.05 ml

TEMED 0.005 ml

4.21 5% (w/v) Stacking SDS-PAGE gel

The solution was mixed as follows:

0.5 M Tris-HCl (pH 6.8) 1.25 ml

Distilled water 3.0 ml

10% (w/v) SDS 0.05 ml

30% (w/v) Acrylamide solution 0.655 ml

10% (w/v) Ammonium persulphate 0.25 ml

TEMED 0.005 ml

5. Buffer solutions for BLM technique

5.1 1 M KCl in 20 mM HEPES pH 7.4 or 8.0

4.766 g of HEPES (MW 238.3) and 74.55 g of KCl (MW 74.55) were dissolved in 900 ml of distilled water and adjusted pH to 7.4 or 8. Then final volume was adjusted to 1000 ml.

5.2 1 M KCl in 20 mM MES pH 5.5

3.90 g of MES (MW 195.2) and 74.55 g of KCl (MW 74.55) were dissolved in 900 ml of distilled water and adjusted pH to 5.5. Then final volume was adjusted to 1000 ml.

5.3 2 mM Stock of chitohexaose (Mr = 1237.2 g/mol, GlcNAc$_6$)

0.0025 g of GlcNAc$_6$ was dissolved in 1 ml of 1 M KCl in 20 mM HEPES pH 7.4, 8.0/ or 1 M KCl in 20 mM MES pH 5.5 and stored at -20 $^{\circ}$C before used.

5.4 2 mM Stock of chitopentaose (Mr = 1034 g /mol, GlcNAc$_5$)

0.0021 g of GlcNAc$_5$ was dissolved in 1 ml of 1 M KCl in 20 mM HEPES pH 7.4, 8.0/ or 1 M KCl in 20 mM MES pH 5.5 and stored at -20 $^{\circ}$C before used.

5.5 2mM Stock of chitotetraose (Mr = 830.78 g/mol, GlcNAc$_4$)

0.0017 g of GlcNAc$_4$ was dissolved in 1 ml of 1 M KCl in 20 mM HEPES pH 7.4, 8.0/ or 1 M KCl in 20 mM MES pH 5.5 and stored at -20 $^{\circ}$C before used.

5.6 2 mM Stock of chitotriose (Mr = 627.6 g/mol, GlcNAc$_3$)

0.0013 g of GlcNAc$_3$ was dissolved in 1 ml of 1 M KCl in 20 mM HEPES pH 7.4, 8.0/ or 1 M KCl in 20 mM MES pH 5.5 and stored at -20 $^{\circ}$C before used.

5.7 2 mM Stock of chitobiose (Mr = 424.4 g/mol, GlcNAc$_2$)

0.0008 g of GlcNAc$_2$ was dissolved in 1 ml of 1 M KCl in 20 mM HEPES pH 7.4, 8.0/ or 1 M KCl in 20 mM MES pH 5.5 and stored at -20 $^{\circ}$C before used.

5.8 2 mM Stock of *N*-acetylglucosamine (Mr = 221.208 g/mol, GlcNAc)

0.0004 g of GlcNAc was dissolved in 1 ml of 1 M KCl in 20 mM HEPES pH 7.4, 8.0/ or 1 M KCl in 20 mM MES pH 5.5 and stored at -20 $^{\circ}$C before used.

5.9 5 mg/ml Diphytanoyl phosphatidylcholine (DPhPC)

5 mg of DPhPC was dissolved in *n*-pentane and stored at -20 $^{\circ}$C.

5.10 1% Hexadecane in *n*-hexane

10 μl of hexadecane was diluted in 990 μl of *n*-hexane and stored at -20 $^{\circ}$C.

6. Medium for growth rate experiments

- Make M9 salts

- To make M9 Salts aliquot 800 ml H_2O and add

  o 64 g $Na_2HPO_4-7H_2O$

  o 15 g KH_2PO_4

  o 2.5 g NaCl

  o 5.0 g NH_4Cl

  o Stir until dissolved

  o Adjust to 1000 ml with distilled H_2O

  o Sterilize by autoclaving

- Measure ~700 ml of distilled H_2O (sterile)

- Add 200 ml of M9 salts

- Add 2 ml of 1M $MgSO_4$ (sterile)

- Add 20 ml of 20% glucose (or other carbon source)

- Add 100 µl of 1M $CaCl_2$ (sterile)

-Adjust to 1000 ml with distilled H_2O

APPENDIX B

COMPETENT CELL PREPARATIONS AND PLASMID

TRANSFORMATIONS

1. Preparation of competent cells

The *E. coli* DH5α, XL1 Blue and Omp8 Rosetta strain are bacterial strain used for the competent cell preparations. The single colony was picked up from LB agar plate and grown in 10 ml of LB broth and incubated at 37 °C for overnight (16 hr) at 200 rpm. Then 1 ml of the overnight cell cultured was subjected into 100 ml of LB broth (ratio 1:100) and grown at 37 °C until OD_{600} reached about 0.4-0.5. The cell cultured was transferred into a pre-chilled polypropylene tube, chilled on ice for 10 min, and the cell pellets were collected by centrifugation at 4,500 rpm at 4 °C for 15 min. The cell pellets were gently resuspended in 20 ml of pre-chilled 100 mM $CaCl_2$ solution on ice, then centrifuged at 4,500 rpm at 4 °C for 15 min. Then, the cell pellets were gently resuspended again in 10 ml of pre-chilled 100 mM $CaCl_2$ solution incubated 30 min on ice. The cell pellets were collected as describe above, then 1 ml of 100 mM pre-chilled $CaCl_2$ and 1 ml of 30% glycerol were used to resuspend the cell. Finally 100 μl of suspension competent cells were aliquoted into 1.5 ml eppendroft tube. The competent cells were frozen using snap-freeze technique under liquid nitrogen and stored at -80 °C.

2. Plasmid transformation (Heat shock method)

The frozen competent cells were gently thawed on ice and then added 50-100 ng recombinant plasmid DNAs of ChiP into 100 µl of the competent cells and kept on ice 30 min. The mixture were immediately placed at 42 °C for 45 second and then rapidly placed on ice again for 2 min. Then 900 µl of pre-warmed LB broth at 37 °C was added into the transformed cells and incubated at 37 °C at 200 rpm for 45 min. 800 µl of supernatant were removed by centrifugation at 4,500 rpm for 5 min, and the remaining 200 µl of cells were spread on an LB agar plate containing the appropriate antibiotic and then incubated at 37 °C overnight (16 hour).
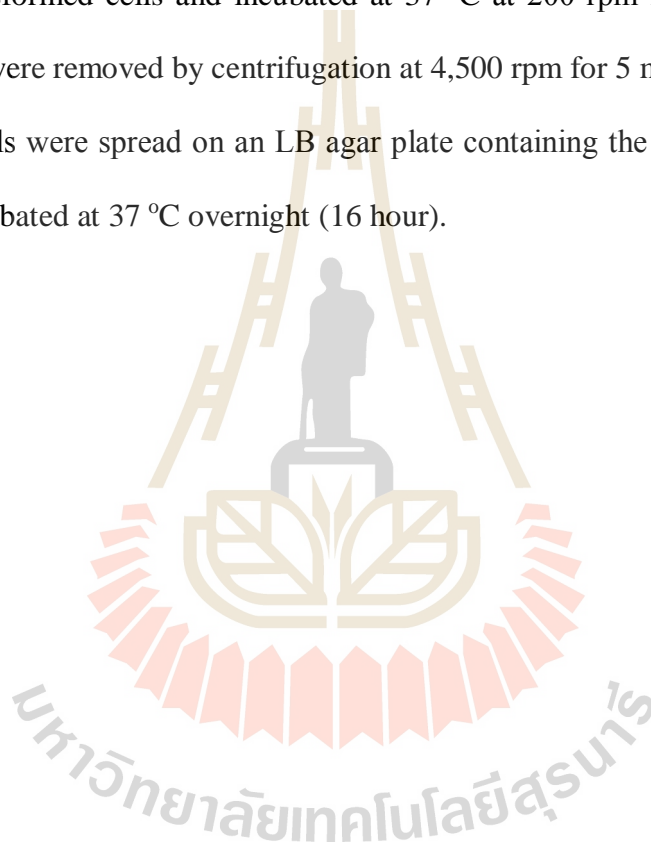
APPENDIX C

SDS-PAGE ANALYSIS

The castings frames were set on the casting stands and distilled water was added and waited 15 min to check whether the gel caster is leak. Then water was removed and the separating gel was added into the gap between glass plates to 3 cm below the top edge of the glass plates. To make the top of the separating gel be horizontal, the water was filled into the gap until an overflow and waited for 20-30 minutes to let it gelate. Then water was discarded and stacking gel was loaded until an overflow. The well-forming comb was inserted and the comb was taken out after complete gelation. The glass plates were took out of the casting frame and set in the cell buffer dam. The running buffer was poured into the chamber and sample with reducing buffer (loading buffer) and protein marker were loaded into the well. Then the voltage (120 V) was set and run the electrophoresis around one hour.

APPENDIX D

SUPPORTING INFORMATIONS
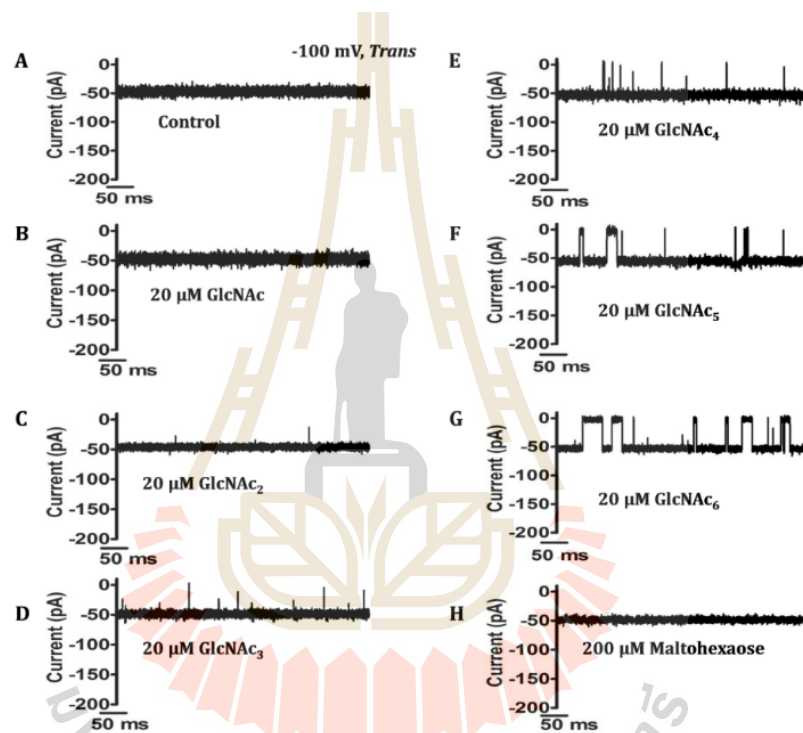
Supplementary Figure 1: Ion current recordings of single *Ec*ChiP channels in the presence of different chitooligosaccharides, of various chain lengths. Here, only current traces for 500 ms at -100 mV, *trans* are presented. (A) A fully open state of *Ec*ChiP before sugar addition. Then (B) *N*-acetylglucosamine (GlcNAc), (C) chitobiose (GlcNAc$_2$), (D) chitotriose (GlcNAc$_3$), (E) chitotetraose (GlcNAc$_4$), (F) chitopentaose (GlcNAc$_5$) or (G) chitohexaose (GlcNAc$_6$) were added on the *trans* side of the chamber, to a final concentration of 20 µM. (H) Control recording with maltohexaose at a final concentration of 200 µM.
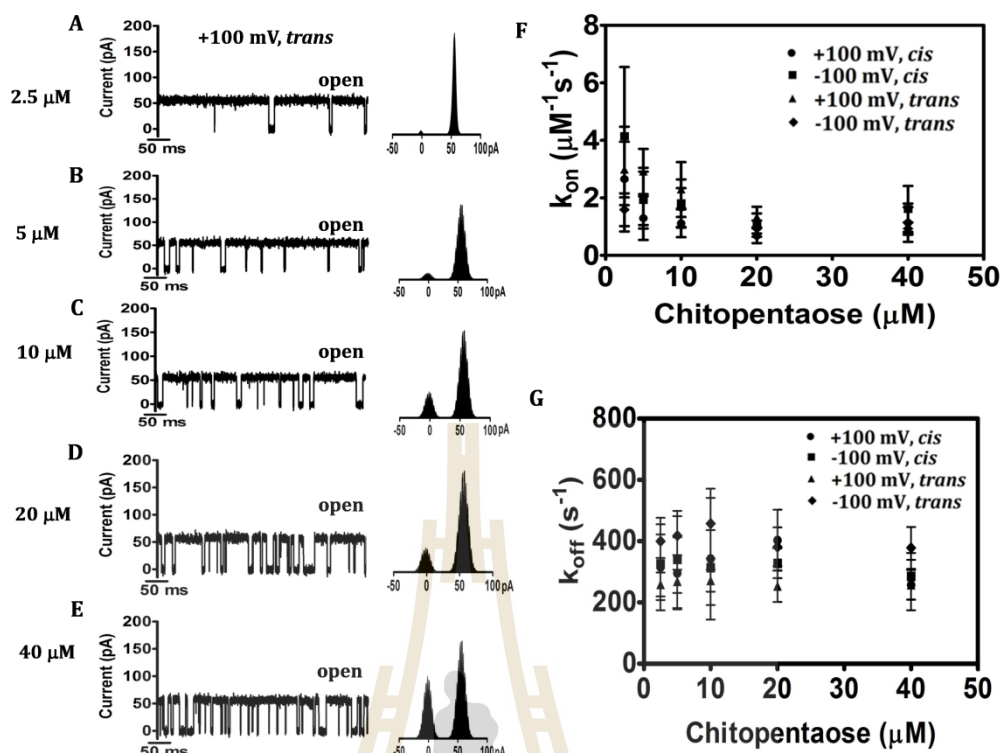
Supplementary Figure 2: Reduction of single *Ec*ChiP channel conductance with increasing chitopentaose concentration and single channel analysis. Ion current fluctuations were monitored for 120 s at applied potentials of ±100 mV with chitopentaose addition on either the *cis* or the *trans* side. Here only current traces for 500 ms are presented, with five different concentrations at + 100 mV *trans* (A-E). (F) Association rate (G) Dissociation rate.
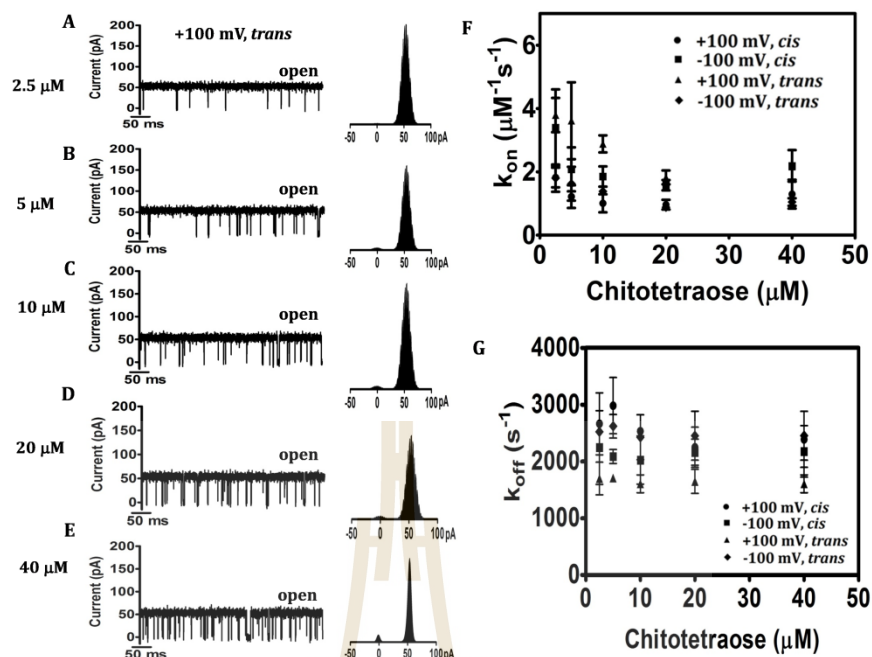
Supplementary Figure 3: Single channel analysis of the reduction of single *Ec*ChiP channel conductance by increasing concentrations of chitotetraose. Ion current fluctuations were monitored for 120 s at applied potentials of ±100 mV with chitotetraose addition on either the *cis* or the *trans* side. Here only current traces for 500 ms are presented, with five different concentrations at + 100 mV *trans* (A-E). (F) Association rate (G) Dissociation rate.
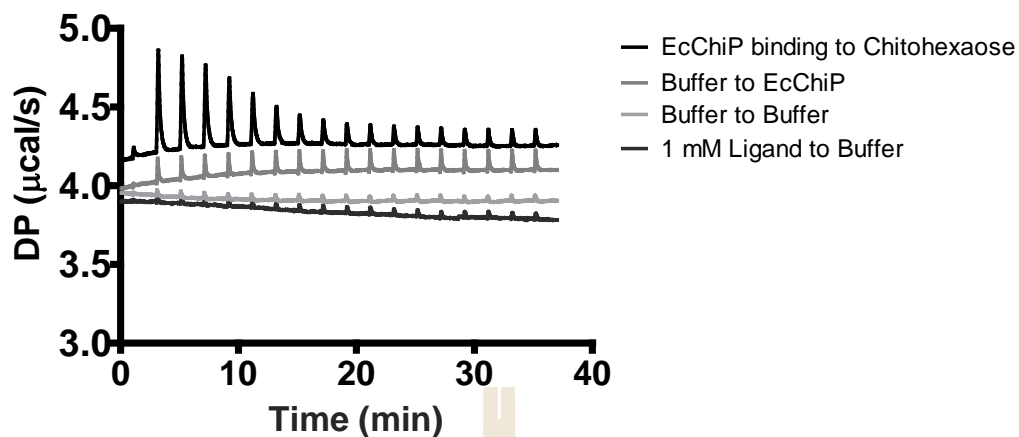
Supplementary Figure 4 *Ec*ChiP binding to chitohexaose, in comparison with controls, in ITC experiments. Control experiments were performed by injecting ligand solution into buffer, buffer solution into protein solution and buffer into buffer in an identical manner and the resulting heat changes were subtracted from the measured heat of binding.
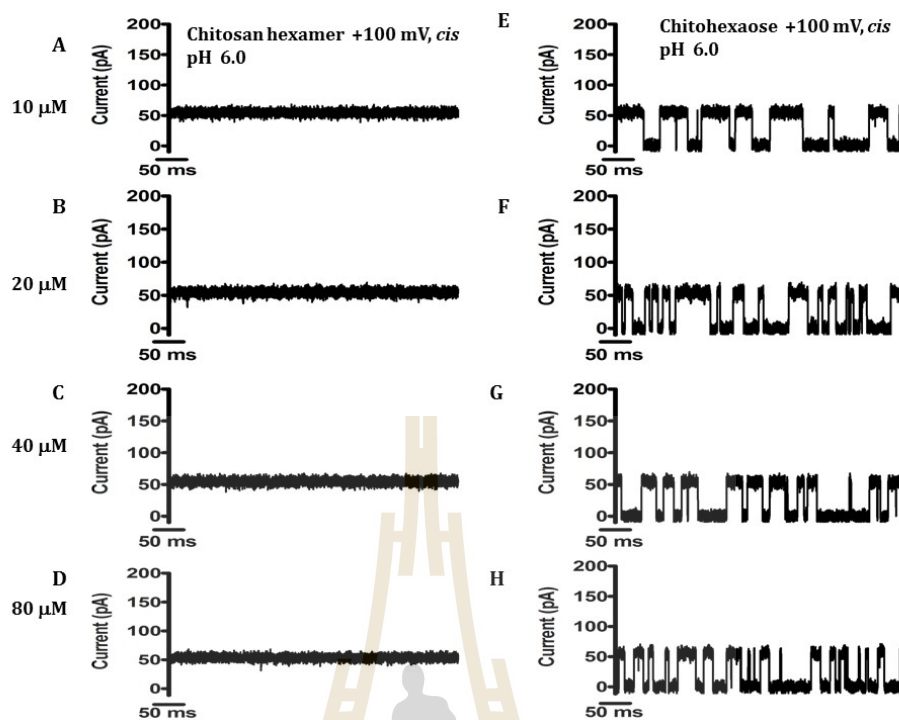
Supplementary Figure 5 Effect of N-acetyl functionality on *Ec*ChiP at pH 6.0 (sugar on the *cis*, positive membrane potentials). Ion current fluctuations were monitored for 120 s at applied potentials of + 100 mV with sugar addition on the *cis* side. Here only current traces for 500 ms are presented, with four different chitosan hexaose concentrations (A-D, left panels) and four different chitohaxaose concentrations (E-H, right panels).
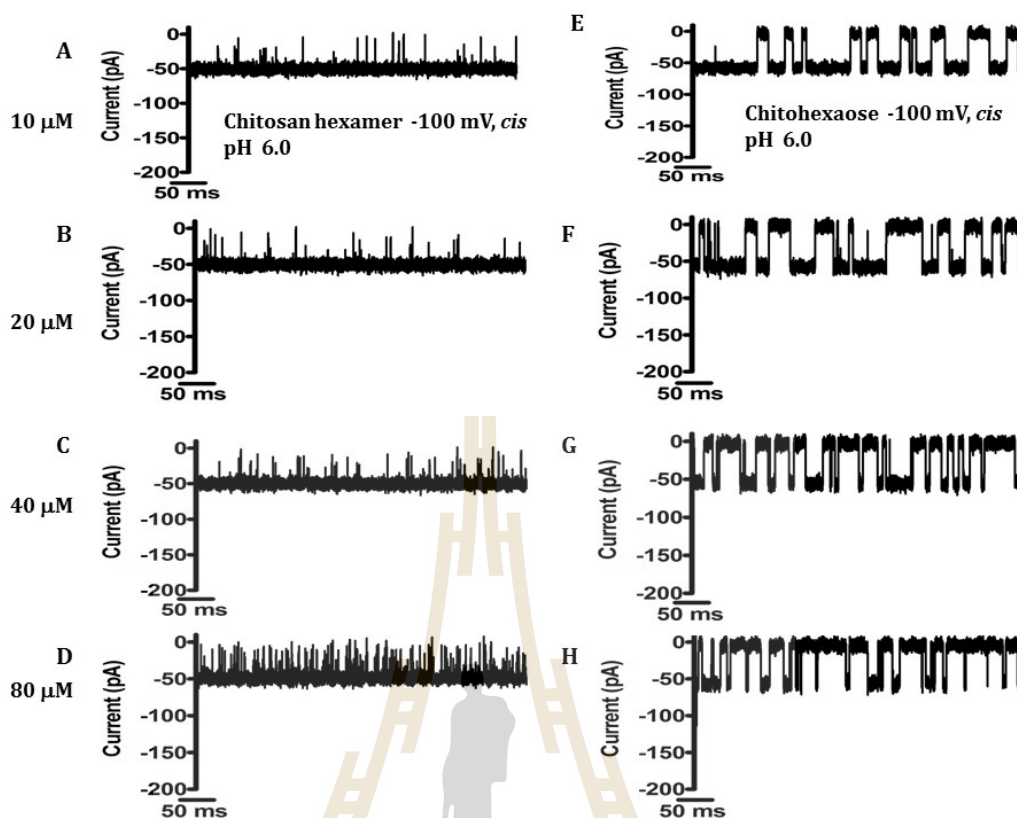
Supplementary Figure 6 Effect of N-acetyl functionality on *Ec*ChiP at pH 6.0 (sugar on the *cis*, negative membrane potentials). Ion current fluctuations were monitored for 120 s at applied potentials of – 100 mV with sugar addition on the *cis* side. Here only current traces for 500 ms are presented, with four different chitosan hexaose concentrations (A-D, left panels) and four different chitohaxaose concentrations (E-H, right panels).
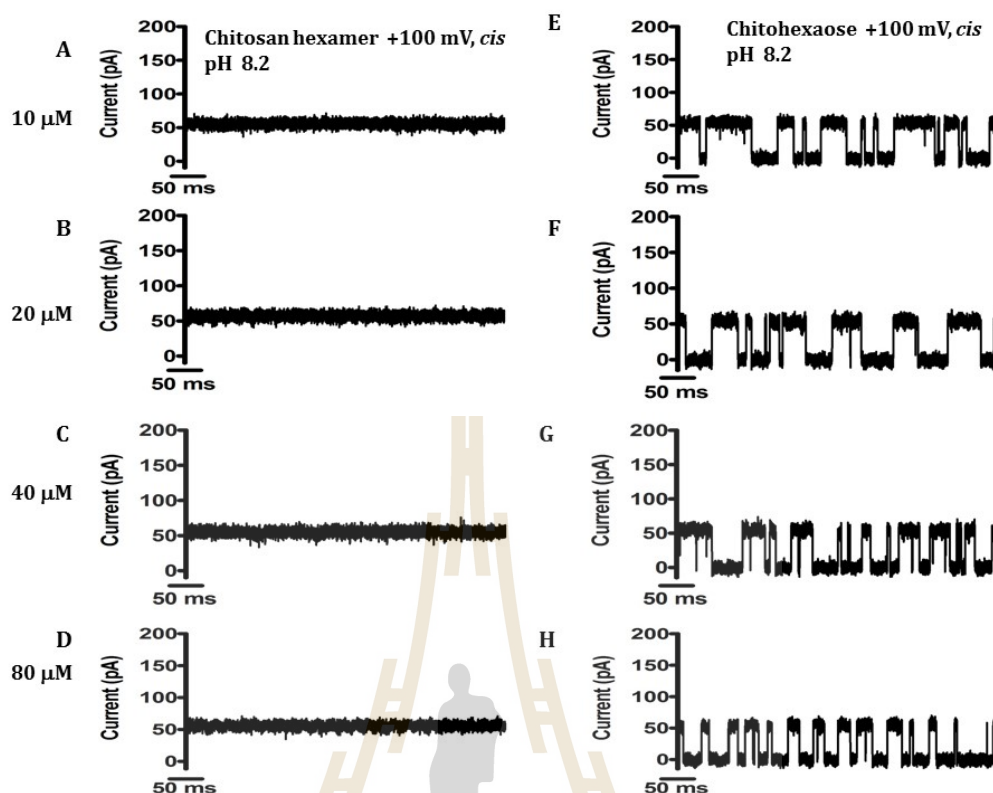
Supplementary Figure 7 Effect of N-acetyl functionality on *Ec*ChiP at pH 8.2 (sugar on the *cis*, positive membrane potentials). Ion current fluctuations were monitored for 120 s at applied potentials of + 100 mV with sugar addition on the *cis* side. Here only current traces for 500 ms are presented, with four different chitosan hexaose concentrations (A-D, left panels) and four different chitohaxaose concentrations (E-H, right panels).
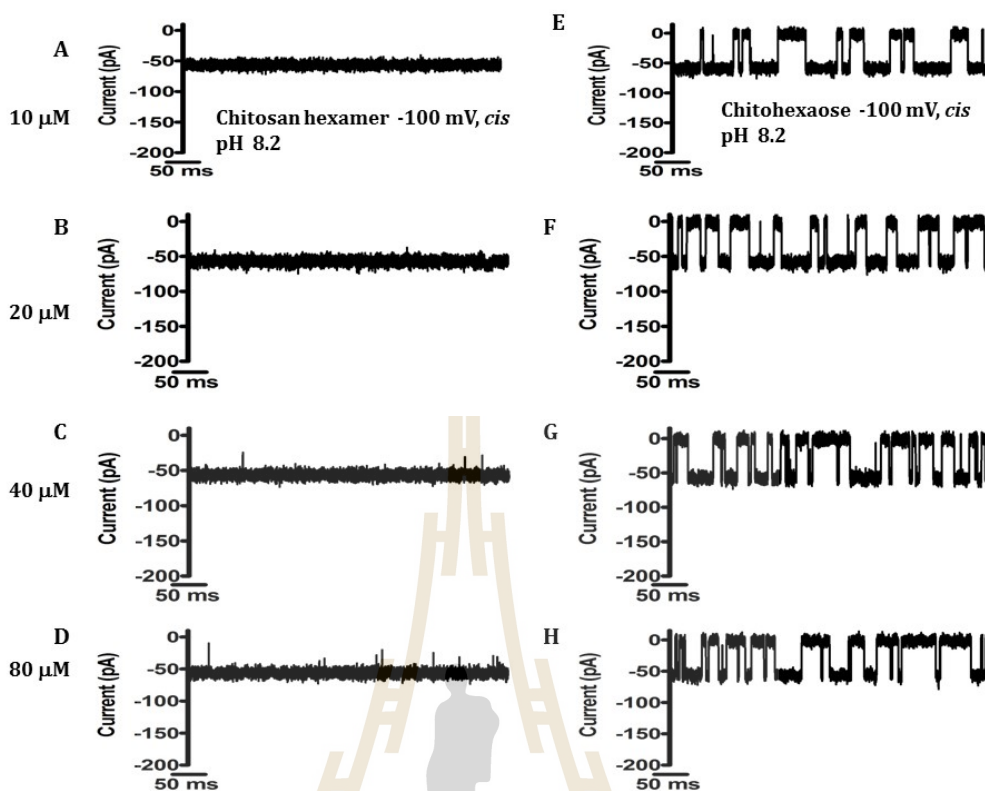
Supplementary Figure 8 Effect of N-acetyl functionality on *Ec*ChiP at pH 8.2 (sugar

on the *cis*, negative membrane potentials). Ion current fluctuations were monitored for

120 s at applied potentials of – 100 mV with sugar addition on the *cis* side. Here only

current traces for 500 ms are presented, with four different chitosan hexaose

concentrations (A-D, left panels) and four different chitohaxaose concentrations (E-H,

right panels).
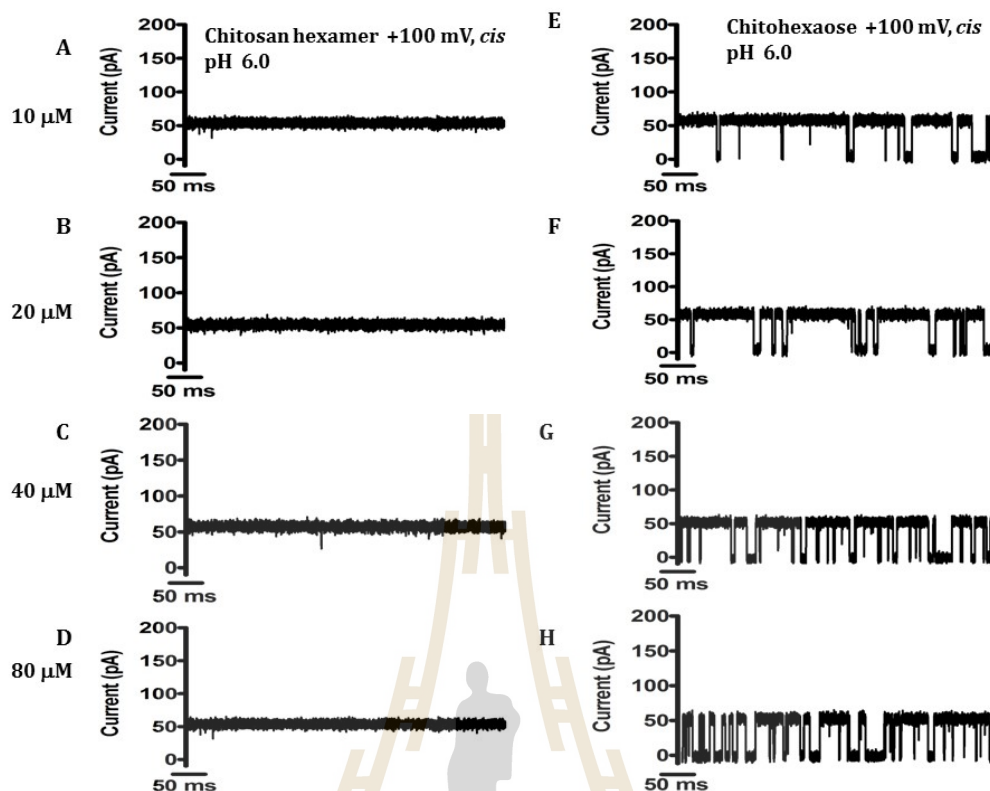
Supplementary Figure 9 Effect of N-acetyl functionality on *Sm*ChiP at pH 6.0 (sugar on the *cis*, positive membrane potentials). Ion current fluctuations were monitored for 120 s at applied potentials of + 100 mV with sugar addition on the *cis* side. Here only current traces for 500 ms are presented, with four different chitosan hexaose concentrations (A-D, left panels) and four different chitohaxaose concentrations (E-H, right panels).
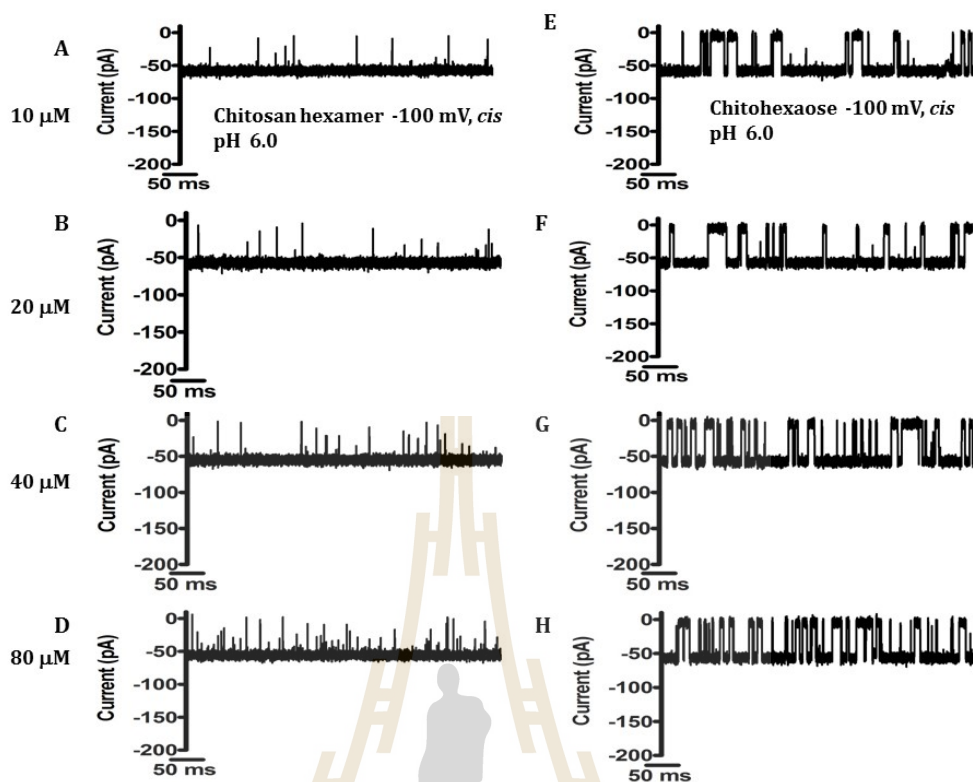
Supplementary Figure 10 Effect of N-acetyl functionality on *Sm*ChiP at pH 6.0 (sugar on the *cis*, negative membrane potentials). Ion current fluctuations were monitored for 120 s at applied potentials of – 100 mV with sugar addition on the *cis* side. Here only current traces for 500 ms are presented, with four different chitosan hexaose concentrations (A-D, left panels) and four different chitohaxaose concentrations (E-H, right panels).

Supplementary Table 1 Effects of pH on the binding constant of *Ec*ChiP towards charged and uncharged chitooligosaccharides.

pH	Chitohexaose (GlcNAc$_6$), -100 mV, *cis*			Chitosan hexaose (GlcN$_6$), -100 mV, *cis*		
	[a]Binding constant (K, M^{-1})	[b]On-rate constant 10^6 (k_{on}, M^{-1}s^{-1})	[c]Off-rate constant (k_{off}, s^{-1})	[a]Binding constant (K, M^{-1})	[b]On-rate constant 10^6 (k_{on}, M^{-1}s^{-1})	[c]Off-rate constant (k_{off}, s^{-1})
6.0	86500 ± 4960	7.0	78 ± 1	1020 ± 230	19	18600 ± 3120
8.2	47700 ± 7140	5.5	118 ± 28	-	ND	ND

[a] The equilibrium binding constant (K) = k_{on} /k_{off}

[b] The on-rate (k_{on}, M$^{-1}\cdot$s^{-1}) is given by number of blocking events(s^{-1})/[sugar concentration]. Here sugar GlcNAc$_6$ concentration = 1.25 μM,

GlcN$_6$ concentration = 1.25 μM.

[c] The off-rate (k_{off}, s^{-1}) was obtained from 1/ τ_c, where τ_c is the average residence (dwell) time of the sugar molecule in the channel.

ND, No well-resolved blocking events.

Supplementary Table 2 Effect of deurerium bond on sugar transport.

Experimental condition	*Trans* side addition							
	+100 mV				-100 mV			
	[a](k_{on}) 10^6	[b](k_{off})	[c](K)	[d](K)	[a](k_{on}) 10^6	[b](k_{off})	[c](K)	[d](K)
GlcNAc$_6$ in H$_2$O	5	93±2	55330±5136	100755	2	98±1	19548±205	16383
GlcNAc$_6$ in D$_2$O	2	26±2	68014±19875	212450	1	29±2	44250±20649	74350

[a] The on-rate (k_{on}, $M^{-1} \cdot s^{-1}$) is given by number of blocking events(s^{-1})/[sugar concentration].

Here [GlcNAc$_6$] = 1.25 μM.

[b] The off-rate (k_{off}, s^{-1}) was obtained from $k_{off} = 1/\tau_c$ where τ_c is the average residence (dwell) time (s) of the sugar molecule in the channel.

[c] The equilibrium binding constant (K, M^{-1})= k_{on}/k_{off}

[d] The equilibrium binding constant (K, M^{-1}) was estimated from the reduction of ion conductance in the presence of increasing concentrations of sugar.

Supplementary Table 3 Binding constant of *Ec*ChiP and its mutants with chitohexaose.

	cis side addition					
Protein	+100 mV			-100 mV		
	[a]$(k_{on}).10^6$	[b](k_{off})	[c](K)	[a]$(k_{on}).10^6$	[b](k_{off})	[c](K)
	$(M^{-1}s^{-1})$	(s^{-1})	(M^{-1})	$(M^{-1}s^{-1})$	(s^{-1})	(M^{-1})
*Ec*ChiP (WT)	4	80±1	46615±28660	54765	5	78±1
(W138A/Y421A)	2	110±4	24014±12757	26795	3	91±8
(W138A)	3	107±15	29715±20726	21276	4	115±6
(Y421A)	2	111±4	15909±4744	23142	3	108±5

[a] The on-rate (k_{on}, $M^{-1} \cdot s^{-1}$) is given by number of blocking events(s^{-1})/[sugar concentration].

Here [GlcNAc$_6$] = 1.25 μM.

[b] The off-rate (k_{off}, s^{-1}) was obtained from $k_{off} = 1/\tau_c$ where τ_c is the average residence (dwell) time (s) of the sugar molecule in the channel.

[c] The equilibrium binding constant (K, M^{-1}) = k_{on}/k_{off}

Supplimentary Table 4 Effects of pH on the binding constant of *Sm*ChiP towards charged and uncharged chitooligosaccharides.

pH	Chitohexaose (GlcNAc$_6$), -100 mV, *cis*			Chitosan hexaose (GlcN$_6$), - 100 mV, *cis*		
	[a]Binding constant (K, M^{-1})	[b]On-rate constant 10^6 (k_{on}, M^{-1}s^{-1})	[c]Off-rate constant (k_{off}, s^{-1})	[a]Binding constant (K, M^{-1})	[b]On-rate constant 10^6 (k_{on}, M^{-1}s^{-1})	[c]Off-rate constant (k_{off}, s^{-1})
6.0	15800 ± 4730	5.0	330 ± 52	410 ± 64	4	11570 ± 596
8.2	12000 ± 2185	3.5	278 ± 18	-	ND	ND

[a] The equilibrium binding constant (K) = k_{on} /k_{off}

[b] The on-rate (k_{on}, M$^{-1} \cdot$s^{-1}) is given by number of blocking events(s^{-1})/[sugar concentration]. Here sugar GlcNAc$_6$ concentration = 2.5 μM, GlcN$_6$ concentration = 5 μM.

[c] The off-rate (k_{off}, s^{-1}) was obtained from 1/ τ_c, where τ_c is the average residence (dwell) time of the sugar molecule in the channel.

ND, No well-resolved blocking events.

APPENDIX E

PUBLICATIONS

Publication outputs:

<u>**Soysa, H. S.,**</u> and Suginta, W. (2016). Identification and functional characterization of a novel OprD-like chitin uptake channel in non-chitinolytic bacteria. **J. Biol. Chem.** 291(26): 13622-13633.

In submissions:

<u>**Soysa, H. S.,**</u> Suginta, W., Moonsap, W., and Smith, M. F. (2017). Chitosugar translocation by an unexpressed monomeric protein channel **Biophys. J.** (under review).

In preparations:

<u>**Soysa, H. S.,**</u> and Suginta, W. (2017). Kinetic and thermodynamic characteristics of sugar-channel interactions of monomeric chitoporin from *Escherichia coli*. **J. Biol. Chem.** (In preparations).

<u>**Soysa, H. S.,**</u> and Suginta, W. (2017). Chitoporin from pathogenic *Vibrio cholerae* exhibit channel gating. **J. Biol. Chem.** (In preparations).

<u>**Soysa, H. S**</u>., Schulte, A. and Suginta, W. (2017). Probing the chitooligosaccharides uptake through chitinolytic *Serratia marcescens* monomeric chitoporin. **FEBS.**

Journal. (In preparations).

<u>**Soysa, H. S.,**</u> and Suginta, W. (2017). Chitooligosaccharides translocation through *E. coli* chitoporin: Temperature dependent and effect of deuterium bonds on sugar transport. **FEBS Lett.** (In preparations).

<u>**Soysa, H. S.,**</u> Schulte, A. and Suginta, W. (2017). Effects *N*-acetyl side chains for chitooligosaccharides translocation in chitoporin from chitinolytic and non-chitinolytic bacteria. (In preparations).
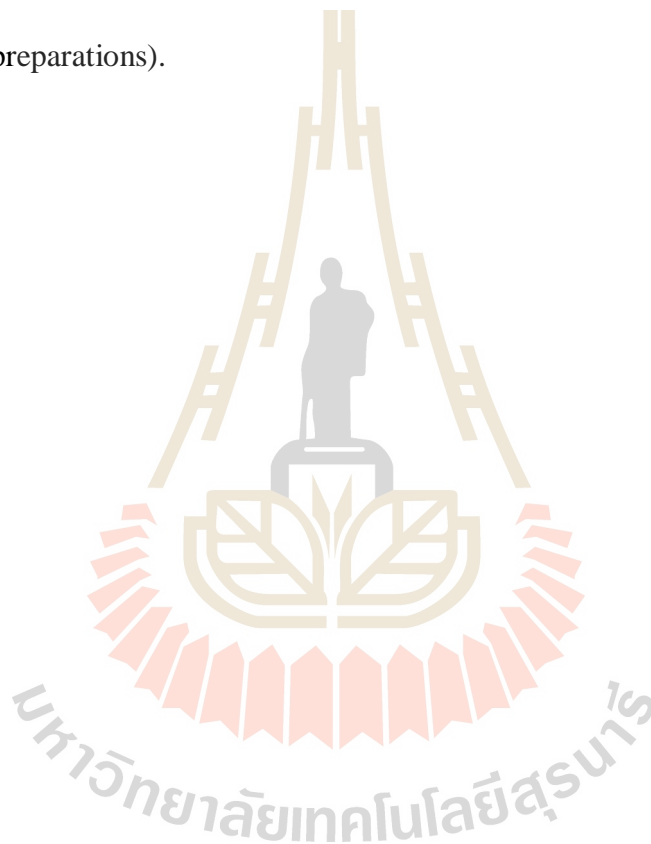
Identification and Functional Characterization of a Novel OprD-like Chitin Uptake Channel in Non-chitinolytic Bacteria[*]

H. Sasimali M. Soysa[‡1] and Wipa Suginta[‡§2]

From the ‡Biochemistry-Electrochemistry Research Unit and School of Chemistry, Institute of Science and §Center of Excellence in Advanced Functional Materials, Suranaree University of Technology, Nakhon Ratchasima 30000, Thailand

Chitoporin from the chitinolytic marine *Vibrio* has been characterized as a trimeric OmpC-like channel responsible for effective chitin uptake. In this study we describe the identification and characterization of a novel OprD-like chitoporin (so-called *Ec*ChiP) from *Escherichia coli*. The gene was identified, cloned, and functionally expressed in the Omp-deficient *E. coli* BL21 (Omp8) Rosetta strain. On size exclusion chromatography, *Ec*ChiP had an apparent native molecular mass of 50 kDa, as predicted by amino acid sequencing and mass analysis, confirming that the protein is a monomer. Black lipid membrane reconstitution demonstrated that *Ec*ChiP could readily form stable, monomeric channels in artificial phospholipid membranes, with an average single channel conductance of 0.55 ± 0.01 nanosiemens and a slight preference for cations. Single *Ec*ChiP channels showed strong specificity, interacting with long chain chitooligosaccharides but not with maltooligosaccharides. Liposome swelling assays indicated the bulk permeation of neutral monosaccharides and showed the size exclusion limit of *Ec*ChiP to be $\sim$200–300 Da for small permeants that pass through by general diffusion while allowing long chain chitooligosaccharides to pass through by a facilitated diffusion process. Taking *E. coli* as a model, we offer the first evidence that non-chitinolytic bacteria can activate a quiescent *ChiP* gene to express a functional chitoporin, enabling them to take up chitooligosaccharides for metabolism as an immediate source of energy.

Escherichia coli is a Gram-negative, heterotrophic bacterium that lives in open environments, such as soil, manure, and water, but the persistence of *E. coli* populations depends upon the availability of carbon substrates in each natural environment. *E. coli* usually grows on glucose-enriched nutrients such as starch, cellulose, and hemicellulose (1) but not on chitin polysaccharides as it intrinsically lacks competent chitin-utilization machinery (2, 3). The chitin degradation pathway is known to be highly active in marine *Vibrio*, the growth of which depends on the utilization of the chitin biomass as their sole source of cellular energy. The chitin degradation pathway of *Vibrio* incorporates a large number of chitin-degrading enzymes and transporters for chitooligosaccharides and *N*-acetyl glucosamine (4–6). Roseman and co-workers (6) first reported the identification and molecular cloning of the gene encoding chitoporin (*Vf*ChiP)[3] from *Vibrio furnissii*. *Vf*ChiP was expressed on induction with $(GlcNAc)_n$, $n = 2–6$, but was not induced by GlcNAc or by other sugars. In contrast to the parental strain, a mutant strain lacking *Vf*ChiP did not grow on $GlcNAc_3$, implying that *Vf*ChiP was selective for chitooligosaccharides (6). We recently identified and characterized the chitin uptake channel (so-called *Vh*ChiP) from the bioluminescent marine bacterium *Vibrio harveyi* (7, 8). *Vh*ChiP is a trimeric OmpC-like porin located in the outer membrane and responsible for the molecular uptake of chitin breakdown products that are generated by the action of secreted chitinases (4, 9–11). Single-channel recordings and liposome swelling assays confirmed that *Vh*ChiP is a sugar-specific channel that is particularly selective for chitooligosaccharides, chitohexaose having the greatest rate of translocation.

Unlike *Vibrio* species, the chitin catabolic cascade of non-chitinolytic bacteria, such as *Candida albicans* (12), *Xanthomonas campestris* (13), *Shewanella oneidensis* (14), and *E. coli* (15–17) was innately inactive although presumed to be preserved. Yang *et al.* (14) proposed the three-step biochemical conversion of GlcNAc (the monomer of chitin) to fructose 6-phosphate in *E. coli* through sequential phosphorylation, deacetylation, and isomerization-deamination reactions. The gene *ChiP* (formerly *ybfM*) encoding chitoporin was previously identified in *E. coli* and *Salmonella* sp. as a silent gene controlled by a non-coding small RNA (16). However, this *ChiP* gene was sporadically expressed as an adaptive strategy for the bacterium to thrive in glucose-deficient environments (16, 18–21). To date, *E. coli* chitoporin (so-called *Ec*ChiP) has not been functionally characterized, and our study used electrophysiological and biochemical approaches to uncover the physiological roles of *Ec*ChiP.

Experimental Procedures

Bacterial Strains and Vectors—E. coli strain DH5α, used for routine cloning and plasmid preparations, was obtained from Invitrogen. *E. coli* BL21(DE3) Omp8 Rosetta (Δ*lamBompF*::

[3] The abbreviations used are: *Vf*ChiP, *V. furnissii* chitoporin; *Ec*ChiP, *E. coli* chitoporin; IPTG, isopropyl 1-thio-β-D-galactopyranoside; BLM, black lipid membrane; $GlcNAc_2$, chitobiose; $GlcNAc_3$, chitotriose; $GlcNAc_4$, chitotetraose; $GlcNAc_5$, chitopentaose; $GlcNAc_6$, chitohexaose; nS, nanosiemen(s).

Tn5 Δ*ompA*Δ*ompC*) mutant strain was a gift from Professor Dr. Roland Benz, Jacobs University, Bremen, Germany. The pET23d(+) expression vector was a product of Novagen (Merck). pUC57 vector carrying the *E. coli ChiP* gene was obtained from GenScript USA Inc. Piscataway, NJ.

Chitosugars—Chitooligosaccharides, including chitobiose, chitotriose, chitotetraose, chitopentaose, and chitohexaose were purchased from Dextra Laboratories (Science and Technology Centre, Reading, United Kingdom).

Structural Prediction and Sequence Analysis—Amino acid sequences of four bacterial ChiPs from *E. coli* (P75733), *Salmonella* (Q7CQY4), *Serratia marcescens* (L7ZIP1), and *V. harveyi* (L0RVU0) were aligned and displayed using the program CLC Main Workbench v6.0. The secondary structure of the *E. coli* ChiP was constructed by ESPript 3.0 (22) according to the three-dimensional structure of *Pseudomonas aeruginosa* OprD (pdb 2odj).

Cloning and Sequencing—The nucleotide sequence encoding chitoporin was identified in the *E. coli* strain K-12 substrain MG1655 chromosome in the NCBI database (gi 49175990), and the *ChiP* gene was commercially synthesized using the GenScript Gene Synthesis Service. The ChiP DNA fragment ligated in the pUC57 cloning vector was excised and then transferred into the pET23d(+) expression vector using the NcoI and XhoI cloning sites so that the *ChiP* gene could be expressed under the control of the T7 promoter. The oligonucleotides used for colony detection of the ChiP PCR product were 5′-ATA<u>CCATG-G</u>CCATGCGTACGTTTAGT-3′ for the forward primer and 5′-AAC<u>CTCGAG</u>TCAGAAGATGGTGAA-3′ for the reverse primer (sequences underlined indicate the restriction sites). Nucleotide sequences of sense and antisense strands of the PCR fragment were determined by automated sequencing (First BASE Laboratories SdnBhd, Selangor DarulEhsan, Malaysia).

Protein Expression and Purification—Expression and purification of the recombinant *Ec*ChiP were carried out as previously described (8). Briefly, the expression vector pET23d(+), harboring the full-length *ChiP* gene, was transformed into *E. coli* BL21(DE3) Omp8 Rosetta strain, which lacks major endogenous Omps, including OmpF, OmpC, OmpA, and LamB. The transformed cells were grown at 37 °C in Luria-Bertani (LB) broth supplemented with 100 μg·ml^{-1} ampicillin and 25 μg·ml^{-1} kanamycin. During the exponential growth phase ($A_{600} \sim 0.6-0.8$), *Ec*ChiP expression was induced with 0.5 mM final concentration of isopropyl thio-β-D-galactoside (IPTG). After 6 h of additional incubation at 37 °C, the cell pellet was harvested by centrifugation at 2,948 × *g* for 20 min at 4 °C.

For protein purification, the cell pellet was resuspended in lysis buffer (20 mM Tris-HCl, pH 8.0, 2.5 mM MgCl$_2$, 0.1 mM CaCl$_2$) containing 10 μg·ml^{-1} RNase A and 10 μg·ml^{-1} DNase I. Cells were disrupted with a high speed ultrasonic processor (EmulsiFlex-C3, Avestin Europe, Mannheim, Germany) for 10 min. After this, 20% (w/v) SDS solution was added to obtain a final concentration of 2%, and the suspension was further incubated at 50 °C for 60 min with 300 rpm shaking to ensure complete lysis. Cell wall components were removed by centrifugation at 100,000 × *g* at 4 °C for 1 h. The pellet, containing recombinant *Ec*ChiP, was extracted twice with 2.5% (v/v) *n*-oc-

tylpolyoxyethylene (Alexis Biochemicals, Lausanne, Switzerland) in 20 mM phosphate buffer, pH 7.4, and centrifuged again. The supernatant was then dialyzed thoroughly against 20 mM phosphate buffer, pH 7.4, containing 0.2% (v/v) lauryldimethylamine oxide (Sigma).

To obtain protein of high purity, the solubilized *Ec*ChiP was subjected to ion-exchange chromatography using a Hitrap Q HP prepacked column (5 × 1 ml) connected to an ÄKTA Prime plus FPLC system (GE Healthcare). Bound proteins were eluted with a linear gradient of 0–1 M KCl in 20 mM phosphate buffer, pH 7.4, containing 0.2% (v/v) lauryldimethylamine oxide. The purity of the eluted fractions was confirmed by SDS-PAGE. Fractions containing *Ec*ChiP were pooled and subjected to size exclusion chromatography using a HiPrep 16/60 Sephacryl S-200 high resolution column. The purity of the *Ec*ChiP fractions obtained after the size exclusion step was verified by SDS-PAGE before they were pooled, and the protein concentration of the freshly prepared *Ec*ChiP was estimated using the Novagen BCA protein assay kit (EMD Chemicals Inc., San Diego, CA).

Peptide Mass Analysis by MALDI-TOF MS—The purified *Ec*ChiP was electrophoresed on a 12% polyacrylamide gel, and the *Ec*ChiP bands were excised and sent to BGI Tech Solutions (HongKong) Co. Ltd. for MALDI-TOF MS analysis. Briefly, protein in the gel was digested with trypsin and eluted to obtain a peptide mixture, then MALDI-TOF mass spectrographic analysis was performed, and the obtained peptide masses were identified using Mascot software v2.3.02.

Molecular Weight Determination of EcChiP—Standard proteins and dyes of known molecular weight were resolved on a HiPrep 26/60 Sephacryl S-300 HR column. Dextran-2000 was used to obtain the void volume (V_0), whereas DNP-lysine was used to calculate the volume of the stationary phase (V_i) and the elution volume of each protein sample, denoted as V_e. The elution of a protein sample was characterized by the distribution coefficient (K_d) derived as in Equation 1,

$$K_d = \frac{V_e - V_0}{V_i} \qquad \text{(Eq. 1)}$$

A calibration curve was created by plotting K_d *versus* logarithmic values of the corresponding molecular weights of the standard proteins and was used to estimate the molecular weight of *Ec*ChiP. The standard proteins used in this experiment were ferritin (440 kDa), catalase (250 kDa), aldolase (158 kDa), bovine serum albumin (66 kDa), ovalbumin (43 kDa), carbonic anhydrase (29 kDa), and ribonuclease A (13.7 kDa).

Black Lipid Bilayer Measurements of Pore Conductance and Chitin Oligosaccharide Translocation—Black lipid membrane (BLM) reconstitution was carried out in electrolyte containing 1 M KCl and 20 mM HEPES, pH 7.5, at room temperature (25 °C). Solvent-free bilayer (Montal-Mueller type) formation was performed using 1,2-diphytanoyl-*sn*-glycero-3-phosphatidylcholine; Avanti Polar Lipids, Alabaster, AL). First, the aperture was prepainted with a few microliters of 1% (v/v) hexadecane in hexane, then a planar bilayer was formed across the aperture by lowering and raising the liquid level (23). Ionic currents were detected using Ag$^+$/AgCl electrodes with a patch-

Identification of Chitin-uptake Channel in E. coli

clamp amplifier connected to a two-electrode bilayer headstage (PC-ONE plus PC-ONE-50; Dagan Corp., Minneapolis, MN). The BLM setup was operated within a Faraday cage on a vibration-dampening table with an A/D converter (LIH 1600, HEKA Elektronik, Lambrecht, Germany) and was operated using the software PULSE program (HEKA Elektronik, Lambrecht, Germany). One of the electrodes, immersed in 1 M KCl electrolyte on the *cis* side of the cuvette, was connected to ground, whereas the electrode on the *trans* side was connected to the amplifier head-stage. *Ec*ChiP was always added to the *cis* side of the cuvette. Conductance values were extracted from the current steps observed at different voltages after the addition of the protein. The ion selectivity of *Ec*ChiP was determined using different salt solutions, such as 1 M lithium chloride (LiCl), 1 M cesium chloride (CsCl), and 1 M potassium acetate (KAc).

To investigate sugar translocation, single *Ec*ChiP channels were reconstituted in the artificial lipid membrane as described earlier. To prevent multiple insertions during data acquisition, the protein solution in the chamber was gently diluted after the first insertion by sequential additions of the working electrolyte. Then the fully open *Ec*ChiP channel was titrated with distinct concentrations of different chitooligosaccharides: chitobiose (GlcNAc$_2$), chitotriose (GlcNAc$_3$), chitotetraose (GlcNAc$_4$), chitopentaose (GlcNAc$_5$) and chitohexaose (GlcNAc$_6$). Each sugar was added to the *cis* side of the chamber. Fluctuations of ion flow were observed as a result of sugar diffusion through the reconstituted channel and were usually recorded for 2 min at different transmembrane potentials. To test the substrate specificity of the channel toward chitooligosaccharides, maltodextrin sugars were used as controls.

Liposome Swelling Assay—The *Ec*ChiP- and *Vh*ChiP-reconstituted proteoliposomes were prepared as described elsewhere (24, 25). Soybean L-α-phosphatidylcholine (20 mg/ml, freshly prepared in chloroform) (Sigma) was used to form multilamellar liposomes. For the preparation of proteoliposomes, 200 ng of *Ec*ChiP was reconstituted into 200 μl of the liposome suspension by sonication, and then 17% (w/v) dextran (40kDa) was entrapped in the proteoliposomes. D-Raffinose solutions were prepared in phosphate buffer to obtain concentrations of 40, 50, 60, and 70 mM for determination of the isotonic solute concentration. This value was then used for the adjustment of the isotonic concentration for other solutes. To carry out a liposome-swelling assay, 25 μl of the proteoliposome suspension was added to 600 μl of sugar solution, and changes in absorbance at 500 nm were monitored immediately. The apparent absorbance change over the first 60 s was used to estimate the swelling rate (s^{-1}) following the equation $\varphi = (1/A_i)\mathrm{d}A/\mathrm{d}t$ in which φ is the swelling rate, A_i is the initial absorbance, and dA/dt is the rate of absorbance change during the first 60 s. The swelling rate for each sugar was normalized by setting the rate of L-arabinose (150 Da), the smallest sugar, to 100%. The values presented are averages from three to five independent determinations. Protein-free liposomes and proteoliposomes without sugars were used as negative controls. The sugars tested were D-glucose (180 Da), D-mannose (180 Da), D-galactose (180 Da), *N*-acetylglucosamine (GlcNAc) (221 Da), D-sucrose (342 Da), D-melezitose (522 Da), GlcNAc$_2$ (424

Da), GlcNAc$_3$ (628 Da), GlcNAc$_4$ (830 Da), GlcNAc$_5$ (1034 Da), GlcNAc$_6$ (1237 Da), and maltodextrins.

Results

Cloning, Sequence Analysis, and Structure Prediction—The availability of the nucleotide sequence in the genome of *E. coli* strain K-12 sub-strain MG1655, (complete genome NCBI reference sequence; NC_000913) allowed the putative amino acid sequence of *E. coli* ChiP (so-called *Ec*ChiP) to be identified. The full-length *ChiP* gene corresponding to *Ec*ChiP was synthesized commercially, for which the target gene was ligated into the NcoI and XhoI cloning sites of the pUC57 cloning vector (GenScript). The nucleotide sequence of the *ChiP* gene, comprising 1407 bps, was translated to a putative polypeptide of 468 amino acids, including the 26-amino acid signal sequence. The theoretical mass of the full-length *Ec*ChiP was 52,780 Da, with a predicted isoelectric point of 4.70.

Amino acid sequence comparison of *Ec*ChiP with other bacterial ChiPs in the SwissProt/UniProtKB database is presented in Fig. 1. The putative sequence of *Ec*ChiP showed highest sequence identity to *Salmonella typhimurium* ChiP (Q7CQY4) (90%) (18) followed by *S. marcescens* ChiP (L7ZIP1) (70%) (26). Our sequence analysis indicated that *Ec*ChiP had exceptionally low identity with the ChiP sequences from marine *Vibrio* species, such as *Vibrio cholerae* ChiP (Q9KTD0) (27), *V. furnissii* ChiP (Q9KK91) (6), and *V. harveyi* ChiP (L0RVU0) (8) with 13, 14, and 12% identity, respectively. Unlike marine *Vibrio* species, *E. coli* and *S. typhimurium* are non-chitinolytic bacteria that possess ChiP homologs belonging to the OprD family of porins. The *Ec*ChiP amino acid sequence was submitted to the Swissmodel database for homology structure prediction, and the crystal structure of *P. aeruginosa* OprD (pdb 2odj) (28) was computationally selected as a structure template. Fig. 2*A* shows a side view of the predicted β-barrel structure of *Ec*ChiP, atypically consisting of 19-strands connected by 9 external loops and 9 periplasmic turns. Previous reports of the crystal structures of the maltoporin (LamB) (29) and sucrose-specific porin ScrY (30) suggested that aromatic residues are important for sugar transport. Amino acid residues located within the pore interior, such as Trp-138, Asp-314, Arg-320, and Tyr-421, are predicted to be crucial for sugar transport (residues marked as sticks in Fig. 2*B*, top view). The predicted transmembrane topology for *Ec*ChiP is shown in Fig. 2*C*. The longest loop (L3, Gly-124 to Tyr-145) found inside the channel lumen presumably acts as the pore-confining loop that controls ion flow.

Recombinant Expression, Purification, and Mass Identification—The plasmid pET23d(+) harboring the *ChiP* gene fragment was designed to express recombinant *Ec*ChiP, with the 26-amino acid N-terminal signal sequence aiding channel insertion into the cell wall of the *E. coli* BL21(DE3) Omp8 Rosetta host. When the transformed cells were grown to exponential phase, expression of the recombinant *Ec*ChiP was induced with 0.5 mM IPTG for a period of 6h at 37 °C. Fig. 3*A* shows SDS-PAGE analysis of whole cell lysates of the Ompdeficient *E. coli* expressing *Ec*ChiP. When compared with cells transformed with the empty vector (*lane 1*, no induction; and *lane 2*, IPTG induction), uninduced cells transformed with the pET23d(+)/*ChiP* vector did not produce the heterologous pro-
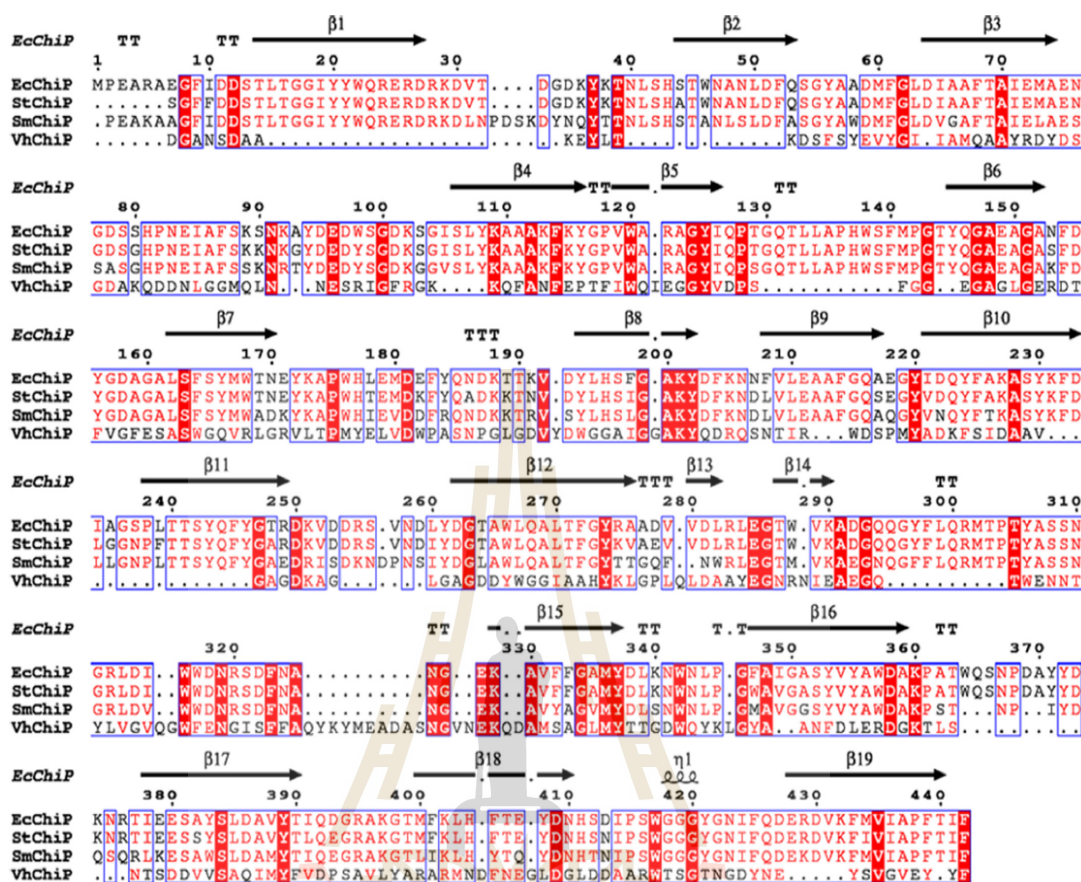
FIGURE 1. **Sequence alignment of *Ec*ChiP, showing the secondary structural elements of *Ec*ChiP.** The amino acid sequences of *S. typhimurium ChiP* (*StChiP*), *S. marcescens* ChiP (*SmChiP*), and *V. harveyi* ChiP (*VhChiP*), without signal peptides, were aligned using CLC Main Workbench 6. The secondary structure of *E. coli* was constructed by ESPript 3.0 according to the structure of *P. aeruginosa* OprD (pdb 2odj). β-Strands are marked with *black arrows*, and an α-helix is marked with *black curl*. Absolutely conserved residues are highlighted in *red*.

tein (*lane 3*), whereas a prominent band of the expected size (50 kDa) appeared on induction with IPTG (*lane 4*). These results confirmed successful production of *Ec*ChiP in the selected host cells.

For purification of *Ec*ChiP, the induced cells were subjected to a two-step detergent extraction. In the first step using 2% (w/v) SDS, most of *Ec*ChiP remained in the insoluble fraction, and in the second step *Ec*ChiP was solubilized with 2.5% (v/v) *n*-octylpolyoxyethylene. The protein purity observed after these steps was >90%. *Ec*ChiP was further subjected to ion-exchange chromatography using a Hitrap Q HP pre-packed column. Fig. 3*B* shows the chromatographic profile, indicating that *Ec*ChiP fractions were eluted in two peaks (P1 and P2) by an applied gradient of 0–1 M KCl. SDS-PAGE analysis shows that the *Ec*ChiP fractions in the first peak (P1) were highly purified (Fig. 3*B*, *inset*), whereas the fractions in P2 included some contaminants (not shown); P2 may, therefore, contain *Ec*ChiP bound to other proteins. Peaks P1 and P2 were, therefore, applied separately to a HiPrep 16/60 Sephacryl S-200 high resolution exclusion chromatography column for final purification. The highly purified *Ec*ChiP obtained after gel filtration chromatography was subjected

to in-gel digestion for MALDI-TOF MS analysis. A MASCOT database search identified 16 peptides (designated P1-P16) that belonged to the internal sequences of the putative chitoporin from *E. coli* (gi 251784171 ref YP_002998475.1) (Fig. 3*C*, sequences in *cyan*). The sequence coverage for the identified peptides was 50%. These results confirmed that the 50-kDa protein expressed in *E. coli* BL21(DE3) Omp8 Rosetta host was *Ec*ChiP.

Determination of the Native State of the EcChiP Channel—All chitoporins identified in marine *Vibrio* species are trimeric channels (8). In the next series of experiments we investigated the native state of *Ec*ChiP. Unlike *Vh*ChiP (8), *Ec*ChiP did not migrate on SDS-PAGE gel to the position corresponding to a trimer under non-denaturing conditions. Fig. 4*A* is an SDS-PAGE analysis showing the migrations of *Vh*ChiP (*lane 1*, unheated; *lane 2*, heated) and *Ec*ChiP (*lane 3*, unheated; *lane 4*, heated). Intact *Vh*ChiP migrated with an apparent molecular mass close to 100 kDa, indicating a trimer (*lane 1*), but the dissociated subunits migrated close to 40 kDa (*lane 2*). Different results were observed with the *E. coli* sample; native *Ec*ChiP migrated with an apparent molecular mass of ~35 kDa (*lane 3*), indicating a monomeric, folded structure according to litera-
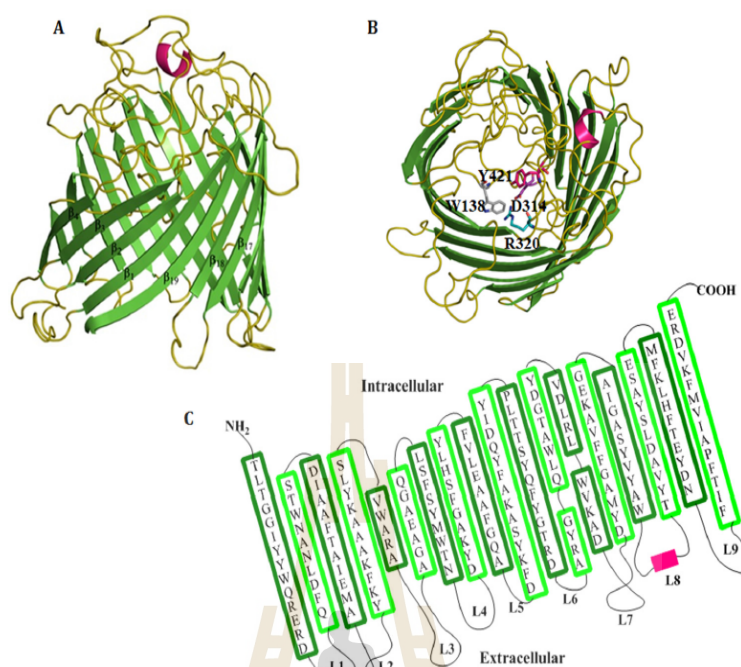
FIGURE 2. **The Swiss-model structure of *E. coli* chitoporin.** *A*, schematic of *Ec*ChiP viewed from the side. *B*, top view of the *Ec*ChiP modeled structure. Important residues in the pore that may be involved in sugar transport; Trp-138, Asp-314, Arg-320, and Tyr-421 are presented in *gray*, *purple*, *teal*, and *pink*, respectively, as stick structures. The x-ray structure of OprD from *P. aeruginosa* (pdb 2odj) was selected as the structure template for *E. coli* chitoporins. *Green*, β-strands; *olive*, loops and turns; *hot pink*, α-helices. *C*, the predicted transmembrane topology of *Ec*ChiP.

ture review (31, 32). After boiling, the apparent molecular mass increased to nearly 50 kDa, presumably due to unfolding of the protein (*lane 4*). Gel filtration chromatography was used to confirm the monomeric structure of native *Ec*ChiP. Fig. 4*B* shows a chromatographic profile of the protein standards eluted from a HiPrep 26/60 Sephacryl S-300 pre-packed column. *Ec*ChiP was eluted at a position between ovalbumin (43 kDa) and bovine serum albumin (66 kDa) (Fig. 4*B*, *black dotted line*), and its apparent molecular mass estimated from its distribution coefficient (K_d) was *ca.* 60 kDa (Fig. 4*C*), consistent with a monomeric molecule. The slightly greater molecular mass than the expected size of *Ec*ChiP (50 kDa) may be added by the molecular mass the detergent lauryldimethylamine oxide (micelle molecular mass 17 kDa) (33), which was included to maintain the protein solubility.

Channel-forming Properties of EcChiP—To examine the pore-forming properties of the isolated channel, *Ec*ChiP was reconstituted into artificial planar phospholipid membranes. An abrupt increase in ion current in response to an externally applied potential was observed soon after the addition of the protein, and the induced current remained steady throughout the subsequent period of data acquisition (usually 2 min). The BLM results clearly demonstrated that *Ec*ChiP was a channel-forming protein. Fig. 5*A* is a representative ion current recording of ~50 pA at +100 mV, signifying a characteristic single *Ec*ChiP insertion under a given condition (<2 ng·ml^{-1} *Ec*ChiP added on the *cis* side of the chamber filled with 1 M KCl, pH 7.5). This channel insertion behavior was observed consistently throughout our study. In Fig. 5*B*, we show typical ion current

traces obtained from multiple insertions in the presence of a high added concentration of *Ec*ChiP (>10 ng·ml^{-1}) in the same electrolyte solution. The Fig. 5*B inset* shows the Gaussian distribution of the pore conductance, derived from 365 channel insertions. The value was fitted with a mean conductance of 0.54 ± 0.04 nS, which corresponded well with the value obtained from the slope of the I-V curve shown in Fig. 5*C*, *inset*. For individual *Ec*ChiP channels, currents were recorded at potentials from −100 to +100 mV, increased in 25-mV steps, as shown in Fig. 5*C*. The plot of current as a function of transmembrane potential was constructed from 17 independent single channel insertions. The conductance of the pore (slope of the curve) was constant over the entire voltage range scanned, yielding the conductance value of 0.55 ± 0.01 nS. *Ec*ChiP was shown to be a relatively stable channel at both negative and positive potentials with a threshold for channel gating observed at approximately −200 mV and +200 mV. An example of channel gating at +200 mV is shown in Fig. 5*D*.

Single-channel experiments were also performed with salts other than KCl to obtain information on the ion selectivity of *Ec*ChiP; the results are summarized in Table 1. Replacement of Cl$^-$ by CH$_3$COO$^-$, a less mobile anion, slightly reduced the single channel conductance from 0.5 to 0.4 nS. However, replacement of K$^+$ by the less mobile cation Li$^+$ resulted in a much larger decrease, from 0.5 nS to 0.25 nS, indicating a preference of *Ec*ChiP for cations (Table 1). Although Li$^+$ and CH$_3$COO$^-$ and K$^+$ and Cl$^-$ have similar aqueous mobilities (34, 35), the conductance of *Ec*ChiP channel was lower in LiCl
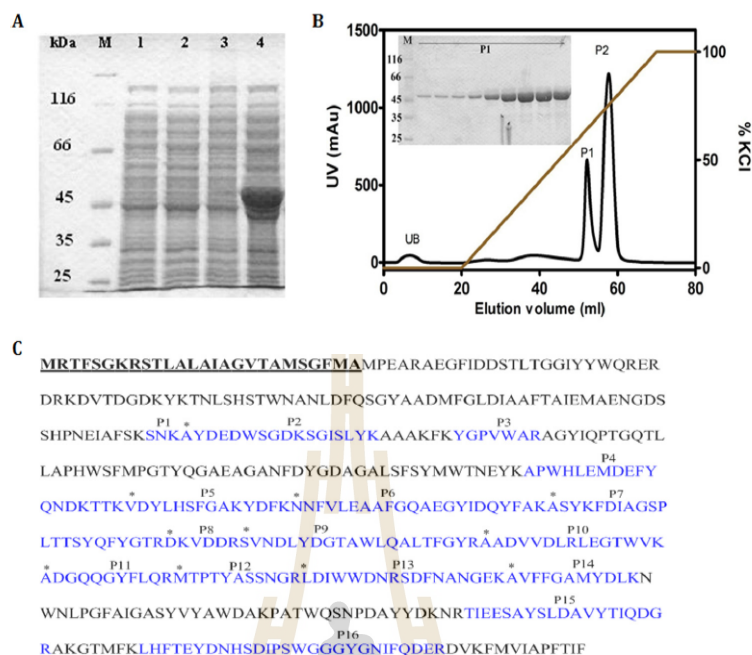
FIGURE 3. **Recombinant expression, purification, and mass identification.** *A*, SDS-PAGE analysis of whole-cell lysate with and without IPTG induction for *E. coli* carrying pET23d(+) and pET23d(+)/*Ec*ChiP. *Lane M*, marker proteins; *lane 1*, *E. coli* Omp8 Rosetta carrying pET23d(+) without IPTG induction; *lane 2*, *E. coli* Omp8 Rosetta carrying pET23d(+) with IPTG induction; *lane 3*, *E. coli* Omp8 Rosetta carrying pET23d(+)/*Ec*ChiP without IPTG induction; *lane 4*, *E. coli* Omp8 Rosetta carrying pET23d(+)/*Ec*ChiP with IPTG induction. *B*, chromatographic profile of *Ec*ChiP purification with a Hitrap Q HP prepacked column (5×1 ml) connected to an AKTA Prime plus FPLC system. Bound proteins were eluted with a linear gradient of 0–1 M KCl in 20 mM phosphate buffer, pH 7.4, containing 0.2% (v/v) lauryldimethylamine oxide. SDS-PAGE analysis of bound fraction P1 is shown in an *inset. mAu*, milliabsorbance units. *C*, identification of tryptic digests of the expressed proteins by MALDI-TOF MS. The 16 identified peptides (P1-P16) that gave a complete match with putative peptides of *Ec*ChiP are shown in *cyan*. The N-terminal ends of peptides P2, P5, P6, P7, P8, P9, P10, P11, P12, P13, and P14 are indicated by *asterisks*. The 26-amino acid signal peptide is in *bold* and *underlined*.
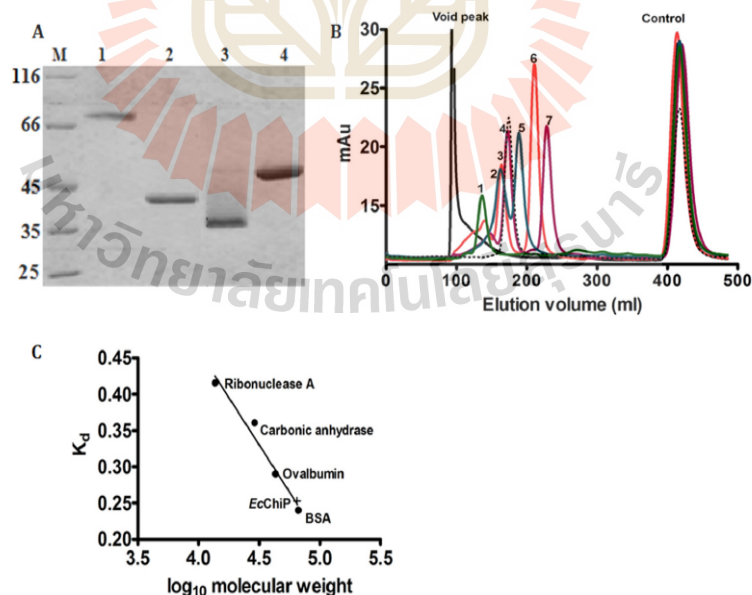
FIGURE 4. **SDS-PAGE analysis of *Ec*ChiP and molecular weight determination.** *A*, SDS-PAGE analysis of purified *Ec*ChiP, with *Vh*ChiP for comparison. *Lane M*, marker proteins; *Lane 1*,*Vh*ChiP (unheated); *lane 2*, *Vh*ChiP (heated); *lane 3*, *Ec*ChiP (unheated); *lane 4*, *Ec*ChiP (heated). *B*, size exclusion chromatogram of standard proteins with *Ec*ChiP. Standards were run separately, together with DNP-lysine (control). Protein standards: *lane 1*, ferritin (440 kDa); *lane 2*, catalase (250 kDa); *lane 3*, aldolase (158 kDa); *lane 4*, bovine serum albumin (66 kDa); *lane 5*, ovalbumin (43 kDa); *lane 6*, carbonic anhydrase (29 kDa); *lane 7*, ribonuclease A (13.7 kDa). *Void peak*, elution peak of blue dextran 2000. *Control*, elution peak for DNP-lysine. *Ec*ChiP was eluted (*black dotted line*) as a monomer within the 43–66 kDa range. *C*, calibration curve to determine the K_d value of *Ec*ChiP.

Identification of Chitin-uptake Channel in E. coli

FIGURE 5. **Single-channel recordings of *Ec*ChiP in artificial lipid membranes.** Lipid bilayers were formed across a 70 μM aperture by the lowering and raising technique, using 5 mg·ml^{-1} 1,2-diphytanoyl-*sn*-glycero-3-phosphatidylcholine in *n*-pentane and 1 M KCl in 20 mM HEPES, pH 7.5, on both sides of the chamber. The protein was added to the *cis* side. *A*, fully open *Ec*ChiP current trace at +100 mV. *B*, multiple channel insertions; *Inset*, histogram of the conductance steps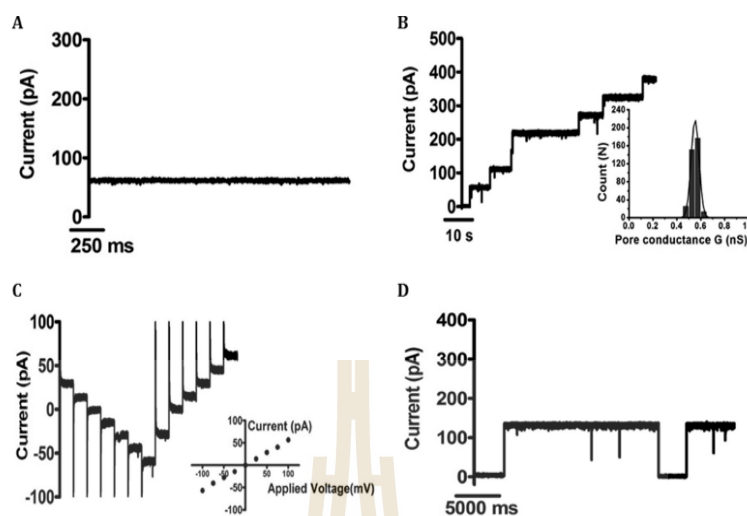 observed with 1,2-diphytanoyl-*sn*-glycero-3-phosphatidylcholine artificial bilayer for 365 independent channel insertions. The *black line* represents a single Gaussian fit. *C*, stepwise ramping of the potential for single insertion. *Inset*, I-V plot for a single *Ec*ChiP single channel. The average current values were obtained by varying the potential from −100 mV to +100 mV in 25 mV steps for 17 independent channel insertions. *D*, gating behavior of *Ec*ChiP at high potential (+200 mV).

TABLE 1

Average single channel conductance (G) of *Ec*ChiP in different salt solutions

The pH of the aqueous salt solutions was around 7.5. G was calculated from the single channel recording by averaging single events as indicated within the parentheses. The applied membrane potential was +100 mV.

Aqueous salt solution	Single channel conductance (G)
	nS
1 M KCl	0.54 ± 0.04 (*n* = 365)[a]
1 M KAc	0.40 ± 0.03 (*n* = 71)
1 M CsCl	0.60 ± 0.04 (*n* = 87)
1 M LiCl	0.25 ± 0.02 (*n* = 65)

[a] *n* represents the number of BLM measurements in which the data were acquired in this experiment.

than in KAc. This result supports the conclusion that the *Ec*ChiP channel was cation-selective.

Investigation of Chitooligosaccharide Interactions with EcChiP—In this set of experiments we performed single-channel measurements in the presence of different chitooligosaccharides to address the substrate specificity of the newly isolated channel. Fig. 6A is a control trace, showing a stably opening channel of conductance ~55 pA at +100 mV in the absence of ligand. The addition of the chitooligosaccharides chitotetraose, pentaose, and hexaose resulted in frequent current blockages in *Ec*ChiP, reflecting strong sugar-channel interactions (Fig. 6, *E–G*). We observed no fluctuation of ion current on the addition of *N*-acetylglucosamine, chitobiose and chitotriose (Fig. 6, *B*, *C* and *D*), and addition of structurally related maltohexaose (Fig. 6*H*) showed no fluctuation of ion current even at a concentration 200-fold greater than that of the chitosugars, indicating that the *Ec*ChiP channel was highly specific for chitooligosaccharides.

LamB has been the subject of intensive studies on sugar binding (36–38). Similarly, our BLM data showed that *Ec*ChiP interacted with chitosugars to various extents depending on the

sizes and the types of the sugars, as shown in Fig. 6. Next, we selected chitohexaose as a substrate to study ion current fluctuation at different sugar concentrations. Fig. 7 shows current recordings obtained from a single *Ec*ChiP channel in the presence of several discrete concentrations of chitohexaose. These traces, recorded at +100 mV, indicated increasing numbers of blocking events as concentrations of chitohexaose were increased from 1.25 to 20 μM, leading to a gradual reduction in the average conductance of the channel (Fig. 7, *A–D*). Similar results were obtained at −100 mV, with the channel more susceptible to sugar occlusion at negative voltages (Fig. 7, *E–H*). At the highest sugar concentration (20 μM), we observed that the sugar molecules fully occupied the channel, leading to more frequent decreases in ion current to zero (Fig. 7, *D* and *H*). We did not detect three-stage transient blockages with *Ec*ChiP measurements on sugar addition, which are usually observed for trimeric channels (8, 36–39). These results provide further evidence that *Ec*ChiP acts as a monomeric channel.

Determination of Channel Specificity Using a Liposome-swelling Assay—Proteoliposome swelling assays were performed to evaluate the bulk permeation of neutral solutes through the *Ec*ChiP channel. *Ec*ChiP-containing proteoliposomes were prepared according to the protocol described elsewhere (24, 25). Swelling of the proteoliposomes caused by diffusion of solute molecules through the protein channel resulted in a decrease in apparent absorbance at 500 nm, whereas under isotonic conditions constant absorbance was maintained. In this assay we used D-raffinose (504 Da), a branched sugar that is unable to diffuse through the porin, to establish the isotonic concentration and enable the comparison of diffusion rates. L-Arabinose (150 Da), the smallest sugar tested in this experiment, had the highest diffusion rate through *Ec*ChiP, and the
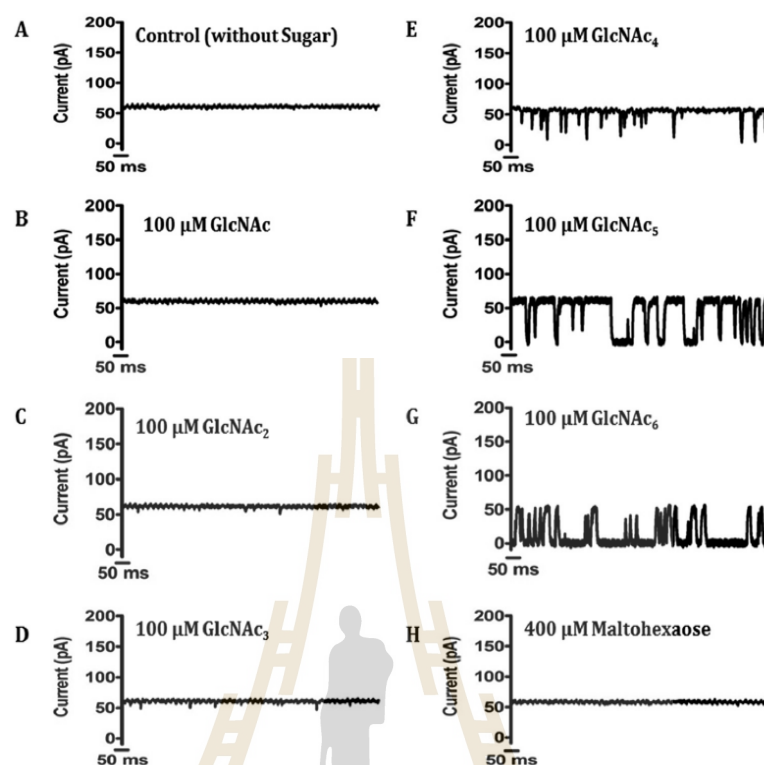
FIGURE 6. **Current recordings of single *Ec*ChiP channels in solutions of different chitooligosaccharides of various chain lengths.** Ion current fluctuations were monitored for 120 s at applied potentials of ±100mV. Here, only current traces for 1 s at +100 mV are presented. *A*, a fully open state of *Ec*ChiP before sugar addition. Then GlcNAc (*N*-acetylglucosamine) (*B*), chitobiose (GlcNAc$_2$) (*C*), chitotriose (GlcNAc$_3$) (*D*), chitotetraose (GlcNAc$_4$) (*E*), chitopentaose (GlcNAc$_5$) (*F*), or chitohexaose (GlcNAc$_6$) (*G*) were added on the *cis* side of the chamber to a final concentration of 100 μM. *H*, control recording with maltohexaose at a concentration of 400 μM.

swelling rates in the other sugars tested were normalized relative to that in L-arabinose, which was set to 100%.

To address the differences between the *Ec*ChiP channel and the chitooligosaccharide-specific porins from the OmpC family, we compared our data with those obtained with *Vh*ChiP-incorporating proteoliposomes. The two chitoporins showed similar diffusion rates for small sugars such as D-glucose, D-mannose, and D-galactose (180 Da) and *N*-acetylglucosamine (GlcNAc, 221 Da) (Fig. 8*A*). However, D-sucrose (342 Da), maltose (360 Da), and D-melezitose (522 Da) showed no diffusion through *Ec*ChiP. In contrast, D-sucrose and maltose permeated *Vh*ChiP, albeit with very low diffusion rates, whereas D-melezitose was impermeant. When *Ec*ChiP was tested with long chain chitooligosacharides it was found that all neutral chitooligosaccharides were permeant (Fig. 8*B*), whereas maltosugars (maltose and maltahexaose) did not show permeation. The results obtained from the proteoliposome swelling assays additionally confirmed the high selectivity of *Ec*ChiP for chitooligosaccharides.

Discussion

Chitin is one of the most abundant naturally occurring polysaccharides, and chitin turnover by marine *Vibrio* species is essential for the recycling of carbon and nitrogen in marine ecosystems (40). *Vibrio* species possess competent chitin degradation and uptake systems that allow the bacteria to metabolize chitinous materials, generating catabolic intermediates that can be used as their sole source of energy (5, 41–47). In marked contrast, *E. coli* is a non-chitinolytic bacterium living primarily in the gastrointestinal tract of animals, and its generation of cellular energy relies on glucose-enriched nutrients. Although the *ChiP* gene, encoding a chitoporin that is responsible for the uptake of chitin-derived chitooligosaccharides, is evolutionarily conserved, it is usually quiescent in non-chitinolytic bacteria. A previous report on *Salmonella* and *E. coli* (16, 18) showed that in the absence of any inducer, the *ChiP* gene (formerly *ybfM*) was constantly suppressed by forming a DNA-RNA duplex with a conserved small RNA, namely *ChiX*. However, silencing was relieved in the presence of chitooligosaccharides, as these sugars produced accumulation of anti-*ChiX* small RNA that paired with *ChiX*, allowing the *ChiP* gene to be expressed. Another study reported co-localization of the genes for *ChiP* and *Hex* (encoding β-*N*-acetylglucosaminidase) in the chromosomes of *Yersinia* and *Serratia* species (14). This suggested a sequential action of ChiP and β-*N*-acetylglucosaminidase in chitin uptake and chitin degradation, respectively, and *E. coli* and *Salmonella* ChiPs have been proposed to be involved in the uptake of chitobiose, an end product of chitin breakdown that is readily transported through the
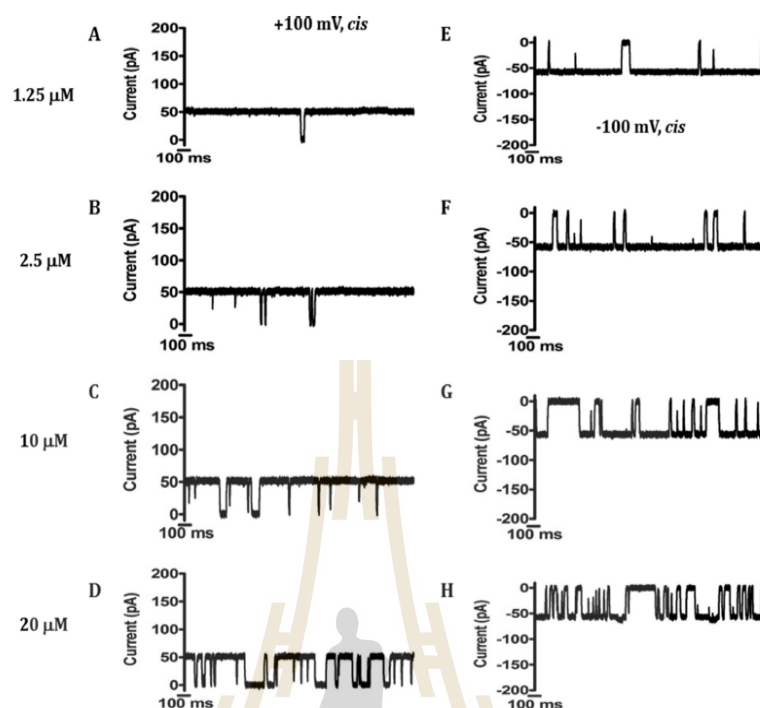
Identification of Chitin-uptake Channel in E. coli

FIGURE 7. **Conductance of the same single *Ec*ChiP channel with increasing chitohexaose concentration at positive and negative potentials.** Ion current fluctuations were monitored for 120 s at applied potentials of ±100 mV with sugar addition on the *cis* side. Here only current traces for 2 s are presented with four different concentrations at +100mV (*A–D*) and at −100mV (*E–H*).

inner membrane by the phosphoenolpyruvate transferase system.

In the present study we identified the *ChiP* gene, encoding a hypothetical outer-membrane chitoporin (*Ec*ChiP) from the genome of the *E. coli* strain K-12, substrain MG1655. Amino acid sequence analysis showed that *Ec*ChiP had exceptionally low sequence identity (<14%) to all ChiPs from the OmpC family, such as *Vh*ChiP from *V. harveyi* and *Vf*ChiP from *V. furnissii* (6, 8). This suggested that the *ChiP* genes from *E. coli* and from *Vibrio* sp. did not share common ancestors, and further sequence analysis showed that *Ec*ChiP was similar to *Sm*ChiP from *S. marcescens* (75% identity), both of which are members of the OprD family.

The recombinant *Ec*ChiP displayed quite different channel behavior from other sugar-specific porins. Its most distinctive feature was that it formed a monomeric channel rather than the trimeric channel observed with other known ChiPs and that the channel was stably open over a wide range of external membrane potentials, with only occasional gating at high voltages (±200 mV). At 0.55 ± 0.01 nS, the single channel conductance of *Ec*ChiP was approximately ⅓ that of the well studied *Vh*ChiP (1.8 ± 0.3 nS) (8), consistent with our observation that *Ec*ChiP formed a monomeric channel, whereas *Vh*ChiP worked as a trimer. Comparison with the monomeric OprD from *P. aeruginosa*, a basic amino acid uptake channel (28), revealed that *P. aeruginosa* OprD had a narrow central constriction zone and displayed a much smaller conductance (28 pS) than that of *Ec*ChiP under the same electrolyte conditions (1 M KCl and pH 7.5). This suggests differences in the amino acids that line the channel interior and regulate the net ion flow in *Ec*ChiP as compared with those in OprD.

Measuring changes in ion flow upon varying the cationic/anionic species could provide some information regarding ion selectivity. For examples, Benz and co-workers (34, 35) used LiCl and KAc to test the channel selectivity of the maltodextrin-specific channel LamB and the glucose-inducible channel OprB. Both channels showed a preference for cations over anions. Following their method, our channel exhibited similar preference. We also measured the K^+/Cl^- selectivity by observing changes in reverse membrane potential at zero current under a 0.1–3.0 M gradient of KCl, yielding a P_c/P_a ratio of 2.8, which was slightly lower than the value obtained for the trimeric *Vh*ChiP ($P_c/P_a = 3.2$) (48). Nonetheless, the ion selectivity study obtained from both techniques confirmed that *Ec*ChiP was a cationic-selective channel.

We further examined sugar-channel interactions with various chitooligosaccharides. Our BLM data showed that *Ec*ChiP interacted strongly with long-chain chitooligosaccharides but not with maltooligosaccharides, implying that the channel was specific for chitooligosaccharide uptake. Strong interaction with the higher molecular weight substrates is also a characteristic of other sugar-specific channels, such as LamB (37, 38, 49), *Vh*ChiP (8, 48), and CymA (50). Consistent with this is an earlier *in vivo* study that showed no growth of *S. marcescens* expressing the null ChiP mutant in the presence of chitooligosaccharides larger than chitotriose (26). Both results confirmed the physiological roles of the OprD-related ChiP in chitooligosaccharide uptake.
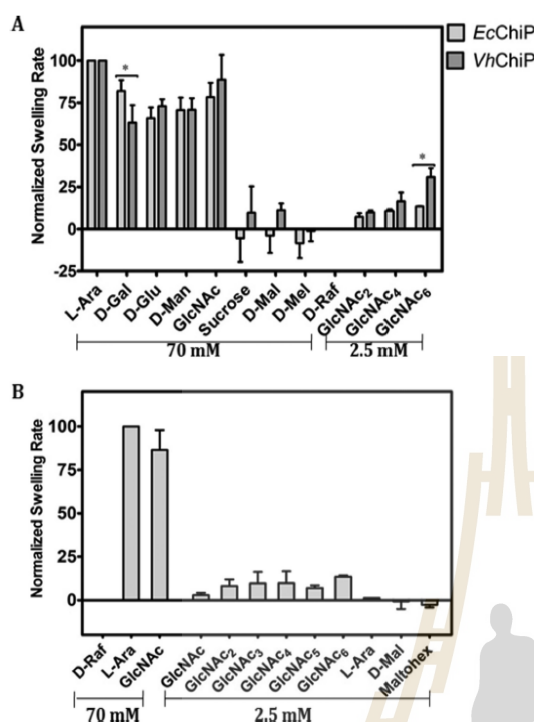
FIGURE 8. **Proteoliposome swelling assays.** In each preparation multilamellar liposomes were reconstituted with 200 ng of *Ec*ChiP or *Vh*ChiP. D-Raffinose was used to determine the isotonic concentrations that produced no change in absorbance at 500 nm of the proteoliposome suspension over 60s. The swelling rate in L-arabinose was set to 100% to obtain normalized swelling rates. The permeability of channels was assumed to be directly proportional to the swelling rate. *A*, permeation of different types of sugar through *Ec*ChiP- and *Vh*ChiP-containing proteoliposomes. Differences between the two data sets were evaluated using a *t* test. Statistically significant differences ($p <$ 0.05) are marked with an *asterisk* (*). Values are the means $\pm$ S.D., obtained from three-five independent sets of experiments. *B*, permeation of chitooligosaccharides through *Ec*ChiP. Maltodextrins were used as controls. L-Ara, L-arabinose; D-*Gal*, D-galactose; D-*Glu*, D-glucose; D-*Man*, D-mannose; GlcNAc, *N*-acetylglucosamine; D-Mal, D-maltose; D-Mel, D-melezitose; D-*Raf*, D-raffinose; *GlcNAc₂*, chitobiose; *GlcNAc₃*, chitotriose; *GlcNAc₄*, chitotetraose; *GlcNAc₅*, chitopentaose; *GlcNAc₆*, chitohexaose; *Maltohex*, maltohexaose.

*Ec*ChiP was tested for its ability to transport neutral sugars of various sizes by use of a liposome swelling assay. All the monosaccharides tested could permeate into *Ec*ChiP-reconstituted liposomes. Similar results were obtained with *Vh*ChiP. Neither channel allowed the passage of neutral sugars of >221 Da, such as maltose, sucrose, melezitose, and raffinose, reflecting the size exclusion limit for small molecules that traverse the channel by general diffusion. In our BLM measurements, we did not observe the occlusion of *Ec*ChiP by GlcNAc, presumably because the short-lived blocking events (<100 μs) produced a residence time too short to be resolved by the currently available BLM setup. This is also the case when molecules with a molecular weight below the size exclusion limit pass through the channel without interacting with it. However, the behavior of the *Ec*ChiP channel was not equivalent to that of other known nonspecific porins, such as *Bps*Omp38 from *Burkholderia pseudomallei* (25, 51, 52) and OmpF from *E. coli* (53), which typically have a size exclusion limit of ~650 Da. In liposome swelling experiments, in agreement with the electro-
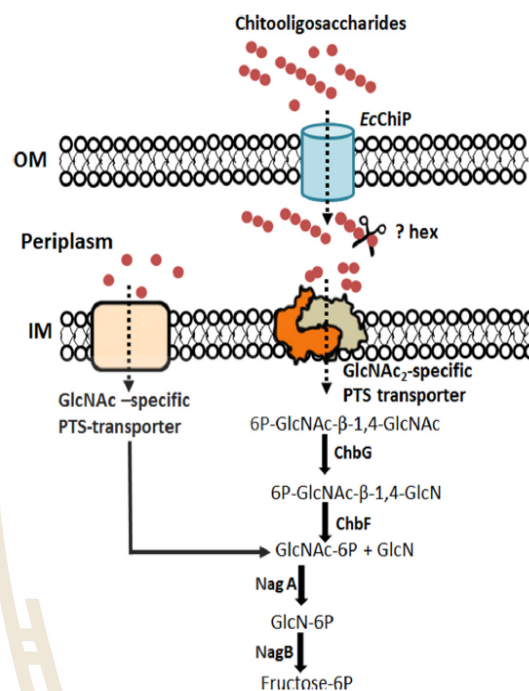
FIGURE 9. **The chitooligosaccharide utilization pathway in *E. coli*.** The scheme is based on the GlcNAc-utilization pathway proposed by Yang *et al.* (14) and Verma and Mahadevan (15). *Solid arrows* denote enzymatic reactions, and *dotted arrows* denote the direction of sugar transport. *PTS*, phosphoenolpyruvate transferase system; *OM*, outer membrane; *IM*, inner membrane; *?Hex*, uncharacterized β-*N*-acetylglucosaminidase (EC 3.2.1.96); *ChbG*, chitooligosaccharide monodeacetylase (EC 3.5.1.105); *ChbF*, monoacetyl-chitobiose 6-phosphate hydrolase (EC 3.2.1.86); *NagA*, *N*-acetylglucosamine-6-phosphate deacetylase (EC 3.5.1.25); *NagB*, glucosamine-6-phosphate deaminase (EC 3.5.1.10).

physiological data, *Ec*ChiP showed sugar-selective behavior, allowing the bulk permeation of chitooligosaccharides at rates that depended on the sizes of the sugar chains, longer chain chitooligosaccharides (chitotetraose, pentaose, and hexaose) tending to show greater permeation rates than short chain sugars such as chitobiose and chitotriose. Additionally, the channel operated even at the low sugar concentration of 2.5 mM, a characteristic of solute-specific channels that has been reported for other well characterized porins, including *E. coli* LamB (54, 55) and *V. harveyi* ChiP (8). As shown in Fig. 8*A*, the rate of permeation of chitohexaose through *Vh*ChiP was much greater than those for other sugars, whereas the permeation rates of chitotetraose, pentaose, and hexaose through *Ec*ChiP were comparable. Both the liposome swelling assays and the BLM data generally showed the lower affinity of *Ec*ChiP than of *Vh*ChiP for the same sugars, and suggested high substrate specificity of the *Vibrio* channel and broad substrate specificity of the *E. coli* channel. This is not surprising, as *Vh*ChiP uses chitin as its sole source of energy, so the channel has evolved to provide every efficient chitooligosaccharide uptake, enabling the bacterium to thrive even in rough seas. On the other hand, *E. coli* uses mainly glucose as a nutrient, its ChiP functioning only under certain environmental conditions, such as a scarcity of glucose in the growth medium.

Identification of Chitin-uptake Channel in E. coli

Taking all of our data together, we reconstructed the chitooligosaccharide utilization pathway of *E. coli* based on the GlcNAc utilization pathway suggested previously (14, 15). As shown in Fig. 9, *E. coli* chitoporin facilitates the uptake of extracellular chitooligosaccharides into the periplasm. The breakdown of high molecular weight chitosugars (chitotriose, chitotetraose, chitopentaose, and chitohexaose) within the periplasm may be initiated by an uncharacterized β-*N*-acetylglucosaminidase (Hex), yielding GlcNAc and GlcNAc$_2$. In the subsequent step GlcNAc is transported through the inner membrane by a GlcNAc-specific phosphoenolpyruvate transferase system transporter, forming GlcNAc-6-phosphate, whereas GlcNAc$_2$ is transported and phosphorylated by the (GlcNAc$_2$)-specific enzyme II permease of a different phosphoenolpyruvate transferase system. Utilization of chitobiose is further mediated by the Chb-BCARFG gene products of the Chb operon (56–58). The deacetylase ChbG removes one acetyl group from chitobiose-6-phosphate, generating monoacetyl chitobiose-6-phosphate, which is then the substrate for a β-glucosidase, ChbF. Its product, GlcNAc 6-phosphate (15), is deacetylated to GlcN 6-phosphate by NagA and then deaminated by NagB to fructose 6-phosphate. This final product of the pathway is metabolized as a carbon source for the bacterial cells. In conclusion, our study is the first elucidation of the physiological function of the OprD-like ChiP and provides an insight into how non-chitinolytic bacteria can utilize chitin as an alternative source of cellular energy during the scarcity of glucose-rich nutrients.

Author Contributions—H. S. M. S. designed, performed, and analyzed all the experiments and co-wrote the paper. WS conceived, designed, and coordinated the study and co-wrote and revised the paper.

References

1. Kim, B. H., and Gadd, G. M. (2008) *Bacterial Physiology and Metabolism*, Cambridge University Press, Cambridge, New York
2. Francetic, O., Belin, D., Badaut, C., and Pugsley, A. P. (2000) Expression of the endogenous type II secretion pathway in *Escherichia coli* leads to chitinase secretion. *EMBO J.* **19,** 6697–6703
3. Francetic, O., Badaut, C., Rimsky, S., and Pugsley, A. P. (2000) The ChiA (YheB) protein of *Escherichia coli* K-12 is an endochitinase whose gene is negatively controlled by the nucleoid-structuring protein H-NS. *Mol. Microbiol.* **35,** 1506–1517
4. Suginta, W., Chuenark, D., Mizuhara, M., and Fukamizo, T. (2010) Novel β-*N*-acetylglucosaminidases from *Vibrio harveyi* 650: cloning, expression, enzymatic properties, and subsite identification. *BMC Biochem.* **11,** 40
5. Li, X., and Roseman, S. (2004) The chitinolytic cascade in *Vibrios* is regulated by chitin oligosaccharides and a two-component chitin catabolic sensor/kinase. *Proc. Natl. Acad. Sci. U.S.A.* **101,** 627–631
6. Keyhani, N. O., Li, X. B., and Roseman, S. (2000) Chitin catabolism in the marine bacterium *Vibrio furnissii*: identification and molecular cloning of a chitoporin. *J. Biol. Chem.* **275,** 33068–33076
7. Suginta, W., Chumjan, W., Mahendran, K. R., Janning, P., Schulte, A., and Winterhalter, M. (2013) Molecular uptake of chitooligosaccharides through chitoporin from the marine bacterium *Vibrio harveyi. PLoS ONE* **8,** e55126
8. Suginta, W., Chumjan, W., Mahendran, K. R., Schulte, A., and Winterhalter, M. (2013) Chitoporin from *Vibrio harveyi*, a channel with exceptional sugar specificity. *J. Biol. Chem.* **288,** 11038–11046
9. Meekrathok, P., and Suginta, W. (2016) Probing the catalytic mechanism of *Vibrio harveyi* GH20 β-*N*-acetylglucosaminidase by chemical rescue. *PLoS ONE* **11,** e0149228
10. Suginta, W., and Sritho, N. (2012) Multiple roles of Asp-313 in the refined catalytic cycle of chitin degradation by *Vibrio harveyi* chitinase A. *Biosci. Biotechnol. Biochem.* **76,** 2275–2281
11. Sritho, N., and Suginta, W. (2012) Role of Tyr-435 of *Vibrio harveyi* chitinase A in chitin utilization. *Appl. Biochem. Biotechnol.* **166,** 1192–1202
12. Biswas, S., Van Dijck, P., and Datta, A. (2007) Environmental sensing and signal transduction pathways regulating morphopathogenic determinants of *Candida albicans. Microbiol. Mol. Biol. Rev.* **71,** 348–376
13. Boulanger, A., Déjean, G., Lautier, M., Glories, M., Zischek, C., Arlat, M., and Lauber, E. (2010) Identification and regulation of the *N*-acetylglucosamine utilization pathway of the plant pathogenic bacterium *Xanthomonas campestris* pv. campestris. *J. Bacteriol.* **192,** 1487–1497
14. Yang, C., Rodionov, D. A., Li, X., Laikova, O. N., Gelfand, M. S., Zagnitko, O. P., Romine, M. F., Obraztsova, A. Y., Nealson, K. H., and Osterman, A. L. (2006) Comparative genomics and experimental characterization of *N*-acetylglucosamine utilization pathway of *Shewanella oneidensis. J. Biol. Chem.* **281,** 29872–29885
15. Verma, S. C., and Mahadevan, S. (2012) The chbG gene of the chitobiose (chb) operon of *Escherichia coli* encodes a chitooligosaccharide deacetylase. *J. Bacteriol.* **194,** 4959–4971
16. Rasmussen, A. A., Johansen, J., Nielsen, J. S., Overgaard, M., Kallipolitis, B., and Valentin-Hansen, P. (2009) A conserved small RNA promotes silencing of the outer membrane protein YbfM. *Mol. Microbiol.* **72,** 566–577
17. Peri, K. G., Goldie, H., and Waygood, E. B. (1990) Cloning and characterization of the *N*-acetylglucosamine operon of *Escherichia coli. Biochem. Cell Biol.* **68,** 123–137
18. Figueroa-Bossi, N., Valentini, M., Malleret, L., Fiorini, F., and Bossi, L. (2009) Caught at its own game: regulatory small RNA inactivated by an inducible transcript mimicking its target. *Genes Dev.* **23,** 2004–2015
19. Valentin-Hansen, P., Johansen, J., and Rasmussen, A. A. (2007) Small RNAs controlling outer membrane porins. *Curr. Opin. Microbiol.* **10,** 152–155
20. Vogel, J., and Papenfort, K. (2006) Small non-coding RNAs and the bacterial outer membrane. *Curr. Opin. Microbiol.* **9,** 605–611
21. Plumbridge, J., Bossi, L., Oberto, J., Wade, J. T., and Figueroa-Bossi, N. (2014) Interplay of transcriptional and small RNA-dependent control mechanisms regulates chitosugar uptake in *Escherichia coli* and *Salmonella. Mol. Microbiol.* **92,** 648–658
22. Robert, X., and Gouet, P. (2014) Deciphering key features in protein structures with the new ENDscript server. *Nucleic Acids Res.* **42,** W320–W324
23. Montal, M., and Mueller, P. (1972) Formation of bimolecular membranes from lipid monolayers and a study of their electrical properties. *Proc. Natl. Acad. Sci. U.S.A.* **69,** 3561–3566
24. Yoshimura, F., and Nikaido, H. (1985) Diffusion of beta-lactam antibiotics through the porin channels of *Escherichia coli* K-12. *Antimicrob. Agents Chemother.* **27,** 84–92
25. Aunkham, A., Schulte, A., Winterhalter, M., and Suginta, W. (2014) Porin involvement in cephalosporin and carbapenem resistance of *Burkholderia pseudomallei. PLoS ONE* **9,** e95918
26. Takanao, S., Honma, S., Miura, T., Ogawa, C., Sugimoto, H., Suzuki, K., and Watanabe, T. (2014) Construction and basic characterization of deletion mutants of the genes involved in chitin utilization by *Serratia marcescens* 2170. *Biosci. Biotechnol. Biochem.* **78,** 524–532
27. Meibom, K. L., Li, X. B., Nielsen, A. T., Wu, C. Y., Roseman, S., and Schoolnik, G. K. (2004) The *Vibrio cholerae* chitin utilization program. *Proc. Natl. Acad. Sci. U.S.A.* **101,** 2524–2529
28. Biswas, S., Mohammad, M. M., Patel, D. R., Movileanu, L., and van den Berg, B. (2007) Structural insight into OprD substrate specificity. *Nat. Struct. Mol. Biol.* **14,** 1108–1109
29. Wang, Y. F., Dutzler, R., Rizkallah, P. J., Rosenbusch, J. P., and Schirmer, T.

(1997) Channel specificity: structural basis for sugar discrimination and differential flux rates in maltoporin. *J. Mol. Biol.* **272,** 56–63

30. Forst, D., Welte, W., Wacker, T., and Diederichs, K. (1998) Structure of the sucrose-specific porin ScrY from *Salmonella typhimurium* and its complex with sucrose. *Nat. Struct. Biol.* **5,** 37–46

31. Conlan, S., Zhang, Y., Cheley, S., and Bayley, H. (2000) Biochemical and biophysical characterization of OmpG: A monomeric porin. *Biochemistry* **39,** 11845–11854

32. van den Berg, B. (2012) Structural basis for outer membrane sugar uptake in pseudomonads. *J. Biol. Chem.* **287,** 41044–41052

33. Strop, P., and Brunger, A. T. (2005) Refractive index-based determination of detergent concentration and its application to the study of membrane proteins. *Protein Sci.* **14,** 2207–2211

34. Saravolac, E. G., Taylor, N. F., Benz, R., and Hancock, R. E. (1991) Purification of glucose-inducible outer membrane protein OprB of *Pseudomonas putida* and reconstitution of glucose-specific pores. *J. Bacteriol.* **173,** 4970–4976

35. Benz, R., Schmid, A., and Vos-Scheperkeuter, G. H. (1987) Mechanism of sugar transport through the sugar-specific LamB channel of *Escherichia coli* outer membrane. *J. Membr. Biol.* **100,** 21–29

36. Ranquin, A., and Van Gelder, P. (2004) Maltoporin: sugar for physics and biology. *Res. Microbiol.* **155,** 611–616

37. Kullman, L., Winterhalter, M., and Bezrukov, S. M. (2002) Transport of maltodextrins through maltoporin: a single-channel study. *Biophys. J.* **82,** 803–812

38. Bezrukov, S. M., Kullman, L., and Winterhalter, M. (2000) Probing sugar translocation through maltoporin at the single channel level. *FEBS Lett.* **476,** 224–228

39. Schwarz, G., Danelon, C., and Winterhalter, M. (2003) On translocation through a membrane channel via an internal binding site: kinetics and voltage dependence. *Biophys. J.* **84,** 2990–2998

40. Zobell, C. E., and Rittenberg, S. C. (1938) The occurrence and characteristics of chitinoclastic bacteria in the sea. *J. Bacteriol.* **35,** 275–287

41. Bassler, B. L., Yu, C., Lee, Y. C., and Roseman, S. (1991) Chitin utilization by marine bacteria: degradation and catabolism of chitin oligosaccharides by *Vibrio furnissii. J. Biol. Chem.* **266,** 24276–24286

42. Bassler, B. L., Gibbons, P. J., Yu, C., and Roseman, S. (1991) Chitin utilization by marine bacteria: chemotaxis to chitin oligosaccharides by *Vibrio furnissii. J. Biol. Chem.* **266,** 24268–24275

43. Yu, C., Lee, A. M., Bassler, B. L., and Roseman, S. (1991) Chitin utilization by marine bacteria: a physiological function for bacterial adhesion to immobilized carbohydrates. *J. Biol. Chem.* **266,** 24260–24267

44. Keyhani, N. O., and Roseman, S. (1999) Physiological aspects of chitin catabolism in marine bacteria. *Biochim. Biophys. Acta* **1473,** 108–122

45. Park, J. K., Keyhani, N. O., and Roseman, S. (2000) Chitin catabolism in the marine bacterium *Vibrio furnissii.* Identification, molecular cloning, and characterization of a *N,N*′-diacetylchitobiose phosphorylase. *J. Biol. Chem.* **275,** 33077–33083

46. Hunt, D. E., Gevers, D., Vahora, N. M., and Polz, M. F. (2008) Conservation of the chitin utilization pathway in the *Vibrionaceae. Appl. Environ. Microbiol.* **74,** 44–51

47. Pruzzo, C., Vezzulli, L., and Colwell, R. R. (2008) Global impact of *Vibrio cholerae* interactions with chitin. *Environ. Microbiol.* **10,** 1400–1410

48. Chumjan, W., Winterhalter, M., Schulte, A., Benz, R., and Suginta, W. (2015) Chitoporin from the marine bacterium *Vibrio harveyi*: probing the essential roles of trp136 at the surface of the constriction zone. *J. Biol. Chem.* **290,** 19184–19196

49. Danelon, C., Brando, T., and Winterhalter, M. (2003) Probing the orientation of reconstituted maltoporin channels at the single-protein level. *J. Biol. Chem.* **278,** 35542–35551

50. Bhamidimarri, S. P., Prajapati, J. D., van den Berg, B., Winterhalter, M., and Kleinekathöfer, U. (2016) Role of electroosmosis in the permeation of neutral molecules: CymA and cyclodextrin as an example. *Biophys. J.* **110,** 600–611

51. Siritapetawee, J., Prinz, H., Krittanai, C., and Suginta, W. (2004) Expression and refolding of Omp38 from *Burkholderia pseudomallei* and *Burkholderia thailandensis* and its function as a diffusion porin. *Biochem. J.* **384,** 609–617

52. Siritapetawee, J., Prinz, H., Samosornsuk, W., Ashley, R. H., and Suginta, W. (2004) Functional reconstitution, gene isolation, and topology modelling of porins from *Burkholderia pseudomallei* and Burkholderia thailandensis. *Biochem. J.* **377,** 579–587

53. Saint, N., Lou, K. L., Widmer, C., Luckey, M., Schirmer, T., and Rosenbusch, J. P. (1996) Structural and functional characterization of OmpF porin mutants selected for larger pore size. II: functional characterization. *J. Biol. Chem.* **271,** 20676–20680

54. Dumas, F., Koebnik, R., Winterhalter, M., and Van Gelder, P. (2000) Sugar transport through maltoporin of *Escherichia coli*: role of polar tracks. *J. Biol. Chem.* **275,** 19747–19751

55. Van Gelder, P., Dumas, F., Rosenbusch, J. P., and Winterhalter, M. (2000) Oriented channels reveal asymmetric energy barriers for sugar translocation through maltoporin of *Escherichia coli. Eur. J. Biochem.* **267,** 79–84

56. Keyhani, N. O., Bacia, K., and Roseman, S. (2000) The transport/phosphorylation of *N,N*′-diacetylchitobiose in *Escherichia coli*: characterization of phospho-IIB(Chb) and of a potential transition state analogue in the phosphotransfer reaction between the proteins IIA(Chb) AND IIB-(Chb). *J. Biol. Chem.* **275,** 33102–33109

57. Keyhani, N. O., Boudker, O., and Roseman, S. (2000) Isolation and characterization of IIAChb, a soluble protein of the enzyme II complex required for the transport/phosphorylation of *N,N*′-diacetylchitobiose in *Escherichia coli. J. Biol. Chem.* **275,** 33091–33101

58. Keyhani, N. O., Wang, L. X., Lee, Y. C., and Roseman, S. (2000) The chitin disaccharide, N,N′-diacetylchitobiose, is catabolized by *Escherichia coli* and is transported/phosphorylated by the phosphoenolpyruvate:glucose phosphotransferase system. *J. Biol. Chem.* **275,** 33084–33090

Identification and Functional Characterization of a Novel OprD-like Chitin Uptake Channel in Non-chitinolytic Bacteria

H. Sasimali M. Soysa and Wipa Suginta
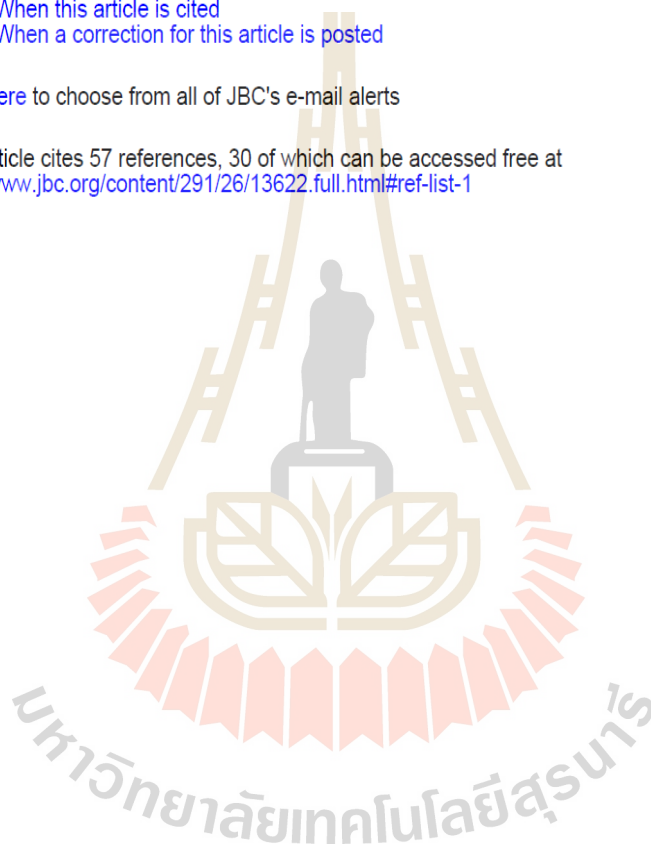
CURRICULUM VITAE

Name   Mrs. H. Sasimali M. Soysa

Date of Birth   28 May 1986

Place of Birth   Panadura, Sri Lanka.

Education

- Academic year 2011, B.Sc. Applied Sciences Special Degree in Chemical Technology, Second Class Upper Division (Gold medal), (In English Medium) Sabaragamuwa University of Sri Lanka, Belihuloya, Sri Lanka.

- Academic year 2013 to date, Ph.D. student, Doctor of Philosophy (Biochemistry), Suranaree University of Technology, Thailand.

Scholaships and Awards

- OROG scholarship, Suranaree University of Technology, Nakhon Ratchasima, Thailand.

- Deutscher Akademischer Austausch Dienst e.V. German Academic Exchange Service (DAAD scholarship), Germany.

- Travel award at the 5th Asia Pacific Protein Association (APPA) Conference and the 12th International Symposium for the Protein Society of Thailand (PST), Bangsaen, Thailand.

Position and Place of Work

- Lecturer (2012 to date), Sabaragamuwa University of Sri Lanka, Sri Lanka.